

A Generalized Approach to g Level Based Equipment Evaluation

by

Christopher William Pichurski

A thesis submitted in partial fulfillment of the requirements for the degree of

Doctor of Philosophy

in

Mining Engineering

Department of Civil and Environmental Engineering

University of Alberta

## **Abstract**

The interaction between operator input, machine and operating surface is highly complex and varied. Time based equipment evaluation metrics are limited in the type of information they can convey. A common alternative to time based evaluation is mechanical modeling, however; these models can be complex and require an advanced understanding of mechanics to construct. The purpose of this research is to provide the framework for a simple vehicle performance indicator which is capable of providing meaningful insight into the physical interaction between the equipment and its operating environment. The value of this indicator is in its versatility, and simplicity which allows it to be implemented by a wide range of researchers and operators who have an understanding of the basic principles of mechanics.

This document proposes a generalized methodology which uses forces measured from the hubs or struts of mobile haulage equipment to quantify, with magnitude and direction, the effects of the interaction between machine and environment. The method proposed is easily adaptable to allow alternative effects and perspectives to be evaluated.

In addition to the formulation of the Generalized g Level Analysis method a scale model investigation is provided to demonstrate the mechanics of g level based evaluation and provide insight into the adverse motions experienced by full scale underground articulated haul trucks. The g Level Analysis method is also applied to field data collected from an ultra class rigid body haul truck operating in Alberta's oil sands. This field data is used to present additional applications of the method including haul road monitoring and equipment efficiency.

This work is dedicated to everyone who has found the joy of learning.

It's a journey which never ends, but we travel it together.

## **Acknowledgment**

In the most profound manner I thank my advisor, mentor, teacher and friend Dr. Tim Joseph for all he has done for me throughout my entire academic career. He has supported me, laughed with me, scolded me, cut red tape for me, advocated for me, encouraged me, believed in me and worked alongside me. There is no way to fully express my gratitude except to hope that in time I can at least partially repay him in kind. There is no greater advocate for the adventure which is learning.

I would also like to acknowledge and thank Dr. Mike Lipsett for his input and comments which undoubtedly increased the quality of this work.

I thank Lucas Duerksen for his help in the lab, discussions on craft beer and for letting me vent when I was frustrated with my other endeavors.

To my father I say “Thank You” for helping to build my desire to learn, work ethic, ambition and love of heavy equipment.

I must thank my dog Phinn, who was literally by my side, or at least my feet, throughout the entire writing process. I couldn’t have made it through without you buddy.

Finally, but certainly not least, I thank my wife, Erin, who is everything to me. In retrospect I should have discussed graduate school with you before I applied as a “hobby”. Thank you for your unwavering support. I love you.



## Table of Contents

<b>1</b>	<b>Introduction .....</b>	<b>1</b>
<b>1.1</b>	<b>Motivation.....</b>	<b>1</b>
<b>1.2</b>	<b>Thesis Statement and Purpose .....</b>	<b>2</b>
<b>1.3</b>	<b>Approach.....</b>	<b>3</b>
<b>1.4</b>	<b>Literature Review .....</b>	<b>3</b>
1.4.1	g Level Based Analysis .....	4
1.4.2	Vehicle Modeling .....	9
1.4.3	Haul Roads and Haul Road Maintenance .....	15
1.4.3.1	Surface Haul Road Construction and Geometry.....	15
1.4.3.2	Haul Road Maintenance .....	19
1.4.4	Whole Body Vibration .....	23
<b>2</b>	<b>Mathematical Investigation .....</b>	<b>28</b>
<b>2.1</b>	<b>Loading Components .....</b>	<b>28</b>
2.1.1	Natural of Tare Force Loading.....	28
2.1.2	Payload Hub force .....	29
2.1.3	Articulation Force.....	29
2.1.4	Force Due to Motion .....	30
<b>2.2</b>	<b>Calculation of Cumulative Hub Forces.....</b>	<b>30</b>
2.2.1	Acknowledgment of Lack of Monitoring Points on Suspension-less Equipment .....	31
<b>2.3</b>	<b>Relationship between Hub Forces and Frame Twist .....</b>	<b>32</b>
<b>2.4</b>	<b>Relationship between Multi-Body Modeling and g Level Analysis.....</b>	<b>35</b>
<b>2.5</b>	<b>Choice of Reference Point .....</b>	<b>38</b>
<b>2.6</b>	<b>Derivation of the Equivalent Force about the Mid-ship .....</b>	<b>39</b>
<b>2.7</b>	<b>Natural Front and Rear Frame Angles .....</b>	<b>39</b>
2.7.1	Definition of Articulation.....	40
<b>2.8</b>	<b>Instantaneous Moment about the Reference Point.....</b>	<b>41</b>
<b>2.9</b>	<b>Equivalent Force and Instantaneous g Level Analysis .....</b>	<b>43</b>
2.9.1	Determination of the Magnitude of <i>FEQ</i> .....	44
2.9.2	Determination of $U \perp$ .....	44

2.10	Final Determination of <i>FEQ</i> .....	46
2.11	Equivalent Force Distributions .....	48
3	Instantaneous g Level Analysis .....	50
3.1	Application of Newton's Second Law .....	50
3.2	Definition of Rack, Pitch, Roll and Twist .....	51
3.2.1	Pitch and Roll .....	52
3.2.2	Rack .....	52
3.2.3	Twist .....	53
3.2.4	g Level Evaluation Process .....	54
3.3	Method Validation .....	58
3.4	Effect of Reference Point Selection .....	68
3.4.1	Pitch Axis .....	68
3.4.2	Roll Axis .....	72
4	Scale Model Testing .....	77
4.1	Scale Model Design and Construction .....	77
4.2	Design .....	77
4.2.1	Detailed Design and Materials .....	78
4.3	Comments on Rigidity .....	83
4.4	Comparison of Test Unit to Full Scale Atlas Copco MT431B .....	83
4.5	Tare Weight Distribution between Test Unit and MT431B .....	84
4.5.1	Tare Weight Balance – Left to Right .....	85
4.6	Testing Method .....	87
4.6.1	Test Axles .....	89
4.6.2	Control of Articulation Angle .....	90
4.6.3	Control of Inclination .....	91
4.6.4	Data Acquisition and Instrumentation .....	92
4.7	Payload and Hub Force Scaling Factor .....	93
4.7.1	Payload .....	93
4.8	Results .....	96
4.8.1	Trials and Data Processing .....	96

4.8.2	Raw Data .....	97
4.8.2.1	Effect of Load Balance on Raw Data .....	99
4.8.2.2	Total Gross Vehicle Weight and Gross Vehicle Weight Distribution .....	100
4.8.3	Moment and g Level Analysis.....	103
4.8.3.1	Key Metrics.....	104
4.8.4	Test Unit Scale.....	104
4.8.4.1	Total Moment, Twist and Axis of Rotation Direction .....	104
4.8.4.2	Roll.....	108
4.8.4.3	Pitch.....	109
4.8.4.4	Q1 Rack.....	110
4.8.4.5	Q2 Rack.....	111
4.8.4.6	Verification Testing.....	112
<b>5</b>	<b>Full Scale Simulations and Operating Hauler Analysis .....</b>	<b>116</b>
5.1.1	Comparison of Test Unit to Simulated Full Scale Articulated Haulers .....	116
5.1.2	Full Scale Articulated Simulation Results .....	119
5.1.3	Sample Detailed Analysis of Full Scale Results – Hauler MT2010 .....	120
5.1.4	General Results for All Simulated Articulated Haulers.....	124
5.1.5	Group Comparison of Hauler Performance .....	128
<b>5.2</b>	<b>Full Scale Analysis of Rigid Body Hauler .....</b>	<b>134</b>
5.2.1	Rigid Body Data .....	134
5.2.2	Caterpillar 797 Analysis.....	135
5.2.2.1	797 Analysis – About Geometric Center.....	135
5.2.2.2	797 Analysis - About Theoretical Centre of Gravity .....	139
5.2.2.3	Haul Road Analysis .....	144
5.2.2.4	Energy Efficiency .....	146
<b>6</b>	<b>Comparison of 2003 Method and gLA .....</b>	<b>150</b>
<b>6.1</b>	<b>Rigid Hauler Comparison.....</b>	<b>150</b>
<b>6.2</b>	<b>2003 vs. gLA With Model Data.....</b>	<b>154</b>
<b>7</b>	<b>Discussion .....</b>	<b>160</b>
<b>7.1</b>	<b>Significant Research Contributions .....</b>	<b>161</b>
7.1.1	Benefits to Researchers and Industry .....	161
7.1.2	Generation and Demonstration of the Generalized g Level Method.....	162
7.1.3	Baseline Study into Adverse Moments Created by UAHT.....	164
7.1.4	Field Data Analysis of Rigid Framed Hauler.....	165
7.1.4.1	Haul Road Analysis .....	167
7.1.4.2	Energy Analysis.....	168

<b>8</b>	<b>Conclusions .....</b>	<b>170</b>
<b>8.1</b>	<b>Future Work .....</b>	<b>171</b>
	<b>Appendix.....</b>	<b>179</b>
<b>1.</b>	<b>Statistical Evaluation of Weight Distribution vs Articulation .....</b>	<b>179</b>
	Tare Weight.....	179
	36% Loading .....	182
	70% Loading .....	185
	100% Loading .....	187
<b>2.</b>	<b>Detailed derivation of the direction of <math>FEq</math> .....</b>	<b>190</b>
<b>3.</b>	<b>Load Cell Calibration Certificates .....</b>	<b>191</b>
<b>4.</b>	<b>Detailed Design Drawings of Test Unit .....</b>	<b>195</b>
<b>5.</b>	<b>Example Equipment Specification Sheets .....</b>	<b>208</b>
<b>6.</b>	<b>Payload Sieve Analysis.....</b>	<b>216</b>
	Sample 1 .....	216
	Sample 2 .....	217
<b>7.</b>	<b>Determination of Scaling Factor .....</b>	<b>218</b>
<b>8.</b>	<b>Scale Model Testing Raw Data .....</b>	<b>220</b>
<b>9.</b>	<b>Complete Full Scale Simulation Results .....</b>	<b>224</b>
	MT431B .....	224
	AD30.....	227
	MT42 .....	231
	AD45B.....	234
	MT5020 .....	238
	AD55.....	241
	MT6020 .....	245
	AD60.....	248
<b>10.</b>	<b>veDYNA Entry Vehicle Parameters .....</b>	<b>252</b>

## List of Tables

Table 1.1: Quarter Vehicle Model Parameters (After Pakowski and Cao, 2013).....	14
Table 3.1: veDYNA Light Truck Basic Parameters (After Tesis, 2014).....	59
Table 3.2: Predicted Pitch Value from Linear Relationship .....	72
Table 3.3: Predicted Roll Value from Linear Relationship .....	76
Table 4.1: Comparison of Test Unit to MT431B.....	84
Table 4.2: Test Unit Vs. MT431B Tare Weight Comparison.....	85
Table 4.3: Completed Trials by Loading, Articulation and Inclination .....	89
Table 4.4: Payload by Replicated Load .....	94
Table 4.5: Test Unit - Left to Right Balance.....	100
Table 4.6: Verification Testing Parameters.....	113
Table 5.1: Sumary Parameters of Simulated Full Scale Haulers .....	117
Table 5.2: Sample Caterpillar 797A Data .....	135
Table 5.3: Caterpillar 797 Data .....	135
Table 5.4: Position Vectors - About Geometric Center.....	136
Table 5.5: 797 Loaded Position Vectors - Ideal COG .....	140
Table 5.6: 797 Empty Position Vectors - Ideal COG .....	141
Table 5.7: Energy Analysis Parameters .....	148
Table 5.8: Energy Analysis Results .....	149

## List of Figures

Figure 1.1: g Level Analysis in a Simplified Scientific Method .....	2
Figure 1.2: Haul Truck Schematic (After Joseph, 2003) .....	5
Figure 1.3: Rack, Pitch and Roll Visualization (After Joseph, 2003) .....	6
Figure 1.4: Articulated Hauler Schematic .....	6
Figure 1.5: Pitch, Rack, Roll Asymmetry Visualization .....	7
Figure 1.6: Balanced Simple Beam.....	7
Figure 1.7: Unbalanced Simple Beam .....	8
Figure 1.8: Simplified Articulated Vehicle, Articulation Equal to Zero .....	8
Figure 1.9: Simplified Articulated Vehicle, Articulation Not Equal to Zero.....	8
Figure 1.10: Roll Model of a Rigid Vehicle (after Jazar,2014) .....	10
Figure 1.11: 14 DOF Full Vehicle Model (Ghike and Shim, 2006) .....	11
Figure 1.12: Typical Articulated Frame Steer Dump Truck (After Huang, Shen, Zang, 2010).....	12
Figure 1.13: Basic Frame Arrangement of Typical ASV (After Huang, Shen, Zang, 2010) .....	13
Figure 1.14: Quarter Vehicle Model (After Pakowski and Cao, 2013) .....	14
Figure 1.15: Typical Haul Road Cross Section (After Tannant and Regensburg, 2001) .....	16
Figure 1.16: Example CBR Design Curve (After Tannant and Regensburg2001) .....	17
Figure 1.17: CSL Design Method (After Tannant and Regensburg 2001) .....	18
Figure 1.18: Minimum Total Cost Solution For Road Maintenance Frequency (After Thompson and Visser, 2003).....	19
Figure 1.19: FBD of RR on Tire (After Plackett, 1985).....	20
Figure 1.20: Components of Real Time RR Based Haul Road Maintenance (After Lee 2010) .....	22
Figure 1.21: Illustration of Circular Rigid Treadband Model (After Hugo et al, 2008).....	23
Figure 1.22: WBV Health Caution Guidance Zones (After ISO 2631-1) .....	25
Figure 1.23: WBV Exposure Monitor Interface (Berezan,2006) .....	25
Figure 1.24: Example Jolt Duration Event (after Miller, 2009) .....	27
Figure 2.1: Caterpillar AD60 Haul Truck.....	33
Figure 2.2: (Left) UAHT Schematic Plan view and Free Body Diagram, (Right) UAHT Free Body Diagram	34
Figure 2.3: (Left) Overview of Test Unit FBD, (Right), Test Unit FBD .....	35
Figure 2.4: Location of Data Collection on 1/4 Vehicle Model .....	36
Figure 2.5: g Level Analysis Vehicle Model .....	37
Figure 2.6: Example Representation of Unit Mo .....	43
Figure 2.7: Example Representation of the Cumulative Moment and the Point P .....	46
Figure 2.8: Unit Sphere Slice .....	47
Figure 2.9: Example Representation of the Equivalent Force Applied Tangent to Point P .....	48
Figure 2.10: Example Vector Representation of Results .....	49
Figure 3.1: Rack, Pitch and Roll Axes .....	52
Figure 3.2: gLA Process Flowchart .....	58
Figure 3.3: Simulated Light Truck Wireframe (Using veDynaware, Thesis, 2014) .....	59
Figure 3.4: Simulated Vehicle .....	60
Figure 3.5: Monte Carlo Course - Plan View (Using veDynaware, Thesis, 2014).....	61

Figure 3.6: Monte Carlo Course - Curvature (Using veDynaWare, Thesis, 2014).....	61
Figure 3.7: Monte Carlo Course - Elevation Profile (Using veDynaWare, Thesis, 2014) .....	62
Figure 3.8: Simulated Suspension Forces .....	63
Figure 3.9: Simulated Light Truck in Left Hand Corner .....	63
Figure 3.10: veDYNA and g Level Pitch Results.....	64
Figure 3.11: Pitch Results with Course Elevation.....	65
Figure 3.12: Vehicle Pitch and Yaw Response.....	65
Figure 3.13: veDYNA vs. g Level Pitch Cross-Plot.....	66
Figure 3.14:veDYNA and g Level Roll Results.....	67
Figure 3.15: veDYNA vs g Level Roll Cross Plot .....	67
Figure 3.16: Pitch Axis Location Description.....	69
Figure 3.17: Pitch Response about Various Axis Locations.....	69
Figure 3.18: Standard Deviation of Pitch Readings with Varied Pitch Axis Locations .....	70
Figure 3.19: Effect of Pitch Axis Location on g Level.....	71
Figure 3.20: Calculated Linear Slope Values for Pitch Axis Variation .....	71
Figure 3.21: Calculated Intercept Values for Pitch Axis Variation .....	72
Figure 3.22: Roll Axis Location Description.....	73
Figure 3.23: Roll Response about Various Axis Locations.....	73
Figure 3.24: Standard Deviation of Roll Readings with Varied Roll Axis Location .....	74
Figure 3.25: Effect of Roll Axis Location of g Level .....	75
Figure 3.26: Calculated Linear Slope Values for Roll Axis Variation .....	75
Figure 3.27: Calculated Intercept Values for Roll Axis Variation .....	76
Figure 4.1: (Left) Setting Left Hand Oscillation Limit, (Right) Setting Right Hand Oscillation Limit.....	78
Figure 4.2:Isometric of Test Unit General Arrangement .....	79
Figure 4.3: Plan View of Test Unit General Arrangement.....	79
Figure 4.4:Section View of Test Unit General Arrangement.....	79
Figure 4.5: (Left) Rear Frame During Construction, (Right) Completed Front and Rear Frames.....	80
Figure 4.6: Welding Shop .....	80
Figure 4.7(Left) Side View of Completed Test Unit Frame, (Right) Isometric View of Completed Test Unit Frame .....	81
Figure 4.8:(Right)Hand Built Test Unit Box, (Left) Front View of Completed Test Unit.....	81
Figure 4.9: Bottom View of Completed Test Unit.....	82
Figure 4.10: (Left) Side View of Completed Test Unit, (Right) Identifying Zero Articulation.....	82
Figure 4.11: Comparison Dimensions .....	83
Figure 4.12: Test Unit With Final Tare Weight Arrangement .....	85
Figure 4.13: Offset Mid-ship Design .....	86
Figure 4.14: Test Unit Weight Distribution by Payload and Hub Location .....	87
Figure 4.15: General Test Setup.....	88
Figure 4.16: Test Axle and Load Cell Arrangement.....	90
Figure 4.17: Articulation Control Plate .....	91
Figure 4.18: (Left)Test Unit in Articulated and Inclined Position, (Right) Inclination Measurement .....	92
Figure 4.19: Test Unit Loading by Replicated Bucket Pass .....	94

Figure 4.20: Replicated Loading Pass #1 .....	95
Figure 4.21: Replicated Loading Pass #2 .....	95
Figure 4.22: Replicated Loading Pass #3 .....	96
Figure 4.23: Raw Data Results by Trial Number .....	98
Figure 4.24: Raw Data Results, Trial #'s 50-90 .....	98
Figure 4.25: Raw Data Results, Trial #'s 90-128 .....	99
Figure 4.26: Gross Vehicle Weight by Test Number .....	101
Figure 4.27: GVW Distribution By Test Number .....	102
Figure 4.28: Proportion of GVW per Axle .....	103
Figure 4.29: Test Unit Total Moment About Reference .....	105
Figure 4.30: Test Unit Total Twist about Reference Point in g Levels .....	106
Figure 4.31: Test Unit Total Moment Unit i & Unit j Coordinates .....	107
Figure 4.32: Test Unit Roll in g Level .....	108
Figure 4.33: Test Unit Pitch in g Level .....	109
Figure 4.34: Test Unit Q1 Rack in g Level .....	111
Figure 4.35: Test Unit Q2 Rack in g Level .....	112
Figure 4.36: Measured vs Calculated FA - Moi .....	114
Figure 4.37: Measured vs Calculated FA - Moj .....	114
Figure 4.38: Measured vs Average Calculated FA - Moi & Moj .....	115
Figure 5.1: Payload to Tare Weight Ratio for Simulated Haulers .....	118
Figure 5.2: Distance from Mid-ship to Front and Rear Axles of Simulated Haulers .....	118
Figure 5.3: Relevant Angles for Simulated Haulers .....	119
Figure 5.4: MT2010 Total Moment About the Reference Point .....	121
Figure 5.5: MT2010 Total Twist about the Reference Point in g Level .....	121
Figure 5.6: MT2010 Total Moment Unit i & Unit j Coordinates .....	122
Figure 5.7: MT2010 Roll in g Level .....	122
Figure 5.8: MT2010 Pitch in g Level .....	123
Figure 5.9: MT2010 Q1 Rack in g Level .....	124
Figure 5.10: MT2010 Q2 Rack in g Level .....	124
Figure 5.11: MT431 Total g Level about Reference and Direction Plot .....	125
Figure 5.12: AD30 Total g Level about Reference and Direction Plot .....	125
Figure 5.13: MT42 Total g Level about Reference and Direction Plot .....	126
Figure 5.14: AD45 Total g Level about Reference and Direction Plot .....	126
Figure 5.15: MT5020 Total g Level about Reference and Direction Plot .....	126
Figure 5.16: AD55 Total g Level about Reference and Direction Plot .....	127
Figure 5.17: MT6020 Total g Level about Reference and Direction Plot .....	127
Figure 5.18: AD60 Total g Level about Reference and Direction Plot .....	127
Figure 5.19: Incremental Total Moment by Payload .....	128
Figure 5.20: Total Moment About Reference .....	129
Figure 5.21: Incremental Increase in g Level .....	129
Figure 5.22: Cumulative Twist By Payload .....	130
Figure 5.23: Incremental Roll By Payload .....	130



Figure 5.24: Cumulative Roll by Payload.....	131
Figure 5.25: Incremental Pitch by Payload .....	131
Figure 5.26: Cumulative Pitch by Payload.....	132
Figure 5.27: Incremental Q1 Rack by Payload .....	132
Figure 5.28: Cumulative Q1 Rack by Payload .....	133
Figure 5.29: Incremental Q2 Rack by Payload .....	133
Figure 5.30: Cumulative Q2 Rack by Payload .....	134
Figure 5.31: Illustrated Position Vectors - Geometric Centre.....	136
Figure 5.32: 797 g Level Results - Total About Geometric Centre .....	137
Figure 5.33: 797 g Level Results Total Twist and Payload.....	137
Figure 5.34: 797 Results Direction Plot - About Geometric Centre .....	138
Figure 5.35: 797 Pitch - About Geometric Centre.....	138
Figure 5.36: 797 Roll - About Geometric Centre.....	139
Figure 5.37: 797 Rack - About Geometric Centre .....	139
Figure 5.38: 797 Illustrated Position Vectors - Loaded COG.....	140
Figure 5.39: 797 Illustrated Position Vectors - Empty COG .....	141
Figure 5.40: 797 Total g Level - About Ideal COG .....	141
Figure 5.41: 797 Total Twist Results - About Ideal COG .....	142
Figure 5.42: 797 Direction Plot - About Ideal COG .....	142
Figure 5.43: 797 Pitch Results - About Ideal COG .....	143
Figure 5.44: 797 Roll Results - About Ideal COG .....	143
Figure 5.45: 797 Rack Results - About Ideal COG .....	144
Figure 5.46: 797 Results - Basic Haul Road Analysis .....	145
Figure 5.47: 797 Vehicle Ground Speed vs g Level .....	145
Figure 5.48: 797 Vehicle Acceleration vs g Level .....	146
Figure 5.49: 797 Moment About Ideal COG - 60s Sample .....	147
Figure 5.50: Absolute Value Slope of Moment About Ideal COG (60s Sample) .....	148
Figure 6.1: Roll Comparison, Loaded Sample .....	151
Figure 6.2: Pitch Comparison, Selected Sample .....	151
Figure 6.3: Roll Cross Plot .....	151
Figure 6.4: Pitch Cross Plot .....	152
Figure 6.5: Total Twist vs. Rack Comparison, Selected Sample .....	152
Figure 6.6: Total Twist vs. Rack Cross Plot .....	152
Figure 6.7: Q2 Rack vs. Rack Cross Plot.....	153
Figure 6.8:(Left) 2003 Resultant Construction, (Right) Q1 Rack Projection .....	153
Figure 6.9: gLA Q2 Rack vs. 2003 Constructed Q2 Rack .....	154
Figure 6.10: 2003 Articulated Pitch .....	155
Figure 6.11: 2003 Articulated Roll .....	155
Figure 6.12: 2003 Articulated Rack.....	155
Figure 6.13: Articulated Roll Cross Plot, 100% Loading .....	156
Figure 6.14: Articulated Pitch Cross Plot, 70% Loading Sample .....	156
Figure 6.15: 2003 Articulated Constructed Q1 Rack.....	157

Figure 6.16: Articulated Q1 Rack Cross Plot, 100% Loading .....	157
Figure 6.17: Articulated Direction Plot, All Loadings .....	158
Figure 6.18: Articulated Unit i Cross Plot .....	158
Figure 6.19: Articulated Unit j Cross Plot .....	158
Figure 6.20: Articulated Unit i vs. Unit j Cross Plot .....	159
Figure 6.21: Articulated Unit j vs. Unit i Cross Plot .....	159
Figure 7.1: 1g Roll Event .....	163
Figure 7.2: 2g Roll Event .....	164

## Definitions, Abbreviations and Symbols

### Definitions

The following list of definitions covers terms defined specifically in this document. Where appropriate the corresponding symbol for the term is also provided.

Natural or Tare Hub Force		One of the four loading components defined in this paper. The natural tare or curb weight of the vehicle is defined as the stationary unloaded operational weight of the vehicle. Additionally; the hub forces under tare conditions are defined as the specific forces at each wheel under zero articulation tare conditions and evaluated on even ground
Payload Hub Force		The incremental increase over tare weight as payload is applied and the vehicle is in the non articulated position such that the articulation angle of the vehicle is zero.
Articulation Force		The incremental change in force at each hub as a result of a change in vehicle articulation. Defined as zero for rigid bodied equipment.
Force Due to Motion		The force generated at the hub as the vehicle moves over uneven terrain or experiences linear or centrifugal acceleration due to changes in velocity or direction respectively.
Cumulative Hub Force		The instantaneous net effect of tare, payload, articulation and force due to motion at each hub.
Mid-ship		The point on an articulated piece of equipment where the front and rear frame components are physically pinned together. This is also the point of articulation.
Theta	$\Theta$	Natural front frame angle in degrees.
Beta	$\beta$	Natural Rear Frame angle in degrees.
Phi	$\phi$	Articulation angle in degrees defined as the deviation of the axis OY' from the initial position parallel to the axis OY. See Figure 2.3
Instantaneous Cumulative Moment	$\vec{M}_{oT}$	The resultant moment about the reference point created by the instantaneous moment at each hub.
Equivalent Force	$\vec{F}_{EQ}$	The force which replicates $\vec{M}_{oT}$ .
Instantaneous Vehicle Mass	$m_i$	The instantaneous mass of the vehicle and payload not including the effects of motion.
Pitch		The degree of rotation about the vehicles lateral axis originating at the reference point. See Section 3.2.
Roll		The degree of rotation about the vehicles longitudinal axis originating at the reference point. See Section 3.2.
Rack		the degree of rotation about an axis which runs through the reference point O in the XY plane and at a 45° angle from the X and Y axes. Has sub components Q1 and Q2

		Rack. See Section 3.2
Twist		The degree of total rotation about any axis. See Section 3.2
Underground Articulating Haul Truck	UAHT	Any underground hauler which articulates when steering.
Payload Scaling Factor	<i>PSF</i>	Scaling factor relating the payload of a full scale hauler to the required scale model payload.

## Abbreviations

The following list of abbreviations is used throughout the remainder of this paper.

gLA	Generalized g level based equipment analysis method
$F_{Hubj}$	Cumulative hub force at the jth hub of the vehicle.
$F_T$	Instantaneous total force exerted by the vehicle on the ground.
$n$	The number of hubs on the vehicle.
$\vec{F}_A$	Cumulative hub force at hub A
$\vec{F}_B$	Cumulative hub force at hub B
$\vec{F}_C$	Cumulative hub force at hub C
$\vec{F}_D$	Cumulative hub force at hub D
$\vec{A}$	Position vector describing the line from O to A
$\vec{B}$	Position vector describing the line from O to B
$\vec{C}$	Position vector describing the line from O to C
$\vec{D}$	Position vector describing the line from O to D
$\vec{M}_{o_T}$	Total Resultant Moment about the reference point O
$\vec{U}_{M_o}$	Vector describing the axis about which $\vec{M}_{o_T}$ rotates. Normalized to fall on a unit sphere.
$\vec{F}_{EQ}$	Equivalent Force.
$\vec{U}_\perp$	A vector perpendicular to $\vec{M}_{o_T}$ .
$P$	The coordinates of a point on the unit sphere orthogonal to $\vec{U}_{M_o}$ . Determined by normalizing $\vec{U}_\perp$ . $\vec{F}_{EQ}$ is applied tangent to this point.
$\ell$	A line which runs tangent to point $P$ .
kg	Kilogram
g	Gravitational Constant (9.81m/s <sup>2</sup> )
N	Newton

## Symbols

The symbols in the following list are used throughout this paper.

A	Location of the front right wheel hub
B	Location of front left wheel hub
C	Location of the rear left wheel hub
D	Location of the rear right wheel hub
O	Reference point
$\Theta$	Natural front frame angle in degrees
$\beta$	Natural rear frame angel in degrees
$\Phi$	Articulation angle in degrees defined as the deviation of the axis OY' from the initial position parallel to the axis OY
$r$	Radius of an arbitrary unit circle.

# 1 Introduction

## 1.1 Motivation

Modern construction and mining equipment is expected to operate continuously at high levels of efficiency with low maintenance costs and little downtime. Factors which affect the ability of the equipment to meet these expectations are diverse and complex. Environmental factors can include the prevalent weather conditions and the geotechnical parameters of the operation's location. Operational factors such as employee skill level and site specific practices and procedures impact equipment and component life as organizations operate equipment differently. Even if environmental and operational factors could be considered essentially equivalent, business conditions and management preferences could result in very different fleets in terms of models and size being employed between operations.

The immense variation in which mining and construction equipment operates leads to a scenario where equipment evaluation and monitoring between operations is very difficult. Conventionally time based metrics have been used for equipment evaluation. The mining and construction industries are very comfortable with time and motion studies and reliability metrics such as mean time between failures. Time based approaches to equipment evaluation are limited in ability to compare an operation's performance against another, as well as against other equipment types both internally and externally as time based metrics often miss the impact the operators decisions have on the equipment and operating surface. Time is also limited in the information it can convey. For example knowing the cycle time of a shovel loading trucks can allow the observer to calculate how many trucks per hour can be expected from the shovel operator but it provides no information as to how precise the operator is in his load placement, which can have a large negative effect on the overall cost to run the equipment. This research demonstrates the mechanics and values which a generalized g level based analysis model can add to equipment evaluation. Time based approaches to equipment monitoring can help to build confidence in how long components will last or when components will fail. However, the g Level Analysis (gLA) method captures information about the physical interaction between the equipment and its operating surface. This reaction is inherently highly influenced by operator input and as a result gLA can provide insight into operator performance as well. The ability to collect information regarding the equipments interaction with its environment, operator and its own dynamic weight allows the observer to understand why components fail rather than only when they will fail. Combining the observation of how the equipment interacts with its environment with sufficient domain expertise can assist in

directing changes in an attempt to improve equipment performance. Once these changes have been implemented, for example to haul road maintenance or load placement practices, the effect of these changes can be evaluated using gLA. Figure 1.1 shows how an equipment improvement practitioner can view the g level based analysis as part of a standard scientific observational model.

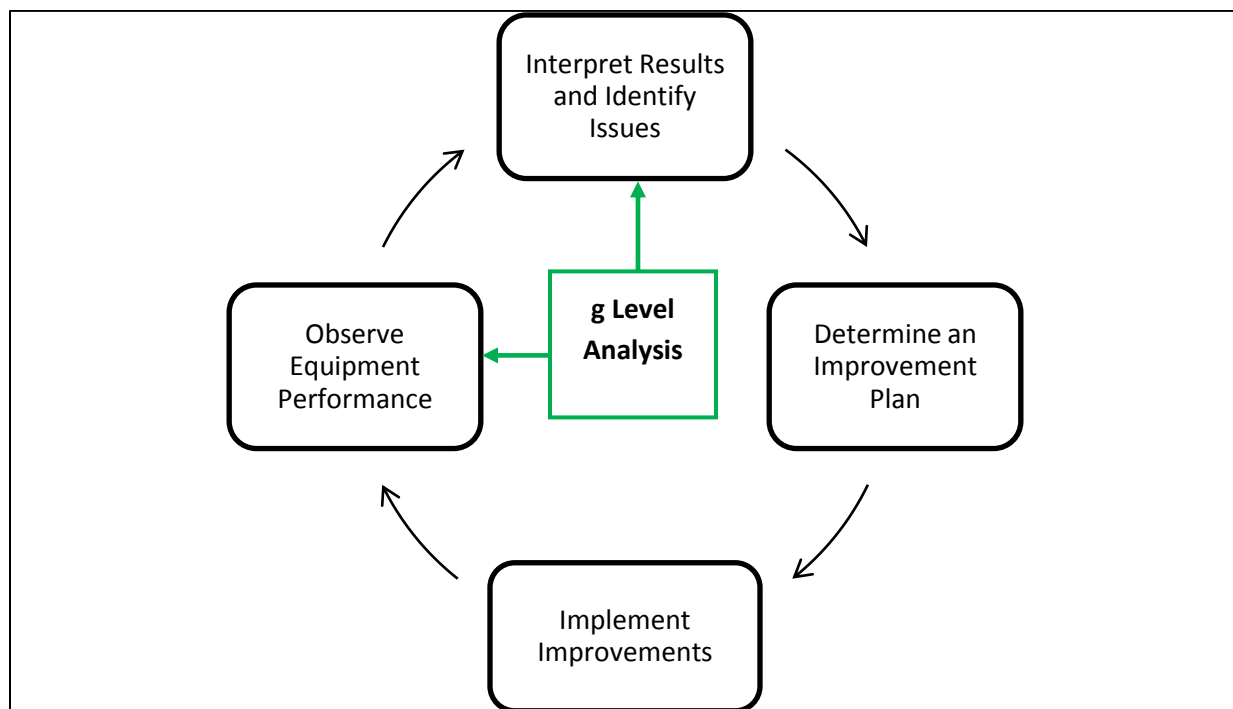


Figure 1.1: g Level Analysis in a Simplified Scientific Method

## 1.2 Thesis Statement and Purpose

Time based equipment evaluation models are limited in the type of information they can convey. A common alternative to time based evaluation is mechanical modeling, however; these models can be complex and require an advanced understanding of mechanics to construct. The purpose of this research is to provide the framework for a simple vehicle performance indicator which is capable of providing meaningful insight into the physical interaction between the equipment and its operating environment. The value of this indicator is in its versatility, and simplicity which allows it to be implemented by a wide range of researchers and operators who have an understanding of the basic principles of mechanics.

### 1.3 Approach

This study was carried out in four phases: a literature review, the mathematical formulation of the proposed gLA method, a scale model application of the derived mathematical models which focuses on articulated equipment, and finally the approach is applied to real field data from a typical ultra class haul truck operating in Alberta's oil sands.

The formulation of the method uses a summation of moments approach to derive the mathematical and geometrical relationships necessary to understand the frame twisting interactions between machine, load and ground under various operating conditions. The general case of an underground articulated haul truck is used to derive the method which can then be simplified for application to rigid framed equipment. Following this mathematical investigation, a scale model of a typical articulated underground haul truck was constructed to provide a platform to demonstrate the application of the mathematical model. Data from the scale model was recorded as articulation, payload, and inclination, and was varied through positions and quantities typically found in an operating environment. This test data was then processed through the gLA model and the results interpreted and discussed in Chapter 5.

It was decided to utilize a scale model study for this investigation after considering the potential challenges associated with attempting to study full scale equipment which are active in an operating profit driven environment. Operations are understandably, not easily persuaded to release revenue generating assets to academic study and as a result research time is not easily obtained. Other problems which can arise from attempts at working with full scale operating equipment are from the unpredictable nature of breakdowns and availability as well as the dynamic nature of production requirements which leave the researcher with many repeatability problems [1]. Another major driver in the decision to use a scale model of a haul truck was the difficulty in securing time with underground articulated suspension-less equipment in Alberta.

### 1.4 Literature Review

Although there is limited work done directly in the field of dimensionless equipment KPI's there is much written which is related to this original research in either application or alternative techniques. The following literature review has been designed to highlight areas within which the following original research is expected to be of use. Because the research which follows provides a tool useful for examining the connection between the performance of: the operator, equipment and operating surface the majority of the literature reviewed focuses specifically on haul roads, operator well being and education, and equipment monitoring. A section on rigid body dynamics based modeling provides the



reader with a background to the most common alternative technique and the challenges associated with modeling an operating haul truck.

#### 1.4.1 g Level Based Analysis

The concept of the moment in classical mechanics refers to the product of a force's magnitude and its perpendicular distance from the point the force is applied to the point or axis about which the force will generate a rotational tendency [2]. The concept of the moment is central to the study of statics and dynamics and is generally introduced in first year engineering classes. As it applies to this body of work the moment and its vector properties have been used to determine the cumulative effect of the machine ground interactions at each hub of a mobile haulage unit.

The natural unit of the moment is force-distance such as Newton Meters (Nm) or pound feet (lbft) and while these units do provide a somewhat intuitive sense of rotation they are not as useful for describing the cumulative effects on an object, such as a haul truck, which is not generally thought to be in rotation. Joseph, 2003 used the notion of g level to describe adverse hauler and cable shovel motions specifically because the g level unit was thought to be more accessible to a broader range of industry [3]. This paper by Joseph is considered the definitive work to date on g level based equipment evaluation. The method presented by Joseph in this paper uses varying levels of acceleration to explain varying strut pressures in large haul trucks even when the instantaneous mass of the vehicle remains constant. It is also in this paper that Joseph defines a rack event larger than 1.5g to be detrimental to the frames and super structures of large mining haul trucks and shovels.

The 2003 approach to g Level analysis developed by Joseph (2003) has proven to be a useful equipment evaluation tool. However; to date the method has only been applied to equipment with fixed geometry such as rigid body haul trucks and track mounted loading tools. Figure 1.2 shows a simple schematic of a rigid body haul truck where the indexes 1,2,3 and 4 denote the struts at the front left, rear left duals, rear right duals and front right wheel sets respectively. This figure and notation system corresponds to the subscript notation used by Joseph to define rack, pitch and roll in terms of dimensionless g-units as in Equation 1.1 through Equation 1.3 Where  $a_1$ ,  $a_2$ ,  $a_3$  and  $a_4$  are the incremental accelerations of the sprung mass calculated at the left front, right front, left rear and right rear struts respectively and  $g$  represents the gravitational constant.

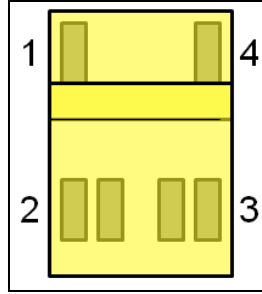


Figure 1.2: Haul Truck Schematic (After Joseph, 2003)

$$Rack = \frac{1}{g}[(a_1 + a_4) - (a_2 + a_3)]$$

Equation 1.1 (After Joseph, 2003)

$$Pitch = \frac{1}{g}[(a_1 + a_2) - (a_3 + a_4)]$$

Equation 1.2 (After Joseph 2003)

$$Roll = \frac{1}{g}[(a_1 + a_3) - (a_2 + a_4)]$$

Equation 1.3 (After Joseph, 2003)

Built into Joseph's method is an assumption of symmetry regarding the strut locations relative to one another. Analysis of Equation 1.1, 1.2 and 1.3 shows that pitch can be interpreted as the difference in balance between the front and rear axles while roll is interpreted as the difference in balance between the left and right; while rack represents the difference in balance along lines running between opposite corners. From the simple schematics of rigid frame equipment shown in Figure 1.3, it is intuitive that pitch is a measure of the vehicles response front to back while roll is a measure of response left to right and rack is a measure of the twisting response of the vehicle.

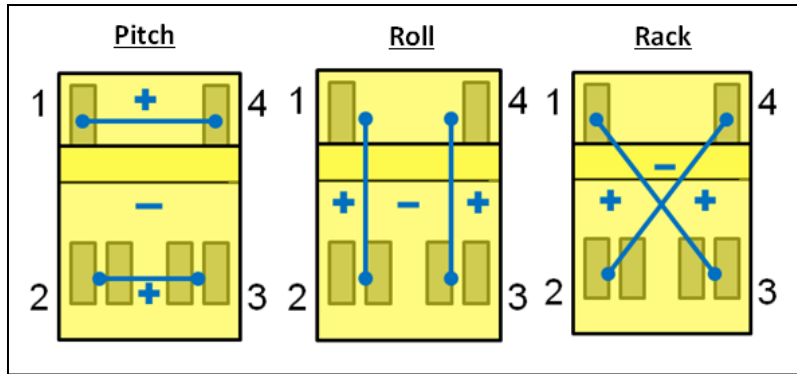


Figure 1.3: Rack, Pitch and Roll Visualization (After Joseph, 2003)

While Joseph's method has been demonstrated to provide a useful analysis of equipment behavior it is not clear how the method handles the geometry of the vehicle and direction of the resultant response accurately. When applying the 2003 method to an articulated vehicle in the zero articulation position, as represented by Figure 1.4, the same logic and interpretation of rack, pitch and roll are applicable. However; if the method is applied to an articulated vehicle, as represented in Figure 1.4, it is less obvious if the original rack, pitch, and roll calculations are still representative of the vehicles response. As Figure 1.5 shows, the inherent symmetry associated with rack, pitch and roll calculations for a rigid frame hauler is lost when considering an articulated hauler vehicle.

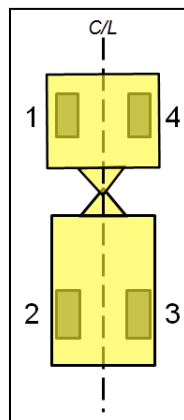


Figure 1.4: Articulated Hauler Schematic

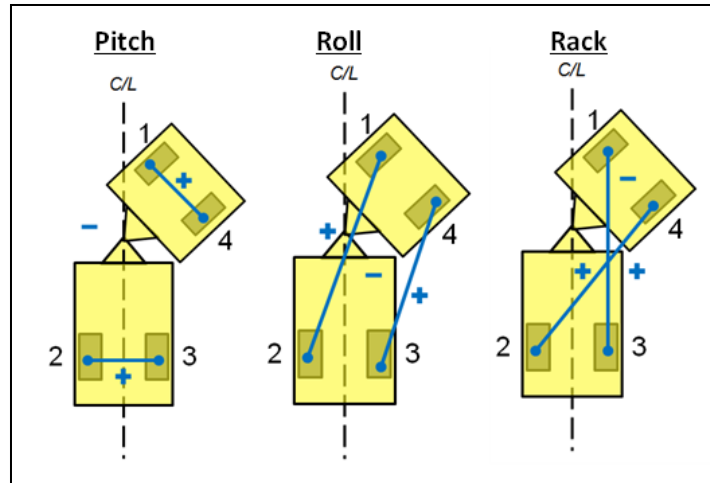


Figure 1.5: Pitch, Rack, Roll Asymmetry Visualization

To begin demonstrating the importance of the location of a strut force; first consider a simple beam as shown in Figure 1.6. If, for example,  $F_1$  and  $F_2$  represent the net summation of forces across the front and rear axles respectively this beam represents the vehicle pitch response described by the g Level method proposed by Joseph. A simple statics analysis shows that the reaction at the fixed point A would be equal to  $-2F_1$  in the vertical direction and zero moment about point A, implying also that the vehicle is enduring zero pitch. If the location of the fixed point is moved as shown in Figure 1.7 the same statics analysis reveals that the reaction at the fixed point is still  $-2F_1$  in the vertical direction, however the moment at A is now equal to  $(-LF_1)/3$  and so it is apparent that the geometry of the applied forces is important. What is not apparent is if the vehicle should be considered to be enduring a pitch response.

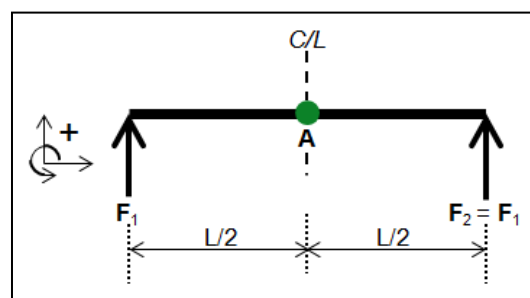


Figure 1.6: Balanced Simple Beam

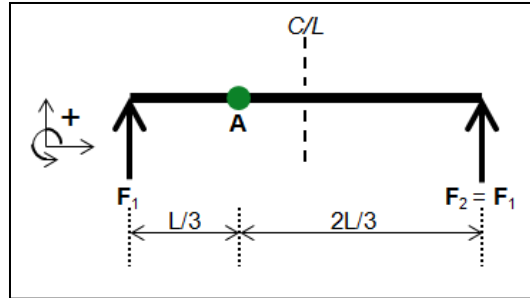


Figure 1.7: Unbalanced Simple Beam

To extend the previous example to a more realistic vehicle scenario, consider the simple articulated vehicle as shown in Figure 1.8 and 1.9 in the non-articulated and an arbitrary position of articulation respectively. If each of the strut forces at 1, 2, 3 and 4 in both figures are equal to  $F_1$  in the vertical direction out of the page, then using the original 2003 method both vehicles would show rack, pitch and roll all equal to zero.

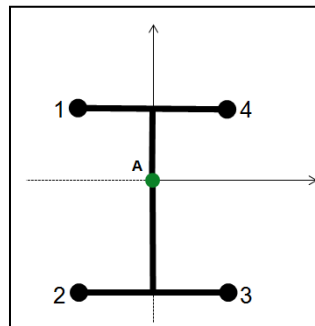


Figure 1.8: Simplified Articulated Vehicle, Articulation Equal to Zero

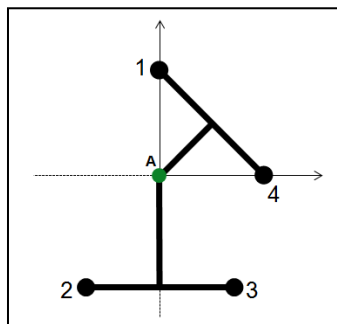


Figure 1.9: Simplified Articulated Vehicle, Articulation Not Equal to Zero

This shows the importance of geometric scaling as it is not logical to interpret the vehicles in Figure 1.8 and 1.9 as being equally in balance about the fixed point A. A primary goal of gLA is to address this issue.

### 1.4.2 Vehicle Modeling

Vehicle modeling and simulation is in itself an entire field of research and application. Multi-body simulation is often used to study dynamic vehicle behavior and there is a wide range of literature available. Wheeled vehicles inherently share some degree of similarity and so while much of this literature is not directly related to heavy mining equipment, the results and principals derived can still be useful.

It is important to note that the intent of the research contained in this study is not to directly model vehicle motion but rather to provide an analysis method which can be used as a performance indicator either by itself or in conjunction with efforts such as simulation. Texts such as “*Vehicle Dynamics*” and “*Ground Vehicle Dynamics*” provide instruction in both fundamental and advanced topics related to the description and modeling of vehicles in general [4, 5].

Mobile equipment interacts directly with the ground upon which it operates via tire-terrain interactions. In off road operations these tire-terrain interactions dominate vehicle performance [6] and it is therefore essential that appropriate tire models exist in order to accurately model the ground influence in more comprehensive off road vehicle models. For example, recent work by Senatore and Sandu, 2011 has generated an off road tire model which predicts the traction, torque, sinkage and the multi-pass compaction effect [6]. The choice of tire model depends on many factors including: physical terrain properties, required accuracy, required outputs and computational and laboratory requirements. Due to the large variation in each of these parameters there are many tire models spread across several analysis methods, fortunately Taheri et al (2014) conducted a thorough survey of the terramechanics models used in the modeling and simulation of wheeled vehicles which is designed to assist readers in selecting an appropriate model for their particular application [7].

In many cases whole vehicle models are generated with various levels of complexity to investigate specific problems. Figure 1.10 shows the basic diagram associated with a dynamic model of a vehicle capable of forward, lateral yaw and roll motions [4]. This model is referred to as a four Degree of Freedom (DOF) model meaning that that the motion of such a model is described completely by four variables, leading to four equations.

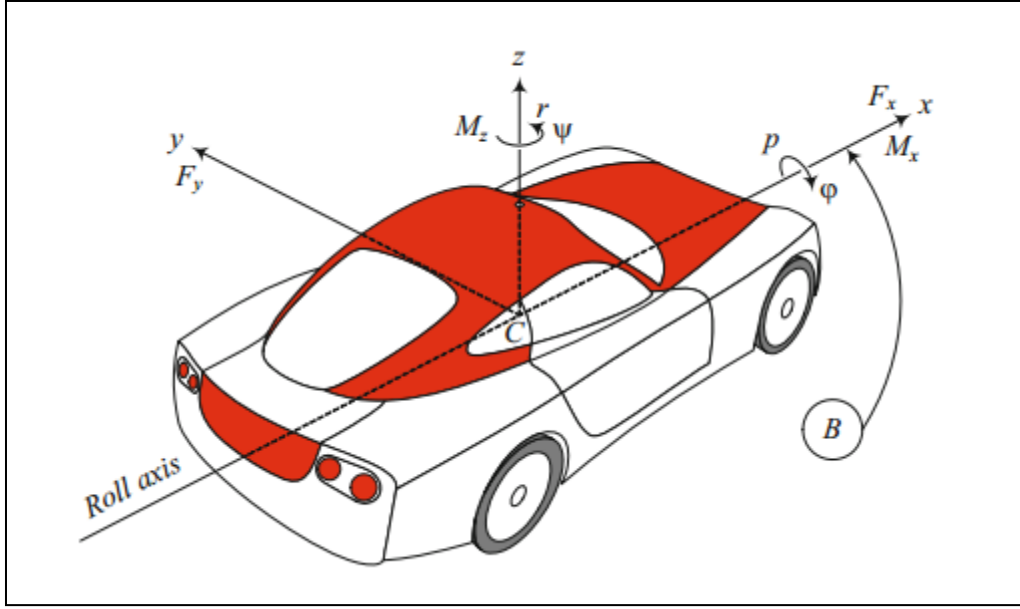


Figure 1.10: Roll Model of a Rigid Vehicle (after Jazar,2014)

Equation 1.4 to Equation 1.7 below presents the four Newton-Euler equations of motion as derived in Jazar, 2014. Note that the four equations describe the motion in the x and y directions and the moments about the z and x axes. As this model was derived to describe a rigid body with roll freedom the force in the z direction and moment about the y axis (pitch) motions are defined as constraints specifically to prevent pitch.

$$F_x = m\dot{v}_x - mr\dot{v}_y$$

Equation 1.4 (Jazar, 2014)

$$F_y = m\dot{v}_y - mr\dot{v}_x$$

Equation 1.5 (Jazar, 2014)

$$M_z = I_z\dot{\omega}_z$$

Equation 1.6 (Jazar, 2014)

$$M_{xz} = I_x\dot{\omega}_x$$

Equation 1.7 (Jazar, 2014)

The pitch limitation in the above four DOF model may be acceptable if the vehicle is operating on a perfectly smooth and level surface however; given that mining equipment frequently operates on substantial degrees of slope and over uneven terrain the pitch component is considered important. The addition of a pitch degree of freedom to the model of a rigid body results in a vehicle which moves

completely in three dimensional space. The model of a vehicle or generally a rigid body which moves in space is also derived by Jazar (2014). The Newton equations of a six DOF model are presented in Equation 1.8 and the corresponding Euler equations are presented in Equation 1.9. Note that the allowance of the vehicle to move in a pitch motion results in a model with six DOF.

$$\begin{bmatrix} F_x \\ F_y \\ F_z \end{bmatrix} = m \begin{bmatrix} \dot{v}_x + \omega_y v_z - \omega_z v_y \\ \dot{v}_y + \omega_z v_x - \omega_x v_z \\ \dot{v}_z + \omega_x v_y - \omega_y v_x \end{bmatrix}$$

Equation 1.8 (Jazar, 2014)

$$\begin{bmatrix} M_x \\ M_y \\ M_z \end{bmatrix} = \begin{bmatrix} \dot{\omega}_x I_1 - \omega_y \omega_z I_2 + \omega_y \omega_z I_3 \\ \dot{\omega}_y I_2 + \omega_x \omega_z I_1 - \omega_x \omega_z I_3 \\ \dot{\omega}_z I_3 - \omega_x \omega_y I_1 + \omega_x \omega_y I_2 \end{bmatrix}$$

Equation 1.9 (Jazar, 2014)

Jazar, (2014) derives the Newton-Euler equations in both the four and six DOF models mentioned above around the concept of modeling a vehicle, however the general equations of motion described by Equation 1.7, Equation 1.8 and Equation 1.9 are actually the equations of motion for any rigid body. A substantial deficit of these models when applied to any typical vehicle is that they do not include the dampening effects of either tires or suspension components. Ghike and Shim, (2006) have generated a fourteen DOF model which models a basic 2 axle vehicle allowing for the six DOF of the vehicles center of mass as well as vertical suspension travel and wheel spin at each tire location [8]. Figure 1.11 below shows the schematic presented by Ghike and Shim (2006).

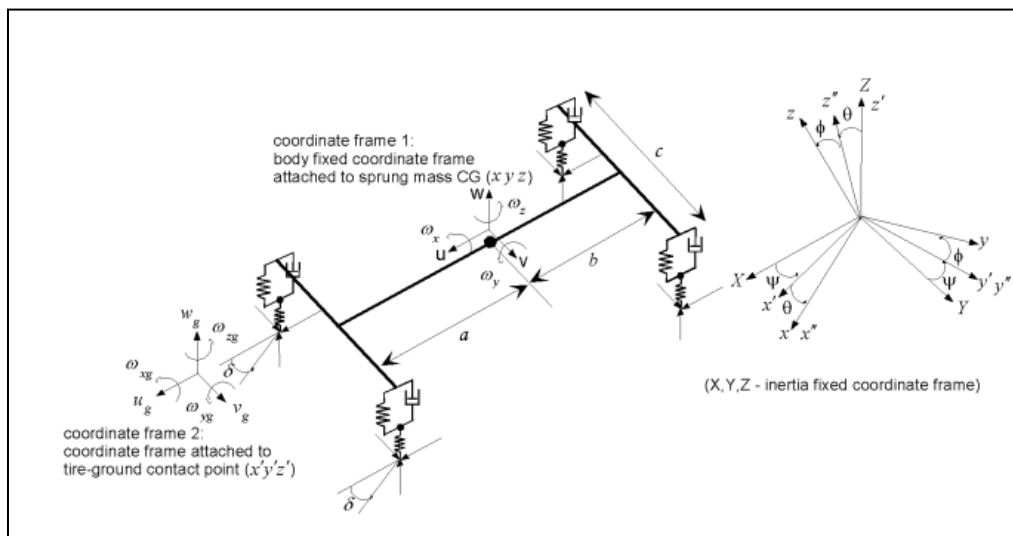


Figure 1.11: 14 DOF Full Vehicle Model (Ghike and Shim, 2006)



This model was derived specifically for automated roll over prevention systems in the automobile industry. Details of the model Ghike and Shim developed are left to the reader to investigate. As in the case of Ghike and Shim, vehicle models are often derived for specific purposes, even relatively simple vehicle models are not trivial. For example the U.S. Army Research Laboratory used a 26 DOF model to investigate chassis performance with predictive vehicle control algorithms [9]. In contrast to the model used in Brown et al, Laghari (2011) used an 8 DOF model to investigate the effect of tire and suspension non-linearity [10].

Due to the prevalence in both on and off road environments, there is substantially more modeling research directed towards rigid framed vehicles than articulated frame or Articulated Steer Vehicle (ASV). Within this research the terms Articulated Frame, or simply Articulated, refers specifically to an ASV where the main vehicle frame is comprised of two parts connected by a hinge[11, 12] as opposed to the work concerning articulated heavy vehicles in the sense of traditional highway based tractor trailer units [13-16]. A typical ASV dump truck is shown in Figure 1.12 and Figure 1.13 Below.

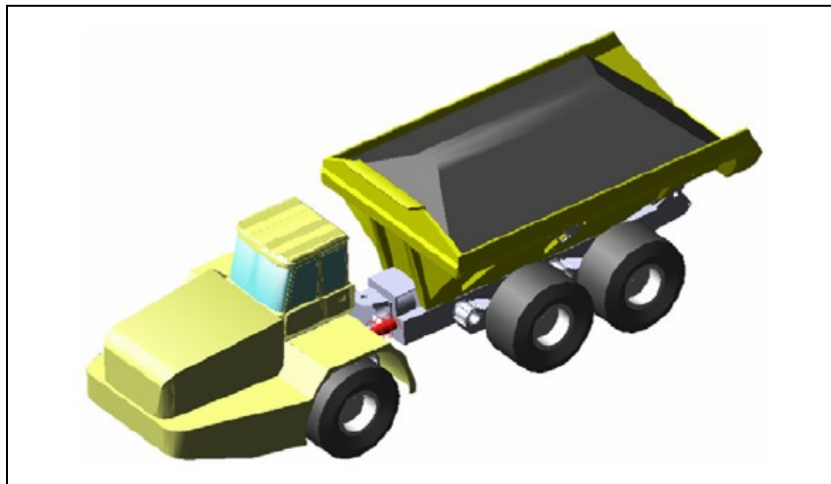


Figure 1.12: Typical Articulated Frame Steer Dump Truck (After Huang, Shen, Zang, 2010)

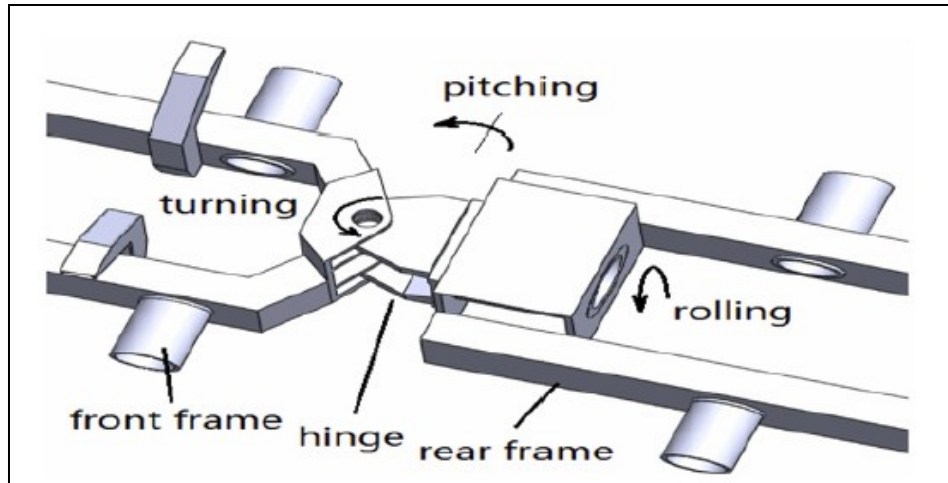


Figure 1.13: Basic Frame Arrangement of Typical ASV (After Huang, Shen, Zang, 2010)

In the area of ASV, Pazooki (2012), constructed a complete vehicle model of an ASV truck, including the hydraulic steering mechanism at the articulation joint, for investigation of vehicle stability and ride dynamics for both the suspended and unsuspended case[17]. Additional complete ASV models have been created by Li et al (2013), Yavin (2005), Langer et al (2013) and [18]. While Li et al (2013) and Yavin (2005) both modeled articulated loaders, their work is still relevant to the motion of all ASV[19, 20]. Pazooki et al (2011) and Langer et al (2013) both compared the chassis motion of unsuspended vehicles to those with a suspension mechanism. Although Pazooki et al (2011) modeled a vehicle with rear torsio-elastic suspension while the vehicle modeled by Langer et al (2013) incorporated a front hydraulic suspension, both were able to show that the suspended models tend to generate substantially less chassis accelerations than their unsuspended counterpart[21, 22]. As ASV are typically unsuspended and are known to subject the operator to higher levels of WBV it is increasingly likely that ASV will incorporate some form of suspension.

While formal modeling of haulage vehicles is possible and has very practical purposes the strength of the gLA presented in this study is in its ability to use very few inputs (strut pressures, geometry and load) to provide a substantial amount of insight into the performance of not only the actual vehicle but the haul road and operator. The generalized nature of this gLA also allows for comparison across vehicle designs which would otherwise require separate mathematical models.

The whole vehicle models discussed above are presented to provide the reader with an overview of models with varying complexity, however, when studying the effect of ground conditions on vehicle performance the quarter-vehicle model is often used. A typical quarter-vehicle model is shown in Figure

1.14 and Table 1.1 below. This model is modified from Pakowski and Cao (2013) who used a quarter vehicle model to derive equivalent soil stiffness values for several different soil types [23]. This model is presented here to show that all ground profiles and properties, such as deformability impact vehicle response as it travels over real world terrain. Vehicle models, such as Ghike and Shimm (2006) and Pazooki (2012) often simplify their models by either combining the soil and tire reactions or neglecting the ground deformation which has been shown to be non negligible within mining environments such as Alberta’s oil sands [8, 17, 24]. While modeling has proven very valuable these common simplifications show that even comprehensive modeling is a simplification of real world conditions. Due to this inherent simplification and the substantial effort required to generate reliable, comprehensive models there is an obvious value in methods such as gLA which are capable of using real world field data to investigate the combined effect of equipment-ground interactions.

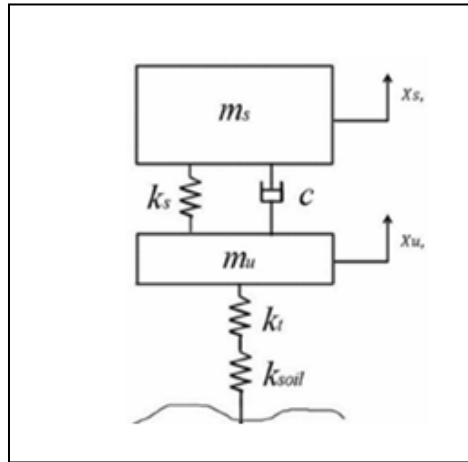


Figure 1.14: Quarter Vehicle Model (After Pakowski and Cao, 2013)

Parameter	Symbol
Sprung Mass (kg)	$m_s$
Unsprung Mass (kg)	$m_u$
Suspension Stiffness Coefficient ( $\text{kNm}^{-1}$ )	$k_s$
Tire Stiffness Coefficient ( $\text{kNm}^{-1}$ )	$k_t$
Soil Stiffness Coefficient ( $\text{kNm}^{-1}$ )	$k_{soil}$
Suspension Damping Coefficient ( $\text{kNsm}^{-1}$ )	$c$
Sprung Mass Displacement (m)	$x_s$
Unsprung Mass Displacement (m)	$x_u$

Table 1.1: Quarter Vehicle Model Parameters (After Pakowski and Cao, 2013)

The quarter vehicle model derives its name from the assumption that the sprung mass in the model is equal to one quarter of the sprung mass of the overall vehicle. Note that at each corner of the model in

Figure 1.11 a quarter-vehicle model is used to describe the interaction between the vehicle and the ground.

### 1.4.3 Haul Roads and Haul Road Maintenance

The haul road is the primary component of the transportation network used by any mining or earthworks operation that has chosen mobile haulage as the primary method of moving earth. Although underground haulage-ways serve the same function as their surface counterparts they differ primarily in the degree of construction associated with each. Surface haul roads are now highly engineered travel-ways designed to withstand the impact and degradation expected from continuous travel of haul trucks with up to 400t payloads. Conversely, while design is still very important in underground haulage-ways, the fact that the haulage-way is excavated directly from either waste or ore and typically in stronger substrates and carrying lighter loads leads to less necessity for extreme design work. Given these differences there is still a similarity to both surface and underground haul roads in that they are the only point of direct interaction between the haulage equipment and the ground. This interaction has the ability to induce deterioration on both the truck and the road which ultimately leads to higher truck/road maintenance costs and lower production rates; perhaps this simple relationship is what generated the now common expression that “roads make loads”. The following discussion is intended to provide a brief overview to haul road construction and to look at two maintenance optimization techniques which rely on analysis similar to the original research which follows in this work.

#### 1.4.3.1 Surface Haul Road Construction and Geometry

In 2001 Tannant and Regensburg generated an overview of haul road construction and maintenance practices in the form of a manual intended as an aid to geotechnical engineers, mining engineers and management of mining and construction companies. One of the foundations of this manual is a 1977 document by Kaufman and Ault of the title *Design of Surface Mining Haulage* (Information Circular 8758, 2001) from the United States Department of Interior. A component of both works is a survey of 13 mines conducted as part of both the manual created by Tannant and Regensburg and Ault and Kaufman. From Tannant and Regensburg’s more recent work, a snapshot of average haul road geometry consisted of grades less than 8% with super-elevations below 4% and typical running widths of greater than 25m for trucks with greater than 200t payloads [25]. Although road design is largely influenced by the environmental and physical constraints of each mining operation, the primary goal of road design is to strike the common balance between safety and the combined effect of capital and operating costs. Also of note is that due to the inherent temporary nature of a mining operation,

surface mining haul roads have expected lives which feed into the design and maintenance process. Tannant's 2001 survey found that typical expected lives of in pit roads range between 1 and 2 years while out of pit roads could have lives ranging between 5 and 10 years. Figure 1.15 below shows a typical haul road cross section as depicted in Tannant and Regensburg's manual.

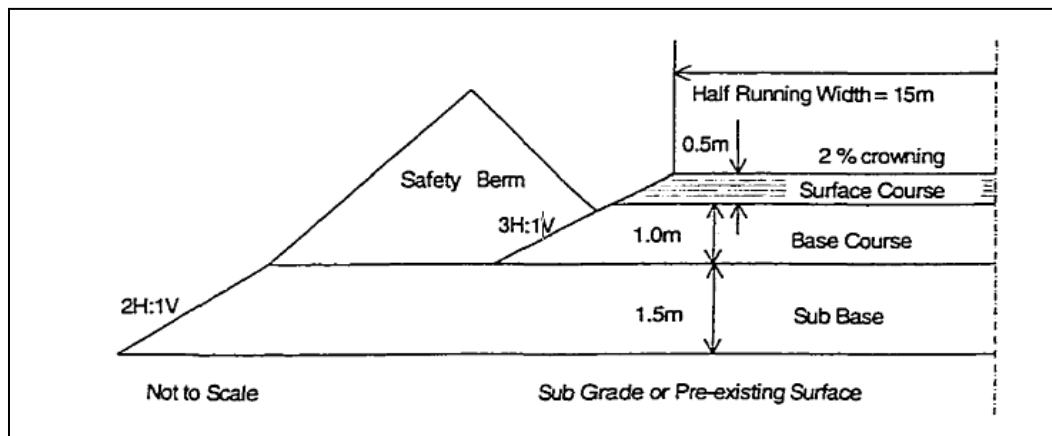


Figure 1.15: Typical Haul Road Cross Section (After Tannant and Regensburg, 2001)

It is understandable that mining operations attempt to reduce costs by constructing haul roads as much as possible from materials on hand. Because operations typically have an abundance of materials such as run of mine waste and ore processed tailings it is common that road design is dictated by the properties of these materials. The generally accepted pioneering work of haul road design was that of Ault and Kaufman (1977). Kaufmann and Ault's work relied on the California Bearing Ratio (CBR), which is used to evaluate the strength of the materials used as the base and sub base layers [26]. When following the procedure developed for haul road design using the CBR method, the thickness of each construction layer is determined from an empirically derived table and the anticipated single wheel load, of the equipment which is to be operated on a road. An example of the table included in Tannant and Regensburg's manual is included below in Figure 1.16.

The primary goal of this method is to prevent overstressing and deformation of the subgrade . However; there are problems with the CBR method which stem from its original function of evaluating sub-grade performance beneath pavement or cemented materials. Thompson (2011) compares the CBR method to a more modern mechanistic design method, discussed below, and found that the CBR

method would over design a temporary haul road with an expected life of less than 5 years by approximately 21%, and would significantly under design a road with a longer design life [27]

While the CBR method is still used and has a simplistic advantage, the method has largely been superseded by a mechanistic structural design method which uses elastic beam theory to determine the

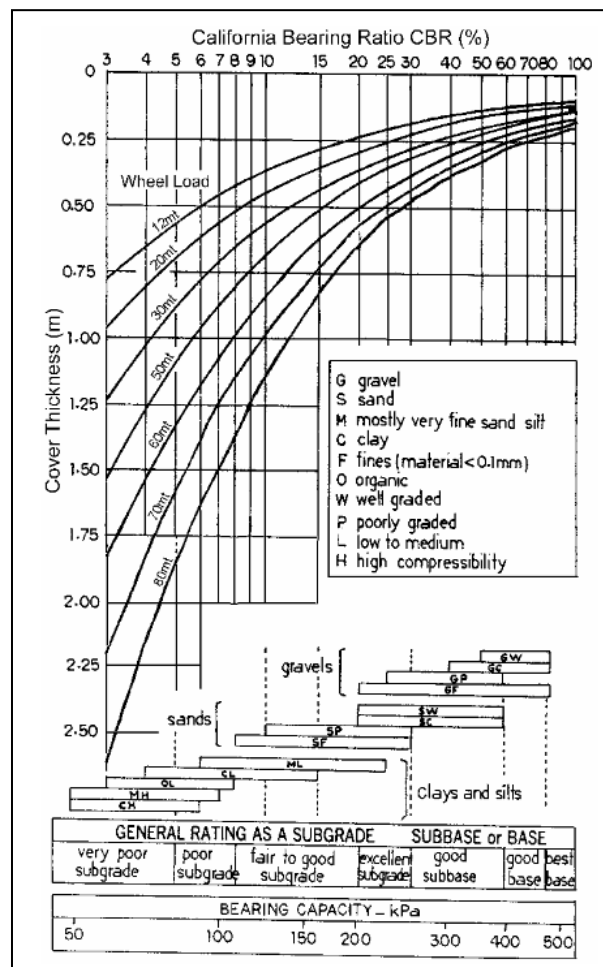


Figure 1.16: Example CBR Design Curve (After Tannant and Regensburg2001)

required thickness of each road construction layer. In this methodology the vertical compressive strain in each layer created by loaded haul trucks traveling over the surface is treated as the primary design criteria. In his original work on the subject Thompson suggests typical haul road designs should fall in the range of 1500 to 2000 micro-strain where lower allowable micro-strain would indicate a more robust road design [28]

Whereas in Ault and Kaufman's work CBR is the primary material property; Thompson's mechanistic approach relies on an estimation of the resilient modulus of the haul road construction as well as the

stress profile generated by the anticipated tire loads. While the resilient modulus can be estimated or tested directly, a stress strain model is most commonly used to estimate tire loads. Figure 1.17 below shows a flow chart of the Critical Strain Limit methodology as illustrated in Tannant and Regensburg's haul road design manual.

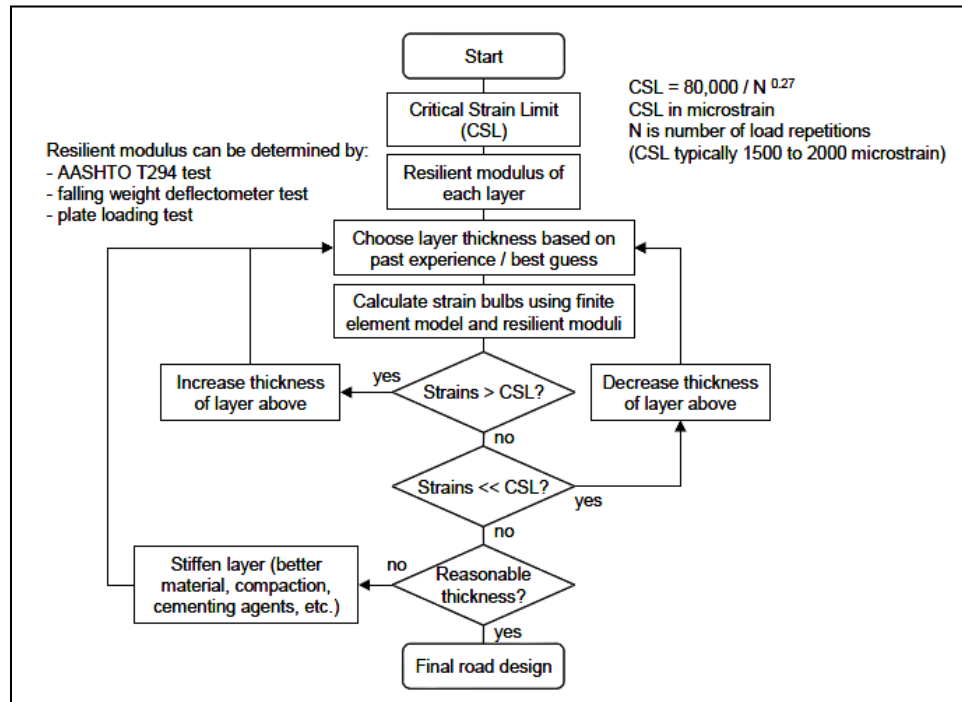


Figure 1.17: CSL Design Method (After Tannant and Regensburg 2001)

In addition to primary construction considerations the selection and maintenance of wearing course material can have a significant impact on overall operating costs, production and operator comfort. Thompson and Visser (2006) found that based on a road user assessment the defect types most detrimental to hauling operation performance included [29]:

- Wet and dry skid resistance
- Dust generation
- Loose material
- Corrugations
- Stoniness (loose and fixed)
- Potholes
- Rutting
- Cracks (slip, longitudinal, crocodile)

Reviewing the above list it can be pictured how each could impact the suspension responses of haulage vehicles as they travel over the defects.

#### 1.4.3.2 Haul Road Maintenance

Haul roads are the transportation network of a mine site and as such are travelled by all mobile equipment operating at the mine. This interaction between machine and road deteriorates the entire system (vehicle and road) through the transmission of energy from the equipment to the road way [30]. The maintenance of multiple machines in a deteriorating environment is a complex task which is complicated by the presence of uncertainty in factors that affect haul road deterioration such as environmental conditions[31-33]. A mining operation's investment in a haul road maintenance management system can result in lower mobile equipment operation costs, higher equipment availability and less impact on operator well being; the cost of road maintenance should reflect an optimum between both haul road and overall vehicle operation costs as pictured in Figure 1.18 below [34]. Thompson summarizes the motivation for haul road maintenance with his introduction to the topic in the SME Mining Engineering Handbook (2011) chapter on haul road design and maintenance:

*“Design and construction costs for the majority of haul roads represent only a small proportion of the total operating and road maintenance costs; in particular, the use of an appropriate road maintenance management strategy has the potential to generate significant cost savings, particularly in the light of increases in rolling resistance because of the interactive effects of traffic volume and wearing course deterioration”. [35]*

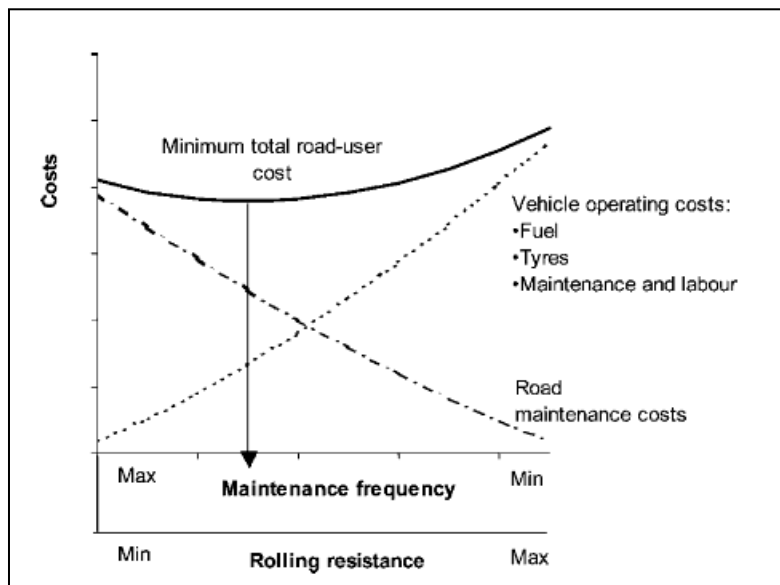


Figure 1.18: Minimum Total Cost Solution For Road Maintenance Frequency (After Thompson and Visser, 2003)



As noted in the above excerpt, the deterioration of a haul road detrimentally affects road and equipment performance as measured by rolling resistance. Rolling resistance (RR) and its effect on vehicle performance has been studied extensively in terms of classical and theoretical soil mechanics, however for the purposes of this discussion an acceptable definition of RR can be taken as the sum of the forces resisting the motion of a vehicle due to the compaction of the operating surface, the horizontal displacement of the operating surface and the flexure of the vehicle tire [36]. The resisting forces as described by Plackett (1985) are summarized in the following free body diagram.

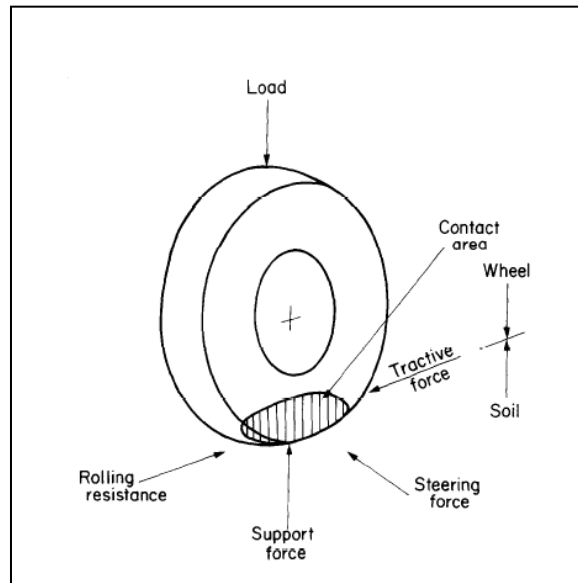


Figure 1.19: FBD of RR on Tire (After Plackett, 1985)

Referring to Figure 1.19, it is reasonably easy to picture how increases in rutting, potholes, washboarding, swales, bumps or generally any form of road roughness leads to an increased rolling resistance [29]. In the case of a vehicle operating on a soft soil, an increase in rolling resistance essentially indicates that the tire and hence the vehicle are forced to continuously climb out of a soil depression which leads to increases in fuel consumption and decreased productivity due to lower travel speeds. Undulations, potholes and washboarding do lead to higher fuel consumption and lower production rates but also create high impact events to vehicle components, [37]. It is because of this increase in rolling resistance and an inherent increase in costs, that mines spend considerable resources on road maintenance usually in the form of grading (for both smoothness and debris removal), compaction, and scarifying, watering and aggregate addition [38].

Although the maintenance methods of haul roads are rather simple there has been considerable work done which attempts to optimize haul road maintenance efforts. Key to optimizing these condition based maintenance efforts is the characterization of defects and mapping of the haul road profile which is then used with either simulation or other appropriate algorithm to identify defect types and severity. However the dynamic and complicated nature of haul road condition means modeling approaches are very challenging and direct profiling often involves specialized aftermarket equipment [30, 39-41]. Ngwangwa and Heyns, (2014), successfully profiled a haul road using vehicle mounted accelerometers and an Artificial Neural Network technique, however the accuracy of the profile was sensitive to speed vehicle speed and a lack of control over the vehicles operation[42]. Heyns, de Villiers and Heyns, (2007), used measured speed, vehicle mounted accelerometer data and target speed as inputs to a Gaussian regression analysis which generated a dynamically calibrated severity metric for road condition classification [43]. While this method yielded promising results, to the knowledge of this author, the method has yet to be tested under real world conditions.

Lee (2010) focused on improving haul road maintenance by using real time data to generate a haul road deterioration profile which feeds into a decision analysis model which optimizes maintenance timing and trigger levels by considering additional economic and production parameters [39]. Lee's work utilized an instrumentation cart to gather rolling resistance data and mentions that practical implementation of his methods requires a low cost instrumentations system. It may be that modern haul trucks are already collecting appropriate data which can be used with the method to be presented in this research to provide the road deterioration profile required for Lee's optimization routine. Figure 1.20 shows the general data flow of Lee's work in a practical implementation, while this figure is specific to Lee, 2010, it represents the general information flow for most real time haul road maintenance methods even if the metrics used to establish haul road condition change.

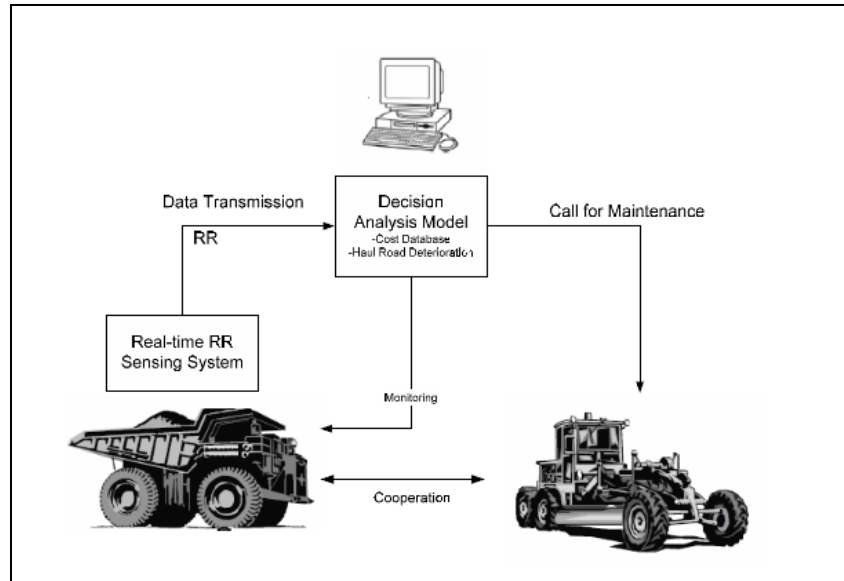


Figure 1.20: Components of Real Time RR Based Haul Road Maintenance (After Lee 2010)

All of the previously mentioned work on haul road profiling and defect identification has been attempted with the aid of additional instrumentation. However, some work has been done which uses actual strut responses from operating haul trucks to recognize road defects. Thompson, Visser, Heyns and Hugo, 2006, used the original equipment manufacturer (OEM) proprietary on board data collection systems in concert with additional accelerometer data to analyze vehicle responses in the form of strut pressure, speed and mode of operation data to determine the degree to which the vehicle racked and pitched during operation. This vehicle response data is then used to determine both the type and degree of haul road defects [44]. While this work by Thompson et al provides the advantage of modeling both the degree and type of road defects, it is admitted by the authors, a complex procedure to calibrate and characterize the haul truck geometry, spring stiffness coefficients, dampening coefficients and other characteristics such as mass and inertia used in the modeling process. Thompson and his colleagues assert that this complexity is warranted because it allows for the algorithms which these parameters feed into to computationally correct for continuously varying parameters such as load and velocity. In 2008 Hugo, Heyns, Thompson and Visser, 2008, simplified the procedure formulated in 2006 and showed that hydro pneumatic suspension pressures in association with OEM GPS data could be used to reconstruct haul road defect profiles by imposing dynamic equilibrium on a quarter vehicle model consisting of a linear spring and circular rigid tread band tire model which is depicted in Figure 1.21[45, 46]. From the tire Model in Figure 1.21 the road profile can be calculated as  $z_r$  in Equation 1.10[46].

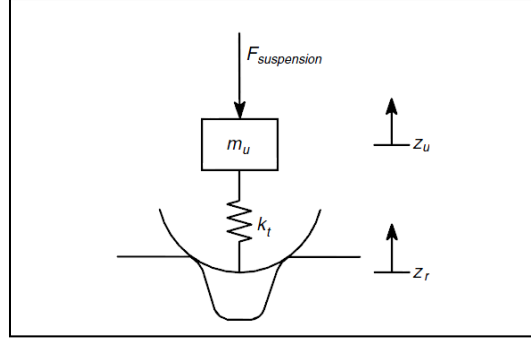


Figure 1.21: Illustration of Circular Rigid Treadband Model (After Hugo et al, 2008)

$$z_r = z_u + \frac{m_u \ddot{z}_u + F_{suspension}}{k_t}$$

Equation 1.10: Road Profile Calculation (After Hugo, Heyns, Thompson and Visser, 2008)

where:

$z_r$  = Road Elevation

$z_u$  = Vertical Displacement of Unsprung Mass

$m_u$  = Unsprung Mass

$\ddot{z}_u$  = Vertical Acceleration of Unsprung Mass

$F_{suspension}$  = Suspension Strut Force

$k_t$  = Tire Spring Constant

#### 1.4.4 Whole Body Vibration

A large part of the motivation behind the research in this study is to present a classical analysis of the interactions between machine, operator and operating surface. When considering the effect of machine and the operating surface on the welfare and productivity of the operator, the concept of Whole Body Vibration (WBV) is essential. The concept of whole body vibration is introduced here because the method of analyzing equipment performance in terms of g level about a point could possibly be extended as an alternative to current WBV monitoring standards by considering the cumulative g level about an axis reflecting the operator's spinal position or about a point representing the operators head, feet or organs.

Research has conclusively shown that operators of heavy construction equipment; including surface haul trucks and underground Load Haul Dump (LHD) units, are at high risk of overexposure to WBV [47-52]. Studies have shown that negative health effects of WBV can include a multitude of symptoms ranging from chronic fatigue to neck pain and irritability, however, the most common ailment is lower back pain (LBP) which is particularly marked in heavy equipment operators [53]. For obvious reasons it is unacceptable to have workers at risk of injury, where in response standards for acceptable dose rate and measurement practice have been developed. The most widely accepted of these standards is ISO 2631-1, *“Mechanical Vibration and Shock Evaluation of Human Exposure to Whole Body Vibration”* [54]. This standard provides a basis for analysis using frequency based root mean square, peak velocity and fourth root analysis. ISO 2631-1 acknowledges that certain methodologies under-represent the peak impacts and do suggest alternatives to account for this. WBV exhibits many of the same characteristics as radiation hazards in that duration is as important as intensity meaning that sustained lower rates of vibration are not necessarily safer to the operator than short durations of high magnitude vibration. Although there are similarities between WBV and radiation exposure, WBV is perhaps more complex to measure and monitor because the direction and the frequency of the vibration or shock are also critical in determining the negative effect on human health [55].

While no clear limits or regulations have been legislated regarding allowable WBV doses, ISO 2631-1 does provide the following Health Guidance chart, shown in Figure 1.22 for total weighted acceleration exposure. The dotted lines represent the allowable exposure for each of the calculation methods presented within the standard. Also note that the standard specifically states that extreme caution must be used when considering short durations of higher acceleration.

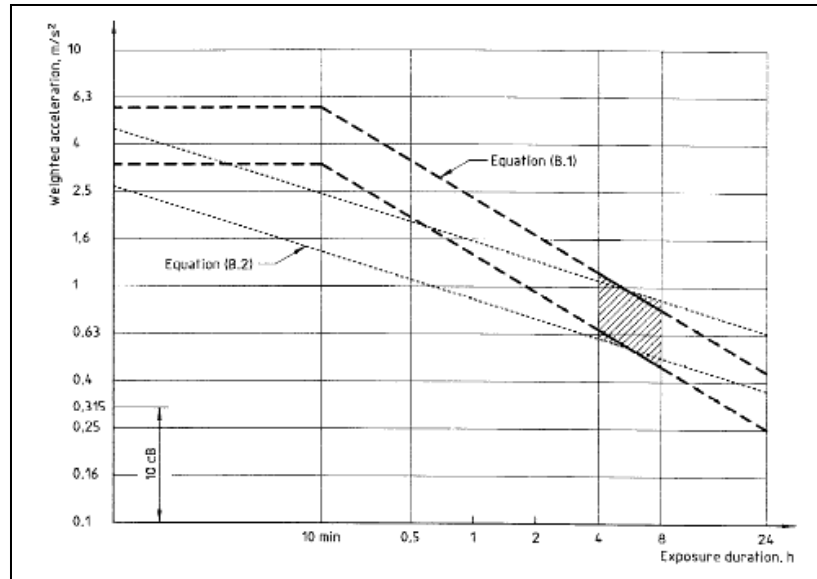


Figure 1.22: WBV Health Caution Guidance Zones (After ISO 2631-1)

Recent work has been completed which attempts to monitor the amount of vibration a heavy equipment operator is exposed to [40, 56, 57]. Specifically the work by Berezan in 2006 showed that there is a correlation between operator exposure vibration levels and equipment rack [1]. Specifically Berezan's contribution was the development of an operator warning system which informed the operator of his or her cumulative vibration exposure over the course of a shift. The goal of the project was to prove that operator exposure to WBV would be lower with the use of the device. Unfortunately it was shown that vibration exposure was actually higher with the system in place due to operator abuse of the system to gain time off. Figure 1.23 shows the operator interface designed by Berezan.

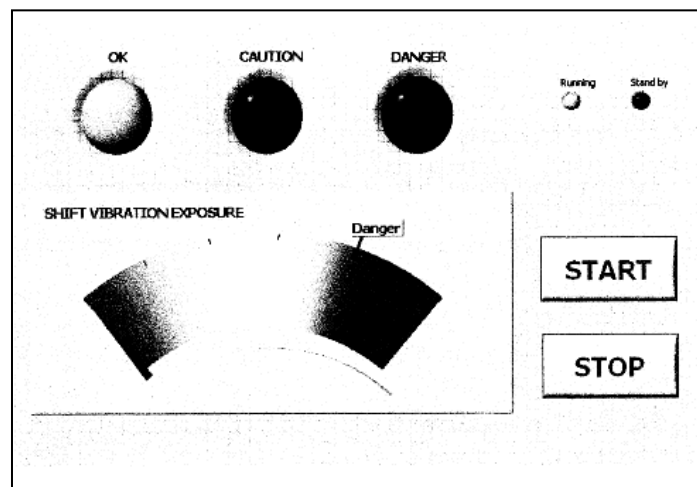


Figure 1.23: WBV Exposure Monitor Interface (Berezan, 2006)

Although Berezan was unsuccessful there is merit in the concept of continuous WBV monitoring which could be explored using the gLA presented in this research about the location of the operator. The primary advantage to using this level is that Berezan's monitoring system could be implemented without additional instrumentation.

To this point the discussion of WBV has centered largely on the root mean square calculation methods presented in ISO 2631-1 and ISO 2631-5, but work has been done which proposes more classical calculations based on acceleration versus time graphs. Much of the foundation of this theory is held in the concept of "Jerk", defined as the first derivative of acceleration with respect to time or the third derivative of position with respect to time [58]. Acceleration versus time methods are particularly appealing when considered in connection with the research in this paper as dynamic gLA could be used to generate the required acceleration versus time graph without the use of additional instrumentation.

Although the ISO 2631-1 standard is still most commonly employed, a 2009 paper by Miller of the National Institute for Occupational Safety and Health proposes a method referred to as the Jolt Duration (JD) Method [59]. The JD method describes each jolting and jarring event as approximated as a half sine wave. Miller describes jolting as any event with a peak greater than 2.0g and jarring events as any event with a peak less than or equal to 2.0g. The excerpt below from Millers work and Figure 1.24 detail Millers method of determining the duration and amplitude of each event from an acceleration versus time graph.

A final note on Miller's Jolt Duration method; Miller claims that if jolting and jarring events (as defined about 2.0g) from his data set are accounted for, the remaining WBV levels fall below the ISO 2631-1 health guidance zones. This is an interesting statement as it implies the possibility that if this correlation is formerly proven, a simpler WBV standard may be achieved.

*"In (Figure 1.24), t2 is the time when the absolute value of the acceleration first exceeds the upper threshold. For the data in this paper, the upper threshold was | 0.60 g |. The amount of time between t2 and t1 is interval2. For this particular example, interval2 was about a millisecond. When the acceleration reaches its apex, that time is marked t3 and the amount of time between t3 and t2 is interval3. Similarly, the amount of time between t4 (when the acceleration falls below the upper threshold on the way down to t5) and the apex, t3, is interval4 and so on. If various intervals are too short or too long, then the waveform may not be ruled as a jolting or jarring event. The amount of time between t5 and the next t1 is also considered." (Miller,2009)*

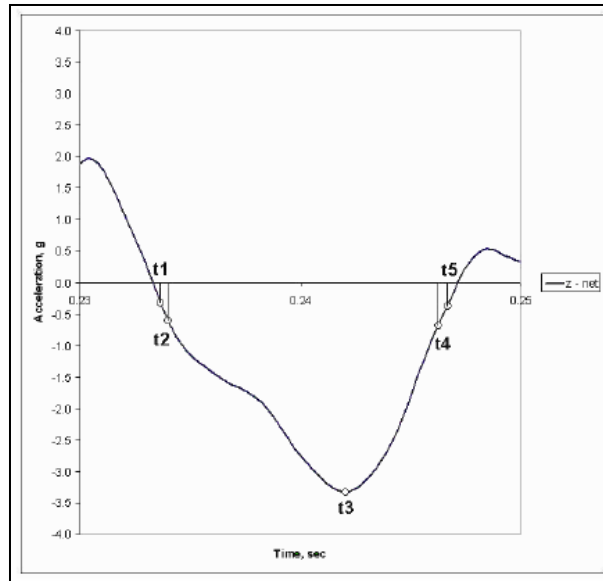


Figure 1.24: Example Jolt Duration Event (after Miller, 2009)

### *Training and Operator Education*

Equipment terrain interactions are impacted not only by terrain and equipment parameters but also by operator decisions and ability. The safe and efficient operation of mining equipment requires skill and experience which is not always practically attainable through operation of full scale equipment. Of paramount importance is the safe operation of mining equipment, however lack of training is a leading cause of haul truck related accidents [60]. In order to meet this training deficit modern mining and construction operations are increasingly turning to simulation and virtual environments to aid in training and re-certification of operators [60-62]. There is also evidence that operator ability and education can increase equipment efficiency and operator well being by decreasing exposure to occupational hazards such as WBV [63-65]. While this research shows operator training is important and will yield valuable results, what is not clear is how to identify the success of such training efforts or when specific operators require additional training. Because the gLA method presented in this paper is conducted from easily obtained field data it is hoped that by using it as performance indicator, in both the simulated and real world environments; a connection between simulation training and actual operator ability can be established.



## 2 Mathematical Investigation

As with many wheeled vehicles an underground articulated haul truck (UAHT) has 4 tires which act as contact points with the ground. As the wheels are the only contact points with the ground any forces acting on the vehicle in the plane normal to the operating surface must be transmitted through these tires. These vertical forces at each wheel create a moment about both the longitudinal (y-axis) and lateral axis (x-axis) of the vehicle; a complete presentation of these forces and the resulting moments is presented in Figure 2.1 through Figure 2.3 below. Importantly; the vehicle at any moment, stationary or otherwise, has a weight which is transmitted through the tires to the ground. It is this ground tire interaction which results in the forces which consequently twist the vehicle frame. Although the mass of the vehicle is instantaneously constant, it is not implied that the loading at each wheel must be equal or, unless the vehicle is completely stationary, that the sum of the forces at the contact points must equal to the weight of the vehicle. In concept the hub forces of any vehicle and the account of their distribution to each wheel can be described as the cumulative effect of the following four force loadings on the vehicle: natural or tare, payload, articulation, and motion. Although these four sets of forces can be used to describe the net hub force for any vehicle it follows naturally that the force due to articulation is zero when the vehicle is rigid (non-articulating) and that the forces due to motion are zero when the vehicle is stationary.

### 2.1 Loading Components

#### 2.1.1 Natural of Tare Force Loading

Vehicle curb weight is defined by the Society of Automotive Engineers as *“The weight of the base vehicle (standard equipment only), with all fluids filled to maximum (fuel, oil, transmission, coolant, etc.). For heavy trucks, the curb weight does not include engine fuel”* [66]. For the purposes of this analysis the tare or curb weight of the vehicle is defined as the stationary unloaded operational weight of the vehicle. Additionally; the hub forces under tare conditions are defined as the specific forces at each wheel under zero articulation tare conditions and evaluated on even ground; this distinction that tare forces at each wheel may be different is important as this analysis procedure does not require that each wheel is under symmetrical loading. Although this analysis is derived around suspension-less equipment, the procedure is also valid for equipment with suspension systems which may or may not

have non symmetrical tare hub forces which may occur if, for example, a suspension system is damaged or altered.

### **2.1.2 Payload Hub force**

Most vehicles are designed for the purpose of transporting material or people. The weight of this additional load is considered payload which in the context of mining vehicles is generally a material such as dirt or rock loaded into the box of the vehicle via large shovels, wheel loaders or hoppers. The weight of the payload, like the tare weight of the vehicle, must also be passed through the wheels to the operating surface and thus adds directly to the vehicles tare hub forces creating gross vehicle hub forces. The total payload force distributed amongst each of the hub forces must not be greater than the weight of the material comprising the payload but there is no restriction as to how the payload weight may be distributed amongst the hub forces. The notion that payload is not distributed evenly across all hub forces is intuitively pictured, as shovel and loader operators cannot reasonably be expected to place loads in exact positions and in general payload is carried primarily by the rear wheels as heavy vehicle components such as engines are loaded over the front axle. Although it has been established that force due to payload does not need to be distributed evenly amongst all wheels this paper will define payload force as the incremental increase over tare weight as payload is applied and the vehicle is in the non-articulated position, such that the articulation angle of the vehicle is zero.

### **2.1.3 Articulation Force**

The primary difference between rigid bodied and articulated vehicles is the fact that in an articulated vehicle the front and rear axles are not constantly aligned when either at rest or during travel. This dynamic relationship has many implications for articulated vehicle designers and operators, however, the two primary differences as concerned by this study are that with articulated vehicles the vehicle weight distribution at each hub changes as the vehicle articulates and, further; as the vehicle articulates the distances of the hub forces relative to the mid-ship and opposite axles change. We will see that this dynamic geometry will play a pivotal role in this proposed method of equipment monitoring. The Appendix 1 contains a study which shows statistical proof using polynomial regression that the force at each hub in fact varies with articulation, following a quadratic relationship, while the vehicle is stationary and gross vehicle weight constant.

#### 2.1.4 Force Due to Motion

The above described hub forces due to vehicle tare, payload and articulation are all present when the vehicle is either stationary or in motion. The final force contributing to total hub force is the force due to motion which, in other words, means the force generated at the hub as the vehicle moves over uneven terrain or experiences linear or centrifugal acceleration due to changes in velocity or direction respectively. The overall approach to frame twist analysis described in this paper is in many ways a continuation of the work done by Joseph in 2002 who used Newton's 2<sup>nd</sup> Law to prove that the dynamic force on any strut of a large tonnage class rear dump haul truck is due to the mass over the strut in a static scenario combined with the reduction or enhancement of acceleration relative to gravity created by the vehicles motion over uneven terrain [3]

### 2.2 Calculation of Cumulative Hub Forces

The preceding section served to introduce the four forces which contribute to the total instantaneous hub force of any vehicle, specifically these forces are due to: Natural/Tare weight, Payload, Articulation (which is defined as zero for rigid bodied vehicles), and motion (which will be zero if the vehicle is stationary or otherwise experiencing zero acceleration). Equation 2.1 describes the cumulative hub force for each hub of a vehicle.

$$F_{Hubj} = \sum_{i=1}^4 F_i$$

Equation 2.1

Where:

$F_{Hubj}$  = Cumulative hub force at the  $j$ th hub of the vehicle

And

$i =$ :

1 = Tare Weight

2 = Force due to Payload

3 = Force Due to Articulation

4 = Force Due to Motion

It is important to note that the hub force at each hub of the vehicle is equal to the action/reaction force at the ground level which also implies that the total ground force exerted by the vehicle can be defined as the summation of all hub forces; this relationship is presented Equation 2.2.

$$F_T = \sum_{j=1}^n F_{Hubj}$$

Equation 2.2

Where:

$F_T$  = Instantaneous total force exerted by the vehicle on the ground

$n$  = The number of hubs on the vehicle

$F_{Hubj}$  = The cumulative hub forces at each hub, as described by Equation 2.1

### 2.2.1 Acknowledgment of Lack of Monitoring Points on Suspension-less Equipment

The work of Joseph utilizes the pressure in an oleo pneumatic suspension system found on most heavy haulers to determine the reaction forces transferred from the ground through these suspension cylinders to the frame of the vehicle [3]. As many large haulers either have existing data acquisition systems, such as Caterpillar's VIMS or Komatsu's VHMS systems, monitoring strut pressures or have ports which ease the installation of monitoring equipment to collect force information in this manner is by far the simplest approach to obtaining hub forces. It is acknowledged that, in practice, it is very

difficult to directly obtain hub forces from suspension-less equipment as without suspension cylinders the remaining choices for data collection become strain gauges or optical readings neither of which are reasonably expected to survive very well in the typical operating environments of articulated mining or construction equipment. It is for this reason that this research uses the theory of an equivalent force and g level loading about a mid-ship reference point as support to suggest measuring frame twist directly at the mid-ship or via the mid-ship pins which although not simple to implement would move the monitoring equipment to a less hazardous location and simplify data analysis as the forces measured directly, would be the resultant twisting force about the vehicle mid-ship. However, given the practical challenges regarding direct hub force measurement on suspension-less vehicles this analysis uses hub forces to derive the equivalent reaction about the mid-ship of the vehicle for several reasons: firstly it provides insight into how the machine ground interactions affect frame twisting, secondly it allows a more detailed analysis into how machine weight is transferred during loading, inclination and articulation; and lastly with the use of a scale model truck direct wheel/hub forces were measured by effectively replacing the tires with load cells. Specifics regarding the scale model test vehicle and procedures are provided in Section 4.

## **2.3 Relationship between Hub Forces and Frame Twist**

The moment of a force about a point or axis is formally defined as “the measure of the tendency of the force to cause a body to rotate about a point or axis” [67]. From this definition it stands logically that the cumulative hub forces described in Section 2.1 will create a resultant moment of force on the vehicle frame about the centre of gravity. The remainder of this analysis is concerned with the moment these cumulative hub forces generate, about the mid-ship of the articulated vehicle under various loading, articulation combinations. These moments about the mid-ship are then expressed as an equivalent force and g level response located on a unit sphere about the mid-ship of the vehicle. For articulated vehicles it makes logical sense to use the mid-ship as the reference point for analysis because as the single connection between the front and rear sections of the vehicle all moments, or twisting, must be transmitted through this point. Furthermore, because all twisting force is directed through the mid-ship in all makes of articulated vehicles using this point as the point of reference would allow the easiest performance comparisons across articulated vehicle sizes and makes. Specifically the point of reference used is the point located directly in the center of the mid-ship pin when viewing the vehicle in plan view and at an elevation equal to the center of the wheel hubs. This exact position is chosen to ensure that

vehicle rotation about either the longitudinal or lateral axis does not change the location of the reference point. Figure 2.2 and Figure 2.3 illustrate the reference point and free body diagrams from the model truck used in this investigation. While this point may in fact not be physically located on the vehicle it is located on the simplified free body diagram used to represent the vehicle during analysis. It is important to note that an inertial reference frame or the COG of the vehicle would be used for a moment analysis such as in the Newton-Euler approaches to vehicle modeling presented in the literature review section. However; the mid-ship is a simpler point to use for derivation and basic analysis of articulated equipment as this point is constant whereas the COG would move as the vehicle articulates to steer. Using any point other than the COG of the vehicle will introduce error, however because this method is intended as an indicator, rather than true dynamic modeling, the location of reference can be relaxed and still provide useful monitoring.



Figure 2.1: Caterpillar AD60 Haul Truck

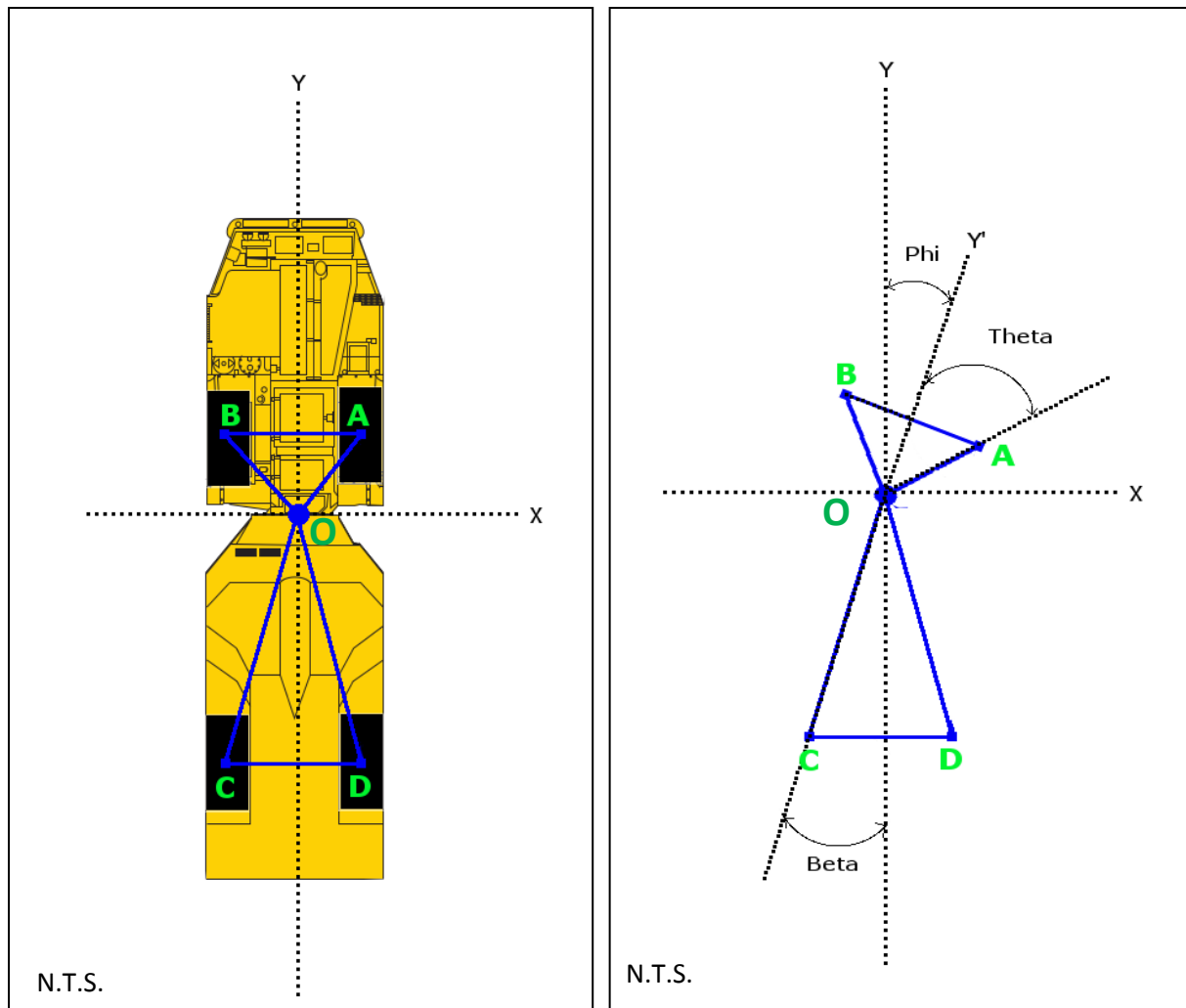


Figure 2.2: (Left) UAHT Schematic Plan view and Free Body Diagram, (Right) UAHT Free Body Diagram

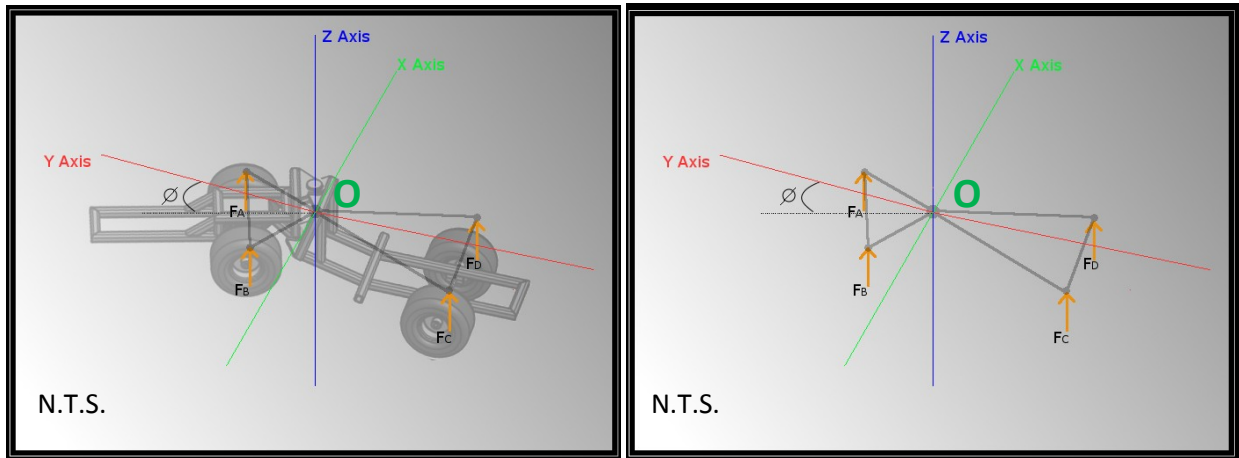


Figure 2.3: (Left) Overview of Test Unit FBD, (Right), Test Unit FBD

## 2.4 Relationship between Multi-Body Modeling and g Level Analysis

As discussed in the literature review section, multi-body vehicle modeling is a very common and useful method of performance investigation but drawbacks including necessary simplification of real world interactions and technical complexity of comprehensive models mean that it is not desirable in all situations. The g Level based analysis presented here is a relatively simple method which conveys similar information as conventional modeling but with several differences.

Figure 2.4 highlights the location used to measure the hub/strut forces used as variable inputs into the gLA. This measurement location captures the overall reaction as the sprung and unsprung masses interact with each other in response to terrain excitation. Using information from each of these 1 DOF quarter vehicle models, located at each strut, a simple vehicle model can be created as shown in Figure 2.5. As will be shown, gLA calculates simple pitch and roll moments about a single reference point. When the chosen reference point is the vehicles COG the result is similar to a simple 6 DOF sprung mass multi-body vehicle model where the sprung mass is treated as a rigid body with 2 DOF (pitch and roll) and each suspension strut has 1 DOF. Note that the DOF of either a rigid or articulated vehicle is the same because gLA is a series of snapshots within each an articulated vehicle is treated as a single rigid body.



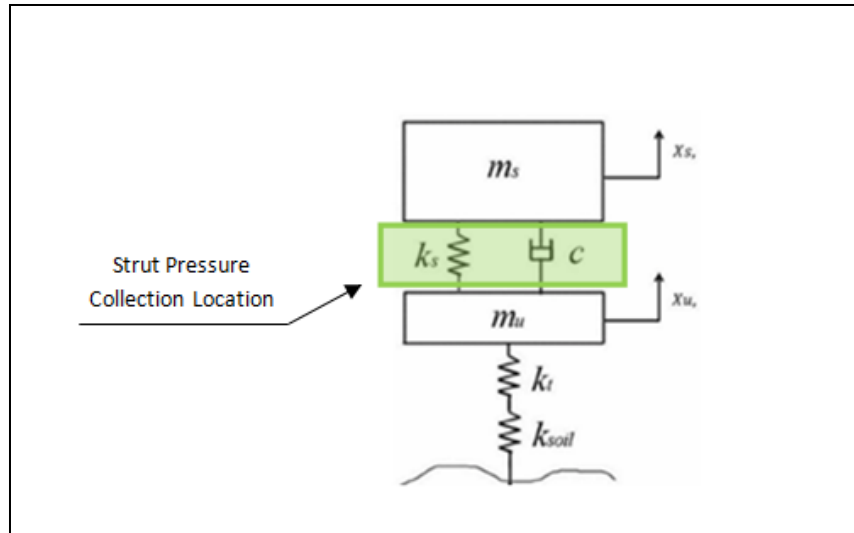


Figure 2.4: Location of Data Collection on 1/4 Vehicle Model

The reason the g Level model can only be considered similar to a conventional multi-body vehicle model is that gLA uses the terms pitch and roll to describe the overall moment generated about the x and y axis (see Figure 3.1) and does not imply any degree of actual movement as is implied by the use of the terms in vehicle dynamics. Secondly; the gLA method is an equipment model which is a projection of a three dimensional vehicle, which operates in a three dimensional world, down to the two dimensional model as represented by the free body diagram in Figure 2.3. Although these simplifications from typical vehicle models are considerable, gLA remains a useful vehicle performance monitoring tool because the input is real suspension data from operating equipment, to explain this statement consider the following: Although gLA has no calculation for load transfer due to cornering; this analysis method will capture the impact of a cornering event due to the accompanied increase in suspension pressure at the struts on the outside of the corner. It is these strut/hub forces which form the basis of gLA and so this method is able to provide information on any interactions which create suspension responses. In a similar fashion, when using a COG reference point on a loaded haul truck the COG is located above the suspension elevation and is also at an increased elevation from the COG location of an unloaded truck. It is known that raising the COG of the vehicle would decrease the stability of the vehicle on slopes and in corners, due again to load transfer. The gLA model would still place the COG of both the loaded and unloaded vehicles on the same elevation plane (although it will be shown that the y axis COG coordinate will change to reflect the shift of weight rearwards when loaded) but any stability issues will result in load transfer which will affect the gLA readings.

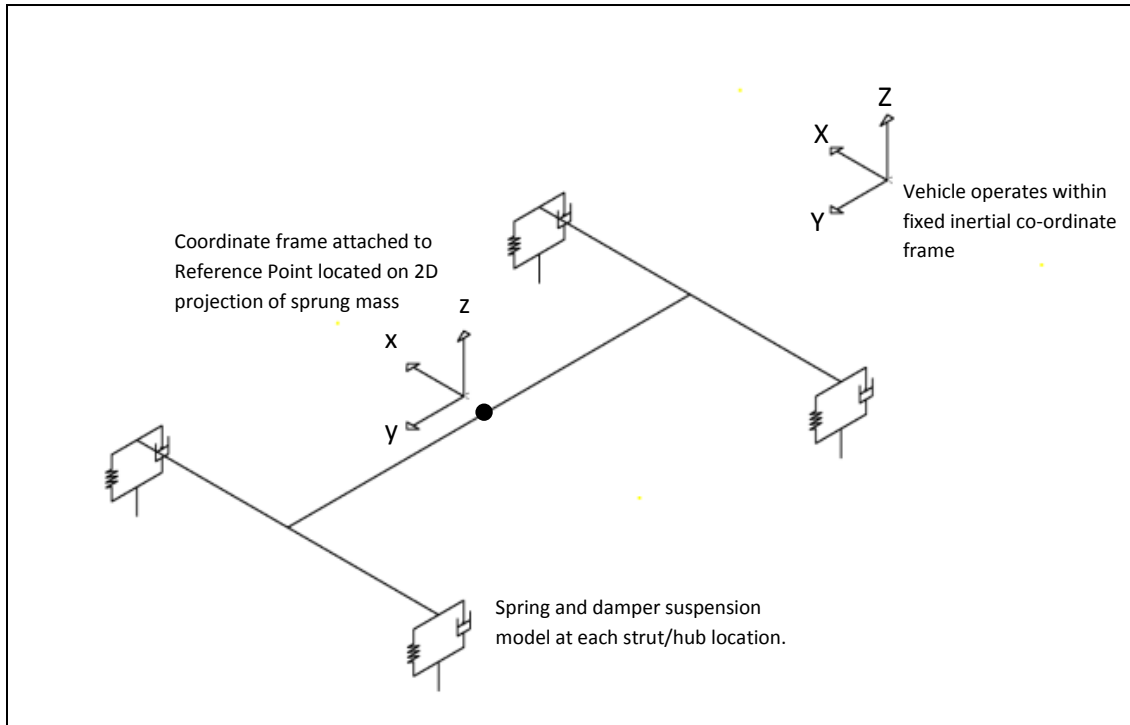


Figure 2.5: g Level Analysis Vehicle Model

### Key Simplifications

Section 2.4 describes the overall relationship between conventional multi-body vehicle modeling and the gLA method. The key simplifications made from dynamic modeling to generate the gLA model include no the following:

- Only forces acting on the point mass of each wheel hub are relevant. This simplification is made in order to develop a model which utilizes data from near vertical suspension struts.
- The inertia tensor of the vehicle is zero. This implies that angular acceleration is neglected and that the calculated approximate accelerations are virtual, linear accelerations only, in the vertical direction due to excitation at the point mass of the wheels.
- The analysis is quasi-static as each sample point is treated as a snapshot of the vehicle at that point.

By working with the above simplifications gLA provides a simple vehicle model based on a moment analysis approach calculated about the vehicles approximate centre of gravity. These simplifications are

made in order to develop a model which can be calculated from easily observed data, using existing technology.

## 2.5 Choice of Reference Point

Although the formal derivations in this work are based on the geometry of an articulated haul truck the analysis can be simplified for application to rigid frame vehicles.

When applying this analysis method the COG of the vehicle is recommended as the first choice of reference point as it will provide the largest degree of agreement with results from classical multi-body analysis. While the COG is recommended as the reference point this location is not necessarily static throughout the vehicles duty cycle, for example the COG of a loaded haul truck travelling from a loading tool to dump location, is different than the COG of the same vehicle travelling empty on a return route to the loading tool. Also of note is that in the real world example of the hauler the COG location would likely change in the x,y and z coordinates, however; because gLA is a two dimensional projection only the x and y coordinates would be affected. This concept is applied in Section 5.2. Another simplification regarding COG in the g Level method is to perform the analysis about the Ideal Centre of Gravity (ICOG). The ICOG is the location where under ideal loading the vehicles COG would be, in reality the COG of the vehicle will vary slightly between loads based on operator ability and if any large fragments are placed off centre. While this assumption will affect the absolute accuracy of the g Level method versus a true classical analysis the g Level method will still capture the overall effect of varying loading conditions as they these variations will be associated with an off-centered suspension response.

The previous paragraph discussed utilizing the ICOG as the reference point instead of the actual COG. This simplification will impart error into the g Level method results when compared to a classical analysis but it is the author's opinion that the results of gLA under these conditions are still a valuable performance monitoring tool. There are also situations where a more extreme deviation from the COG or ICOG will yield useful performance information. One such example of a situation is the application of the method to an articulated vehicle. In the case of an articulated vehicle the COG of the vehicle will shift from in front of to behind the mid-ship location when empty and loaded respectively. The effect of this is that the COG will rotate about the mid-ship from one instance to the next as the vehicle articulates. Analyzing loaded conditions separately from empty conditions would minimize the variation in results however, if it is desired to compare whole duty cycles simultaneously it would be beneficial to

use a point of reference, such as the mid-ship pin, which does not vary during articulation. Although this reference location will impact results, overall the method will still function as a performance indicator and can be used to monitor equipment performance and road conditions as long as all vehicles under analysis use the same reference points. This discussion is also applicable to other potential monitoring points such as the geometric centre of the wheel base as demonstrated in Section 5.2.

## 2.6 Derivation of the Equivalent Force about the Mid-ship

Unless otherwise noted all pertinent vehicle components and general geometries are referenced to Figure 2.2 and Figure 2.3. Additionally it should be noted that a standard  $x,y,z$  and  $i,j,k$  Cartesian coordinate system is used consistently and that all counter clockwise rotations are considered positive.

Where in Figure 2.2, and Figure 2.3:

A = Location of the front right wheel hub

B= Location of front left wheel hub

C=Location of the rear left wheel hub

D=Location of the rear right wheel hub

O= Reference point as described in Section 2.3

$\Theta$ =Natural front frame angle in degrees

B= Natural rear frame angel in degrees

$\Phi$ = Articulation angle in degrees defined as the deviation of the axis  $OY'$  from the initial position parallel to the axis  $OY$

## 2.7 Natural Front and Rear Frame Angles

The term Natural Frame angles refer to the angles beta and theta in Figure 2.3 and are defined as the angle between the longitudinal axis of the vehicle and a line originating from the point of reference/origin “O” of any vehicle which travel through the wheel hubs. These angles are used to simplify the representation of the vehicle free body diagram. These angles are constant as they are a function of vehicle construction. All of the relevant dimensions required for analysis can be estimated

from general arrangement drawings or, if available, CAD drawings can be used for more accurate determination.

### 2.7.1 Definition of Articulation

If the vehicle under investigation is articulating the geometry between the wheel hubs and the reference point “O” will change as the vehicle articulates. See Figure 2.3. By convention established in this investigation articulation is defined as deviation of the longitudinal axis OY, which bisects the front axle from its location at zero articulation to the location of the bisecting axis OY’ and will be denoted by the Greek letter phi,  $\phi$ . Arbitrarily the rear section of the vehicle is considered stationary relative to the reference point; therefore all articulation is expressed through the angle  $\phi$ . The decision to arbitrarily hold the rear section of the vehicle stationary serves to simplify evaluation as this condition forces the geometry of hubs C and D to remain constant relative to point O in the XY plane.

As mentioned in Section 2.2.1 there is substantial difficulty in attempting to measure hub forces directly on suspension-less vehicles. However, cumulative hub forces will be used to derive the general relationship for an equivalent force about the mid-ship as it is a more general approach and because hub forces were obtained directly during scale model testing. The derivation of this equivalent force from hub forces also provides a more thorough understanding of the machine/ground interactions which take place to create the overall twisting effect on the vehicle. The cumulative forces acting at each of the wheel locations can be computed using Equation 2.1 and will be denoted according to the alphabetical convention displayed in Figure 2.2 where, moving counterclockwise from front right to rear right:

$\vec{F}_A$  = Cumulative hub force at hub A

$\vec{F}_B$  = Cumulative hub force at hub B

$\vec{F}_C$  = Cumulative hub force at hub C

$\vec{F}_D$  = Cumulative hub force at hub D

At each instant the forces described above can be written in vector notation as:

$$\vec{F}_\alpha = x\vec{i} + y\vec{j} + z\vec{k}$$

Equation 2.3

Where  $\vec{F}_\alpha$  is the cumulative hub force at either the A, B, C, or D hub location and x,y,z are the magnitude of the cumulative hub force in the  $\vec{i}, \vec{j}, \vec{k}$  directions respectively. In this analysis, when using the vector notation the x and y components of hub force are zero as the monitored forces are in the  $\vec{k}$  direction only which simplifies the vector notation to:

$$\vec{F}_\alpha = z\vec{k}$$

Equation 2.4

It is a relatively safe assumption that the x and y components of the hub forces are zero as they could only be non zero if the wheels were to be impacted from a direction other than within the z plane which is not a part of normal operating conditions for the equipment under investigation.

## 2.8 Instantaneous Moment about the Reference Point

As this analysis is based on moments, the moment arms of the forces located at the wheel hubs will change as articulation increases or decreases. Referring to Figure 2.3 a simple geometry can be used to develop the instantaneous position of each hub relative to the reference point. These instantaneous positions of each hub, relative to the reference, in effect describes the i,j,k components of the lines OA, OB, OC, and OD which will be denoted as position vectors  $\vec{A}, \vec{B}, \vec{C},$  and  $\vec{D}$  respectively. These position vectors are drawn from the reference point and travel through the line of action of each respective  $\vec{F}_\alpha$  and as such the instantaneous cumulative moment about the reference point created by each  $\vec{F}_\alpha$  can be determined from the cross product  $\vec{a} \times \vec{F}_\alpha$  where  $\alpha$  denotes each hub position. This computation is expressed in Equation 2.5 below as:

$$\vec{M}_{O_\alpha} = \vec{a} \times \vec{F}_\alpha$$

Equation 2.5

Which can be calculated in determinant form as Equation 2.6:

$$\vec{M}_{O_\alpha} = \begin{vmatrix} i & j & k \\ \alpha_x & \alpha_y & \alpha_z \\ F_{\alpha_x} & F_{\alpha_y} & F_{\alpha_z} \end{vmatrix}$$

Equation 2.6

With each of the moments calculated about the common reference points, the resultant moment about the reference point, denoted  $\vec{M}_{o_T}$ , can be calculated as the vector summation of each of the moments created about the reference points by each individual  $\vec{F}_\alpha$ .

$$\vec{M}_{o_T} = \vec{M}_{O_A} + \vec{M}_{O_B} + \vec{M}_{O_C} + \vec{M}_{O_D}$$

Equation 2.7

Which is equal to:

$$\vec{M}_{o_T} = \begin{vmatrix} i & j & k \\ A_x & A_y & A_z \\ F_{A_x} & F_{A_y} & F_{A_z} \end{vmatrix} + \begin{vmatrix} i & j & k \\ B_x & B_y & B_z \\ F_{B_x} & F_{B_y} & F_{B_z} \end{vmatrix} + \begin{vmatrix} i & j & k \\ C_x & C_y & C_z \\ F_{C_x} & F_{C_y} & F_{C_z} \end{vmatrix} + \begin{vmatrix} i & j & k \\ D_x & D_y & D_z \\ F_{D_x} & F_{D_y} & F_{D_z} \end{vmatrix}$$

Equation 2.8

This resultant moment can be expressed in vector form as

$$\vec{M}_{o_T} = M_{o_x}\vec{i} + M_{o_y}\vec{j} + M_{o_z}\vec{k}$$

Equation 2.9

The unit vector  $\vec{U}_{M_o}$ , which provides the direction of the axis about which the resultant moment tends to rotate the vehicle can be calculated as:

$$\vec{U}_{M_o} = \frac{\vec{M}_{o_T}}{\|\vec{M}_{o_T}\|}$$

Equation 2.10

Using the unit vector,  $\vec{U}_{M_o}$ , and the magnitude of the resultant moment,  $M_{o_T}$ , the final form of the resultant moment about the reference can be expressed as:

$$\vec{M}_{o_T} = M_{o_T} \vec{U}_{M_o} = M_{o_T} (\hat{M}_{o_x} \vec{i} + \hat{M}_{o_y} \vec{j} + \hat{M}_{o_z} \vec{k})$$

Equation 2.11

Figure 2.6, is a visual representation of  $\vec{U}_{M_o}$  using the Test Unit frame as an example.

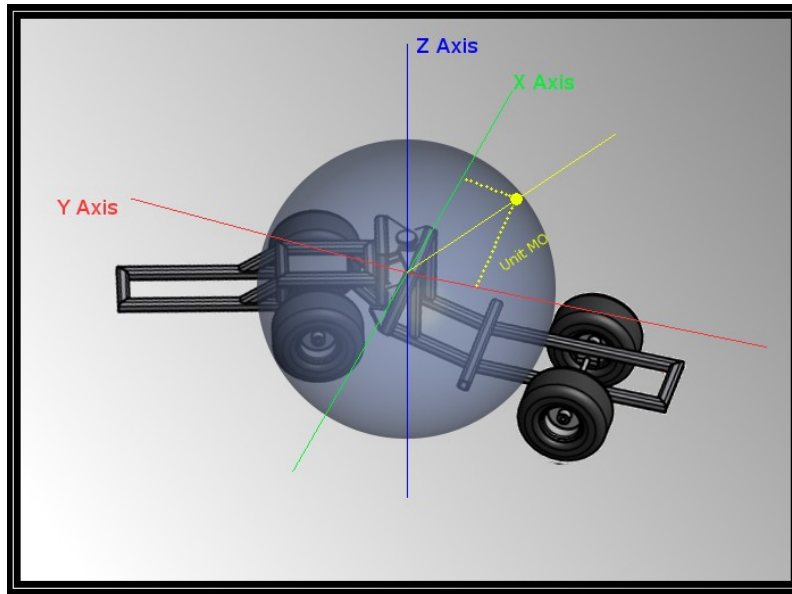


Figure 2.6: Example Representation of Unit Mo

## 2.9 Equivalent Force and Instantaneous g Level Analysis

Thus far the major result has been the derivation of an expression for the magnitude and direction of the resultant moment about the reference point created by each of the cumulative forces acting at the



individual hub locations. The direction of the resultant moment,  $\vec{M}_{oT}$ , is provided by the unit vector  $\vec{U}_{M_o}$ , however this is the direction of the axis about which the vehicle will tend to rotate. Therefore; to replicate this rotation with a single force, the force will need to act in a direction perpendicular to that indicated by  $\vec{U}_{M_o}$ . To determine the direction of this perpendicular equivalent force, denoted as  $\vec{F}_{EQ}$ , first a point,  $P$ , on the unit sphere perpendicular to the point indicated by  $\vec{U}_{M_o}$  will be found and then the required  $\vec{F}_{EQ}$  will be applied tangent to the point  $P$ . Figure 2.6 above along with Figure 2.7 and Figure 2.9, in the following sections, show the progression of the representation of the  $\vec{M}_{oT}$  by the equivalent force  $\vec{F}_{EQ}$ .

### 2.9.1 Determination of the Magnitude of $\vec{F}_{EQ}$

The purpose of  $\vec{F}_{EQ}$  is to replicate the cumulative moment about the point O. Given that the magnitude of any moment is dependent on both the magnitude of the force and length of the moment arm at which the force is applied the magnitude of the equivalent force,  $\vec{F}_{EQ}$ , will be dependent on the radius of the unit circle chosen for analysis. While the radius of the relevant unit circle is arbitrary caution must be used to ensure that magnitudes of all forces which are to be compared are adjusted to act with a common moment arm. This same statement will be important in the gLA presented in Section 2.11. Once the radius of the unit circle has been set the magnitude of  $\vec{F}_{EQ}$  can be determined from the following equation:

$$F_{EQ} = \frac{M_{oT}}{r}$$

Equation 2.12

Where  $r$  is equal to the radius of the unit circle.

### 2.9.2 Determination of $\vec{U}_{\perp}$

A commonly employed and useful property of vectors is that two non-zero vectors are orthogonal if and only if the dot product between the two vectors is equal to zero [68]. To find a vector which is

orthogonal to  $\vec{U}_{M_o}$  this dot product property is used to determine an arbitrary vector  $\vec{U}_\perp$  which satisfies the condition that  $\vec{U}_{M_o}$  dot  $\vec{U}_\perp$  is equal to zero. Specifically to determine  $\vec{U}_\perp$  the following is used:

$$\vec{U}_\perp = U_{\perp x} \vec{i} + U_{\perp y} \vec{j} + U_{\perp z} \vec{k}$$

Equation 2.13

$$\vec{U}_{M_o} = \hat{M}_{o_x} \vec{i} + \hat{M}_{o_y} \vec{j} + \hat{M}_o \vec{k}$$

Equation 2.14

And

$$\vec{U}_\perp \cdot \vec{U}_{M_o} = 0$$

Equation 2.15

Because all three components of  $\vec{U}_\perp$  are unknown there is no single solution to Equation 2.15. However; since any vector orthogonal to  $\vec{U}_{M_o}$  is adequate any arbitrarily assumed values for two of the variables in  $\vec{U}_\perp$  will result in a solution to Equation 2.15. This solution will actually be a vector from the plane which is orthogonal to the vector  $\vec{U}_{M_o}$ . By convention stated here the  $\vec{j}$  and  $\vec{k}$  components of  $\vec{U}_\perp$  will be assumed to be equal to one leaving only the  $\vec{i}$  component to be determined. This solution simplifies Equation 2.16 as follows:

$$\vec{U}_\perp \cdot \vec{U}_{M_o} = 0$$

$$(U_{\perp x} \vec{i} + U_{\perp y} \vec{j} + U_{\perp z} \vec{k}) \cdot (\hat{M}_{o_x} \vec{i} + \hat{M}_{o_y} \vec{j} + \hat{M}_o \vec{k}) = 0$$

And with the assumption  $U_{\perp y} = U_{\perp z} = 1$ .

$$(U_{\perp x} \vec{i} + 1\vec{j} + 1\vec{k}) \cdot (\hat{M}_{o_x} \vec{i} + \hat{M}_{o_y} \vec{j} + \hat{M}_o \vec{k}) = 0$$

### Equation 2.16

### Equation 2.17



## 46

The point P represents the location on the relevant unit sphere about the reference point O to which the line of action of the equivalent force  $\vec{F}_{EQ}$  will be tangent. To calculate the direction of  $\vec{F}_{EQ}$  a slice of the relevant unit sphere along the axis indicated by  $\vec{U}_\perp$  yields a unit circle with origin O and point P represented in two dimensional space by the coordinates of  $\sqrt{P_x^2 + P_y^2}$  and  $P_z$  as shown in Figure 2.8.

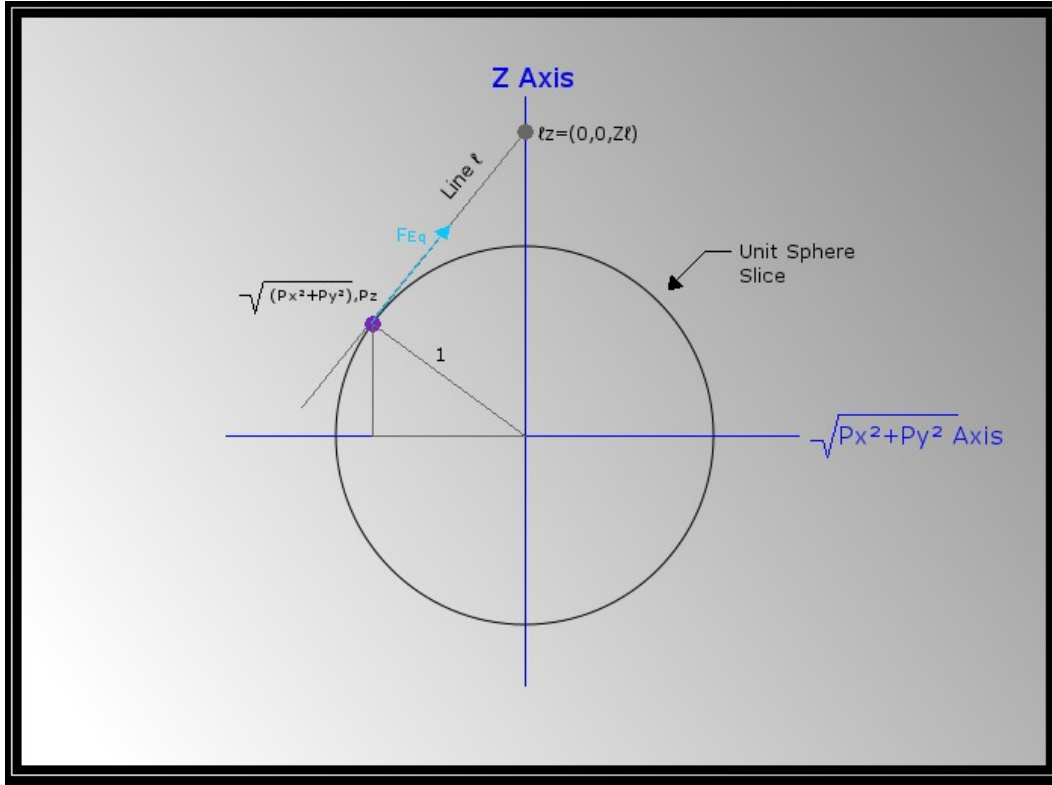


Figure 2.8: Unit Sphere Slice

The direction of  $\vec{F}_{EQ}$  can be determined by evaluating the equation of the line  $\ell$  which is tangent to the unit circle, as illustrated by Figure 2.8, and is oriented to intercept the vertical, Z, axis at the point  $\ell_z = (0, 0, z_\ell)$  as shown in Figure 2.8. The direction of  $\vec{F}_{EQ}$  must be in agreement with the sense of  $\vec{M}_{OT}$ , meaning that if  $\vec{M}_{OT}$  is a positive moment so must be the moment created by  $\vec{F}_{EQ}$ . Specifically the direction of  $\vec{F}_{EQ}$  will be determined as the vector between the point P and  $\ell_z$ . Appendix 2 shows the logic and method used to determine the exact direction of  $\vec{F}_{EQ}$ .

Once the direction of  $\vec{F}_{EQ}$  has been determined it can be stated that:

$\vec{M}_{o_T}$  can be replicated by  $\vec{F}_{EQ}$ , acting in the direction  $(F_{EQ}\vec{i} + F_{EQ}\vec{j} + F_{EQ}\vec{k})$ , located at point P, on a unit sphere which is centered about the reference O. This statement is represented visually in Figure 2.9 below.

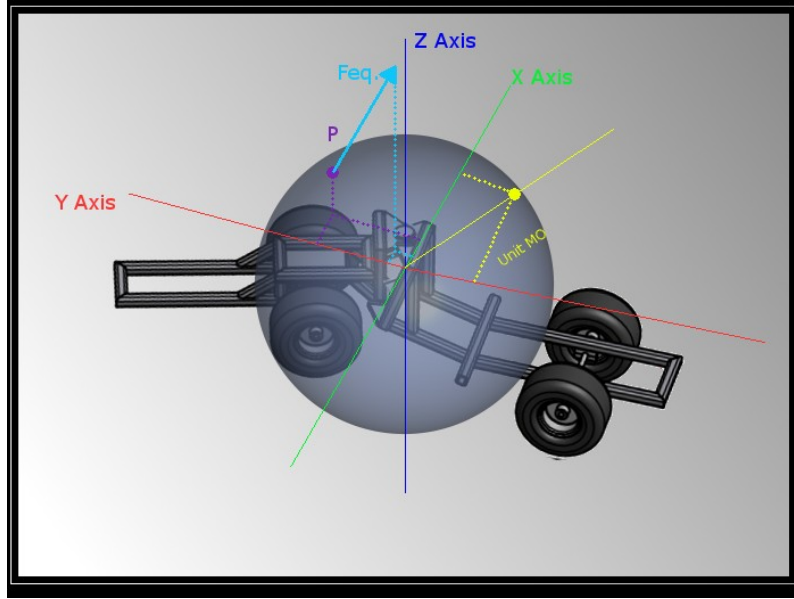


Figure 2.9: Example Representation of the Equivalent Force Applied Tangent to Point P

## 2.11 Equivalent Force Distributions

At this point it should be noted that in situations where real world data is collected the volume of data points for  $\vec{U}_{M_o}$  and correspondingly for  $\vec{F}_{EQ}$  will be very large. In such situations it would be useful to display the data simultaneously on the unit sphere as points and vectors or as a stereographic projection highlighting the most densely populated areas. An example of such a representation using points and vectors has been created with the R software package using the averaged data for each loading and articulation combination collected during this investigations scale model testing. A complete discussion regarding this scale model testing and its results can be found in sections 4 through 4.8 of this report. In Figure 2.10, below, the red points represent the  $\vec{U}_{M_o}$  coordinates and the blue arrows represent  $\vec{F}_{EQ}$  which originate from the points  $\vec{U}_{M_o}$ .

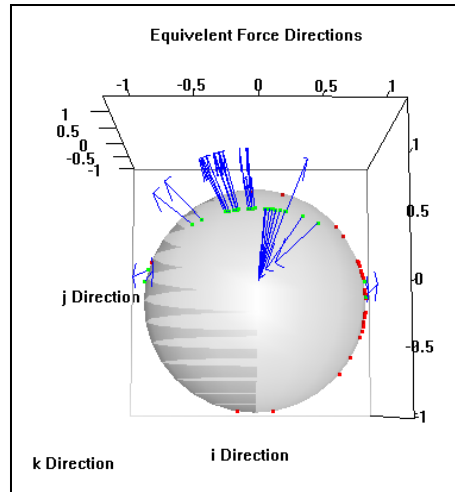


Figure 2.10: Example Vector Representation of Results

### 3 Instantaneous g Level Analysis

The remainder of the mathematical analysis is used to present a method of expressing the moment about the reference point O in terms of relative g units which is more useful for the monitoring of frame conditions and is more relevant for benchmarking the performance of different vehicles and operators. The instantaneous g level can also be used in conjunction with the direction of the equivalent force to facilitate analysis in terms of rack, pitch and roll; this application will be presented in Section 3.2.

#### 3.1 Application of Newton's Second Law

As is commonly understood, Newton's second law of motion states that the sum of the forces acting on a body must equal the mass of the body multiplied by the body's acceleration [67]. This second law can be applied to moments by multiplying the left and right sides by distance yielding the following:

$$Fd = m\vec{a}d$$

Equation 3.1

In terms of components relevant to this investigation Equation 3.1 can be stated as:

$$\vec{M}_{o_T} = \vec{F}_{EQ}r = m_i\vec{a}r \text{ or:}$$

$$\vec{a} = \frac{\vec{M}_{o_T}}{m_i r}$$

Equation 3.2

Where:

$\vec{F}_{EQ}$  = Equivelnet force as calculated in Section 2.9

$r$  = The radius of the unit sphere on which  $\vec{F}_{EQ}$  acts

$\vec{a}$  = The instantaneous acceleration of the vehicle about the reference point

$m_i$  = The instantaneous mass of the vehicle, defined as:

$$m_i = \frac{Tare\ Weight + Payload}{g}$$

Equation 3.3

Note that the instantaneous mass,  $m_i$ , will change as the vehicle is loaded or unloaded but is constant between the addition or reduction of payload. For example the instantaneous mass of the vehicle travelling loaded from the shovel to the dump location is constant but different from the instantaneous mass of the vehicle on the return trip from the dump to the shovel. It is important to use the appropriate loaded or unloaded nominal mass of the vehicle in this analysis.

In Equation 3.2 the instantaneous mass of the vehicle,  $m_i$ , and the radius of the unit sphere are fixed and the total moment about the reference point,  $\vec{M}_{OT}$ , can be calculated as outlined in Section 2.8 therefore the additional moment about the reference must be caused by the forces due to articulation and motion which generate higher or lower accelerations, effectively enhancing or reducing the gravitational constant,  $g$ . The analysis presented in this thesis utilizes the number of  $g$  units about the reference point because with the real world difficulty in monitoring forces on articulated suspension-less vehicles closer to the hubs it is proposed that the final effect could be measured using strain or accelerometer analysis on the mid-ship components as mentioned in Section 2.2.1. If the moment about the reference were to be monitored directly from the mid-ship pin Equation 3.2 could be used without requiring knowledge of the cumulative forces at each of the hubs.

As Joseph states in his 2003 paper; an adverse rack cycle is considered to be greater than 1.5g, therefore; as with Josephs analysis, real world implementation of the analysis outlined in this investigation would also consider rack cycles greater than 1.5g to be detrimental.

### 3.2 Definition of Rack, Pitch, Roll and Twist

The terms rack, pitch and roll in the context of this investigation have specific meanings which are defined in the following section. All positive rotations are defined through use of the right hand rule. Figure 3.1 below shows each axis of rotation as it relates to the typical Underground Articulated Haul Truck (UAHT). The same axes could be used in the evaluation of rigid bodied equipment.



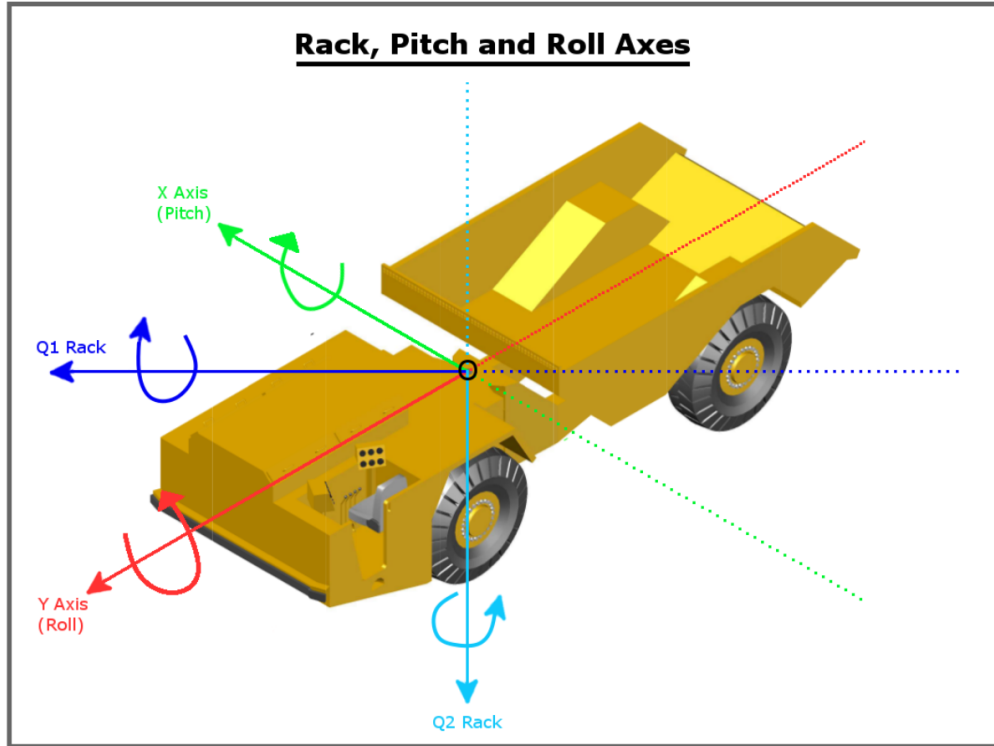


Figure 3.1: Rack, Pitch and Roll Axes

### 3.2.1 Pitch and Roll

Pitch and roll are defined as rotation around the X and Y axes respectively which is consistent with the pitch and roll of an aircraft [69]. Pitch and Roll are calculated as the magnitude of the rotation, in either the units of moment or g level, projected onto the unit vector defining the direction of either the X or Y axes respectively. Equation 3.4 and Equation 3.5 below define pitch and roll in terms of a scalar triple product.

$$Pitch = M_{o_T} \vec{U}_{M_o} \cdot (1,0,0)$$

Equation 3.4

$$Roll = M_{o_T} \vec{U}_{M_o} \cdot (0,1,0)$$

Equation 3.5

### 3.2.2 Rack

This study proposes to define rack as the tendency of the vehicle to rotate specifically about an axis which runs through the reference point O in the XY plane and at a 45° angle from the X and Y axes in either quadrant one or quadrant two. Specifically this study uses the term “Q1 Rack” to refer to rotation about the above described axis located in quadrant one and the term “Q2 Rack” to refer to rotation about the above described axis located in quadrant 2. This study does not propose that there is any distinction between the effects of Q1 Rack or Q2 Rack in terms of overall effect on the vehicle or occupant but rather the definition of rack about a defined axis prevents ambiguity between, for example, rotation about an axis one degree from the y axis which would have essentially the characteristics of roll and the rotation about the defined Q1 or Q2 rack axes which would create very different effects on the vehicle as compared to roll. Equation 3.6 and Equation 3.7 define Q1 Rack and Q2 Rack in terms of a similar scalar triple product as used in pitch and roll.

$$Q1\ Rack = M_{o_T} \vec{U}_{M_o} \cdot (\sqrt{2}/2, \sqrt{2}/2, 0)$$

Equation 3.6

$$Q2\ Rack = M_{o_T} \vec{U}_{M_o} \cdot (-\sqrt{2}/2, \sqrt{2}/2, 0)$$

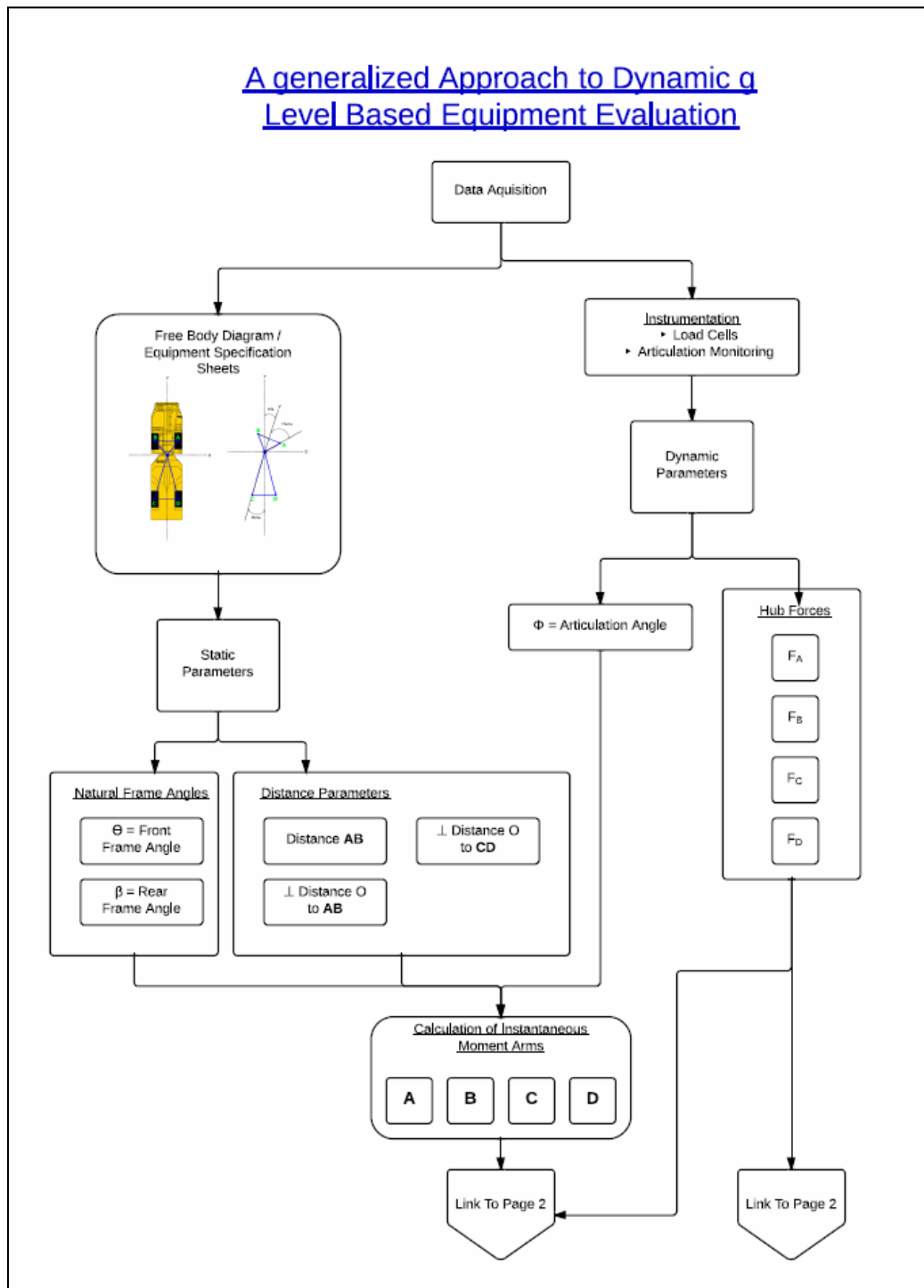
Equation 3.7

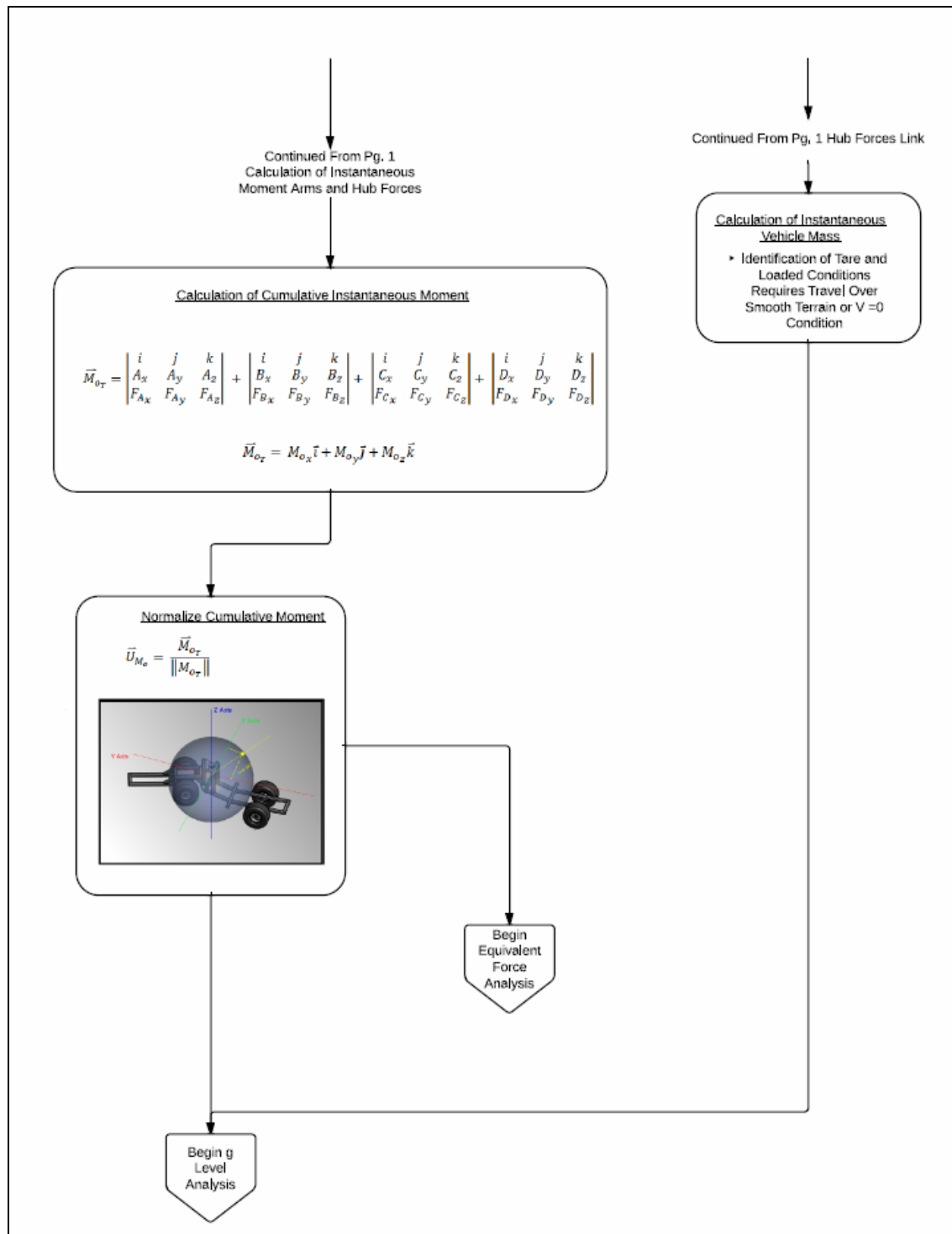
### 3.2.3 Twist

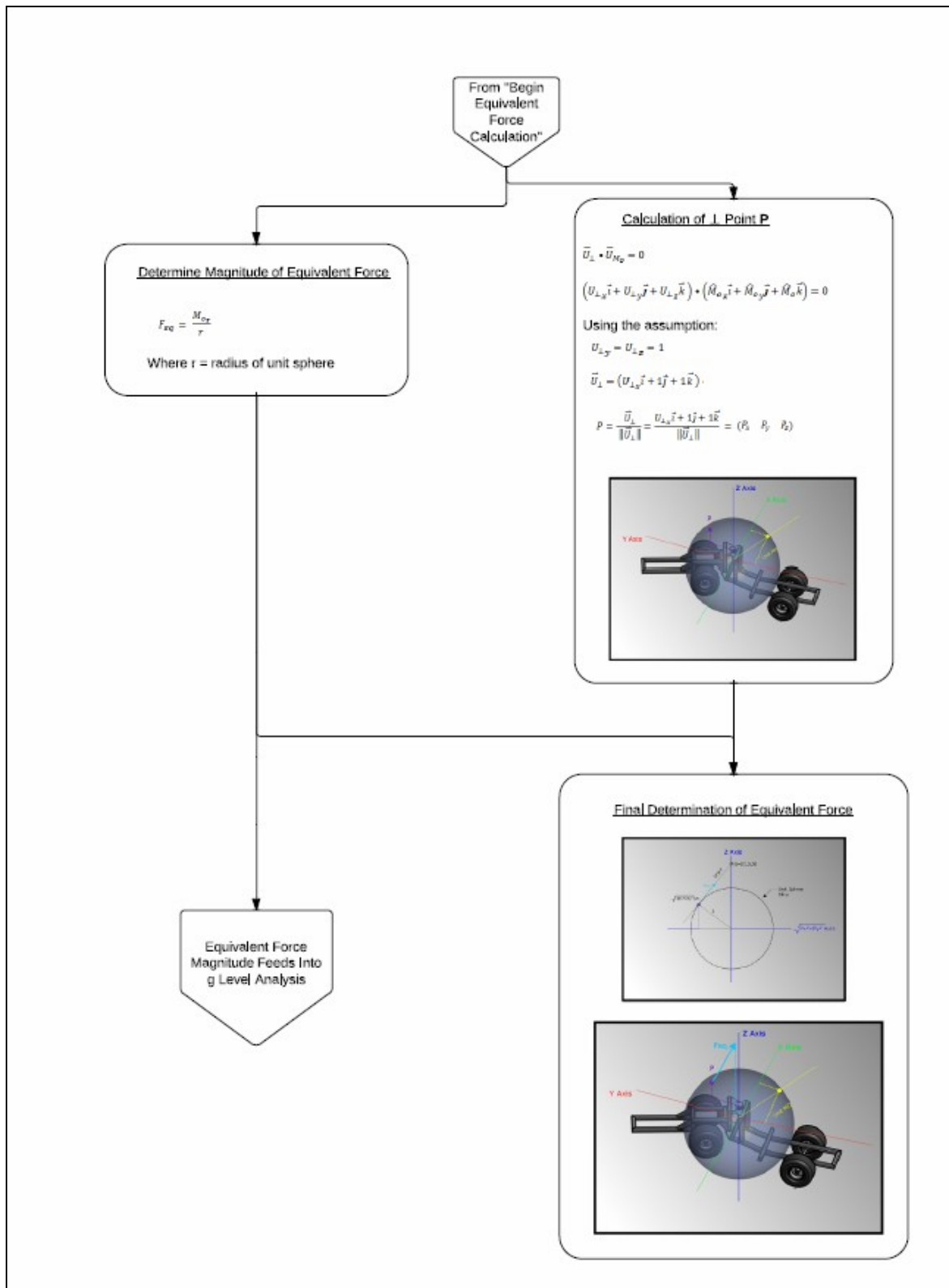
Twist is defined as the total or overall rotation about any axis. Alternatively put, Twist is the term used for resultant rotation due to the cumulative moment whereas Rack, Pitch and Roll imply rotation about specific axes because there is no defined axis associated with Twist it is important that the general direction of the rotation is considered with the magnitude to accurately understand which characteristics, rack, pitch or roll will be most pronounced.

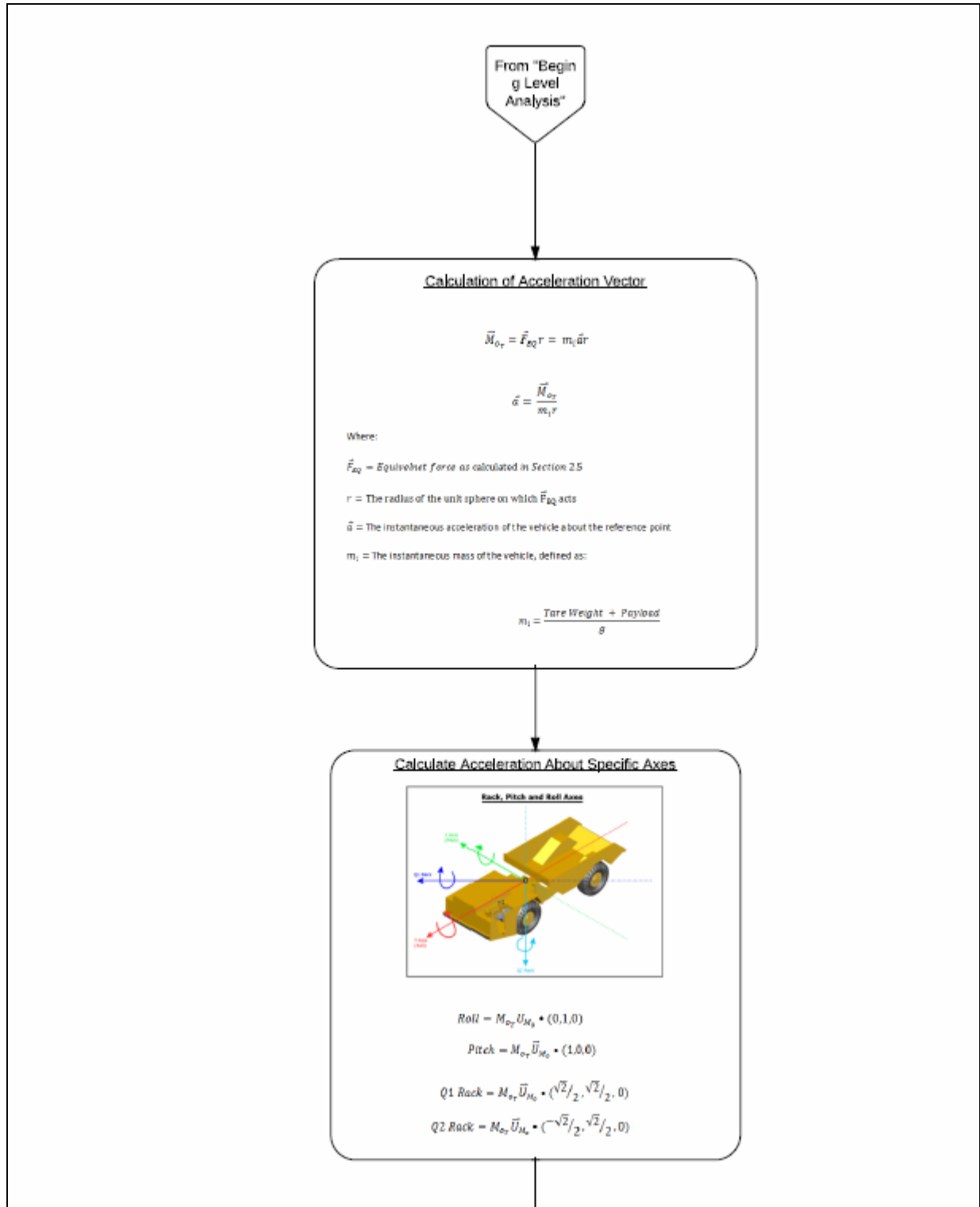
### 3.2.4 g Level Evaluation Process

The flow chart shown as Figure 3.2 summarizes the calculations steps associated with the gLA methodology.









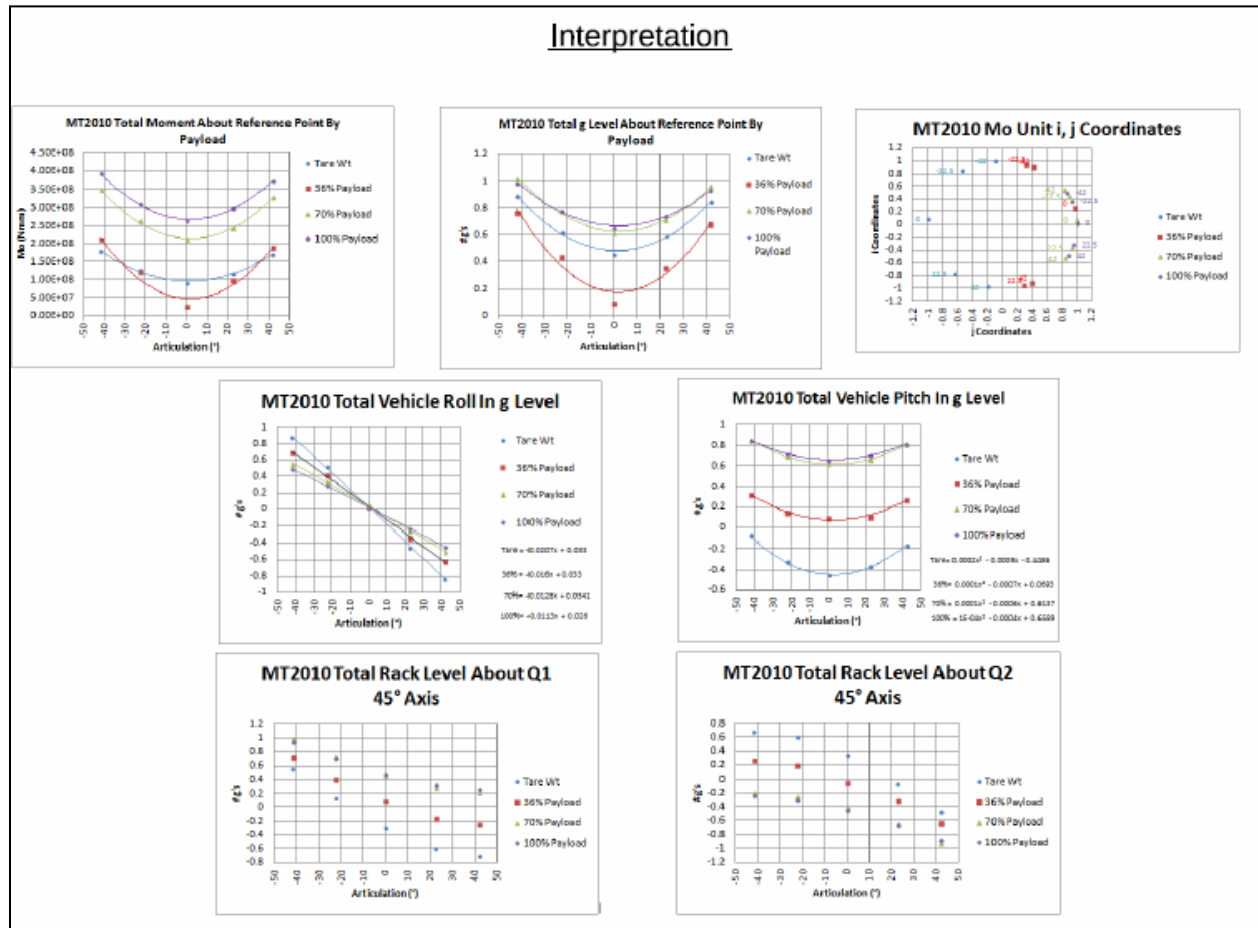


Figure 3.2: gLA Process Flowchart

### 3.3 Method Validation

As discussed in Section 2.4 the gLA method which is proposed is intended to monitor equipment performance as a key performance indicator. In order for this to be accomplished the method should show a reasonable degree of agreement to classical vehicle dynamics analysis.

To demonstrate this agreement the commercially available vehicle dynamics modeling software veDYNA-Entry was used to generate a set of strut data from a pre-configured vehicle and simulation routine [70]. Currently veDYNA does not offer any pre-configured off road vehicle models as part of the veDYNA-Entry modeling suite so a small delivery-type vehicle operating on pavement was chosen. Although this scenario is not specifically what has been discussed in this investigation gLA can be applied. A wire frame of the simulated vehicle is presented in Figure 3.3 and an image of the vehicle

during simulation is shown as Figure 3.4. General vehicle data is presented in Table 3.1 below, complete vehicle data is presented as Appendix 10. Note the yellow sphere in Figure 3.3 represents the vehicle's centre of gravity.

Vehicle Type	Truck
Vehicle Length (m)	7.5
Vehicle Width (m)	2.55
Vehicle Height (m)	3.1
Wheel Track Width (m)	2.2
Vehicle Mass (kg)	8830
Load Mass (kg)	0
Front Spring Stiffness (kN/m)	300
Rear Spring Stiffness (kN/m)	300

Table 3.1: veDYNA Light Truck Basic Parameters (After Tesis, 2014)

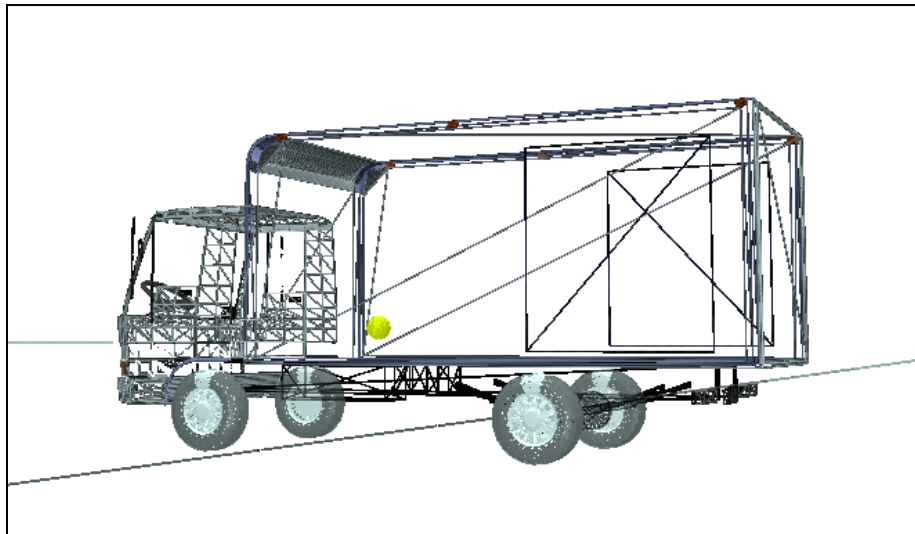


Figure 3.3: Simulated Light Truck Wireframe (Using veDynaWare, Tesis, 2014)



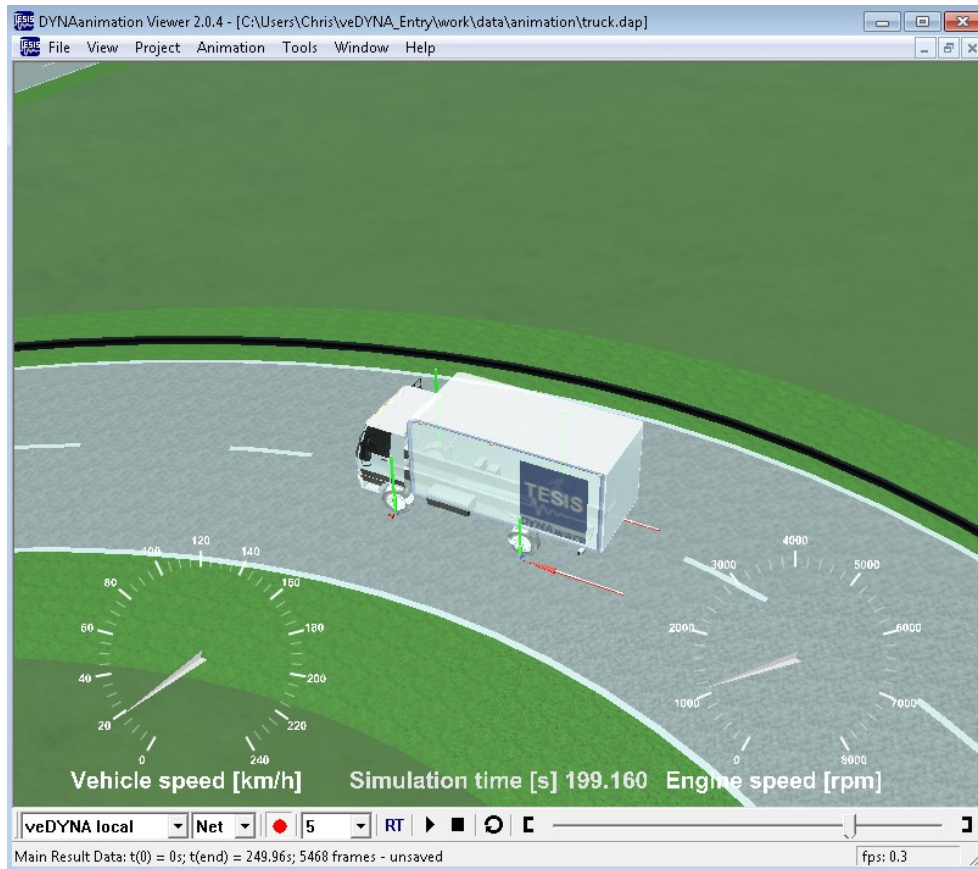


Figure 3.4: Simulated Vehicle

The most realistic road based simulation procedure offered in the veDYNA-Entry software is called the Monte Carlo course. This course is intended for use with the sports car vehicle configuration offered in the software; however, due to curvature and elevation variations this course provided a diverse range of vehicle responses from the truck configuration even with velocity limited to 20km/h. During a simulation veDYNA is capable of monitoring hundreds of vehicle parameters and responses. For the purposes of this study spring and damper forces from each of the four suspension components were monitored to be used as post processing input variables to the g Level method. For comparison the vehicle's pitch and roll Cardan angles were recorded. All parameters were recorded at 0.01s intervals and the simulation was run for 250s during which time the vehicle completed approximately 1500m of the course.

Figure 3.5, Figure 3.6 and Figure 3.7 below show the Monte Carlo course's plan overview, curvature profile and elevation profile respectively. The simulation parameters were left unaltered from veDYNA's standards for a light truck vehicle type executing the go\_monte\_carlo simulation procedure. To maintain stability during cornering the maximum vehicle speed was limited to 20km/h.

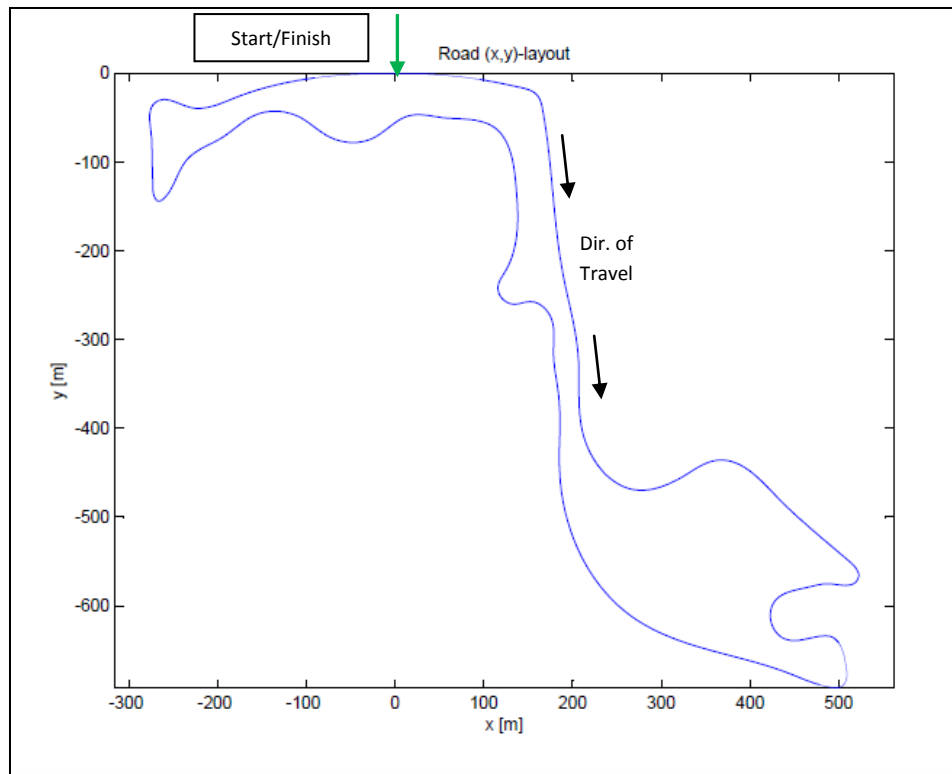


Figure 3.5: Monte Carlo Course - Plan View (Using veDynaware, Tesis, 2014)

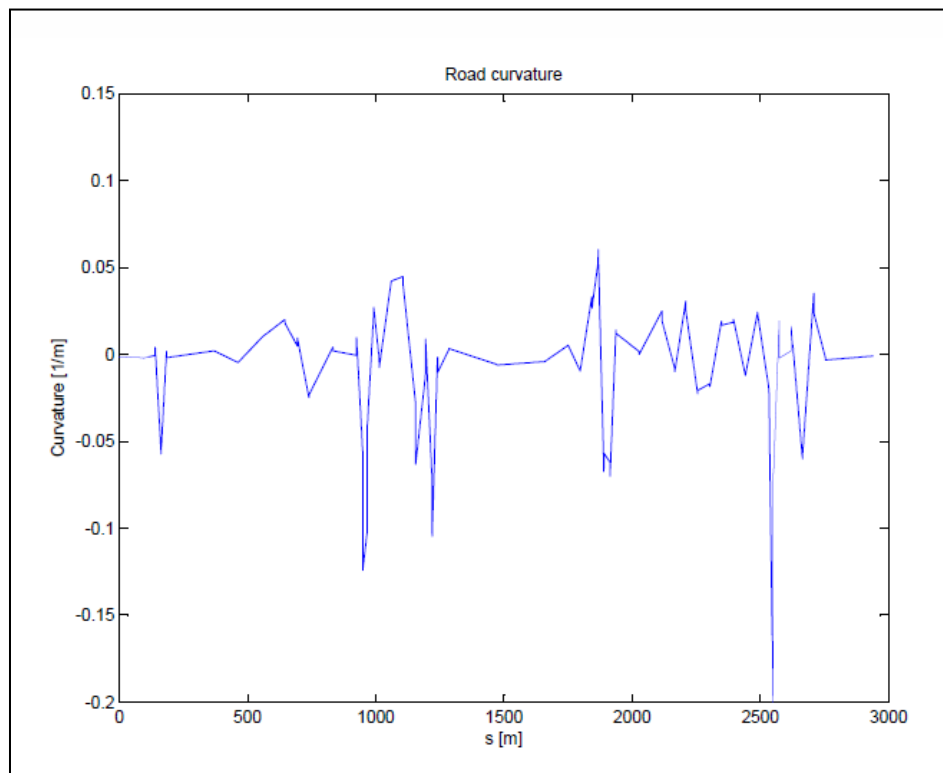


Figure 3.6: Monte Carlo Course - Curvature (Using veDynaware, Tesis, 2014)

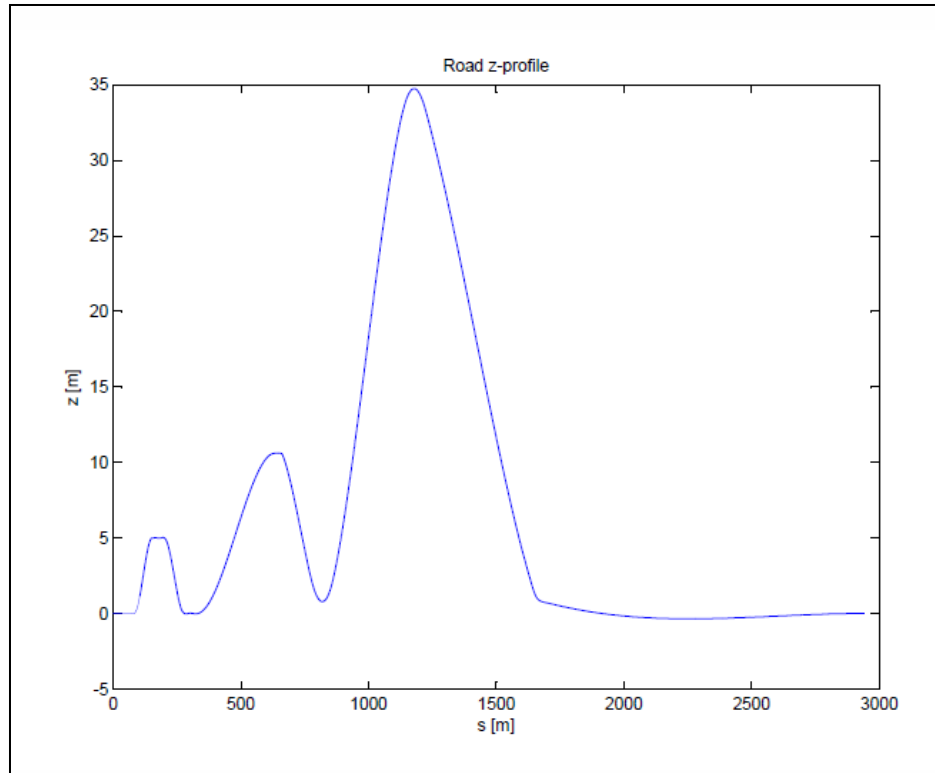


Figure 3.7: Monte Carlo Course - Elevation Profile (Using veDynaWare, Thesis, 2014)

To complete the gLA on the simulated data set the spring forces and damper forces were combined to represent a suspension force similar to the pressure inside a conventional strut. Figure 3.8, below, shows the combined simulated suspension data. As the simulation was run with zero load on the truck it is expected that the left rear and right rear forces would be, on average, lower than the front suspension forces.

Figure 3.9 shows a wireframe view of the simulated truck executing a left hand corner. Note that the simulation shows larger tire reaction forces (green vectors) on the outside of the corner and larger longitudinal forces at the rear wheels, both of these observations are as would be expected from a rear wheel drive vehicle executing a left hand corner. The calculated roll value of 0.19g at the indicated simulation time of 199.2s is also indicates the vehicle is experiencing larger reaction forces at the front and rear suspension on the outside of the corner.

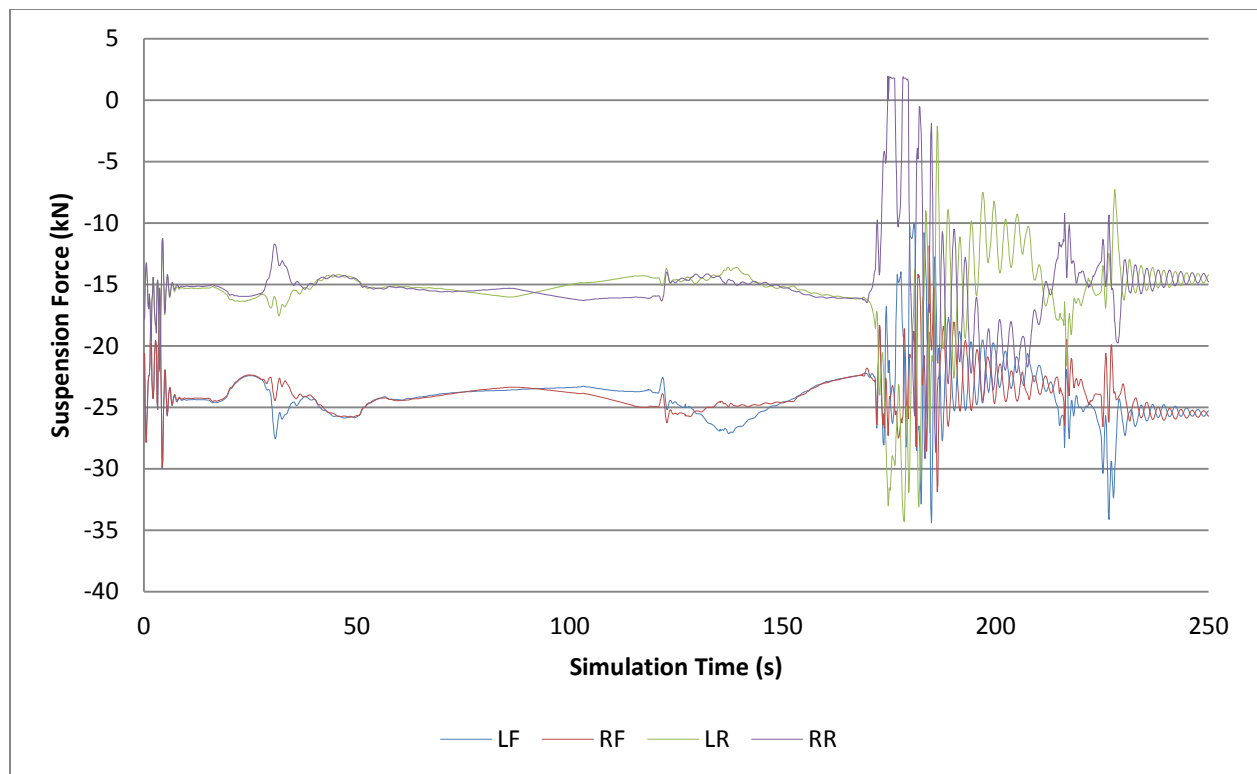


Figure 3.8: Simulated Suspension Forces

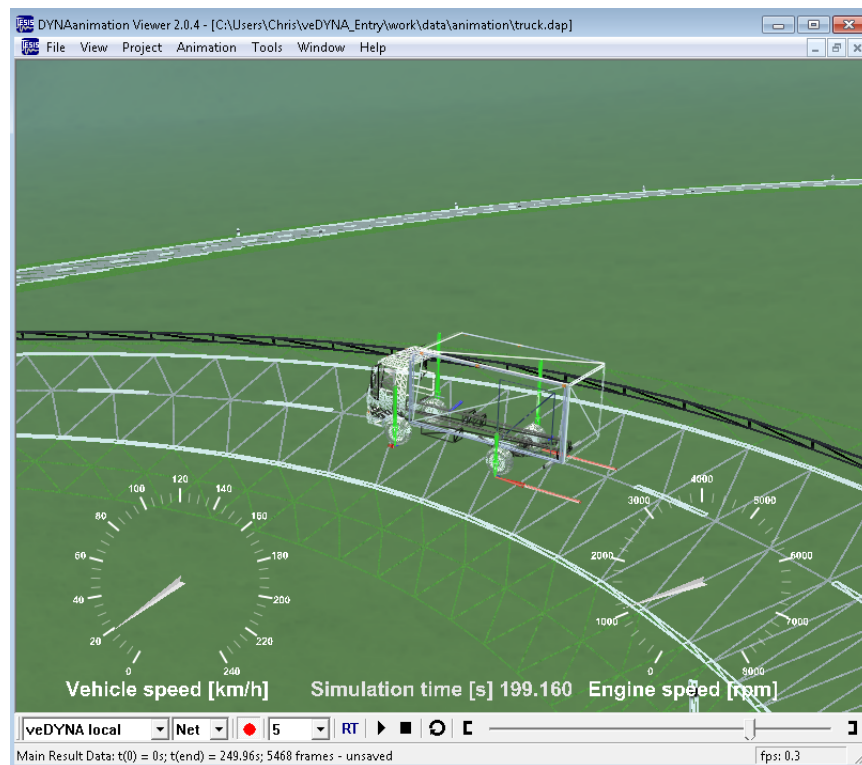


Figure 3.9: Simulated Light Truck in Left Hand Corner

Figure 3.10 shows the veDYNA vehicle pitch angle in radians versus the the gLA calculated pitch in g Level. Figure 3.11 also shows both the veDYNA and g Level pitch calculations but also includes the elevation profile of the simulation course. Note that the gLA trends substantially with both veDYNA pitch angle and that both methods correlate with changes in track elevation. The period of higher pitch volatility at the approximate simulation time of 175s is suspected to be in response to higher degrees of yaw due to a cornering series which compromised vehicle stability. This is supported by Figure 3.12 which shows both pitch calculations as well as the veDYNA calculated vehicle yaw response. For the purpose of this simulation the most important result is that the g Level pitch and veDYNA pitch measurement show a reasonable degree of agreement. Figure 3.13 shows the degree of correlation between the methods at ~51%. While this correlation is far from perfect, careful observation of Figure 3.10 shows that sudden changes in vehicle pitch angle is associated with and slightly preceded by volatility in the g Level pitch value.

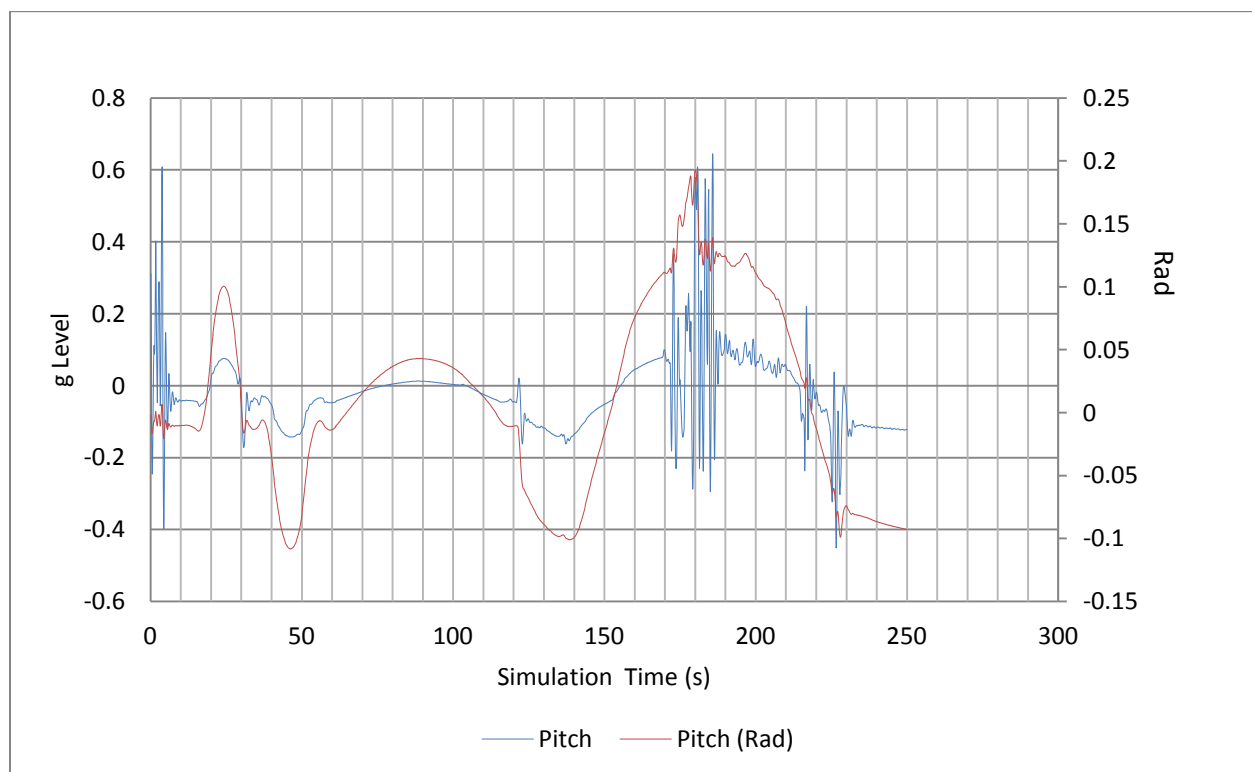


Figure 3.10: veDYNA and g Level Pitch Results

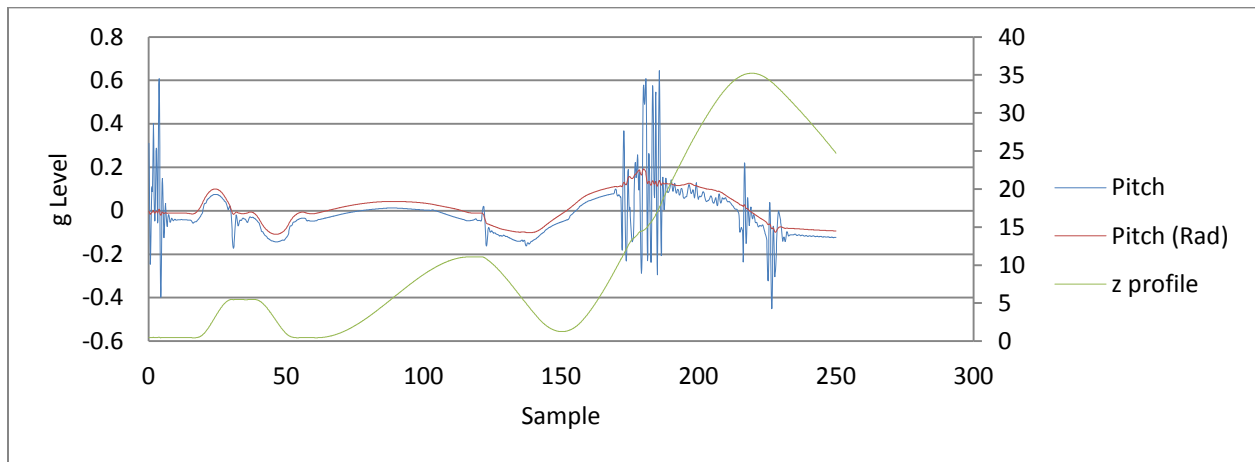


Figure 3.11: Pitch Results with Course Elevation

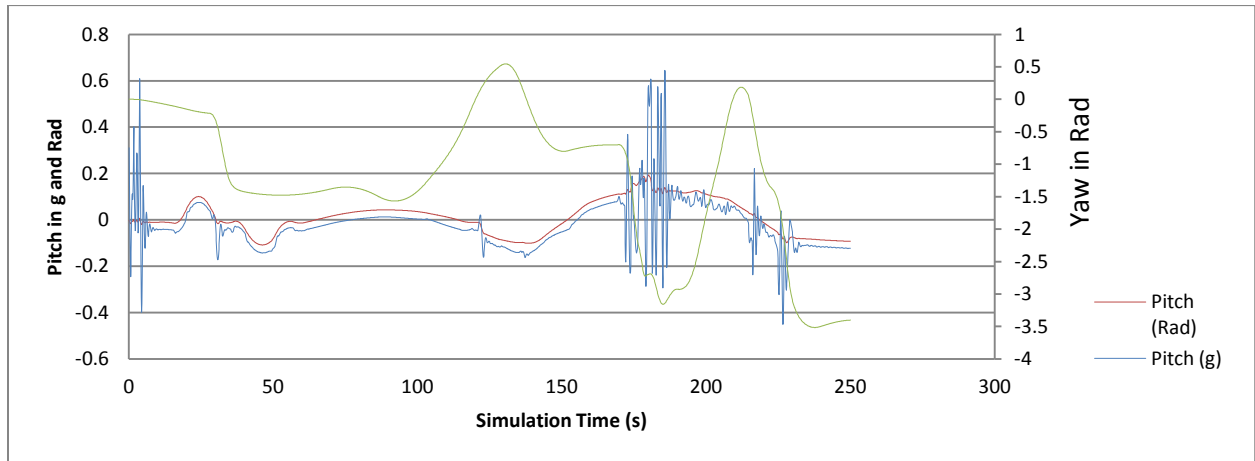


Figure 3.12: Vehicle Pitch and Yaw Response

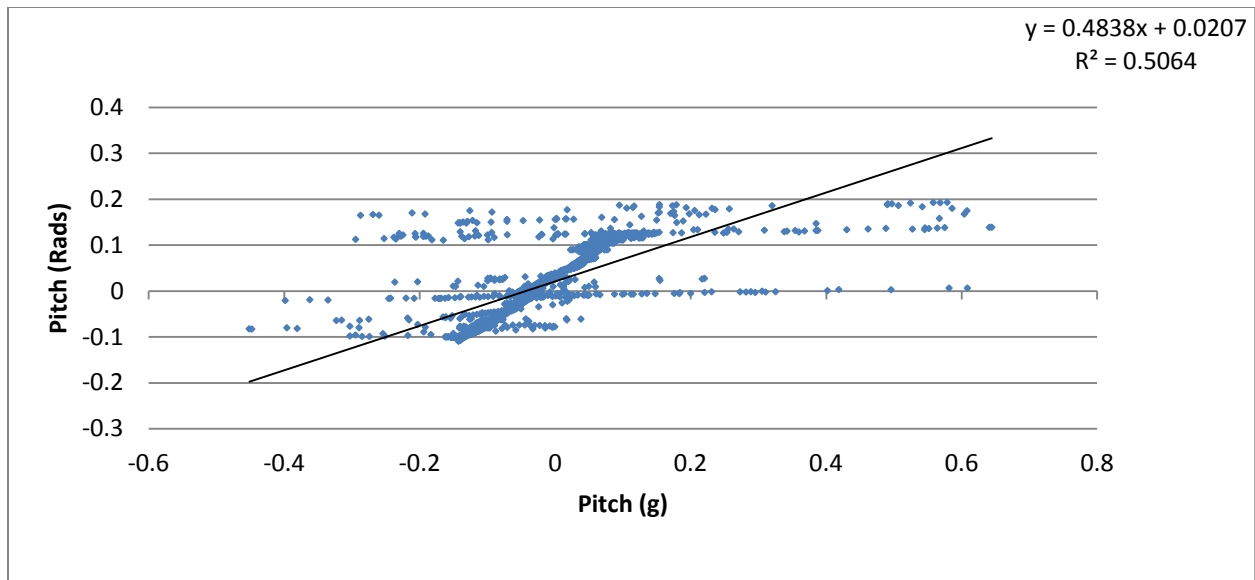


Figure 3.13: veDYNA vs. g Level Pitch Cross-Plot

As indicated in Figure 3.14 and, shown in Figure 3.15, there is a higher degree of correlation between the veDYNA calculated vehicle roll angle and the gLA calculated roll. The correlation coefficient between the two roll calculations is 78%. Figure 3.14 does show similar observation to that which was noted with pitch wherein the g Level response slightly precedes the vehicle angle response although the effect is much slighter for roll than pitch.

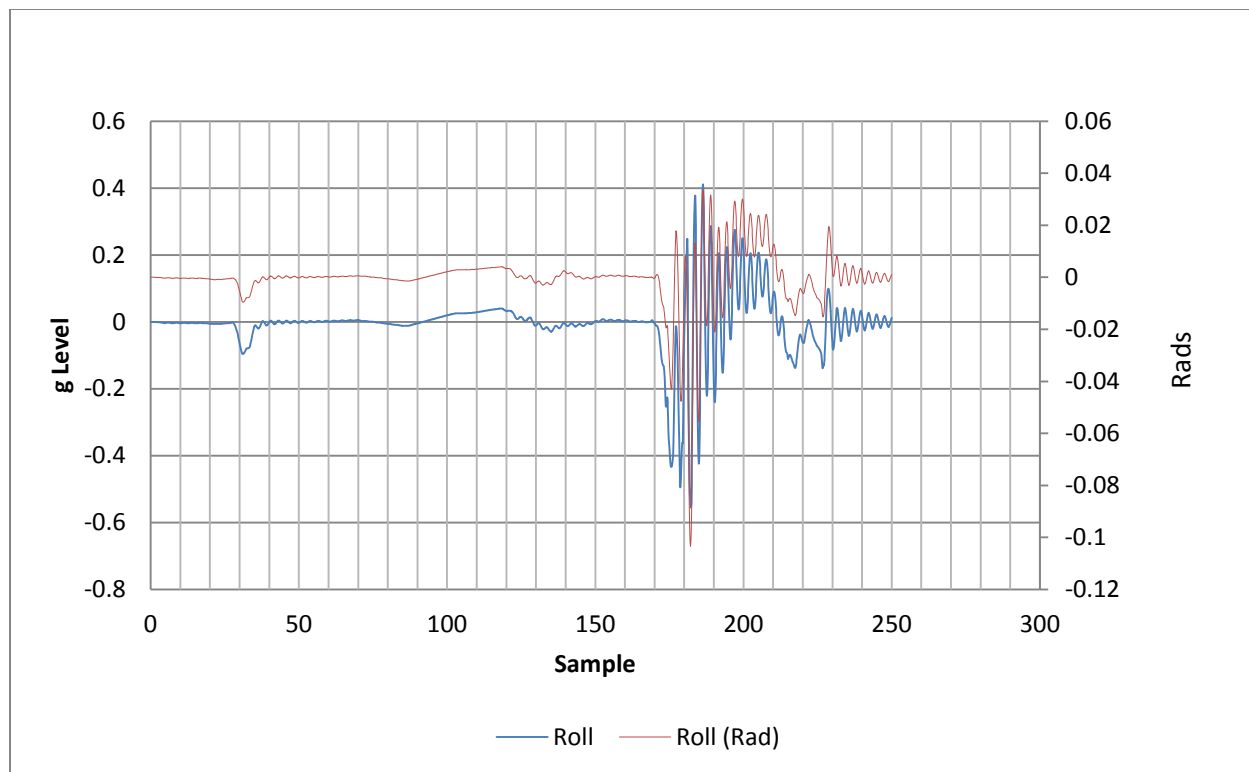


Figure 3.14:veDYNA and g Level Roll Results

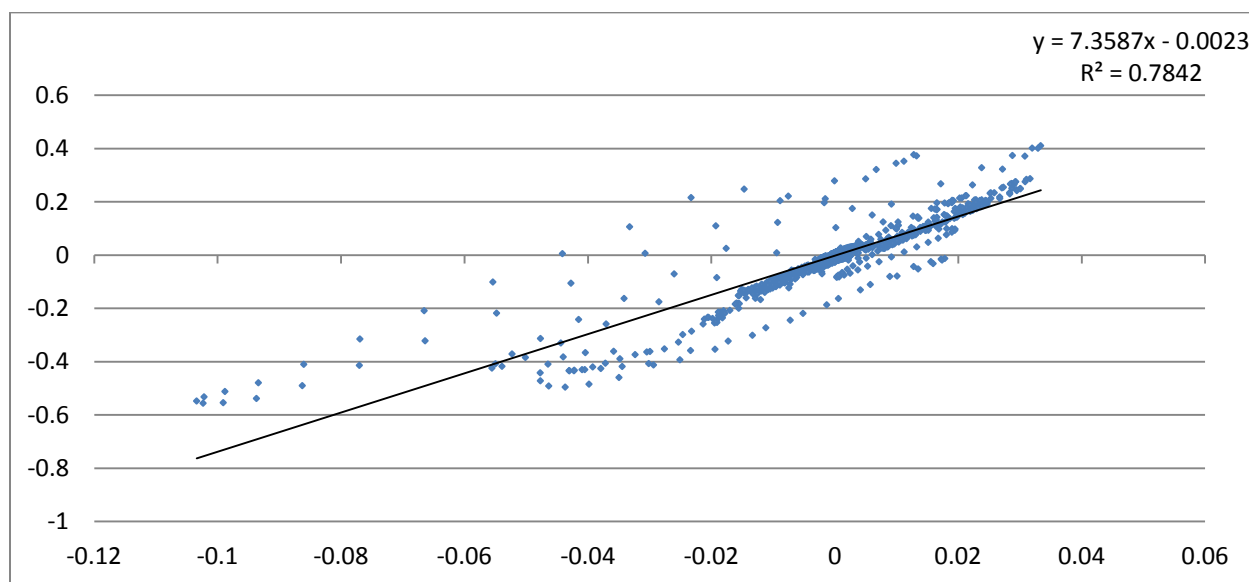


Figure 3.15: veDYNA vs g Level Roll Cross Plot



Section 3.3 showed a correlation between a reputable commercial vehicle dynamics simulator and the gLA method to have  $r^2$  values of 50% and 78% for pitch and roll respectively. It was also shown that the gLA method appears to be more sensitive than conventional modeling techniques. In future applications this sensitivity may be proven to be a useful characteristic of gLA. Overall this section has shown that the gLA method can be a valid indicator of vehicle kinematic performance.

### 3.4 Effect of Reference Point Selection

The gLA method is an indicator of vehicle kinematic performance, but it does not strictly measure vehicle motion. To accurately model a vehicles motion calculations must be performed about the vehicles COG or an inertial reference frame, deviations from these points will result in loss of accuracy. The strength of the gLA are that it conveys information about how the vehicle interacts with its environment, and its simplicity. Due to its simplicity the method is not capable of describing accurately actual vehicle motion on its own, however, in accepting this it can be considered acceptable to relax some of the assumptions required for accurate modeling of vehicle motion. The following section will show the effect of deviating the reference point location point from the COG. It should be noted that the most accurate location to perform the gLA in terms of direct correlation with vehicle motion modeling is the vehicles COG.

#### 3.4.1 Pitch Axis

Figure 3.16 illustrates how the distance to the pitch axis is varied from the front axle location. With the exception of the COG location axis locations were chosen arbitrarily. Figure 3.17, below, shows the g level pitch response from the veDYNA simulation data as the pitch axis location is varied. The results of Figure 3.17 clearly show that varying the location of the pitch axis does have an effect on calculated g levels, the effect is largely translational. Figure 3.18 displays the effect of varying the axis location on the standard deviation of the results. Although varying the location of the reference point does increase the volatility of the results this effect is considered small, for reasonable deviations and highly predictable.

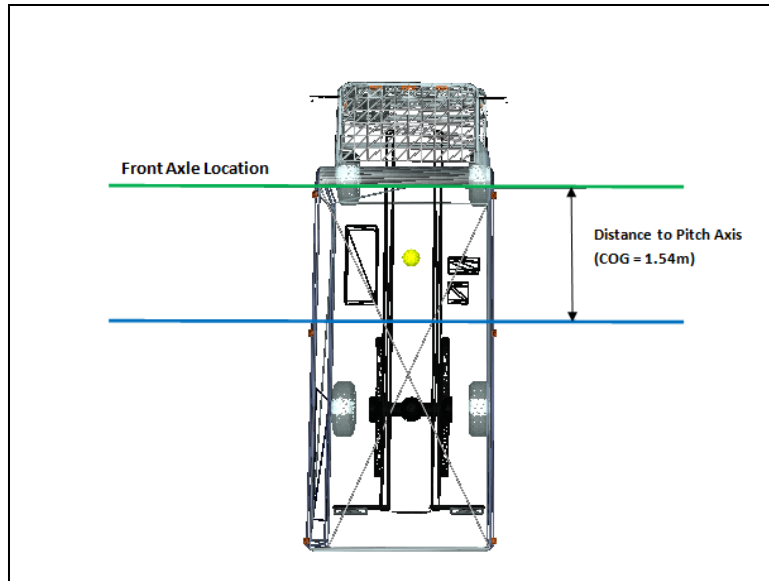


Figure 3.16: Pitch Axis Location Description

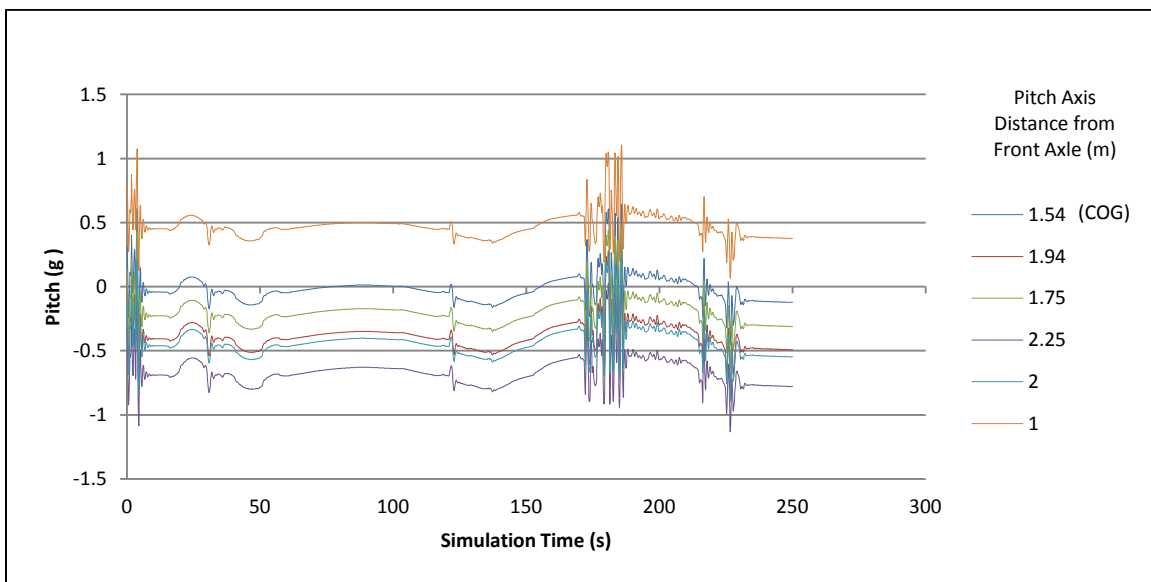


Figure 3.17: Pitch Response about Various Axis Locations

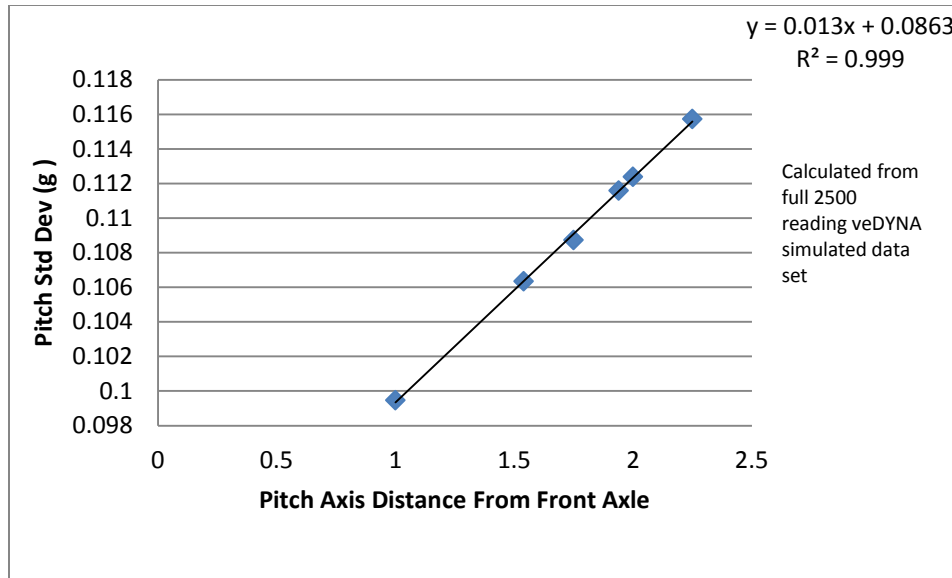


Figure 3.18: Standard Deviation of Pitch Readings with Varied Pitch Axis Locations

Figure 3.19 through Figure 3.21 show that the effect of moving the pitch axis location can be accurately predicted. Figure 3.20 and Figure 3.21 show summary histograms of linear regression analysis for each of the 2500 pitch responses, in g Level, from the simulated data set as pitch axis location was moved varied from 1m through to 2.25m from the front axle. These overall linear regression results were then used to calculate the pitch g Level about an axis 2m from the front axle for each of the 2500 readings. Table 3.2 summarizes the results of this calculation and shows that the effect of moving the axis of rotation can be accurately predicted.

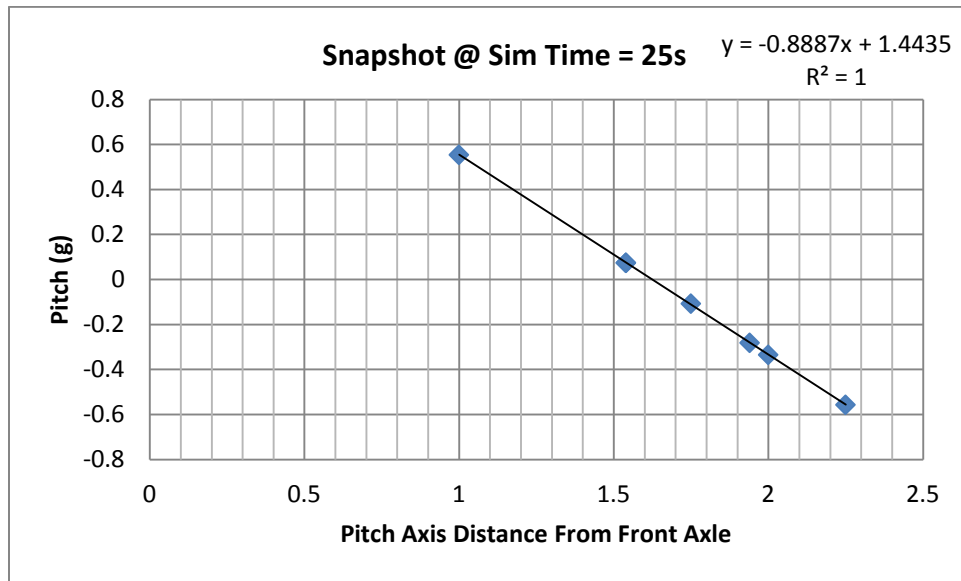


Figure 3.19: Effect of Pitch Axis Location on g Level

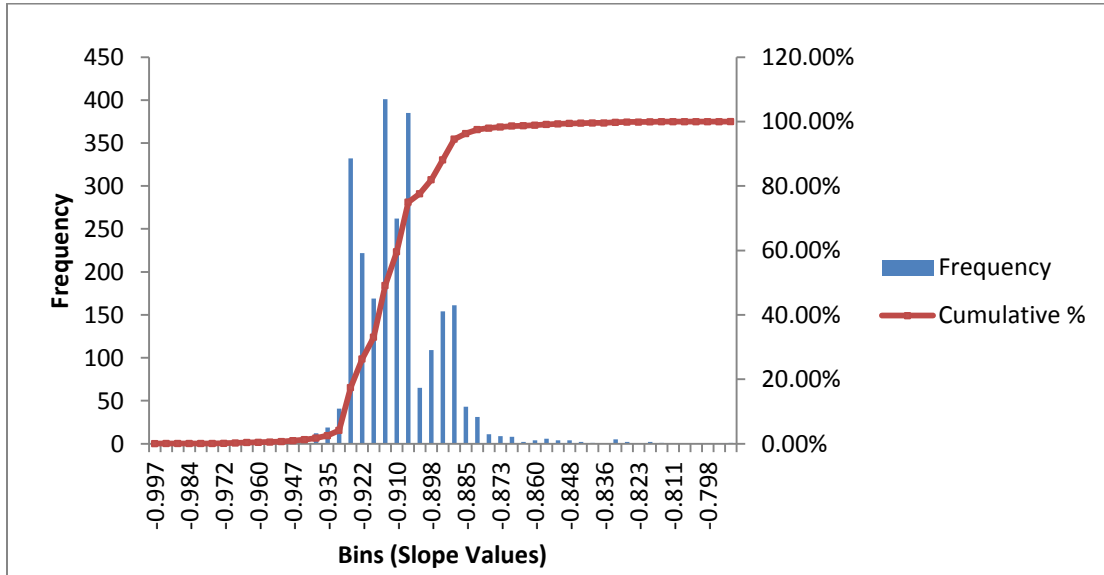


Figure 3.20: Calculated Linear Slope Values for Pitch Axis Variation

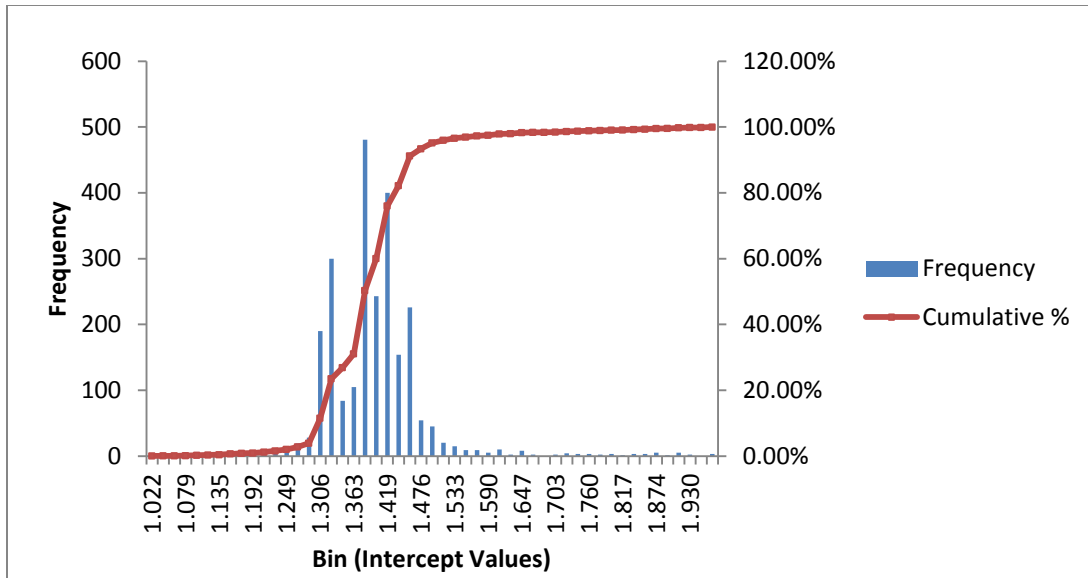


Figure 3.21: Calculated Intercept Values for Pitch Axis Variation

Average Pitch Linear Relationship - 2500 Readings (g Level)		
Slope	-0.911	Pitch = mx+b
Intercept	1.39	
Avg. Error	-0.001	Calc. About Pitch Axis 2m From Front Axle (x=2)

Table 3.2: Predicted Pitch Value from Linear Relationship

### 3.4.2 Roll Axis

Section 3.4.2 considers the effect of moving the location of the roll axis in an analogous manner as Section 3.4.1. Figure 3.22 illustrates the convention used to describe the roll axis location in relation to the vehicle. The results of this section show that, as with pitch, the effect of moving the axis about which roll is calculated results in primarily a translational effect. The effect of axis location on roll response is also shown to have an effect on the volatility of the results, however; the standard deviation in roll response follows a quadratic relationship with axis location. Although this deviation is present it is considered to be small and highly predictable.

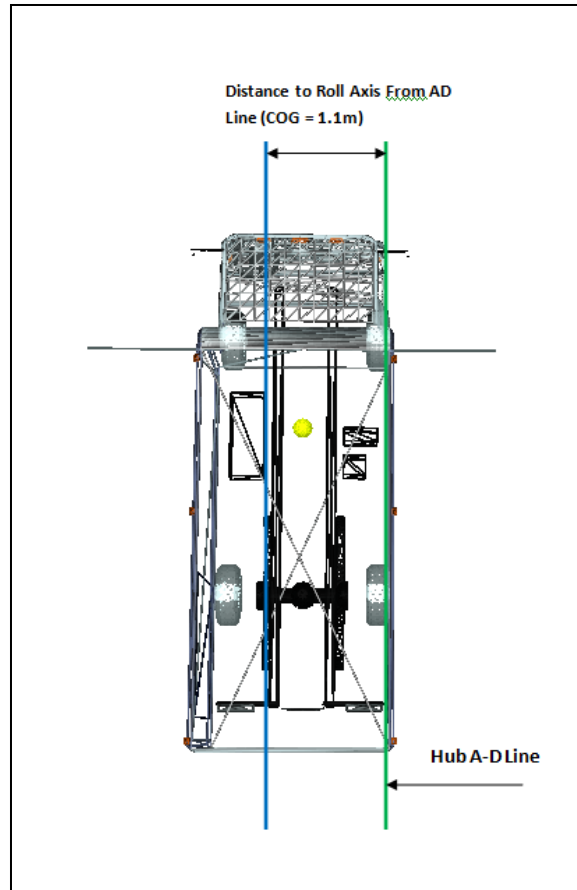


Figure 3.22: Roll Axis Location Description

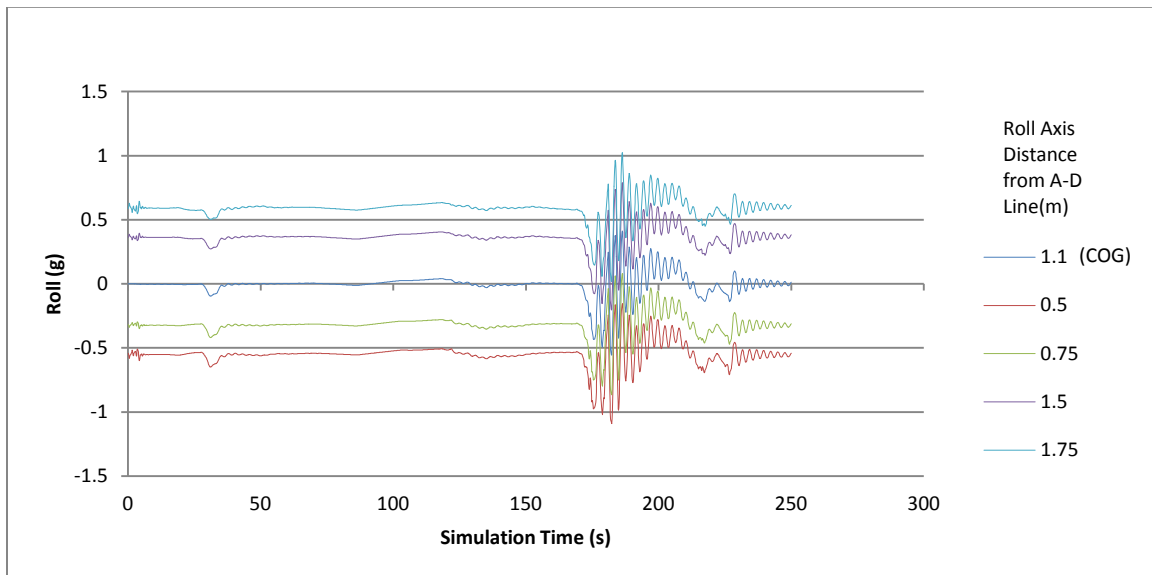


Figure 3.23: Roll Response about Various Axis Locations

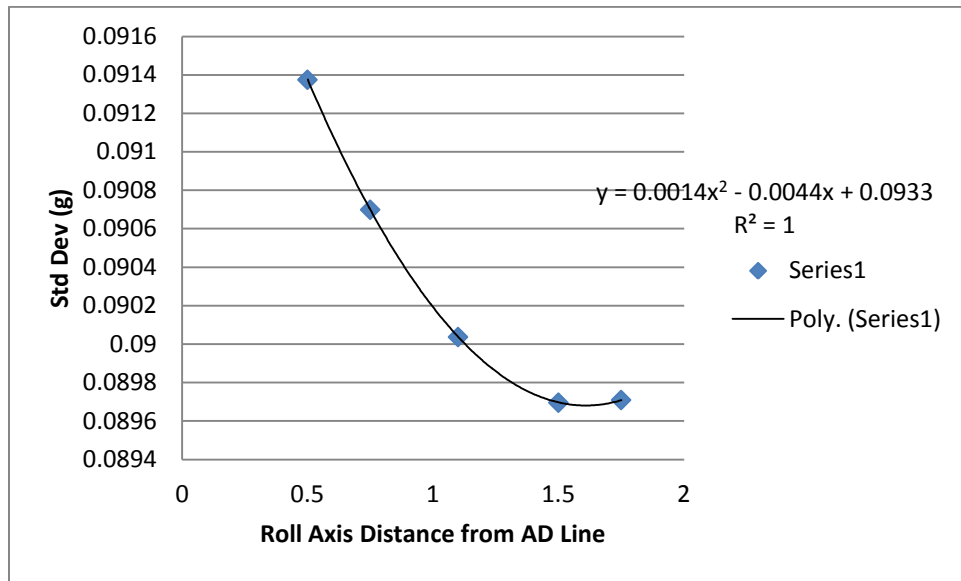


Figure 3.24: Standard Deviation of Roll Readings with Varied Roll Axis Location

Figure 3.25 through Figure 3.27 show that the effect of moving the roll axis location can be accurately predicted. Figure 3.26 and Figure 3.27 show summary histograms of linear regression analysis for each of the 2500 pitch responses, in g Level, from the simulated data set as pitch axis location was moved varied from 0.5m through to 1.75m from the front axle. These overall linear regression results were then used to calculate the pitch g Level about an axis 2m from the front axle for each of the 2500 readings. Table 3.3 summarizes the results of this calculation and shows that the effect of moving the axis of rotation can be accurately predicted.

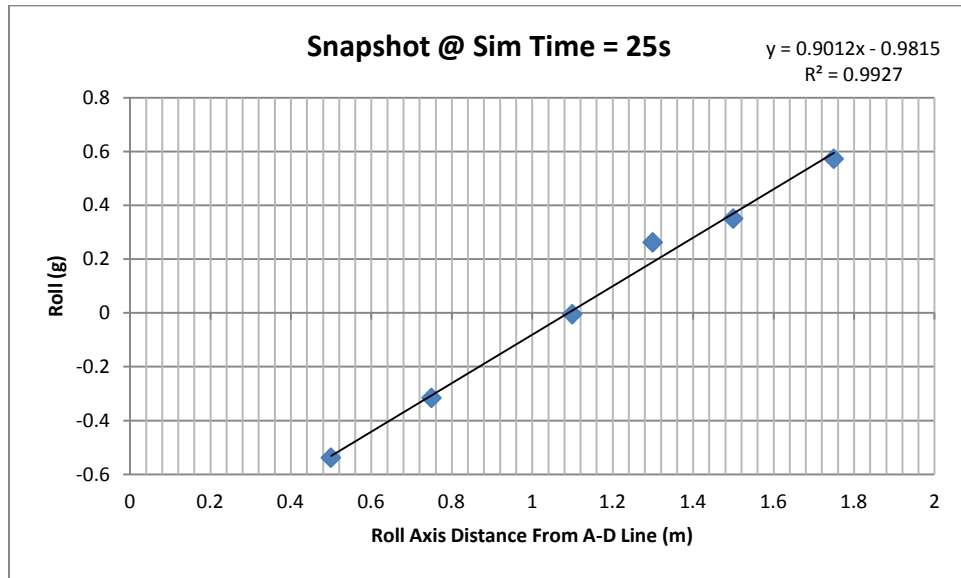


Figure 3.25: Effect of Roll Axis Location of g Level

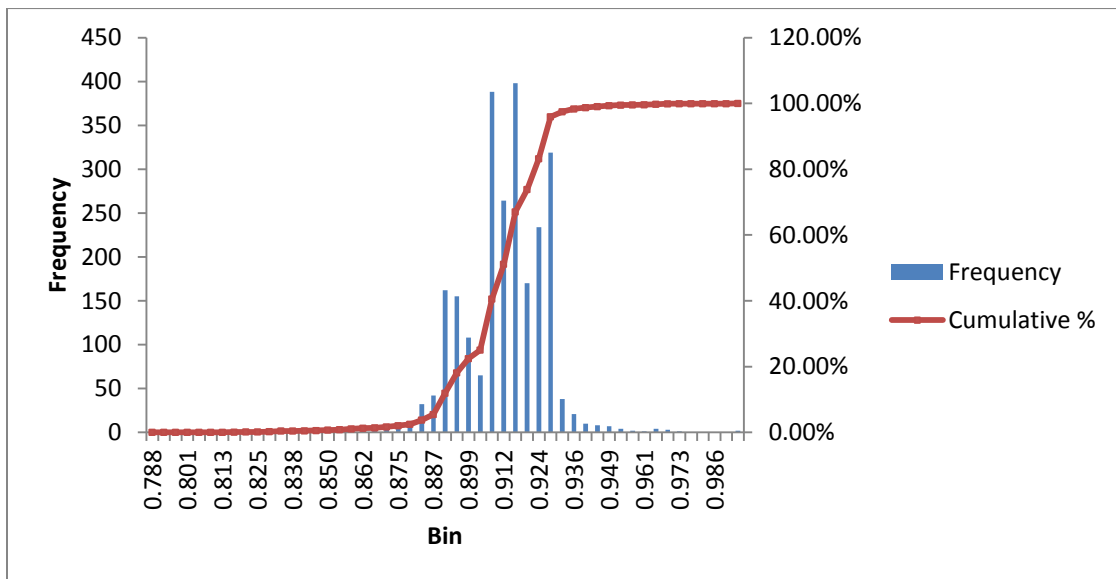


Figure 3.26: Calculated Linear Slope Values for Roll Axis Variation



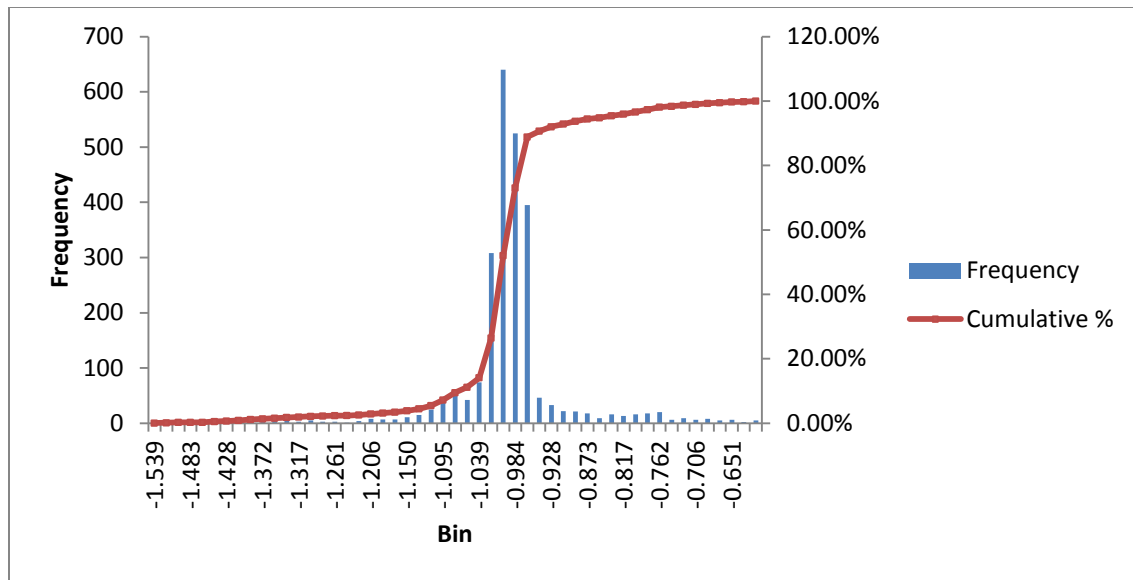


Figure 3.27: Calculated Intercept Values for Roll Axis Variation

Average Roll Linear Relationship - 2500 Readings (g Level)		
Slope	0.909	Roll = mx+b
Intercept	1.005	
Avg Error	0.091	Calc. About Roll Axis 1.3m From A-D Line (x=2)

Table 3.3: Predicted Roll Value from Linear Relationship

Section 3.3 and Section 3.4 have shown that gLA is able to provide a reasonable approximation to a multi-body vehicle dynamics analysis. Specifically gLA has been shown to capture major vehicle responses to variations in road and driving inputs. Further; these sections have shown that deviations in reference point location will still provide useful results and that the effect of these deviations can be accurately predicted.

## 4 Scale Model Testing

### 4.1 Scale Model Design and Construction

Typical operating conditions for a UAHT include periods of inclined and declined travel on ramps created during underground mine development. Because these ramps are typically designed with spiral sections as well as lengthy straight sections a typical haulage cycle demands that the vehicle travel while in many inclination and articulation combinations. The purpose of a UAHT is to remove rock from the mine and therefore most inclined travel is under fully loaded conditions while typical travel down ramp is empty. Because of the availability issues associated with procuring time on an operating UAHT as well as the complications inherent in attempting to reliably instrument a full scale vehicle for force measurements on each axle it was determined that a geometrically similar 1/5<sup>th</sup> scale model would be tested using a stationary snapshot approach to determine hub force readings at articulations and inclinations under dynamically similar loading conditions. These results could then be scaled up to a variety of UAHT classes and typical g level readings could be estimated using the mathematical approaches described in Section 2 and Section 2.11.

### 4.2 Design

Although the testing for this study was to be conducted with the vehicle stationary it was decided that the model should be constructed in such a fashion as to allow for versatility in future testing which could include tests under motion. This implied that geometries such as ground clearance and all load frame proportions must be maintained. Another design consideration was the design of a system which replicates the full scale vehicles front oscillating axle. The oscillating axle is found on all classes of suspension-less UAHT as well as many other articulating vehicles such as front end loaders and forestry equipment. In general the oscillating axle is used on four wheel drive heavy equipment which does not have axle mounted suspension. The purpose of the oscillating axle is to allow for greater stability and traction when operating in rough terrain by keeping all four tires in contact over uneven ground surfaces. In the case of UAHT the front axle is allowed to articulate while the rear axle is of a simple ridged design. The degree of oscillation the oscillating axle on a MT 431B haul truck is specified as 9° on either side of centre. Figure 4.1 below show the setting of the test unit's oscillating axle. Note that in these figures the front axle is being worked on upside down.

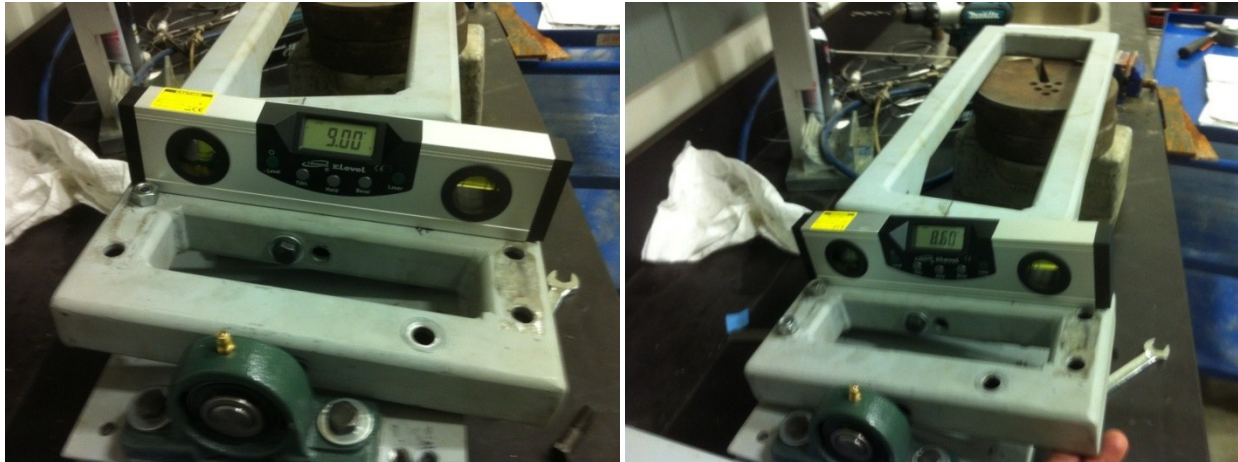


**Figure 4.1: (Left) Setting Left Hand Oscillation Limit, (Right) Setting Right Hand Oscillation Limit**

Final design of the test unit was based on general arrangement specifications for a model 431B Atlas Copco underground haul truck. The 431B was chosen as it is a simple vehicle design. Additionally the 431B is a relatively small haul truck given the modern payload ranges of up to 60,000kg meaning that a scaled gross vehicle weight of approximately 450kg would be considerably more manageable than the 880kg scaled gross vehicle weight which would have been required if a 60,000kg payload class of vehicle was chosen. The 431B was chosen, finally, due to the author's personal experience operating the unit. The test unit was comprised only of a load frame designed to carry a nominal payload of 224kg at a nominal tare weight of 230kg. Although the test unit was not designed as a perfect 1/5<sup>th</sup> scale model it was deemed an adequate model as frame geometries, ground clearance and axle load distribution of both tare and payload weight were designed to match as closely as possible to the full scale version.

#### **4.2.1 Detailed Design and Materials**

Detailed design work was completed at the University of Alberta Department of Chemical and Materials Engineering machine shop. Figure 4.2 through Figure 4.4 below show selected detailed designs; all detailed design drawings can be found as Appendix 4. Regarding construction, all load frame components are 1 ½" mild steel square tubing fillet welded together with all surfaces beveled, where possible all accessible edges were joined in this manner. All welding time was donated by Kevin Pelz of Devon Alberta. Post welding, the required boring of the front and rear mid-ship connections was completed at Devon Machine and Welding as the required equipment was not available at the University machine shop. Figure 4.5 through Figure 4.6 show selected photos of the welding process.

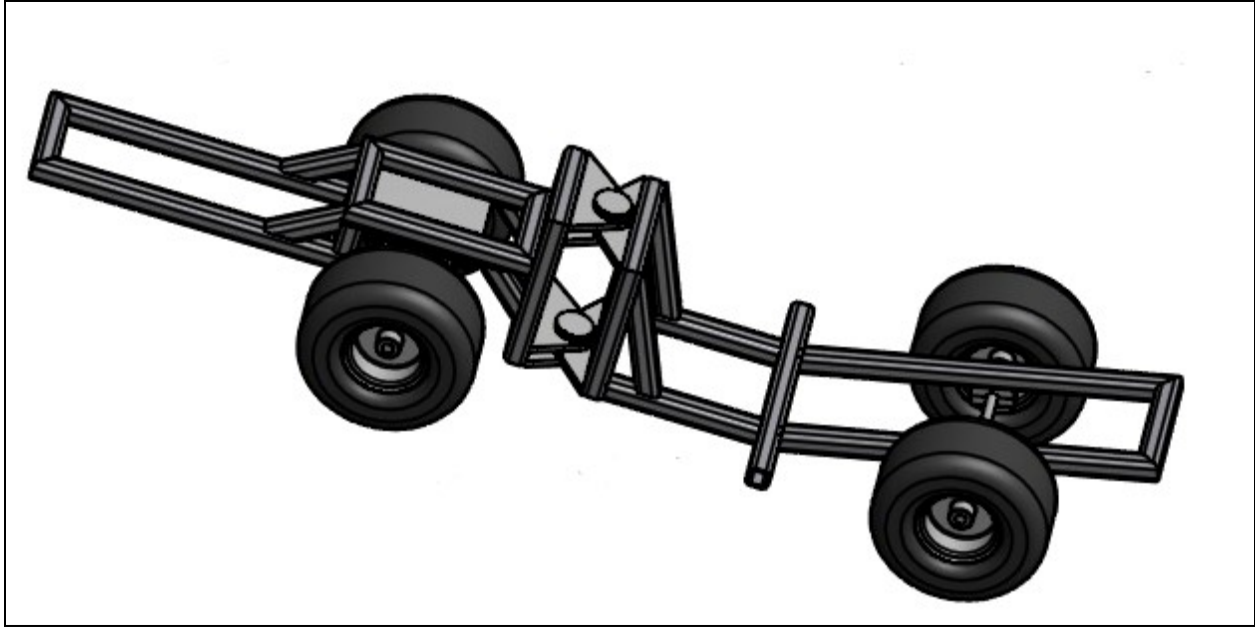


Figure 4.2:Isometric of Test Unit General Arrangement

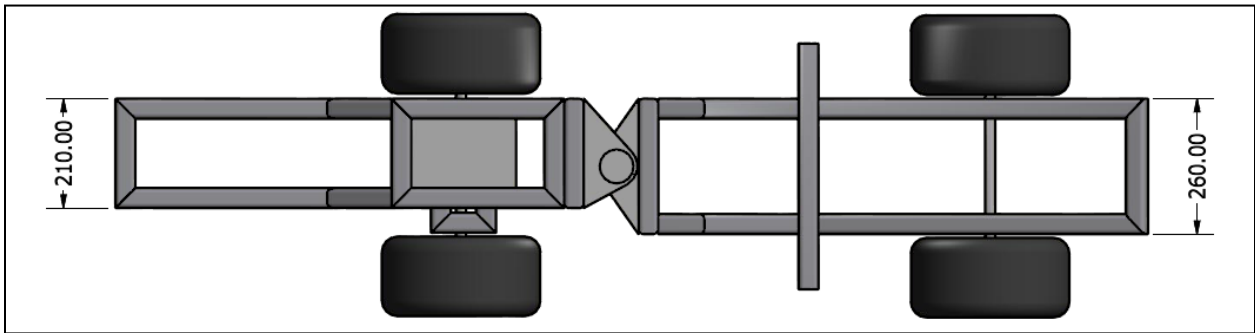


Figure 4.3: Plan View of Test Unit General Arrangement

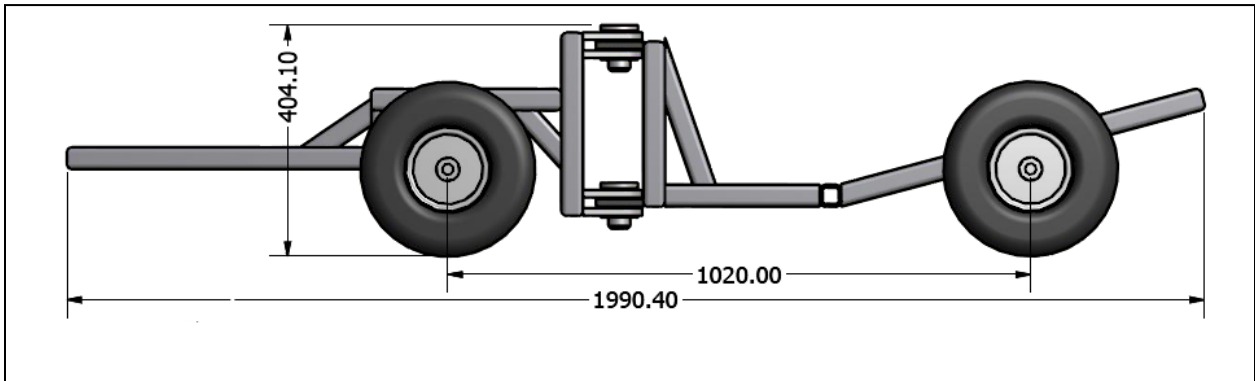


Figure 4.4:Section View of Test Unit General Arrangement



Figure 4.5: (Left) Rear Frame During Construction, (Right) Completed Front and Rear Frames

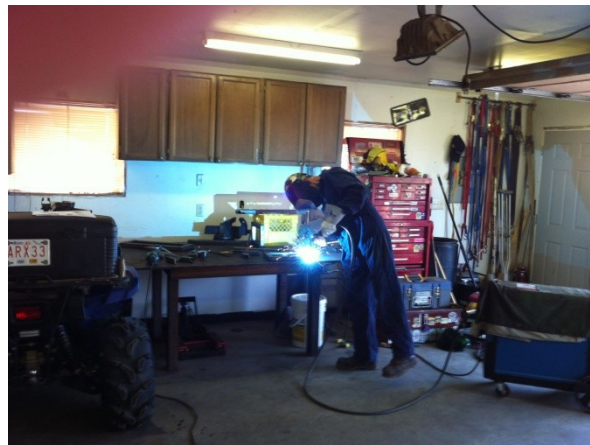


Figure 4.6: Welding Shop

Construction of the box for the test unit was hand built using two 6 cubic foot steel wheel barrows for materials and basic form. The box is not a perfect model of the box found on a full scale 431B haul truck however it can be considered an adequate model as it is formed around the frame which has been made geometrically similar. Although the box is not perfectly similar considerable effort was spent constructing the box in an effort to make the vehicle carry material in a manner reasonably similar to that of a full scale hauler with the end goal being that the distribution of payload force would closely



mimic a full scale hauler. Figure 4.7 through to Figure 4.10 below show the Test Unit in various stages of construction.



Figure 4.7(Left) Side View of Completed Test Unit Frame, (Right) Isometric View of Completed Test Unit Frame



Figure 4.8:(Right)Hand Built Test Unit Box, (Left) Front View of Completed Test Unit



Figure 4.9: Bottom View of Completed Test Unit



Figure 4.10: (Left) Side View of Completed Test Unit, (Right) Identifying Zero Articulation

Although testing was completed without wheels the vehicles tires were scaled from the 18.00R33 tires found on Atlas Copco's 431B general specifications to a 13X6.50-6 smooth tread golf cart tire made by Kenda Tires. This scale tire was chosen to maintain tire height for ground clearance and to provide maximum load capability as this tire is rated for a maximum load of 200kg. In retrospect a closer scale match would have been a Kenda 9X3.50-4 or the Kenda 11X4.00-5 however the choice of tire was not important to testing in this study as the unit was tested without tires.

### 4.3 Comments on Rigidity

No analysis of the test unit's rigidity or overall strength was conducted. This was not deemed necessary as this study is not concerned with stresses developed within the structure of the vehicle but rather the forces exerted on the ground due to tare weight and payload distribution and the resultant overall effect these force distributions have on the frame; this study is not concerned with the frame failure these forces could cause which would be dependent on the engineering parameters of the frame construction.

### 4.4 Comparison of Test Unit to Full Scale Atlas Copco MT431B

Figure 4.11 and Table 4.1 below illustrate the comparison of finished dimensions of the finished test unit frame to those of the MT4361B of which the test unit was based.

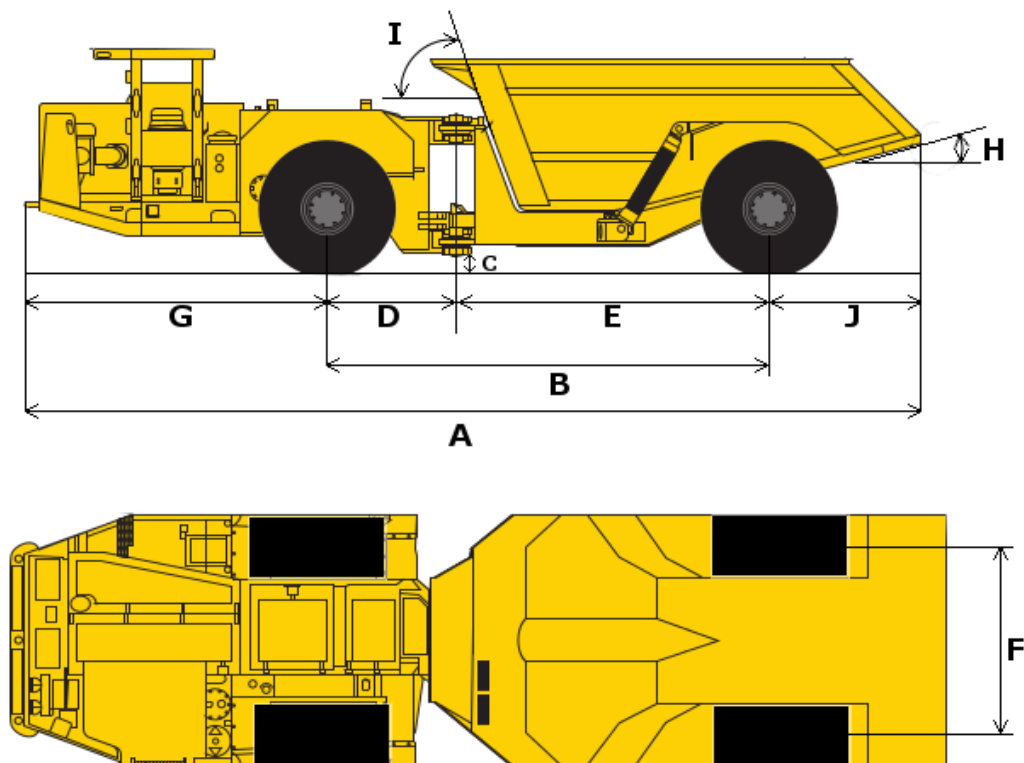


Figure 4.11: Comparison Dimensions



Measurement	Description	Units	Test Unit	431B	Target Scale	% Deviation
A	Overall Length	mm	1990	10180	2036	-2%
B	Wheel Base	mm	1020	5020	1004	2%
C	Clearance At Mid-ship (Not Incl. Pin on Test Unit)	mm	70	370	74	-5%
D	Mid-ship To Front Axle	mm	300	1465	293	2%
E	Mid-ship To Rear Axle	mm	715	3555	711	1%
F	Width Between Hubs	mm	428	2338	467.6	-8%
G	Length Front Axle To Front Of Vehicle	mm	670	3430	686	-2%
H	Box Inclination Angle	Degrees	15	15	14.5	3%
I	Front Box Angle	Degrees	71	76	76	-7%
J	Length Rear Axle To End Of Box	mm	310	1730	346	-10%

Table 4.1: Comparison of Test Unit to MT431B

## 4.5 Tare Weight Distribution between Test Unit and MT431B

The test unit constructed for this study was deemed adequate on geometric similarity to the full scale UAHT and its ability to representatively distribute tare weight and payload to the axle hubs for a full scale vehicle. Because the test unit was constructed as a load frame only without any mechanical components such as the motor, transmission, differentials, and cab amongst others, the test unit weighed 89.1kg as opposed to the ideal scaled tare weight of 224kg. To make up this difference a total of 1.04m<sup>2</sup> of 19.1mm (  $\frac{3}{4}$  ") thick plate steel was added to various areas of the frame. None of this added steel was intended to exactly match the weight of individual components on the full scale vehicle but rather to match the distribution of the vehicles tare weight on the front and rear axles. To achieve this desired distribution between the front and rear axles 53% (84kg) was positioned directly above the front axle and a total of 66% (107kg) was positioned on the front half of the test unit. Table 4.2 below shows the final distribution of tare weight of the test unit and the full scale MT431B haul truck. It should be noted that although the percent difference in axle distribution is large between the test unit and the MT431B this distribution was still considered acceptable as the ratio of front to rear tare weight distribution for the other haulers evaluated in this study ranges from approximately 66/33 to 75/25 front to rear axle distribution, see Section 5.1.1 for more information on parameters of other vehicles included in this study. Figure 4.12 shows the vehicle nearing final tare weight configuration.

	Tare Wt. (kg)	% Tare Wt. By Axle	
		Front	Rear
<b>Test Unit</b>	230	73%	27%
<b>MT431B</b>	28,000	68%	32%
<b>% Difference In Axle Distribution</b>		7%	-16%

Table 4.2: Test Unit Vs. MT431B Tare Weight Comparison



Figure 4.12: Test Unit With Final Tare Weight Arrangement

#### 4.5.1 Tare Weight Balance – Left to Right

Although this study was completed without access to either an operational full scale UAHT or detailed drawings of a full scale hauler it is assumed that under tare conditions a full scale UAHT would distribute the force equally between the left and right side of the vehicle however it was determined from visual inspection of several maintenance drawings that the front half of the load frame is not located in line with the geometric centerline of the vehicle. See Figure 4.13 below. It is assumed this offset is to allow enough lateral room for the four wheel drive system. This configuration may seem odd however it begins to make more sense when considering how narrow a MT432B is at 2,795mm compared with a Volvo A35F which is a 35 ton articulated surface hauler at 3,258mm wide and a common 2013 Ford F150 half ton pickup truck which is 2,463mm wide.

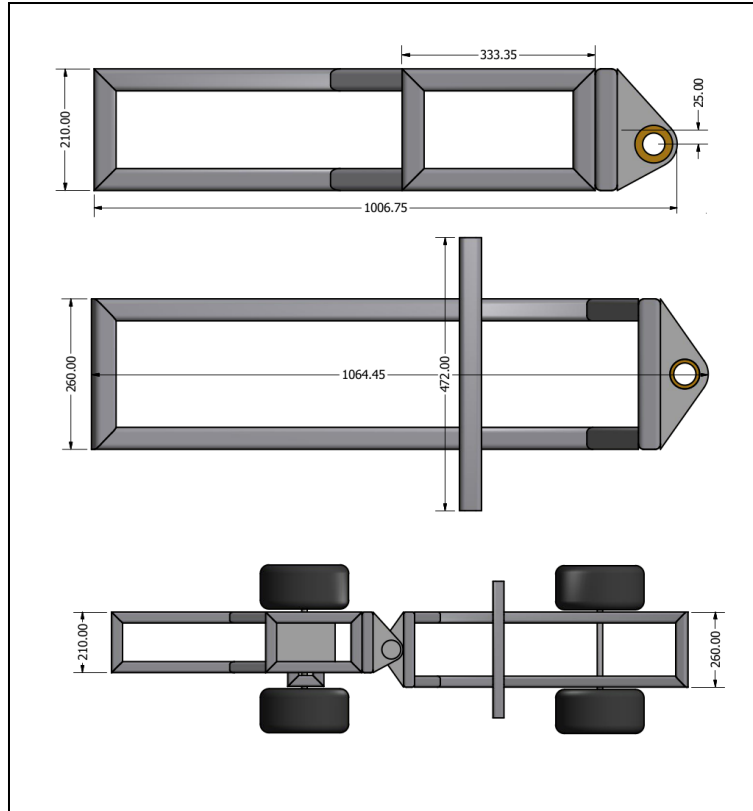


Figure 4.13: Offset Mid-ship Design

This offset load frame was built into the test unit; however because the test unit was not balanced on a component by component basis with the result was that the test unit was unbalanced under tare conditions with the right rear hub taking 11.5kg more weight than the rear left hub. The unbalanced load was shifted to the rear axle as the front must be balanced to prevent the frame from rotating on the oscillating axle. Given the constraints of space and weight, to stay close to scaled tare weight, on the rear half of the test unit it was decided that, although not ideal the unbalanced tare weight would not detrimentally impact the results of the study. Specifically this unbalanced state is acceptable as the effect of the unbalance can be separated mathematically in the results and because once the vehicle is loaded with payload any unbalanced load can be assumed to replicate any number of real world scenarios such as poor load placement, uneven operating surface, or even damaged suspension components if the hauler under investigation were equipped as such. Figure 4.14 below shows the distribution of load on each hub under zero articulation conditions and various loadings; note the convergence towards balance as load is applied. Also note that the front left and front right

distributions remained equal. Many attempts were made to balance the vehicle utilizing the placement of the plate steel used to achieve the required tare weight. Ultimately these attempts all resulted in the imbalance being shifted to the front axle which was deemed to be even more detrimental as it led to the vehicle tipping on the oscillating axle which would severely affect results and create an unnecessary hazard to the testing team. Figure 4.14 shows the Test Unit's convergence of load distribution from approximately a 70% Front, 30% Rear at tare condition to a near ideal 50% Front to 50% Rear distribution under fully loaded conditions.

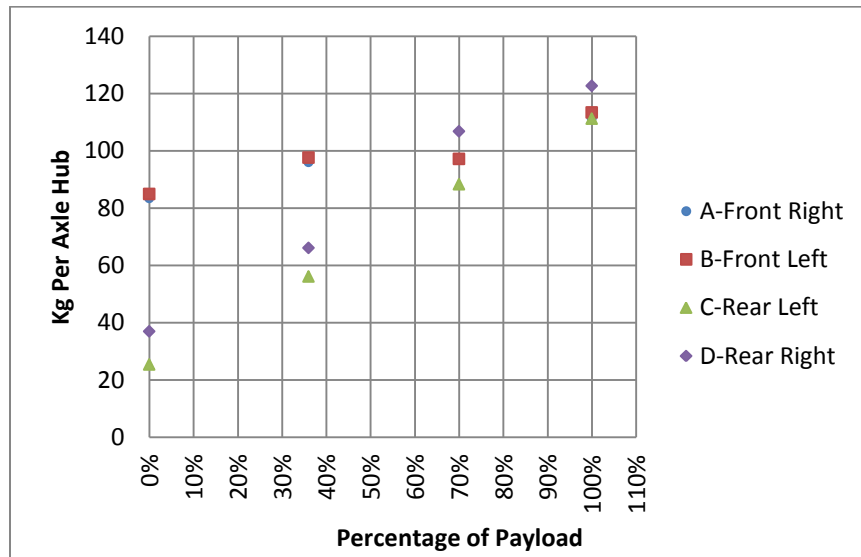


Figure 4.14: Test Unit Weight Distribution by Payload and Hub Location

## 4.6 Testing Method

The goal of scale model testing in this investigation was to obtain representative hub force measurements which could then be applied to several models and classes of UAHT via a payload scaling factor. These measurements and their application also provided an example of the implementation of the mathematical analysis presented in Section 2 and Section 3. In general, testing consisted of positioning the test unit in various loading, articulation and inclination combinations and recording the force at each hub location as indicated by load cells connected to the axles in place of hub assemblies. The articulation positions or  $-42^\circ$ ,  $-22.5^\circ$ ,  $0^\circ$ ,  $+22.5^\circ$ , and,  $+42.5^\circ$  were chosen to represent the extremes typically seen with UAHT, the zero articulation condition and a mid-point, together these angles provide a series of snapshots over the entire articulation range of a typical UAHT. Figure 4.15 below shows the

test unit during measurements in an inclined position. Note that the jack at the front of the unit is not holding any weight.



Figure 4.15: General Test Setup.

Testing began once the vehicle had been modified to approach the required tare weight as described in Section 4.5. Once the test unit had been constructed testing consisted of manually recording the force exerted at each hub location as measured by four 0-1000lb load cells while the load, articulation and inclination were varied for a minimum of three readings for each combination, an exception to this is that only two readings were recorded at 42° articulation, 4.5° inclination, and at 100% loading; it appears a third reading was simply overlooked. Three readings were taken to provide a representative average. Table 4.3 details the number of readings taken at each geometry and loading.

Table 4.3 includes all testing under varied inclinations for completeness. However, no inclined tests are included in the results beyond Section 4.8.2.2 as inclining the vehicle has the same effect as moving the payload of the vehicle closer to the rear axle.

Articulation (°)	Inclination (°)	Load	Number Of Readings	Articulation (°)	Inclination (°)	Load	Number Of Readings
-42	0	0%	4	22.5	0	0%	4
	0	36%	4		0	36%	4
	0	70%	3		0	70%	4
	0	100%	3		0	100%	4
	3.15	100%	3		3.15	100%	4
	4.5	100%	3		4.5	100%	3
	7.7	100%	3		7.7	100%	4
-22.5	0	0%	4	42	0	0%	4
	0	36%	4		0	36%	4
	0	70%	4		0	70%	4
	0	100%	4		0	100%	3
	3.15	100%	4		3.15	100%	3
	4.5	100%	4		4.5	100%	2
	7.7	100%	3		7.7	100%	3
0	0	0%	4				
	0	36%	4				
	0	70%	4				
	0	100%	4				
	3.15	100%	4				
	4.5	100%	3				
	7.7	100%	4				

Table 4.3: Completed Trials by Loading, Articulation and Inclination

#### 4.6.1 Test Axles

To complete testing in a safe and controllable manner, the original axles and wheel assemblies were replaced with 610mm (24") axles made out of 19.1mm (3/4") mild steel hex bar with holes drilled 428mm (17") apart to allow the test axle to be bolted to the top of the load cells. The spacing between the mounting holes on the test axle was equal to the spacing between hubs on the test units rolling axles. Hex bar was chosen to construct the test axles because it allowed for a flat surface of the axles to make direct contact with the flat surface of the load cell and because the six sided cross section of the hex bar fit better into the existing clam shell axle clamps on the test unit. See the Appendix 4 section for detailed design of the clam shell clamps. Although the wheels were removed for testing this was accounted for when setting the tare weight of the vehicle; specifically 18kg was added to the tare

weight of the test unit to account for the weight of the missing wheel assemblies. Figure 4.16 below shows the mounting of the test axle to the vehicle as well as the mounting on the load cell, including spacer and base plate. The load cells are discussed further in Section 4.6.4.

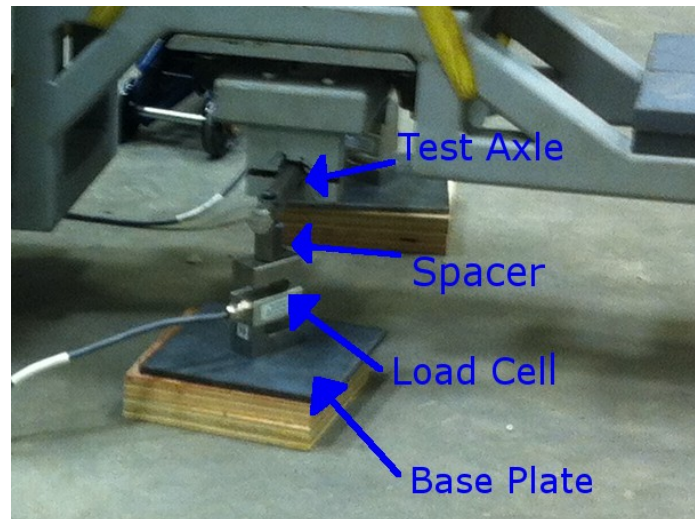


Figure 4.16: Test Axle and Load Cell Arrangement

#### 4.6.2 Control of Articulation Angle

Control and consistency of replication for the articulation angle was achieved by using a strip of  $1/8^{\text{th}}$  inch thick steel with holes drilled at appropriate intervals to set the articulation angle at each of the five settings, bolts were used to secure the front and rear sections with the angle bar. A second reason for the solid connection was to ensure that the vehicle did not unintentionally move during positioning or the recording of data. Figure 4.17 below shows the angle bar holding the vehicle in the positive  $22.5^{\circ}$  articulation position. While it is possible that this connection aided in minimizing the twist on the mid-ship it is assumed that the effect is minimal and that it would more likely simulate the effect of steering cylinders on full scale articulated machines.



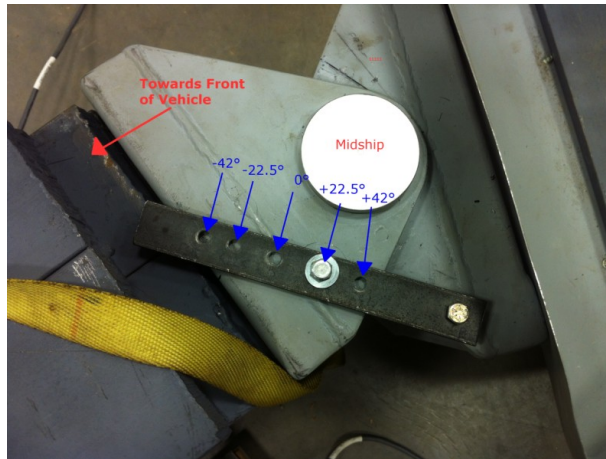


Figure 4.17: Articulation Control Plate

#### 4.6.3 Control of Inclination

Testing was conducted with the test unit level and inclined to angles of 3.2°, 4.5° and 7.7°, these angles were chosen to cover the typical ramp gradients a UAHT is likely to encounter. Each of the chosen inclinations were tested in combination with the unit in each of the five articulation positions. All inclined testing was done with the unit in the 100% loaded state as UAHT primary purpose is to transport rock uphill from the mine to the surface. Declined testing was not completed due primarily to time constraints. Control of the inclination was achieved by using a hydraulic jack to lift the front of the unit and simple wooden blocks were added under the base plates of the load cell until the desired inclination was achieved. Inclination was measured using a 229mm (9") digital iGaging eLevel with  $\pm 0.2^\circ$  accuracy. All inclination readings were taken with the level placed on the steel plate used to create tare weight as shown in Figure 4.18. Figure 4.18 shows the test unit in 7.7° inclination and -22.5° articulation. During all tests where the unit was inclined the axle clamps were loosened to allow the vehicle to move without twisting the load cells. Also, after each change in inclination the rear axle was momentarily lifted until the rear load cells were off the ground to ensure that any twist which may have been inadvertently induced on the load cell was relieved before testing continued.



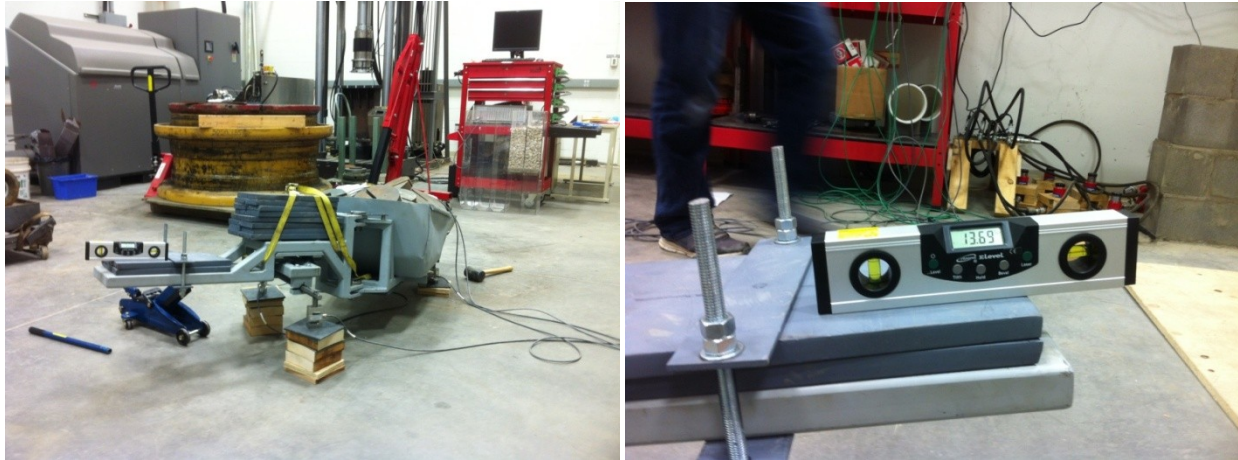


Figure 4.18: (Left) Test Unit in Articulated and Inclined Position, (Right) Inclination Measurement

#### 4.6.4 Data Acquisition and Instrumentation

As this study consists of snapshot measurements, where there was no continuous data recording during testing, the hub forces from each vehicle position were manually recorded into a spreadsheet from the read out of the data acquisition system. Specifically the instrumentation set up consisted of four 0 to 454kgf (1000lb) S-Beam load cells with 10V excitation and 3mV/V output. Accuracy of load cells was stated as  $\pm 0.03\%$  of full scale linearity,  $\pm 0.02\%$  of full scale hysteresis,  $\pm 0.01\%$  of full scale repeatability and  $\pm 1\%$  of full scale zero balance. These load cells input into a SoMat eDAQlite data acquisition processor reading at 10 hertz. Each load cell was powered by a bk precision 1670a power supply outputting the required 10V DC. All four load cells were purchased new for this test; a copy of the five point calibration certificate for each load cell is provided as an Appendix 3. Although the instrumentation used is capable of sub 0.45kgf (1lb) accuracy, all readings were recorded at the nearest 0.45kg (1lb) increment due to the difficulty associated with attempting to read the data which was continuously fluctuating in the tenths of decimal place. The loss of decimal place precision is not considered material, given that the scale of forces read by the load cells represents at most a 0.23 kg error on a 25kg reading, the lowest recorded during testing which equates to an additional 0.9% error. Note that this additional 0.9% error is only on the lowest recorded force, this error reduces to 0.23% at 100kg force readings and 0.15% at 150kg readings.

## 4.7 Payload and Hub Force Scaling Factor

In order to gain insight into the range of g level events created by full scale trucks this study used data captured at the model level to simulate nine haulers considered representative of several size classes of UAHT. For each hauler in the simulation the average hub forces were scaled by payload. Appendix 7 presents the derivation of the appropriate relationship between model and full scale hub forces via the Buckingham Pi Theorem and the payload scaling factor which is defined as follows:

$$PSF = \sqrt[3]{\left( \text{Payload}_{Full\ Scale} / \text{Payload}_{Model} \right)}$$

Equation 4.1

Appendix 7 contains the derivation of the following relationship between scale model and full scale hub forces:

$$F_{H_{Full\ Scale}} = F_{H_{Model}} (PSF^3)$$

Equation 4.2

### 4.7.1 Payload

To replicate the 28,125kg of payload a MT 431B is capable of carrying a 224kg combination of 20mm minus clean crushed gravel and steel dead weights were placed in the box of the test unit. A total of 112kg of gravel and 114kg of steel weights were used during testing. Payload was increased in increments which would approximate three pass loading by a model ST1030 LP scoop tram. The first replicated bucket consisted of 80kg of gravel contained in three plastic sacks. The second replicated pass consisted of the remaining 31.4kg of gravel and 45.4 kg of steel weights. The final replicated bucket consisted of 68.2kg of steel weights. The gravel was loaded first to fill the irregularly shaped box bed and provide a stable base for the steel weights to be added on to. No effort was made to be able to replicate load positioning because testing was completed as the payload was increased to each increment. Also to be noted is that it was not determined to be necessary to position the load in any

specifically desired manner, however; the testing team did add payload in an attempt to balance the load; however it was a visual estimation of where the load should be placed in the box much as a skilled scoop tram operator would under real world conditions. Table 4.4 below summarizes the payload used for testing while Figure 4.19 shows the cumulative loading. Figure 4.20, Figure 4.21 and Figure 4.22 show the test unit under 36%, 70% and 100% loading respectively.

Replicated Load	Gravel (kg)	Steel (kg)	Total
1	80.1	0	80.1
2	31.4	45.4	75.8
3	0	68.2	68.2
	<b>111.5</b>	<b>113.6</b>	<b>224.1</b>

Table 4.4: Payload by Replicated Load

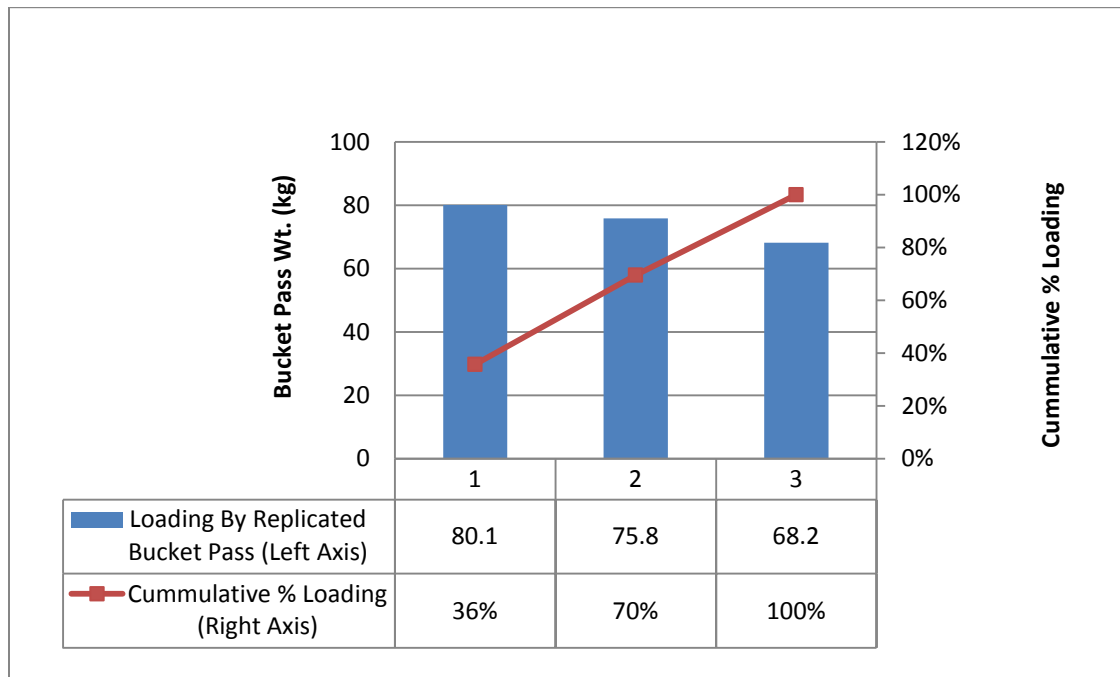


Figure 4.19: Test Unit Loading by Replicated Bucket Pass



Figure 4.20: Replicated Loading Pass #1



Figure 4.21: Replicated Loading Pass #2



Figure 4.22: Replicated Loading Pass #3

## 4.8 Results

The purpose of the scale model testing completed by this study is to demonstrate an application of the analytical method presented in mathematical investigation section and also to study the degree of g level events expected in various classes of UAHT. The following section begins by presenting the findings from experimentation with the scaled test unit followed by the scaling of these experimental forces to the range associated with the MT 431B haul truck and finally, the experimental forces are applied to the geometry and scale of various haul trucks found in both Atlas Copco's and Caterpillar's UAHT product lines.

### 4.8.1 Trials and Data Processing

A total of 128 tests were completed in March 2013. Prior to testing a spreadsheet was developed which carried out the application of the analytical method presented in Section 2 and Section 3, this spreadsheet was also used for manual data collection during testing as well as a simple modeling tool for the investigation which is discussed in the upcoming Section 5 and beyond. Although raw data from the test unit will be presented below, all application of the testing results to larger vehicles was carried out after averaging results from each unique articulation, inclination, loading combination as summarized by Table 4.3. All data was recorded in pounds and subsequently converted to kilograms

and Newtons prior to the calculation of moments, the following sections show all data in metric units however the raw data in standard imperial pounds can be found in Appendix 8.

#### 4.8.2 Raw Data

Figure 4.23 below displays the raw data by test number, expressed in Newtons, as recorded at each of the hub locations A, B, C, and D. From this figure it is obvious that the front locations, Hub A and Hub B, track very closely, with less than 400N separating the maximum and minimum readings. A second observation is that the rear hub locations, Hub C and Hub D, mirror each other. This mirroring effect is to be expected considering that as the vehicle is articulated from the zero articulation position through to the extremes of  $\pm 42.5^\circ$  articulation the total mass of the vehicle does not change however the distribution of this mass does change. The mirroring effect is especially evident with tests 40 through to approximately 55 with the peaks representing instances of extreme articulation. Not as readily apparent from Figure 4.23 is that although there is a higher degree of variation in the distribution of weight between the rear hubs, Hub C and Hub D, when payload is increased from 70% to 100% this variation still follows the mirroring trend. Figure 4.24 and Figure 4.25 show closer snapshots of tests 50 to 90 and 90 to 128 respectively. In these more detailed snapshots the mirroring effect is once again clearly visible. The increased variation in the scatter is due to the positioning of the final replicated scoop tram pass. Referring back to Figure 4.20, Figure 4.21 and Figure 4.22 it can be seen that the final load is positioned very near to the front of the box, this is very likely representative of real world loading conditions and this box location should carry the most payload per square meter of box floor because it is the deepest location in the box. Because this deepest spot is also, and intentionally, the closest to the centre of the wheel base the payload added to this location will proportionally add the largest amount of weight to the front axle. When more weight is added to the front axle of an articulated vehicle more weight is moved nearer and further from the rear axle as articulation occurs. It can be seen from the consistency of distribution at Hub A and Hub B in all three figures below that this additional weight on the front axle is not redistributed across the front axle as articulation occurs but rather the additional weight is distributed to and from the rear hubs, Hub C and Hub D, as the front of the vehicle articulates. It should be noted that as articulation occurs the geometry between the front hubs does not change relative to each other but the geometry between the front hubs and the mid-ship and each rear hub does change, which changes the moment arm with which each hub force operates about the mid-ship.



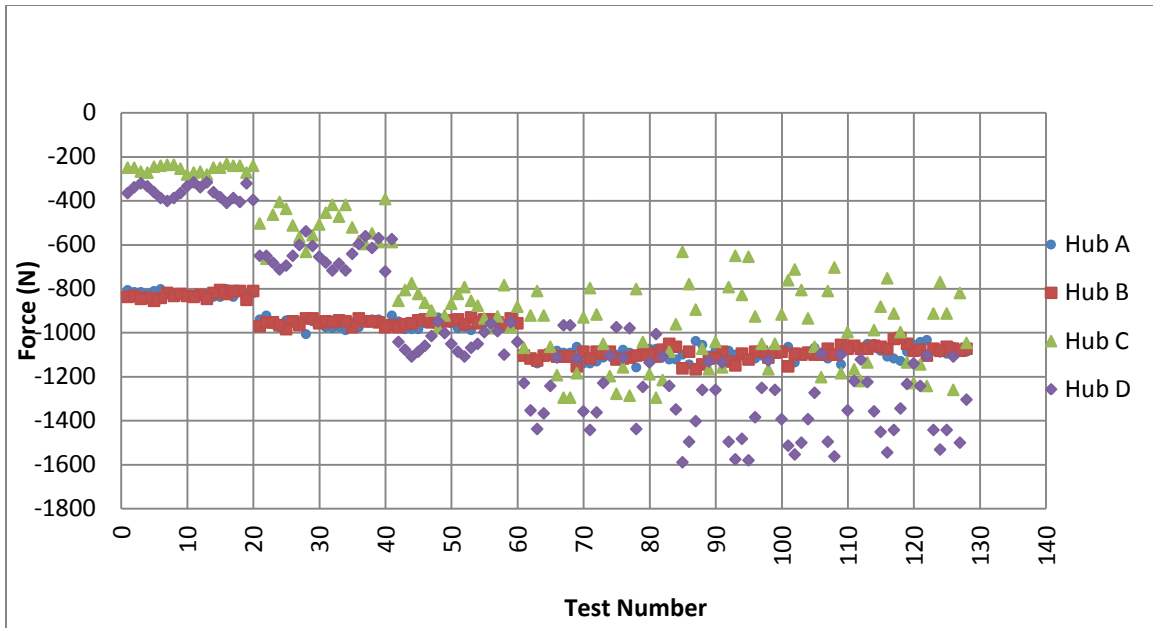


Figure 4.23: Raw Data Results by Trial Number

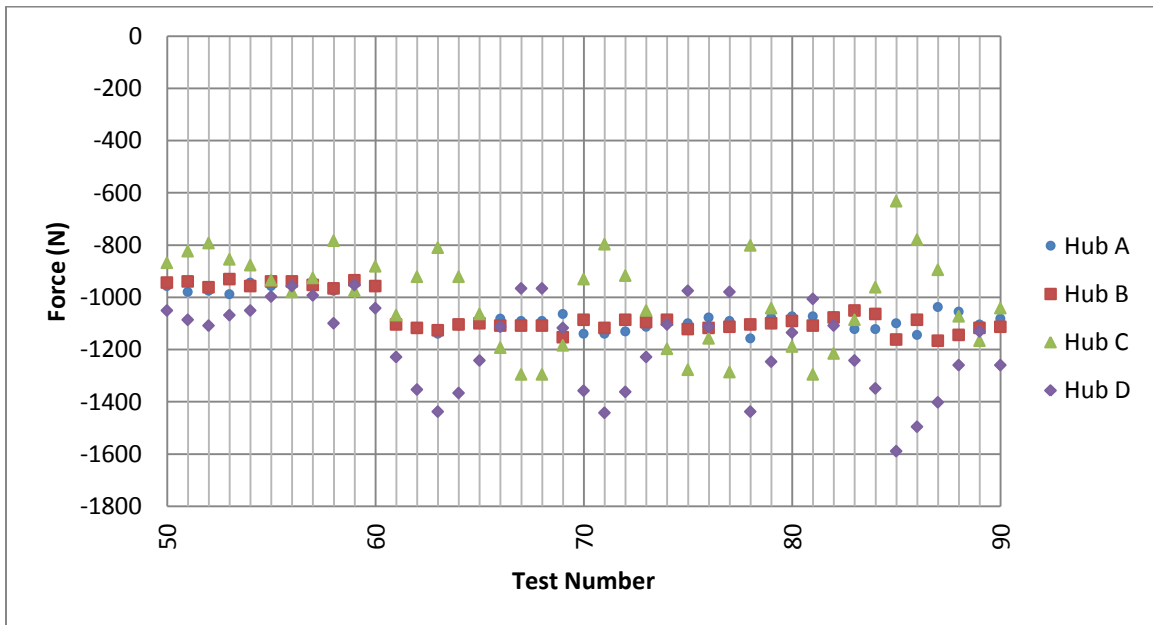


Figure 4.24: Raw Data Results, Trial #'s 50-90

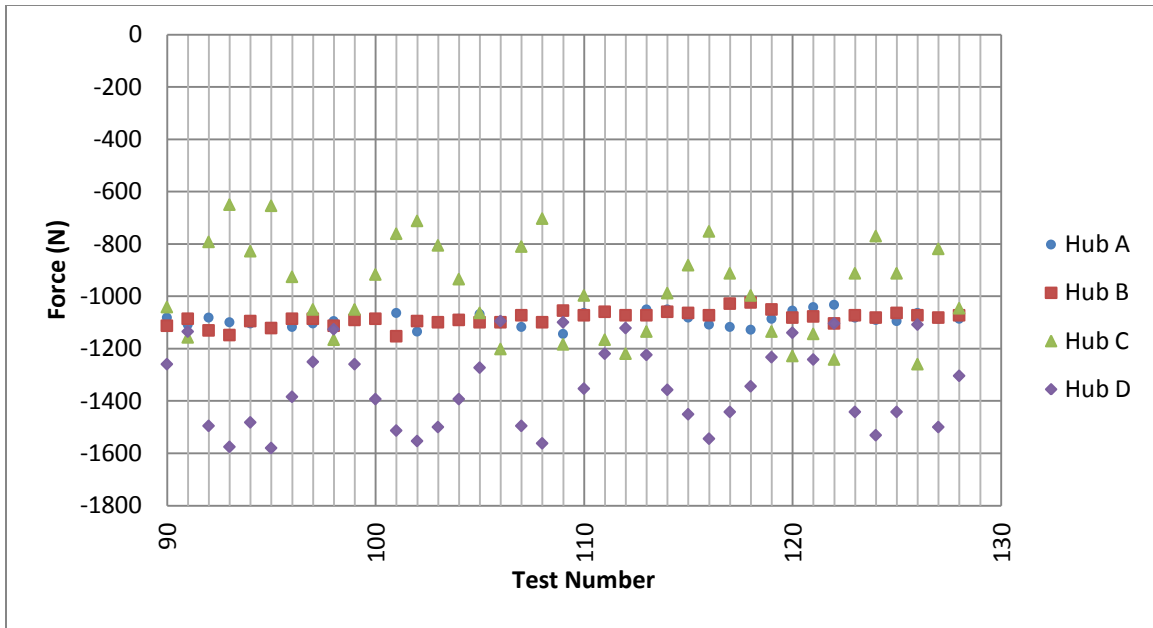


Figure 4.25: Raw Data Results, Trial #'s 90-128

#### 4.8.2.1 Effect of Load Balance on Raw Data

Table 4.5 below summarizes the zero articulation imbalances at the front and rear axles for each major payload increment. Results are also shown for each inclination. The table shows average readings for each combination. The purpose of this table is to show that under tare conditions the vehicle is not balanced across the rear axle. This imbalance is inherent to the offset design of the front load frame on the test unit and although this could be considered a serious design flaw in an actual production machine, as it would imply that all empty travel would be unbalanced not only front to back, as is to be expected, but also from left to right which would wear tires unevenly amongst other things. This study assumes that full scale production vehicles are indeed balanced left to right and that this is accomplished either by the weight and positioning of additional components such as the cab or another design aspect which could not be discerned from the limited information available. Notice how the imbalance is significantly reduced with load placement; although it is not fully understood why the imbalance fluctuates when the vehicle is inclined. The fluctuation with inclination could be caused by either shifting of the load or by undesired torsion being induced into the load cells as the vehicle was lifted to achieve the required incline. Although care was taken not to twist the load cells during any movements or repositioning of the vehicle it would still be a possible source of these fluctuations.



								Balance Left to Right		Balance Left to Right As % Of Axle Load	
% Total Payload	Articulation (°)	Inclination (°)	Hub A (N)	Hub B (N)	Hub C (N)	Hub D (N)	Total (N)	Front Axle	Rear Axle	Front Axle	Rear Axle
0% (Tare)	0	0	-819	-833	-249	-363	-2264	14	113	-0.9%	-18.5%
36%	0	0	-942	-958	-551	-649	-3099	16	98	-0.8%	-8.2%
70%	0	0	-953	-953	-867	-1048	-3821	0	181	0.0%	-9.5%
100%	0	0	-1092	-1112	-1091	-1204	-4500	20	112	-0.9%	-4.9%
100%	0	3.2	-1080	-1097	-1017	-1298	-4492	17	281	-0.8%	-12.2%
100%	0	4.5	-1098	-1087	-926	-1390	-4500	-10	464	0.5%	-20.1%
100%	0	7.7	-1068	-1065	-1056	-1289	-4478	-4	234	0.2%	-10.0%

Table 4.5: Test Unit - Left to Right Balance

#### 4.8.2.2 Total Gross Vehicle Weight and Gross Vehicle Weight Distribution

Although Figure 4.23 shows the degree of variation that occurred across each axle during testing and Table 4.5 shows the imbalance at each axle Figure 4.26 below shows the consistency in measured total Gross Vehicle Weight (GVW). This consistency in GVW is to be expected and was the first metrics analyzed during testing to ensure the results being recorded would be reliable.

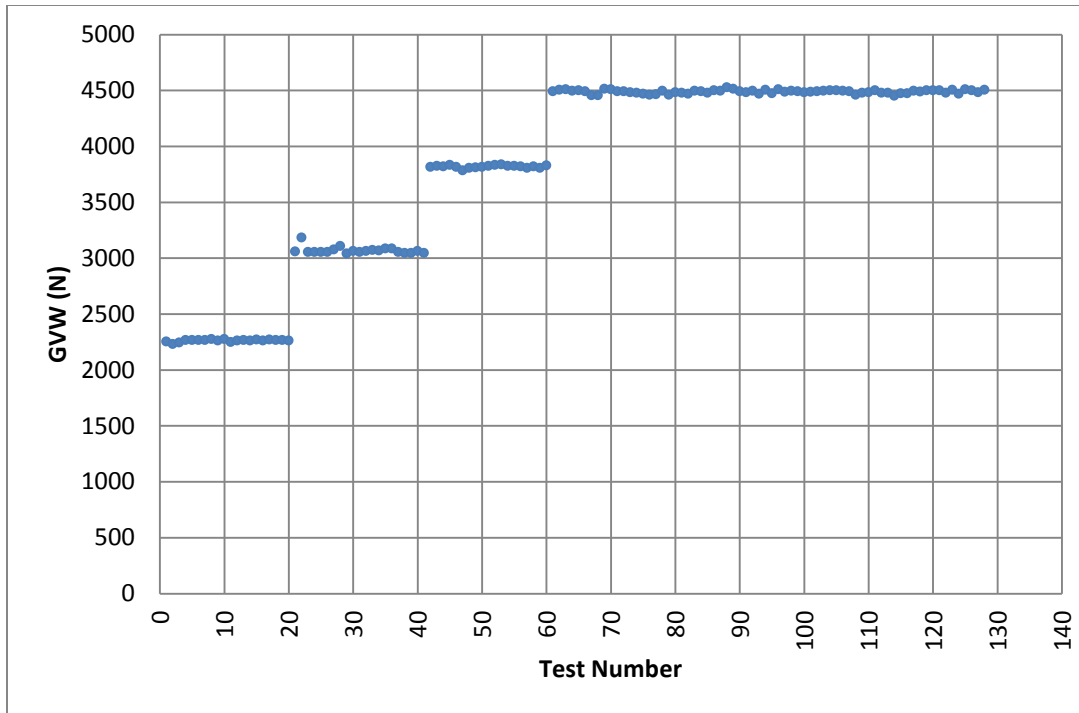


Figure 4.26: Gross Vehicle Weight by Test Number

Although consistency in GVW is to be expected one of the key initial findings of testing was how the test unit would distribute overall GVW across the front and rear axles. It is known from literature on Caterpillar's product line, and it is reasonable to assume that all UAHT designs would strive for this, that under loaded conditions total GVW should be split evenly between the front and rear axles. Figure 4.27 below shows that the GVW distribution does indeed converge on the 50/50 axle distribution as load is applied until test 79 when inclined testing began. Once the vehicle is inclined it stands to reason that more weight would be distributed to the rear axle and less on the front axle as can be seen in Figure 4.27 by the divergence of the load on each axle once inclined testing begins at test 79. This weight distribution behavior of the Test Unit is a major indication that the model is in fact responding as a full scale UAHT would, lending confidence to validity of the collected data. Note the small and consistent cyclical effect that articulation has on the distribution of weight on each axle. This cyclical effect is created in much the same manner as discussed in Section 4.8.2 which highlighted the mirrored effect across the rear axle as the weight on the front axle is moved closer and further away from the rear axle during articulation.

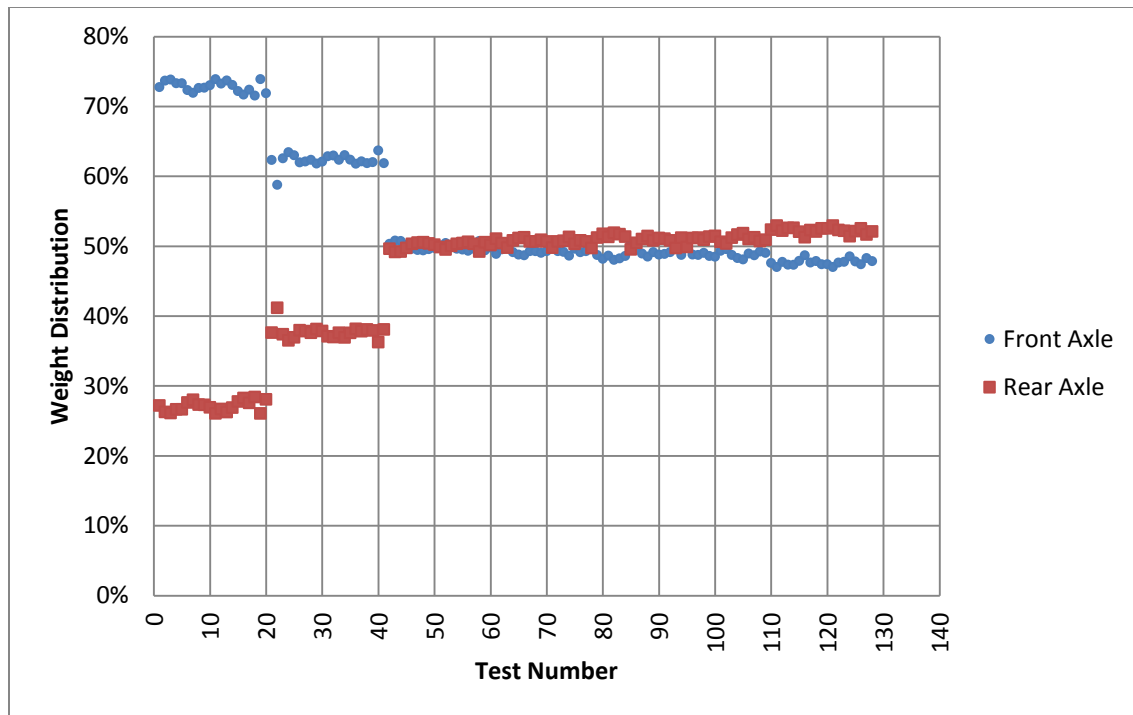


Figure 4.27: GVW Distribution By Test Number

Figure 4.23 through to Figure 4.27 present basic weight distribution and GVW data in relation to each individual test number. Figure 4.28 below shows the average proportion of GVW distributed to each axle at 0% (tare), 36%, 70% and 100% proportion of total payload for all tests with inclination equal to zero.

Figure 4.28 serves to show that under fully loaded conditions the vehicle is nearly in balance, 49%:51% front to rear, implying that any overall moments created about the mid-ship are due to either geometry, which can be interpreted to include the effects of articulation, or imbalance left to right. A key insight provided by Figure 4.27 and Figure 4.28 is that the amount of weight shifted between the front and a rear axle during articulation is very little. This may not be particularly intuitive however it makes sense given that so much of the tare weight on the front half of the vehicle is actually positioned over the axle as the following logic will explain. The motor on the MT431B is listed as a 400hp 12.7L Detroit Diesel which weighs 1193 kg [71] and the total amount of weight on the front axle under tare conditions is 19,880kg. Referring back to Figure 4.11 and Table 4.2 it can be seen that the motor is the only major component positioned ahead of the front axle and with less than 1.5m from the front axle to the mid-ship it is reasonable to assume that the significant majority of the remaining 18,687kg of front axle tare

weight is located directly over the front axle. Because this weight is directly over the axle which moves during articulation the weight it supports does not change only the geometry relative to the mid-ship and rear half of the vehicle changes.

Figure 4.27 shows a trend of convergence towards a 50%:50% weight distribution from test number 1 to approximately test number 60 after which point a divergence is seen. The convergence section is a result of the increase in payload having the effect of equalizing the GVW distribution. Test numbers 1 through 65 were completed at zero inclination, however the divergence seen on tests beyond number 65 is a result of inclination being increased.

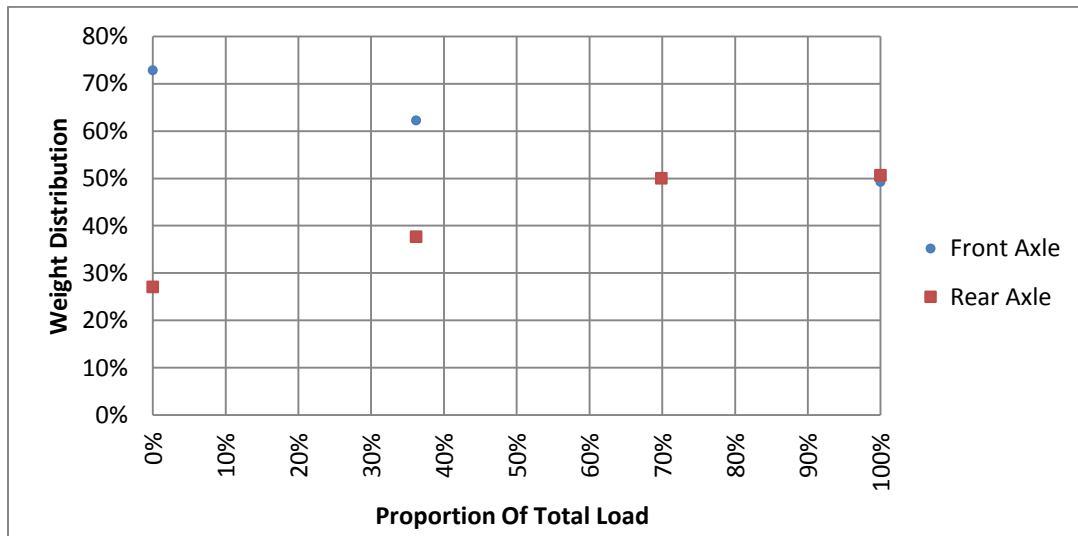


Figure 4.28: Proportion of GVW per Axle

#### 4.8.3 Moment and g Level Analysis

The previous section discussed some of the basic results of this study which can be made from the raw, unprocessed data. The following sections present and discuss the analysis of the raw data using the mathematical procedure outlined in Section 2 and Section 2.11. The goal of this data processing is to present, in terms of moments and gLA, the effects on a UAHT due to changes in loading, articulation and inclination. For simplicity the analysis completed in the following section uses averaged results for each of the loading, articulation and inclination combinations outlined in Table 4.3.

The entire mathematical process used in the following analysis is discussed in detail in the Mathematical Investigation section, however; the most relevant outputs of the analysis are: the magnitude of the resultant moment about point O, the sense of rotation of the resultant moment and the rack, pitch, roll and twist expressed in g levels created by the resultant moment. Note that twist is the description of the overall cumulative moment about its natural axis whereas Rack is defined as specifically about the Q1 or Q2, 45° axis as described in Section 3.2. To give a better representation of magnitude the absolute value of twist is used.

#### **4.8.3.1 Key Metrics**

The analysis presented below focuses on the effect of g levels induced by loading and articulation combinations at various scales of UAHT including the test unit used to conduct experimentation. For both the direct test unit results and the simulated full scaled vehicles the analysis centers on the induced Pitch, Roll, Q1 Rack, Q2 Rack, and absolute value of Twist in g Level units. As well, the total moment in Nmm and the direction of the axis about which the moments rotate are presented. The direction of rotation is useful in that it allows the reader to determine the predominate characteristics of the total moment, Twist, about the reference point in terms of Q1 Rack, Q2 Rack, Pitch or Roll by mentally applying the right hand rule.

#### **4.8.4 Test Unit Scale**

The following section details the moment and gLA yielded directly from experimentation at the test unit scale. Testing results have been broadly categorized into inclined and flatland. Keeping these results separated provides a more equivalent look at vehicle performance by percentage of payload as all inclined testing was completed with 100% payload which, if included, would skew results at the 100% payload level.

##### **4.8.4.1 Total Moment, Twist and Axis of Rotation Direction**

Figure 4.29 below shows the total cumulative moment about the reference point on the test unit, the most notable feature of this figure is the quadratic shape of the results at all loading levels and the order of magnitude of moment created at the scale level. Regarding the shape of the results it can be seen that the least moment is consistently generated at the zero articulation position and the largest

moments created at the most extreme articulations which implies that the machine is most balanced under zero articulation conditions. Also of importance is to not that under tare conditions the moment created at +42° and -42° are  $3.33 \times 10^5$  Nmm and  $3.74 \times 10^5$  Nmm respectively. This imbalance under tare conditions is the effect of the unbalanced construction of the vehicle as described in Section 4.5.1. Assuming that perfect balance would move tare weight moments at these articulations to between the  $3.33 \times 10^5$  Nmm and  $3.74 \times 10^5$  Nmm this construction defect can be seen as providing a  $\pm 5.9\%$  error at tare conditions; once additional payload is added the tare weight defects are either reduced or enhanced depending on the final weight distribution at each loading increment. Because Figure 4.28 shows that as load is applied the distribution per hub trends towards equal this  $\pm 5.9\%$  error due to the construction defect will be diminished rather than enhanced. Note that the moment about the reference point in terms of force per unit distance provides a sense of the mass of the vehicle, both loaded and unloaded, and the affect this mass can have on the structure of the machine however; it does not provide a sense of how this affect compares to other vehicles or other periods of operation which may or may not be under static conditions. To provide a comparable metric the gLA is used.

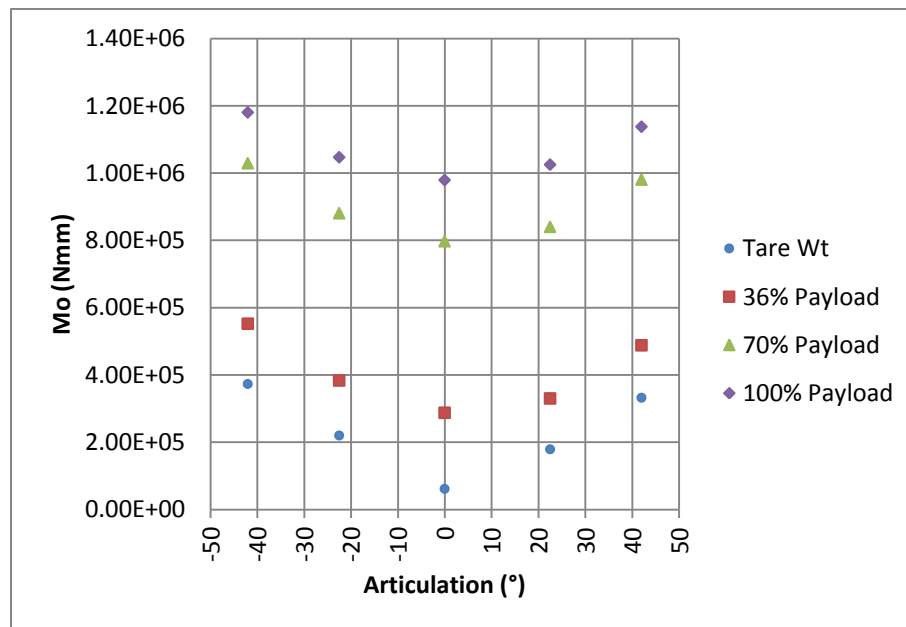


Figure 4.29: Test Unit Total Moment About Reference

Figure 4.30 shows the total Twist, expressed in g Levels, generated by the total moment acting on the Test Unit which are presented in Figure 4.29. Note that shape of the results in Figure 4.30 are not identical to those presented in Figure 4.29, in fact it can be seen that in terms of gLA the 70% payload is essentially as detrimental to the hauler as 100% loading, especially at the  $\pm 22.5^\circ$  and  $\pm 42^\circ$  articulations. This shape inequality may seem counterintuitive however it can be explained via the differing treatment of moment arms in the gLA versus the direct moment calculation. The explanation is as follows. Equation 3.1, Newton's Second Law applied to moments, is the structure of the method under which the total moment generated about the reference point is calculated; specifically the cumulative or resultant hub force is applied at a cumulative or resultant moment arm to generate the cumulative moment. Under these standard calculations the total weight of the vehicle, calculated as mass multiplied by the gravitational constant, is held instantaneously constant between loading increments while the moment arm at which this weight is applied is altered as the vehicle articulates. With the calculation of the gLA the instantaneous mass of the vehicle and the theoretical moment arm, equal to the 1000mm radius of the unit sphere on which the equivalent force will act, are held constant while the acceleration varies to account for the increased or decreased cumulative moment.

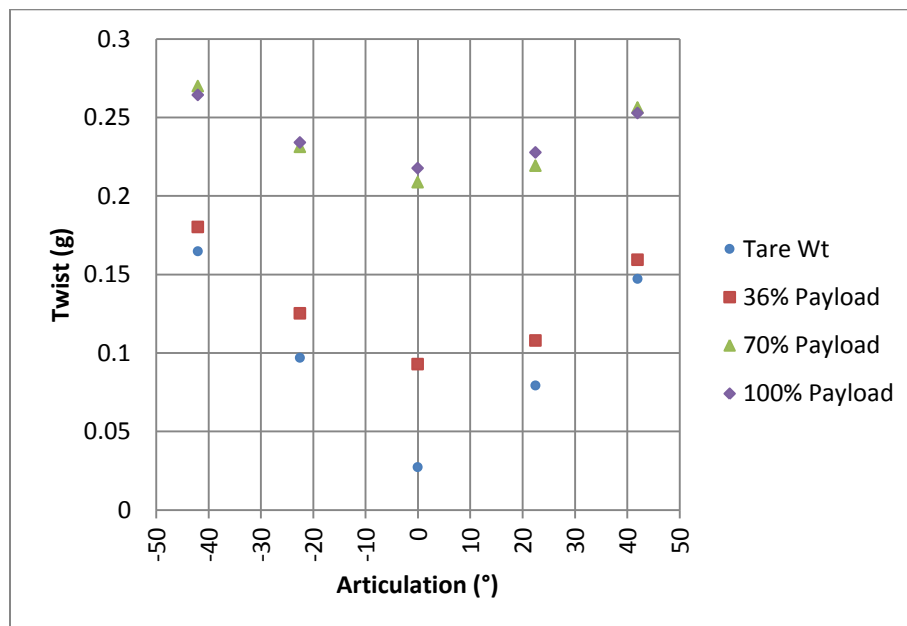


Figure 4.30: Test Unit Total Twist about Reference Point in g Levels

Although the total Twist such as expressed for the Test Unit in Figure 4.30 above, provides a useful reference for the overall g Level induced on the vehicle it does not differentiate between the degree of Rack, Pitch or Roll the vehicle is undergoing at any instant. An initial insight into the how the

components of Rack, Pitch or Roll associated with the total Twist can be gained by examination of the  $\vec{U}_{M_o}$  coordinates for each loading and articulation combination. Figure 4.31 below shows the  $\vec{U}_{M_o}$  coordinates for the Test Unit. As would be expected all points in Figure 4.31 lay on a unit circle, also note that because this study is under the assumption that there is no rotation about the z axis imparted on the vehicle all  $\vec{U}_{M_o}$  lay in the  $\vec{i}, \vec{j}$  plane. At this point it is useful to reiterate that the  $\vec{U}_{M_o}$  coordinates are the direction of the axis about which the instantaneous moment rotates, a corollary of this is that the closer the  $\vec{U}_{M_o}$  are to lying on any of the defined Q1 Rack, Q2 Rack, Pitch or Roll axes the more predominant that particular motion will be in the cumulative rotation. It can also be seen that there are coordinates that show predominant characteristics of Rack, Pitch and Roll. For example it can be seen that under tare conditions the unit is nearly completely experiencing roll when articulated to the  $\pm 22.5^\circ$  and  $\pm 42^\circ$  positions. It can also be seen that the highest degree of rack is found under 36% payload conditions with Q1 Rack dominating at the at the  $-22.5^\circ$  and  $-42^\circ$  articulation and Q2 Rack dominating at the  $+22.5^\circ$  and  $+42^\circ$  articulations. Another observation is that at zero degrees of articulation Pitch is dominant at all loadings and that at all articulation the overall effect converges towards Pitch as payload is increased. Because Rack, Pitch and Roll are calculated as the Scalar Triple Products described in Section 3.2; Figure 4.30 above in conjunction with Figure 4.31 begins to provide an initial estimation into what g Level the vehicle is experiencing about any of the defined axes. The next section examines in detail the components of Q1 Rack, Q2 Rack, Pitch and Roll as calculated from test unit data.

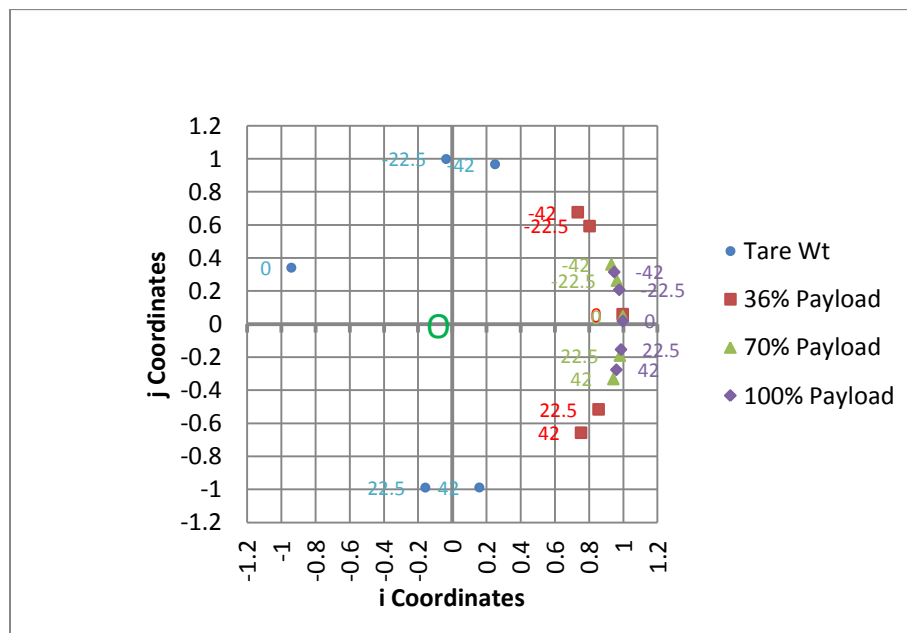


Figure 4.31: Test Unit Total Moment Direction Plot



The following figures and discussion centers around the components of Twist associated with results from experimentation on the Test Unit scale.

#### 4.8.4.2 Roll

Figure 4.32 below shows the degree of roll associated with each articulation and loading combination used during testing. The linear relationship between articulation and the number of g's of roll experienced by the vehicle can be explained in that as the vehicle is articulated the load on the front hubs is positioned nearer or further from the Roll axis. The inverse relationship between slope and the percentage of payload added to the vehicle is also rather intuitive as it is easy to visualize the additional weight on the rear hubs acting to resist the roll motion induced by the movement of the weight on the front hubs relative to the roll axis. It is also rather intuitive that the vehicle would experience minimal absolute roll at zero articulation regardless of loading level.

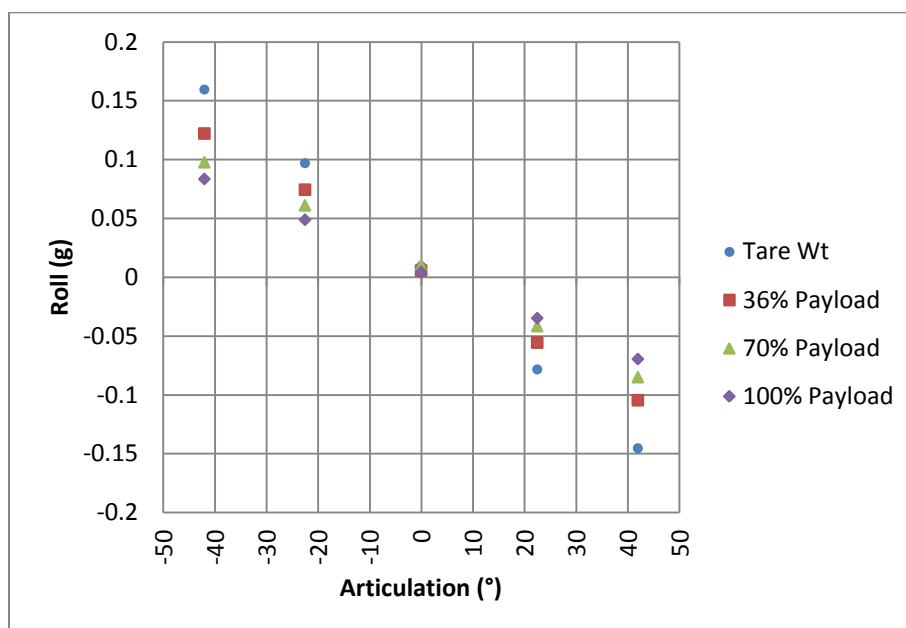


Figure 4.32: Test Unit Roll in g Level

#### 4.8.4.3 Pitch

Figure 4.33 below presents Pitch data as calculated for the Test Unit. Vehicle Pitch is defined as the degree of rotation induced about the  $\vec{i}$  axis of particular note from Figure 4.33 is the transitions from positive pitch to negative pitch as even under tare conditions the vehicle is capable of generating positive and negative pitch rotations. Under tare conditions it would be expected that the vehicle would tend to rotate with a negative sense, using the established right hand convention, about the  $\vec{i}$  axis as it is under a 73% front to 27% rear weight distribution bias however; this as a good example to the benefits of moment or g Level based analysis because it can be seen that at as the 73% front weight bias is move closer to the Pitch axis it is less able to counteract the rotation induced by the 27% vehicle weight on the rear tires. This effect is entire explained by the variation in the moment arms the front hub forces act with as the vehicle is articulated. For example at zero degrees of articulation the front hub forces act on equal moment arms of 300mm from the pitch axis and this is capable of over powering the rotational tendencies of the 27% rear weight acting at 715mm from the pitch axis; however at 42° of articulation the front left and right hub forces act on moment arms of 79.7mm and 366mm respectively which is not capable of overpowering the rotational tendency of the rear hub forces.

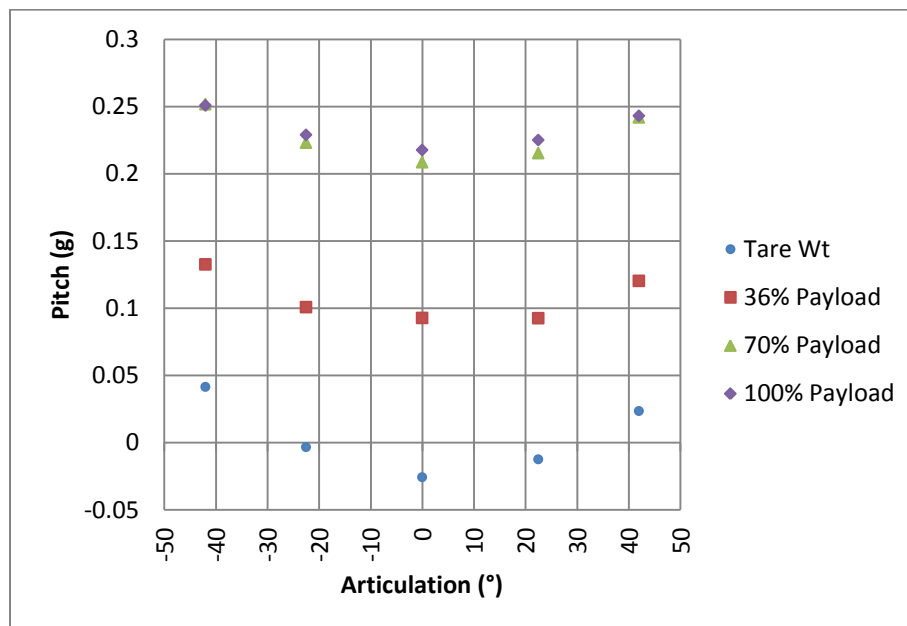


Figure 4.33: Test Unit Pitch in g Level

#### 4.8.4.4 Q1 Rack

Figure 4.34 shows the range of Q1 Rack induced on to the Test Unit during trials. Keeping in mind that the Q1 Rack axis runs at  $45^\circ$  counterclockwise from the x axis in Figure 4.31 it can be visualized that the front wheels/hubs of the vehicle will nearly equally straddle this axis when in the  $-42^\circ$  articulation position. The result being that in this position the ability of the weight over the front axle to counteract the rotation about the Q1 Rack axis induced by the rear wheels is minimized resulting in the largest degree of Q1 Rack occurring in the  $-42^\circ$  articulation position. Note that the maximum Q1 Rack is encountered when the vehicle is 70% loaded rather than the 100% loading which may have been expected. This potential discrepancy can be explained by evaluating the positioning of the payload at the 70% and 100% increments. At 70% loading the vehicle is in near perfect 50/50 front to rear balance however this means that 50% of the weight is acting on the longer rear moment arms which implies, correctly, that the rotation induced by the weight over the rear wheels cannot be eliminated by the rotation induced by the weight acting on the shorter moment arms of the front hub forces. The fact that the 70% to 100% payload addition does not create larger g levels than the 36% to 70% increment is explained by weight distribution and positioning. The addition of the final loading increment keeps the vehicle in near perfect 51% rear to 49% front weight balance it would be expected that g levels would be either equal or greater than at the 70% loading increment. However; further analysis of Figure 4.21 and Figure 4.22 show that the final replicated bucket is positioned closer to the mid-ship pin meaning that the front and rear moment arms with which the final loading increment works is closer to equal, thus limiting the ability of the additional incremental weight to generate higher degrees of g level rack, pitch or roll. It can also be visualized how this same principal can explain the higher degree of variability in Q1 Rack when the vehicle is articulated to the  $+22.5^\circ$  and  $+42^\circ$  positions. When articulated to these positions the front wheels are near orthogonal to the Q1 Rack axis meaning that the weight over the front hubs works with maximum moment arm efficiency to overcome the rotation induced by the rear hub forces. However; we see that the largest absolute value of Q1 Rack in the  $22.5^\circ$  and  $42^\circ$  articulation positions is found with 100% loading, this implies that after the initial payload increase the maximum moment arm efficiency for the front hub forces is still overpowered by the longer moment arms of the rear hub forces.

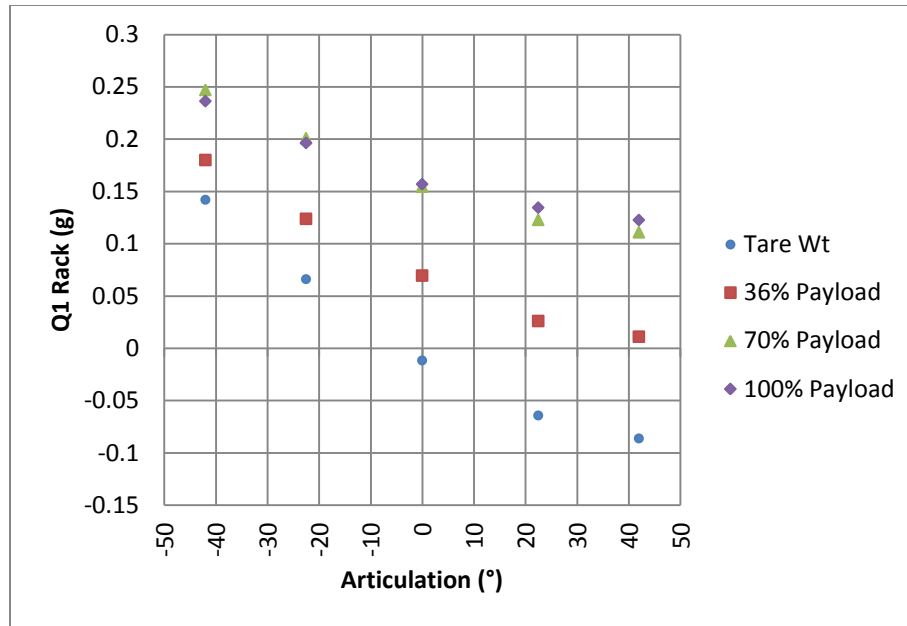


Figure 4.34: Test Unit Q1 Rack in g Level

#### 4.8.4.5 Q2 Rack

This study has defined Q2 Rack as induced rotation about the axis running 45° clockwise from the negative x axis. As this line of rotation is symmetrical about the point of reference from the Q1 Rack axis of rotation it is not surprising that the Q2 Rack results show a high degree of symmetry to the Q1 Rack results. Specifically the Q2 Rack results shown in Figure 4.35 below are centrally symmetric to the Q1 Rack results shown in Figure 4.34 above. With the above stated symmetry the anomalies such as the higher degree of absolute rack levels occurring at 70% payload are, both, to be expected and explained in a similar but opposite manner. Note, however; that the symmetry is not quite perfect due to the slight imbalance in loading.

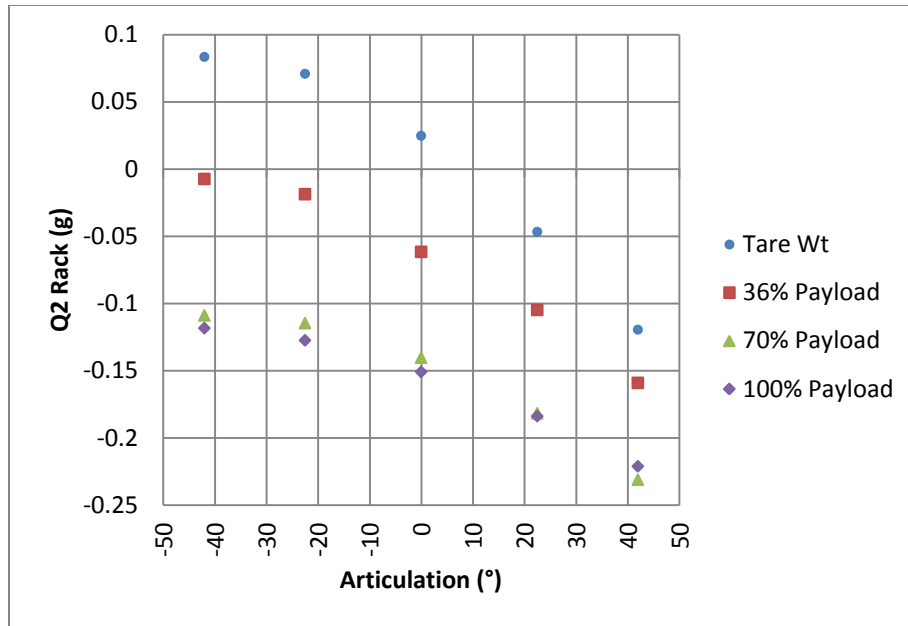


Figure 4.35: Test Unit Q2 Rack in g Level

The previous section has provided detailed information on the results obtained from scale model testing using the purpose built Test Unit. Note that the range of g levels induced as calculated at the model scale are rather small being in the range of  $\pm 0.27g$  which are not near to the range of  $\pm 1.5g$  quoted in Section 2.11 as being detrimental to hauler performance. While the model scale data does not pose reason for concern it must be noted that model testing was completed under static conditions. A dynamic measuring environment would see the addition of hub forces due to motion, as described in Section 2, which would either increment or decrement the resulting g level readings making the numbers in the above section a minimum range of expected readings over perfectly smooth ground. The next section of this investigation utilizes the scale model Test Unit data to estimate and compare the expected performance of full scale haulers.

#### 4.8.4.6 Verification Testing

To verify that the method of calculating the g Level is correct given a set of hub forces, single elimination testing was completed. Using the test unit under the 100% loaded condition an additional 15 measurements were taken at various articulation angles and each of the hub forces was recorded as in section 4.8. Following this data collection the pitch and roll g levels were calculated for each of the

verification tests. Using these results the original hub force at A,  $\vec{F}_A$ , was derived. Table 4.6 provides the parameters used to back calculate the experimentally recorded hub force at A.

Given Parameters and Assumptions	Units and Notes
Pitch, Roll	g Level about the Reference
Articulation Angle, Inclination Angle	° (Degrees), All points at 0° Inclination
$\vec{F}_B, \vec{F}_C, \vec{F}_D$	N
$\vec{F}_{\alpha i} = \vec{F}_{\alpha j} = 0$	Only vertical hub forces exist
Tare Weight =230kg, Payload is known	Required to know $m_i$
Front and Rear Frame Geometries	mm

**Table 4.6: Verification Testing Parameters**

It is important to note that each of the 15 samples can be used to calculate two values for the omitted hub force. This double calculation arises from solving both the i and j components of the moment about the reference caused by the omitted hub force, the two values should be equal. See Figure 4.36 and Figure 4.37 below. While the calculated value of  $\vec{F}_A$  via the j component of the cumulative moment tends to be slightly more accurate the average percent error from all 30 calculated values is -0.05%. The most accurate estimate of  $\vec{F}_A$  is found when using the average between the values calculated about both the i and j components of the moment, this cross plot is found in Figure 4.38. In this case the correlation coefficient,  $R^2$ , between the calculated and measured  $\vec{F}_A$  is 94%. Although there is a minor difference between the calculated hub forces and the actual hub forces at A the calculation method is found to be verified.

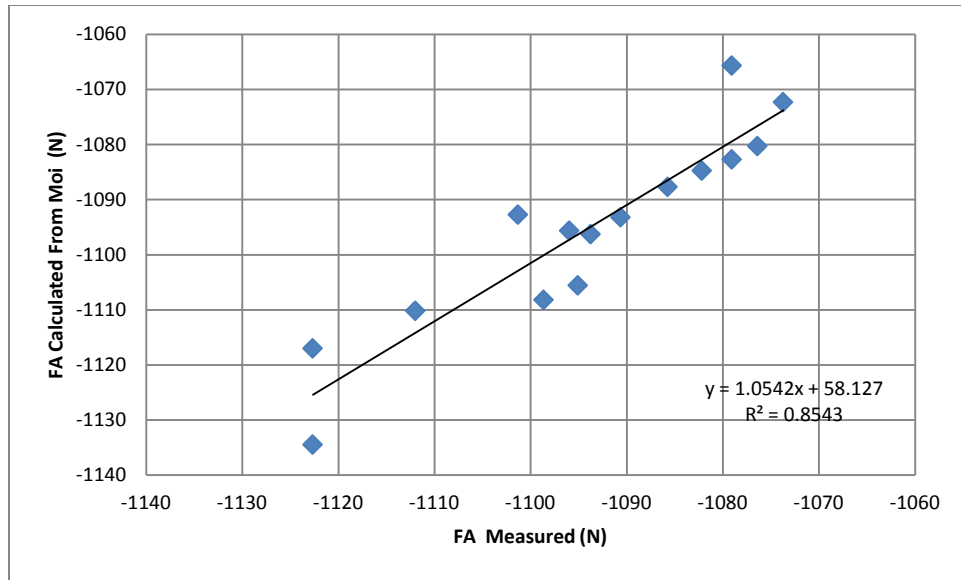


Figure 4.36: Measured vs Calculated FA - Moi

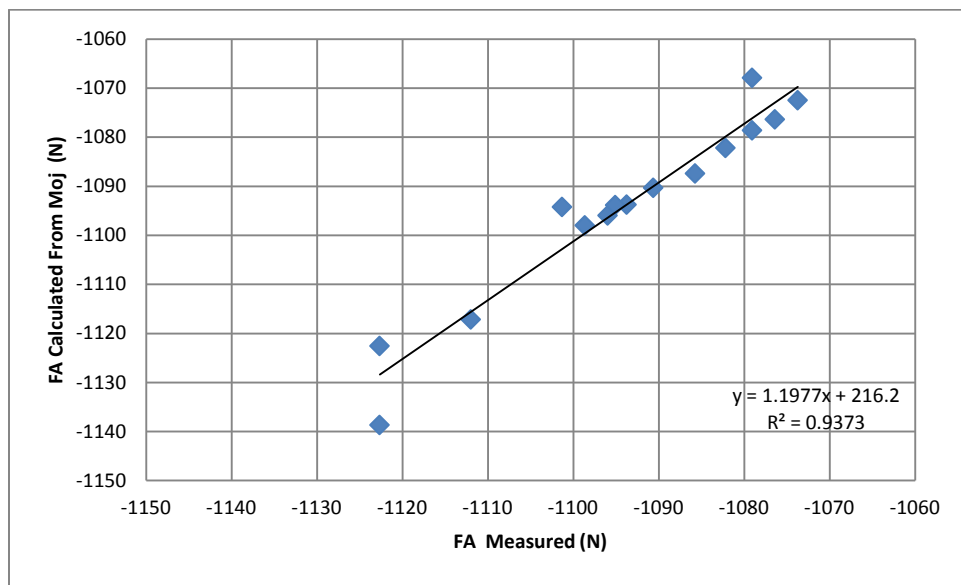


Figure 4.37: Measured vs Calculated FA - Moj

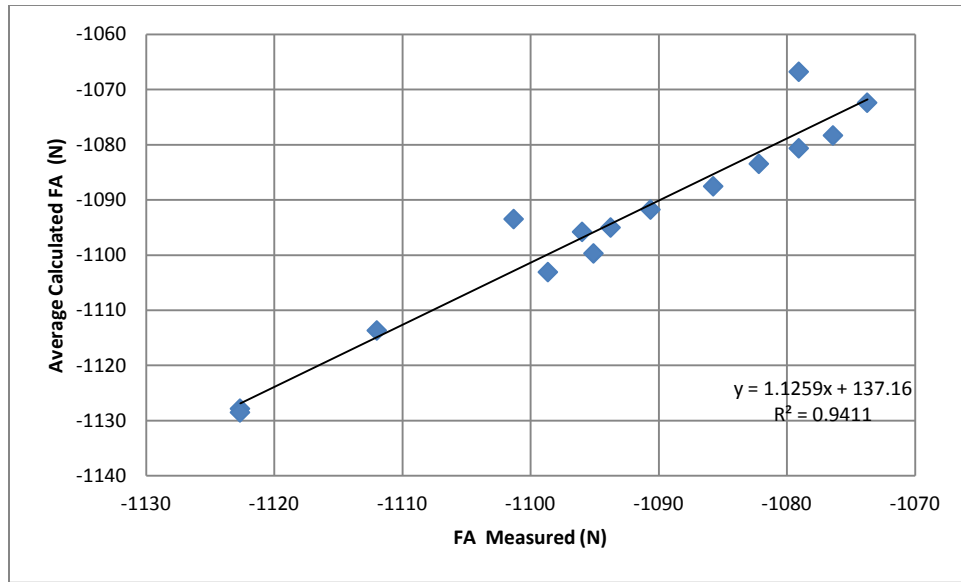


Figure 4.38: Measured vs Average Calculated FA - Moi & Moj



## 5 Full Scale Simulations and Operating Hauler Analysis

This investigation includes three types of full scale hauler analysis. The first analysis uses the articulated scale model data presented in Section 4 to simulate the g level based behavior of ten UAHT with payloads ranging from 20t to 60t. The second full scale study is conducted by applying the methodology presented in this paper to real world data collected from a 360t payload rigid body hauler operating at one of Alberta's major oilsands operations. The final full scale analysis section compares the rigid body results from this methodology to those obtained using the same data set and the methodology presented by Joseph, 2003.

### 5.1.1 Comparison of Test Unit to Simulated Full Scale Articulated Haulers

In addition to scaling model hub forces to represent each hauler the geometries of each respective vehicle were used in the calculations required to arrive at the resultant cumulative moment and gLA as presented for the Test Unit in Section 4.8.4.

Table 5.1 below presents the nine haulers involved in the study along with the pertinent information used to conduct the simulation. For completeness the University of Alberta built Test Unit is included in Table 5.1. All data used to generate Table 5.1 has been taken from specification document available online, examples of these documents are included for reference as part of the Appendix.

The nine full scale haulers included in the study can be broken into five classes by payload; 20t, 30t, 45t, 50t and 60t. The following haulers would fall into each class; 20t: MT2010, 30t: MT431B and AD30, 45t: MT42 and AD45B, 50t: MT5020 and AD55, and finally the 60t class comprised of the MT6020 and AD60 haul trucks. These trucks range in intended use from small production or rapid development as in the case of the MT2010 to large scale, high velocity, high production ramp haulers as in the MT6020 and AD60 vehicles.

General Specifications										
Model	Test Unit	MT 2010	MT 431B	AD 30	MT 42	AD 45B	MT 5020	AD 55	MT 6020	AD 60
Manufacturer	UofA	Atlas Copco	Atlas Copco	Cat	Atlas Copco	Cat	Atlas Copco	Cat	Atlas Copco	Cat
Tramming Capacity (kg)	224	20000	28125	30000	42000	45000	50000	55000	60000	60000
Degree of Articulation (Degrees)	42.5	45	42.5	42.5	45	42.5	42.5	42.5	44	42.5
Tire Width (mm)	165	457	457	673	771	749	889	889	889	889
Overall Width (mm)	560	2217	2795	2690	3050	3000	3200	3346	3440	3346
Payload Scaling Factor (PSF)	1.00	4.47	5.01	5.12	5.72	5.86	6.07	6.26	6.45	6.45
Tare Mass (kg)		230	20500	28,000	28870	34500	40000	42000	47000	49969
	% Front	73%	67%	71%	68%	75%	69%	71%	66%	70%
	% Rear	27%	33%	29%	33%	25%	31%	29%	34%	30%
Loaded Mass (kg)		454	40500	56125	60000	76500	85000	92000	102000	104600
	% Front	49%	Not Stated	Not Stated	44%	Not Stated	46%	Not Stated	47%	Not Stated
	% Rear	51%	Not Stated	Not Stated	56%	Not Stated	54%	Not Stated	53%	Not Stated

Front Frame Geometry										
Front Frame Angle Theta (Degrees)	35.5	27.3	38.6	29.3	33.1	30.4	30.3	32.6	32.8	32.6
Length AB/2 (mm)	214	880	1169	1008	1140	1125	1156	1229	1276	1229
Length O to Perp AB (mm)	300	1702	1465	1800	1750	1920	1980	1920	1980	1920
Length OA (mm)	368	1916	1874	2063	2088	2225	2293	2279	2355	2279

Rear Frame Geometry										
Rear Frame Angle Beta (Degrees)	16.7	16.8	18.2	16.5	17.1	17.1	17.3	17.2	19.0	17.2
Length DC/2 (mm)	214	880	1169	1008	1140	1125	1156	1229	1276	1229
Length O to Perp DC (mm)	715	2921	3555	3400	3700	3650	3700	3980	3700	3980
Length OC (mm)	746	3051	3742	3546	3871	3820	3876	4165	3914	4165

**Table 5.1: Summary Parameters of Simulated Full Scale Haulers**

In addition to Table 5.1, Figure 5.1, Figure 5.2 and Figure 5.3 below compare graphically the important front and rear frame angles as well as payload to tare weight ratios and the ratio of the distance from mid-ship to the front and rear axles of each vehicle divided by the respective axle width. To aid in acceptance of the Test Model as adequate  $\pm 10\%$  error bars have been added to each figure. Although the Test Unit does not match perfectly all haulers in the study it is still considered adequate to provide insight into the expected range of cumulative moment and g levels created by each vehicle.

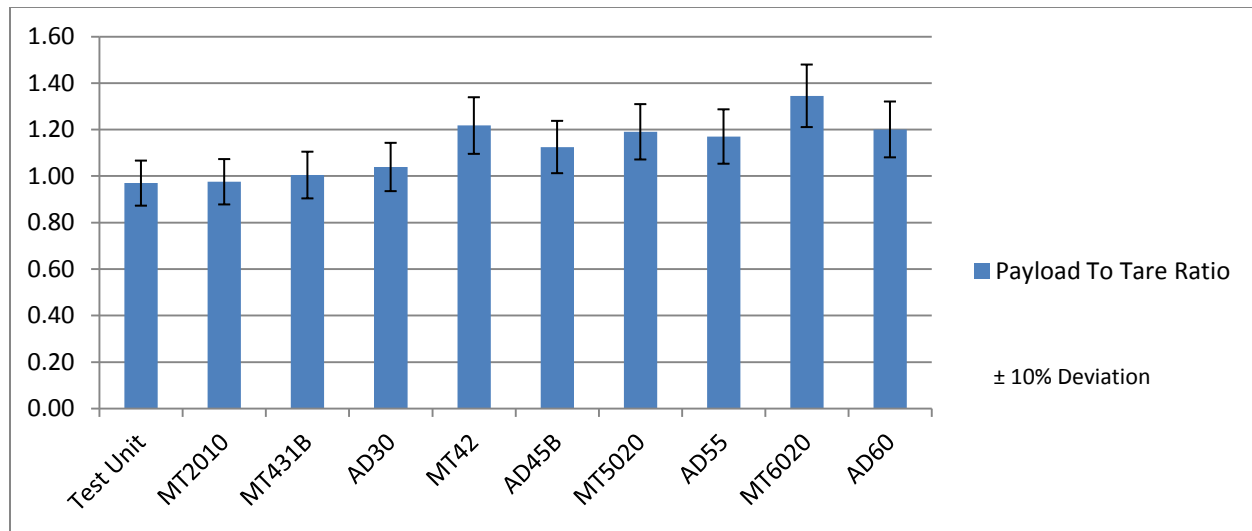


Figure 5.1: Payload to Tare Weight Ratio for Simulated Haulers

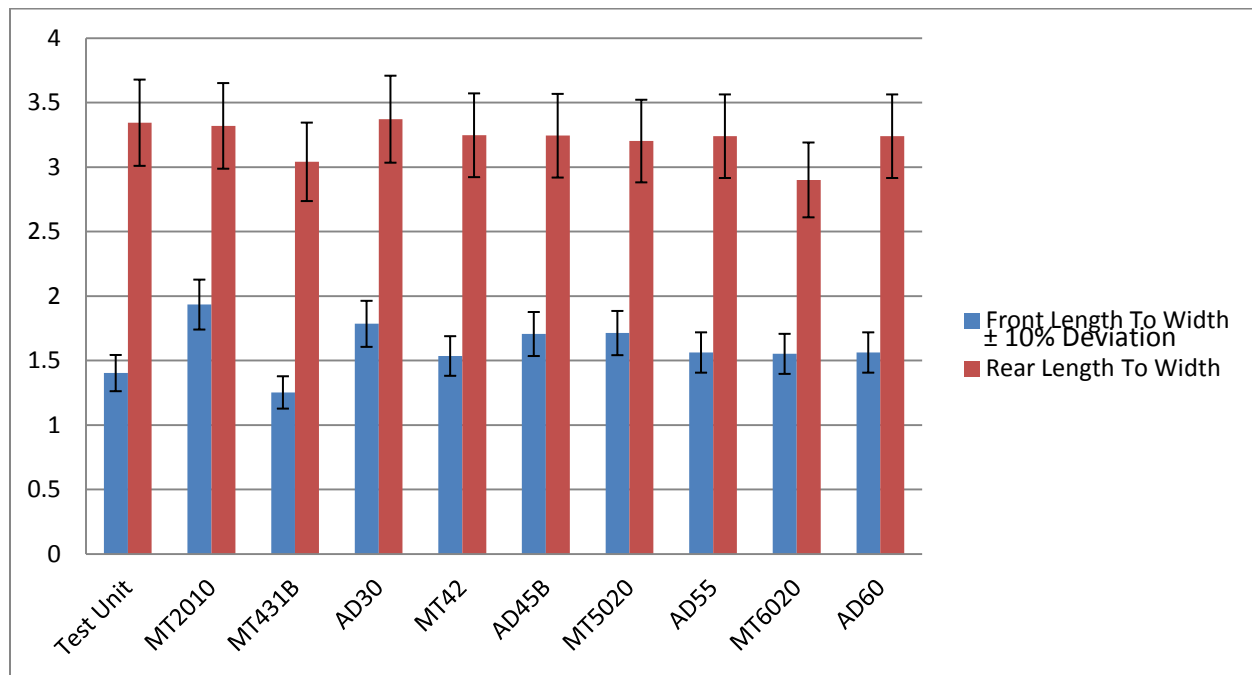


Figure 5.2: Distance from Mid-ship to Front and Rear Axles of Simulated Haulers

Note the consistency found in the ratios presented in Figure 5.1, Figure 5.2 and Figure 5.3. It can be hypothesized that this consistency is very much a function of the space available in a UAHT's working environment. It stands to reason that width and height would be limiting design factors as increases in either result in higher mine development costs as more rock must be excavated to allow equipment clearance. This lack of flexibility in height and width, in turn, requires the vehicle to increase in length as payload is increased. Also of notable consistency is the payload to tare weigh ratio of the haulers

included in the study. Although there appears to be two trends in the ratio of payload to tare weight ratio, with the split coming at the 45t class, it shows that general UAHT design has not made substantial developments within the time period represented by the haulers in this study.

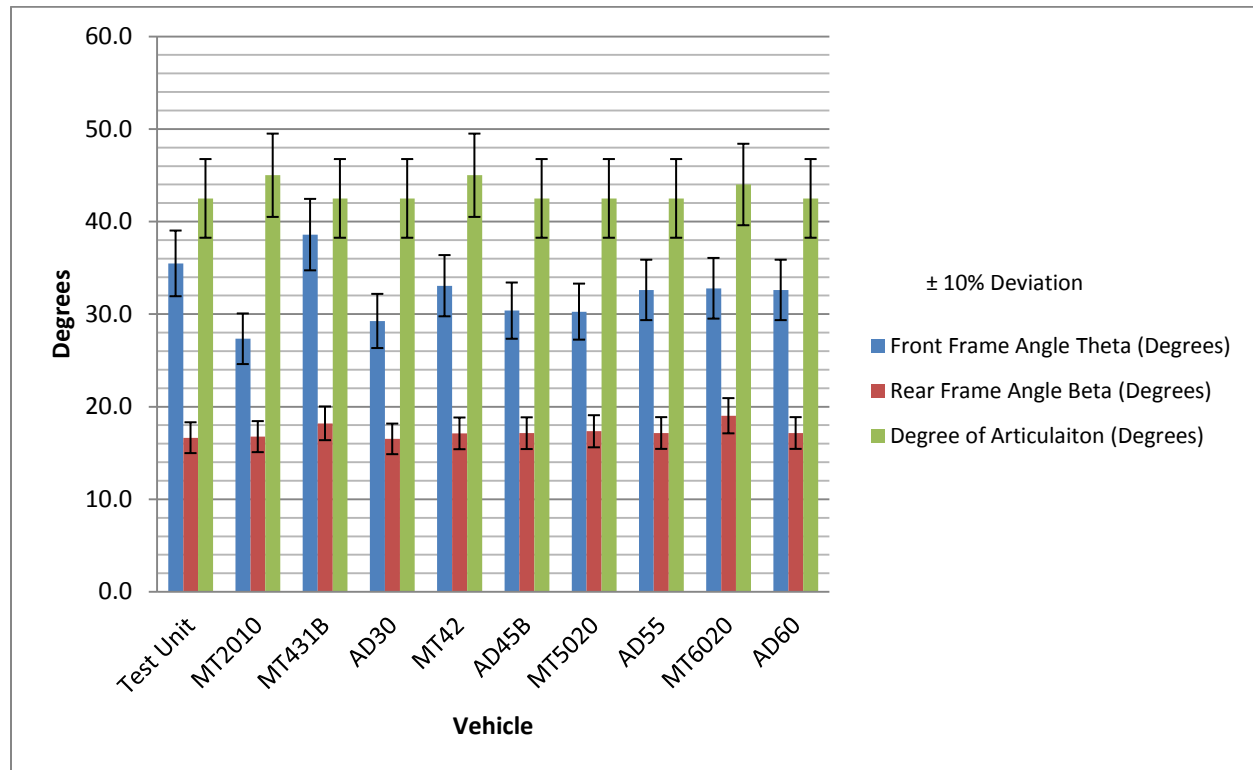


Figure 5.3: Relevant Angles for Simulated Haulers

In the above graph, Figure 5.3, it can be seen that the Test Unit has a slightly high front frame angle compared to the MT2010 hauler, other than this anomaly the angles used in construction of the Test Unit fall very nicely into the range of the other eight comparables.

### 5.1.2 Full Scale Articulated Simulation Results

Results of the full scale simulations are presented in the following section. For clarity the results of a single hauler is presented in the same order as 4.8.4. Following the individual results of the MT2010 hauler the total g level charts and Unit Mo direction plots for each hauler are provided. Although the Test Unit was based closest on the MT431B hauler this model received the same analysis as the other eight units.

### 5.1.3 Sample Detailed Analysis of Full Scale Results – Hauler MT2010

The following are full scale simulations for the MT2010 UAHT. The Payload Scale Factor for the MT2010 is 4.47 derived from the MT2010's stated 20,000kg of Payload compared to the Test Units 224kg payload. Figure 5.4 shows the absolute value of the cumulative moment about the reference point for this truck, note the approximately payload of the MT2010 is approximately two orders of magnitude larger than the Test Unit and that this increase in payload is matched proportionally by a two orders of magnitude larger cumulative moment. Also of interest is that at low degrees of articulation, approximately less than  $\pm 22.5^\circ$  there is less of a moment generated with 36% payload applied as opposed to under tare conditions. This is a state that will appear several times amongst the nine full scale simulations.

Figure 5.5 presents the absolute value of the total g level induced about the reference point. The most important observation from Figure 5.5 is that even with the smallest hauler in the study the absolute g level created by articulation is 1.0g without the effect of motion over undulating terrain. Also note that in terms of g level, where the instantaneous mass of the vehicle is accounted for, the tare weight and 36% payload curves return to the anticipated order. Finally, as with the test unit, it can be seen that the 70% payload creates a more detrimental rotational tendency than when the vehicle is fully loaded.

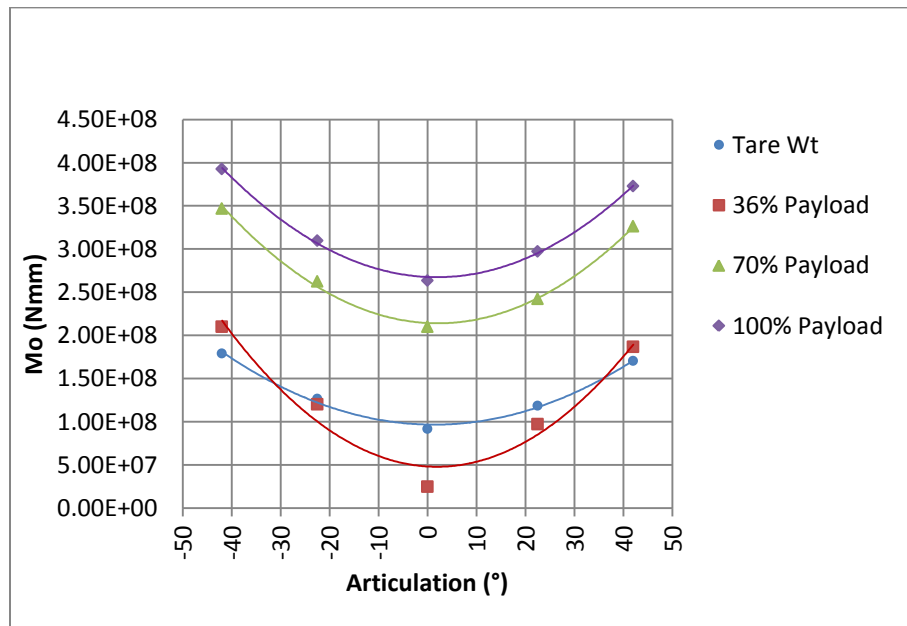


Figure 5.4: MT2010 Total Moment About the Reference Point

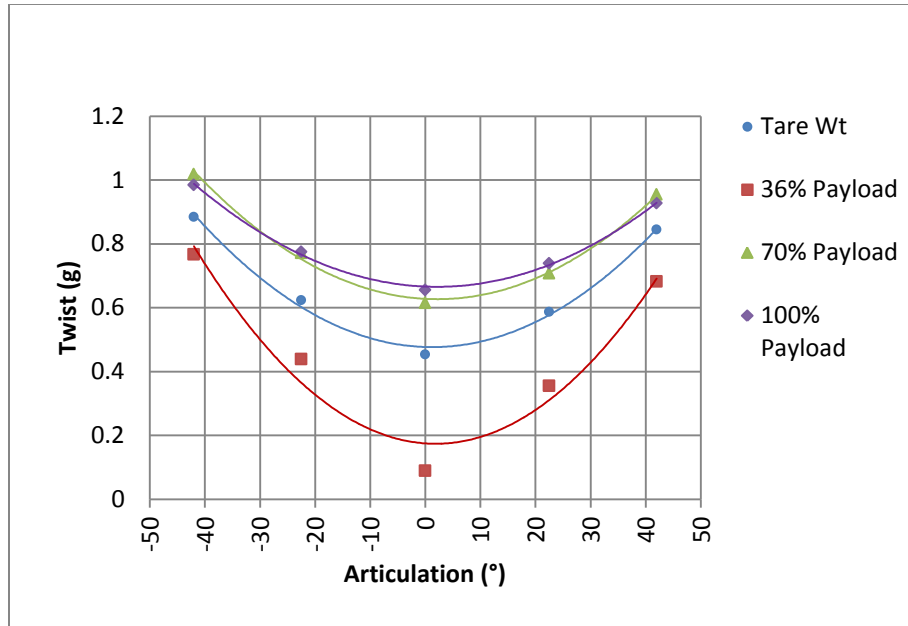


Figure 5.5: MT2010 Total Twist about the Reference Point in g Level

Figure 5.6 below shows the  $\vec{i}, \vec{j}$  coordinates of the resultant moment about the reference point. From observation of this figure compared to Figure 4.31, which shows the same parameters for the Test Unit the MT2010 generates more roll at the 36% loading,  $\pm 22.5^\circ$  and  $\pm 42^\circ$  articulations but less roll under tare weight conditions than the Test Unit. There is also a tendency towards higher Q1 and Q2 rack at the all articulations in the 70% and 100% loadings. These results reflect the effect of geometry on the resultant moments and induced g levels.

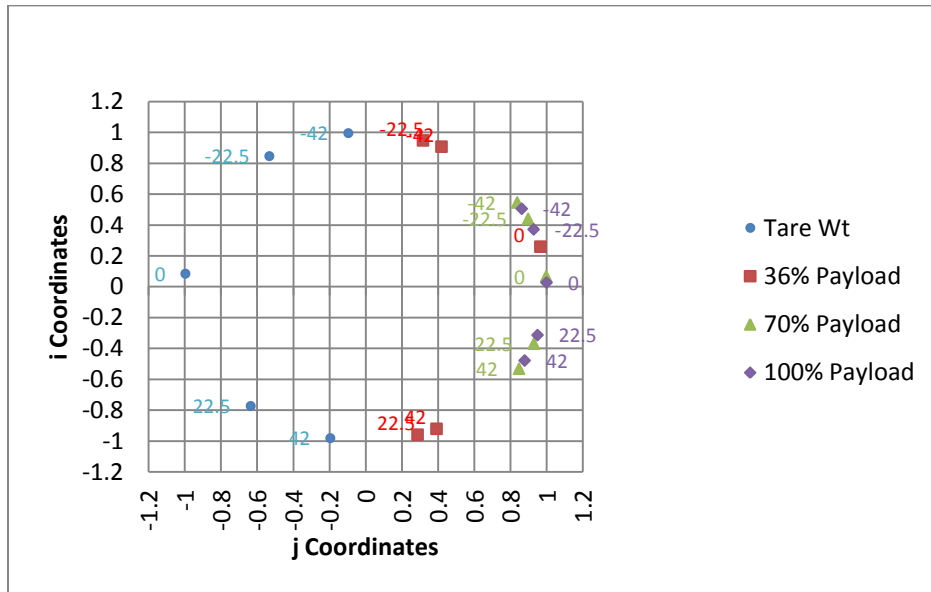


Figure 5.6: MT2010 Total Moment Unit i & Unit j Coordinates

Referring to Figure 5.7 and Figure 5.8 below which show the MT2010 roll and pitch results respectively it is interesting to note that even under tare conditions g levels in single components of the moment can approach 1.0g.

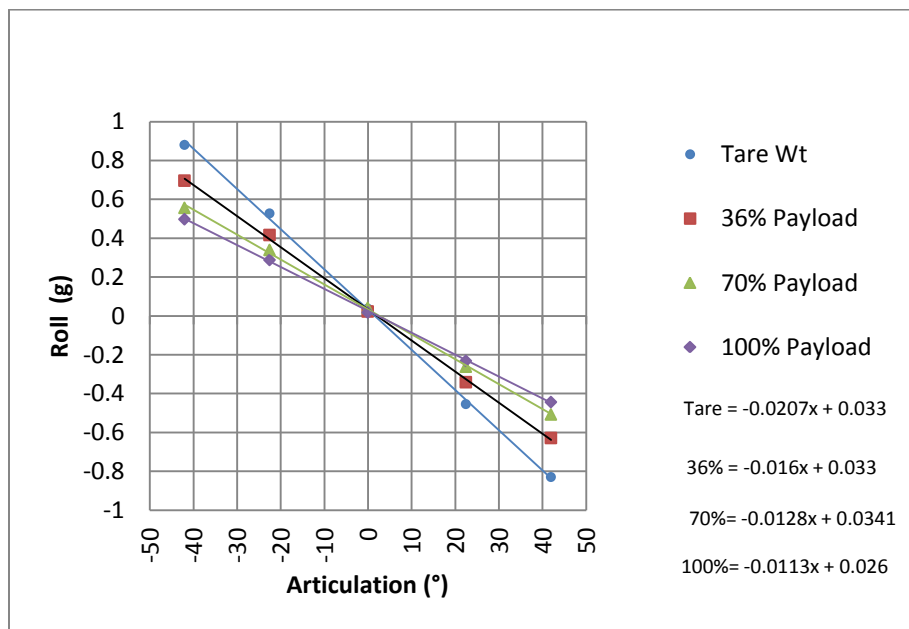


Figure 5.7: MT2010 Roll in g Level

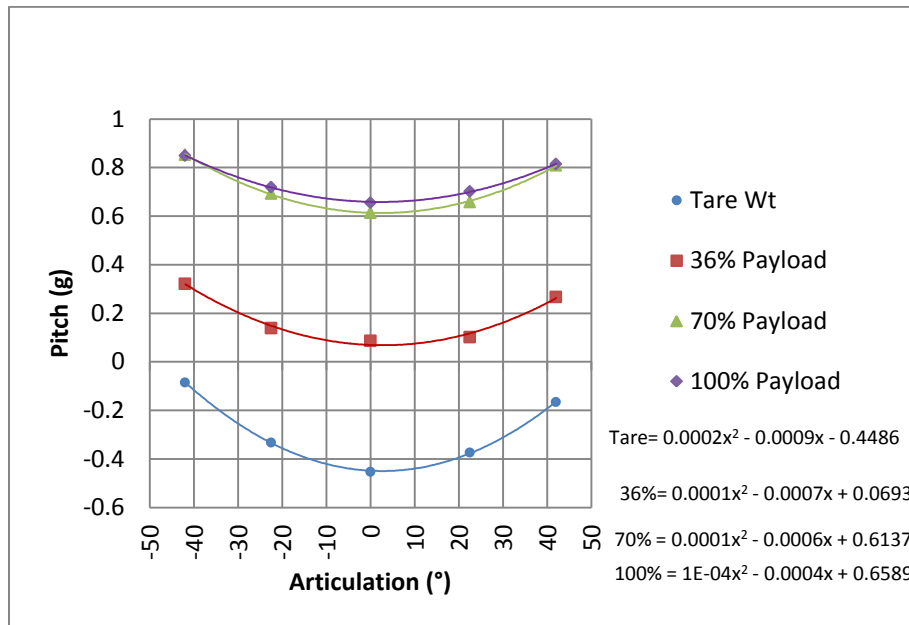


Figure 5.8: MT2010 Pitch in g Level

Figure 5.9 and Figure 5.10 below show the Q1 and Q2 rack respectively. The rack level of the MT2010 shows extremely similar shape to that determined with the Test Unit. The approximately 0.9g range of rack at  $\pm 42^\circ$  of articulation is noteworthy as it demonstrates that payload, as expected, is highly influential to rack levels yet nearly the same absolute levels of rack can be generated under tare conditions as when the vehicle is fully loaded.



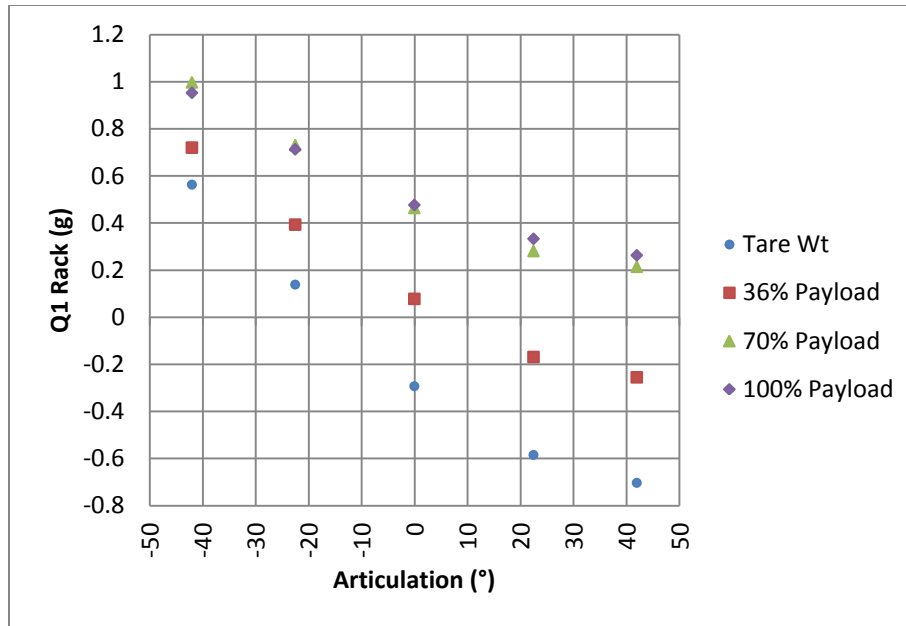


Figure 5.9: MT2010 Q1 Rack in g Level

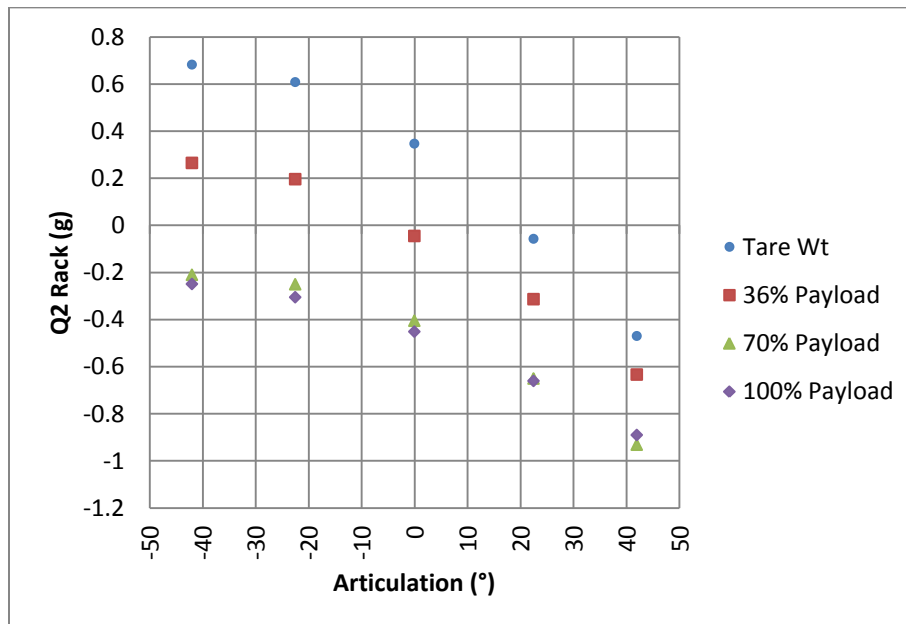


Figure 5.10: MT2010 Q2 Rack in g Level

#### 5.1.4 General Results for All Simulated Articulated Haulers

The above analysis of simulated results for the MT2010 haul truck has been completed for each of the nine haulers in the study and is included as Appendix 9. To provide some insight into the results of all nine haulers the following sections presents figures for each haulers total g level about the reference point and the directions of the cumulative moment about the reference point for each loading and articulation condition. From each set of these results the reader can gain an understanding of the magnitude and predominant characteristics of the twist associated with each hauler class.

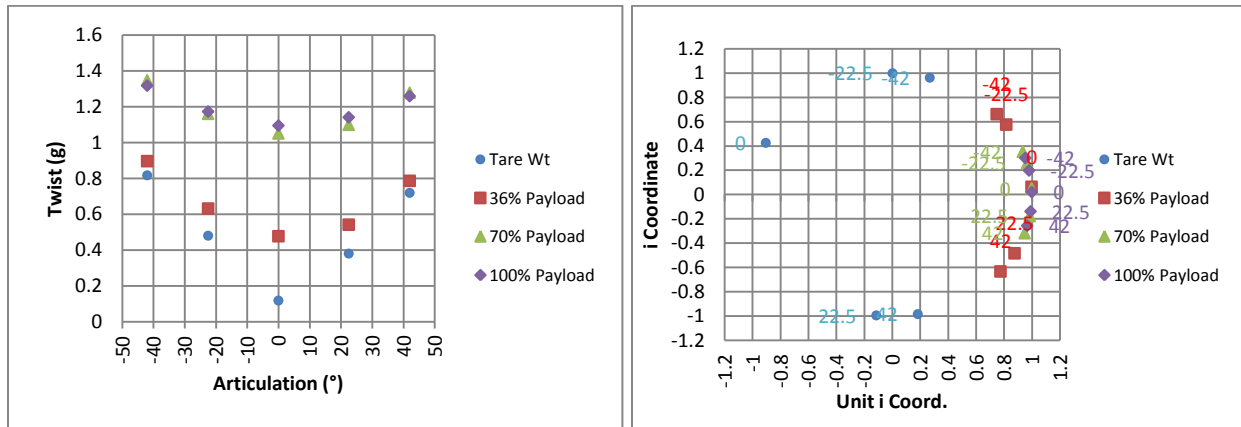


Figure 5.11: MT431 Total g Level about Reference and Direction Plot

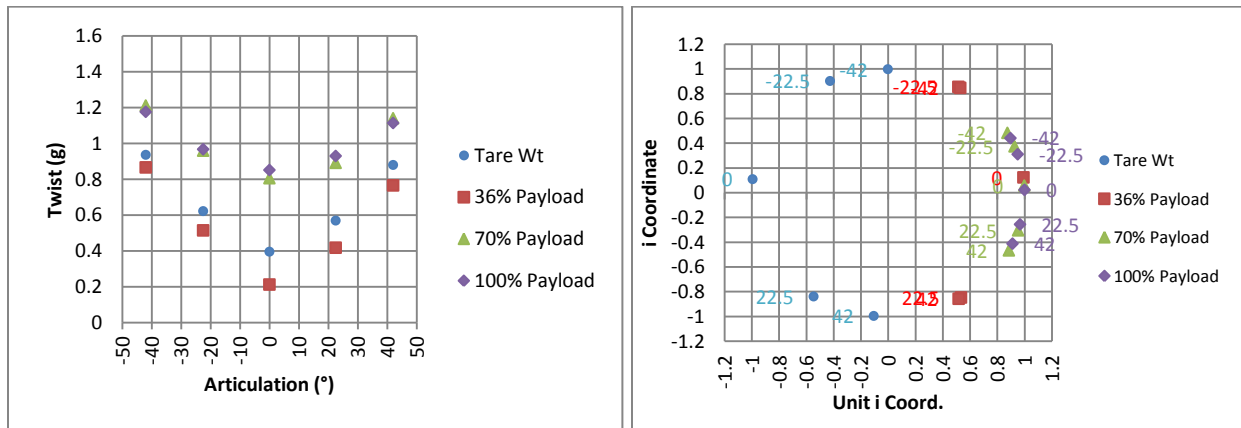


Figure 5.12: AD30 Total g Level about Reference and Direction Plot

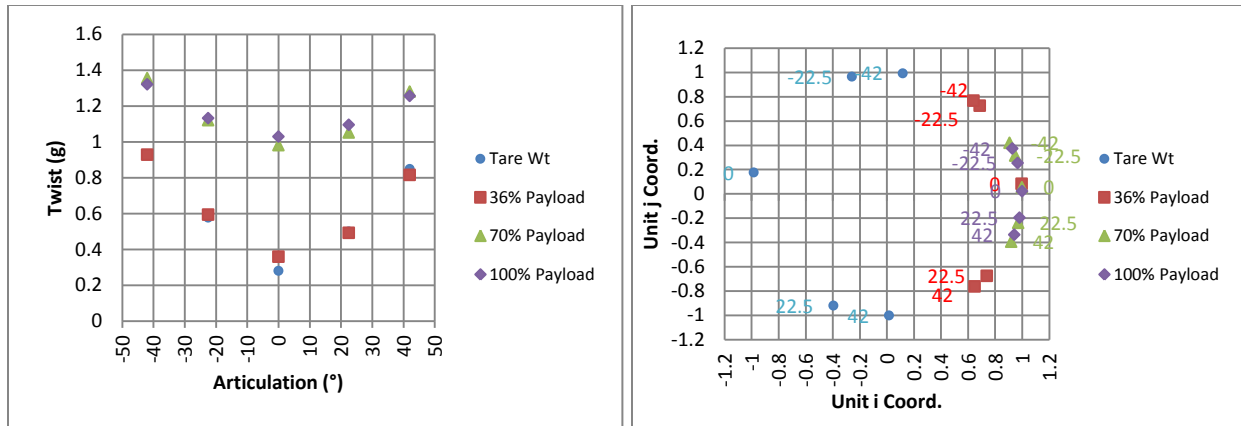


Figure 5.13: MT42 Total g Level about Reference and Direction Plot

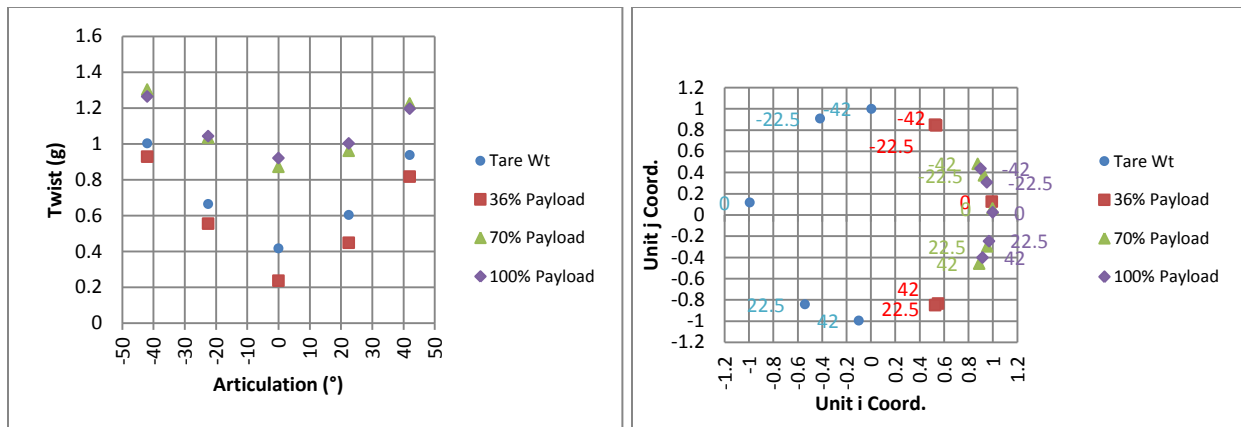


Figure 5.14: AD45 Total g Level about Reference and Direction Plot

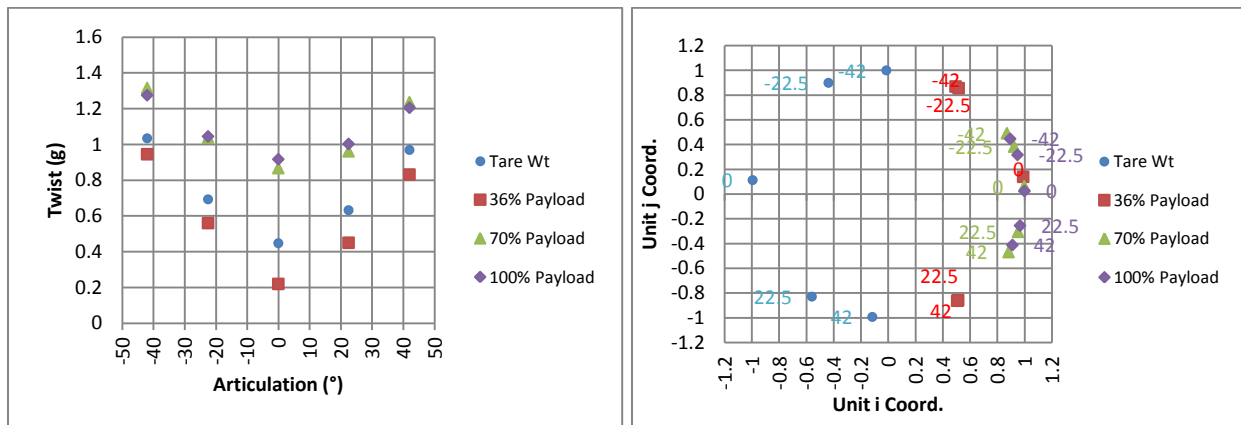


Figure 5.15: MT5020 Total g Level about Reference and Direction Plot

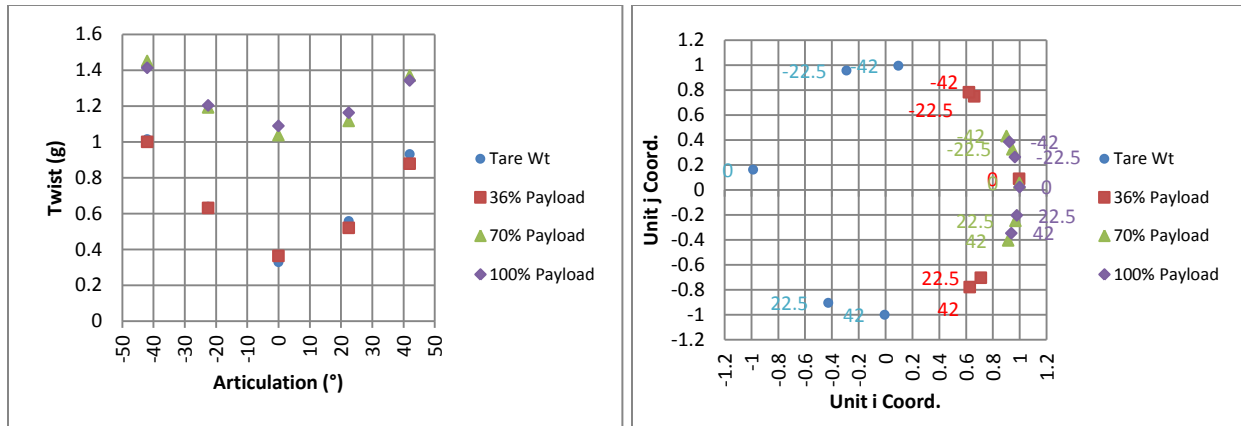


Figure 5.16: AD55 Total g Level about Reference and Direction Plot

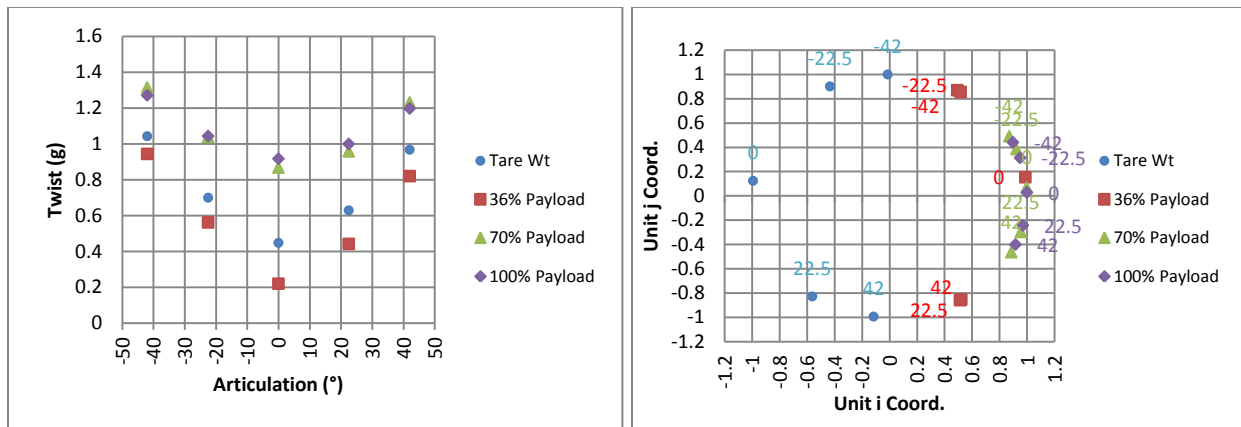


Figure 5.17: MT6020 Total g Level about Reference and Direction Plot

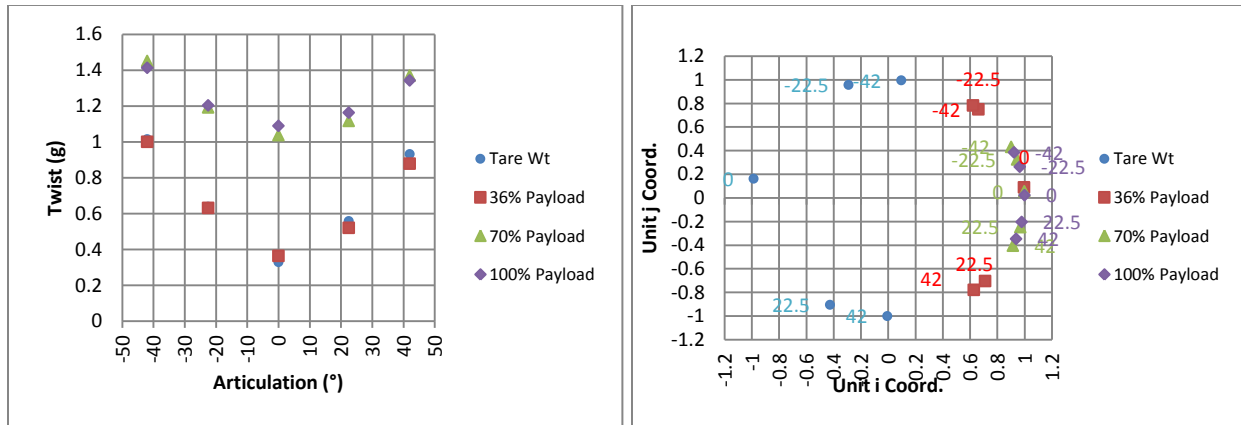


Figure 5.18: AD60 Total g Level about Reference and Direction Plot

### 5.1.5 Group Comparison of Hauler Performance

The following section compares the scaled results for all nine simulated haul trucks. The goal of this section is to provide the basis for discussion on common trends and individual anomalies found in each metric.

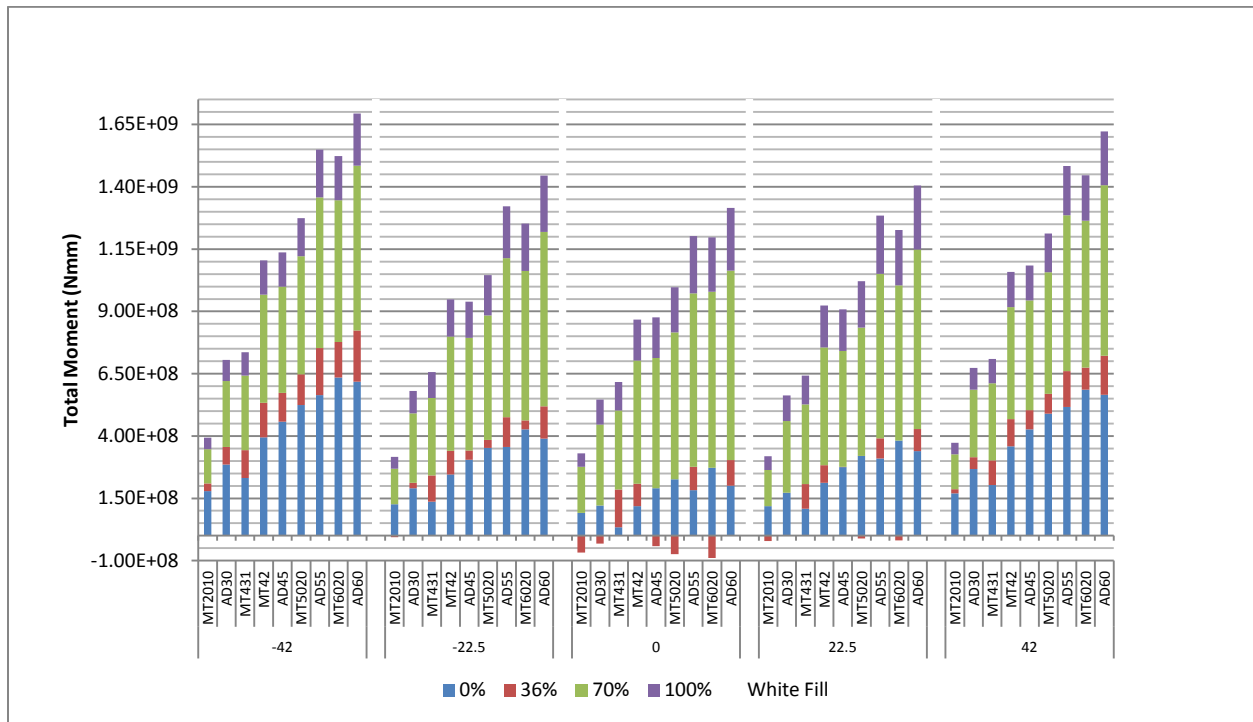


Figure 5.19: Incremental Total Moment by Payload

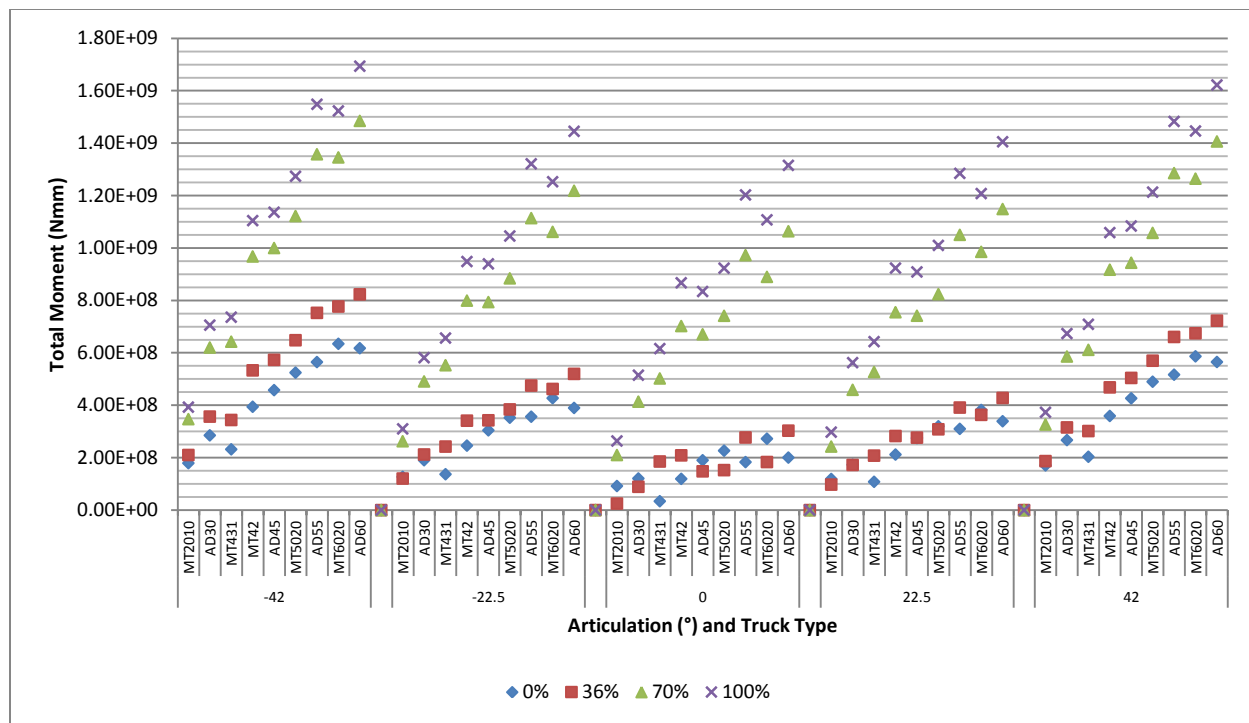


Figure 5.20: Total Moment About Reference

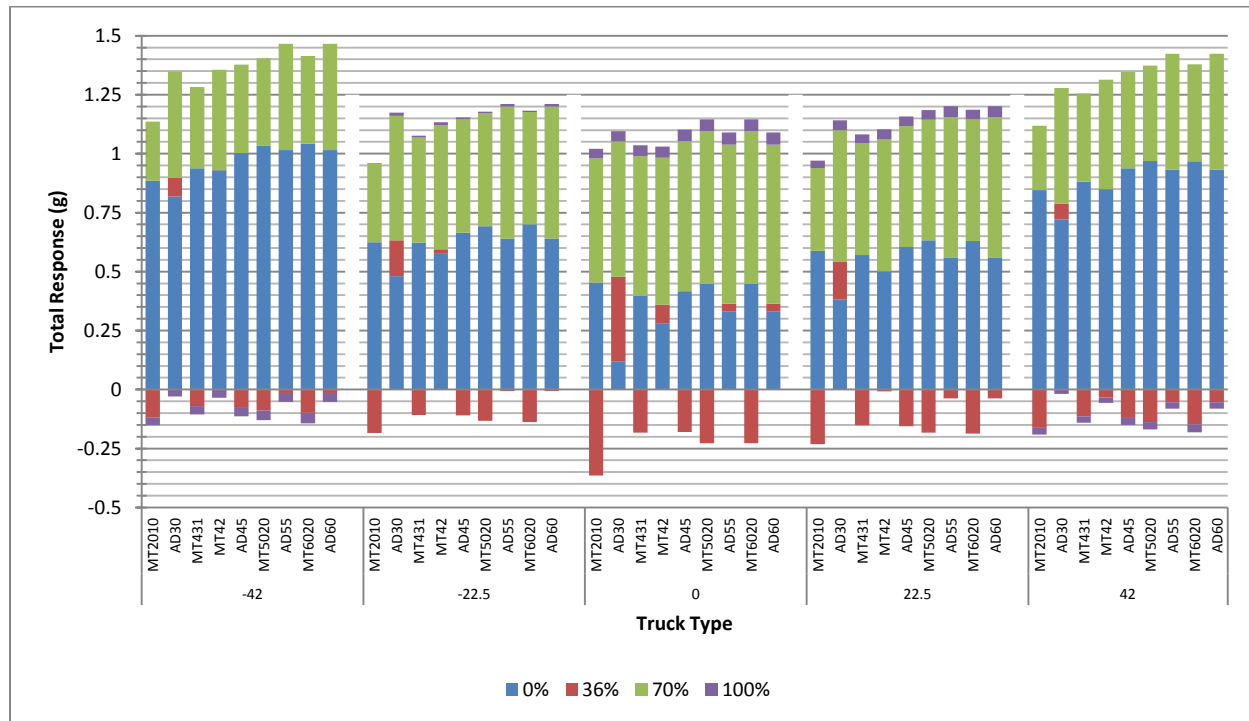


Figure 5.21: Incremental Increase in g Level

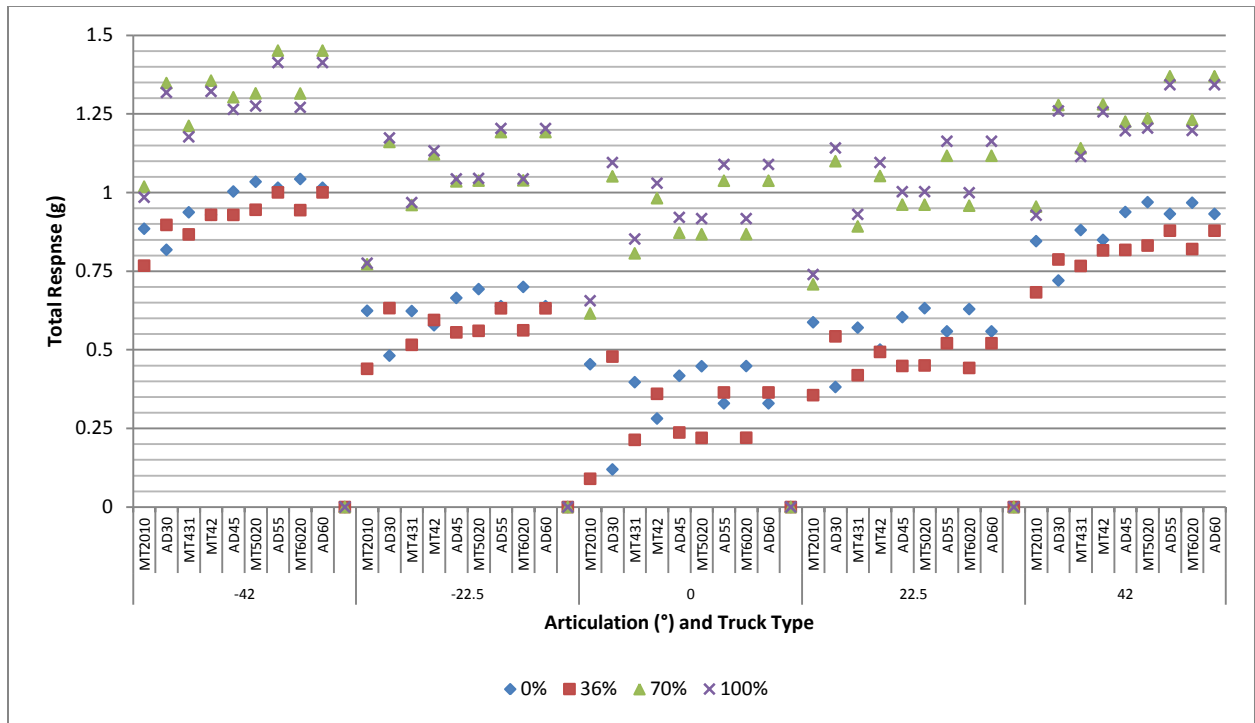


Figure 5.22: Cumulative Twist By Payload

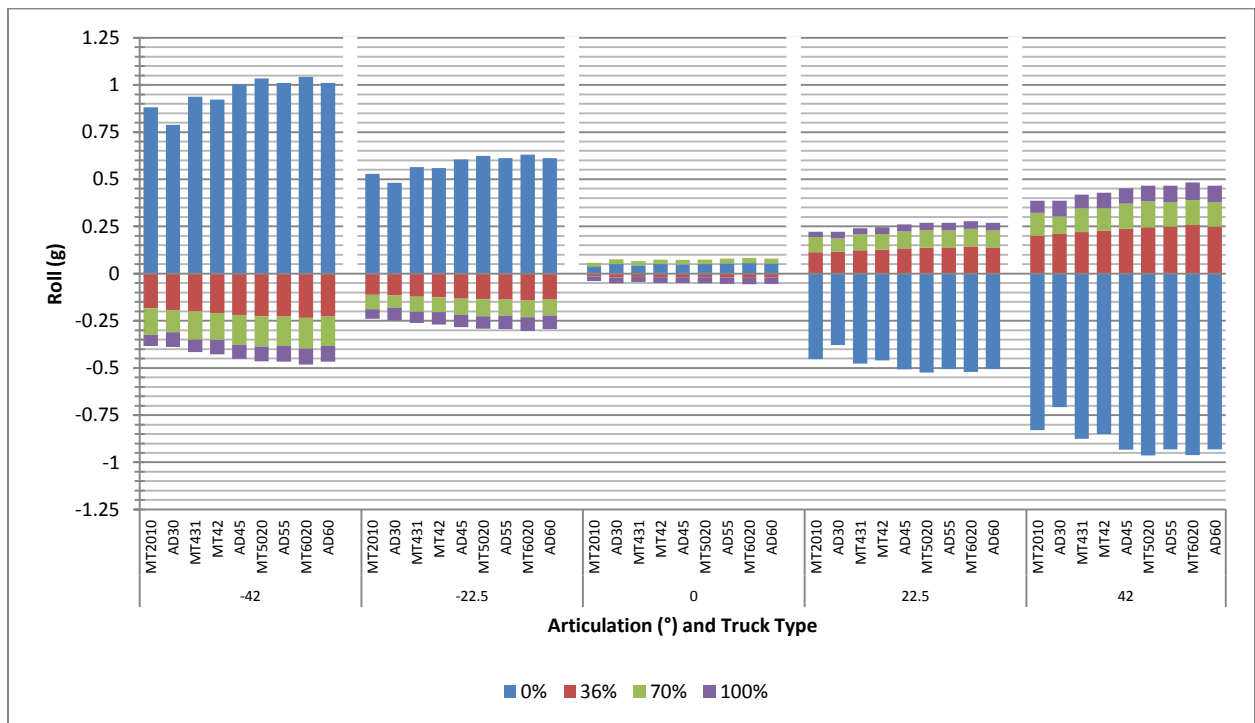


Figure 5.23: Incremental Roll By Payload

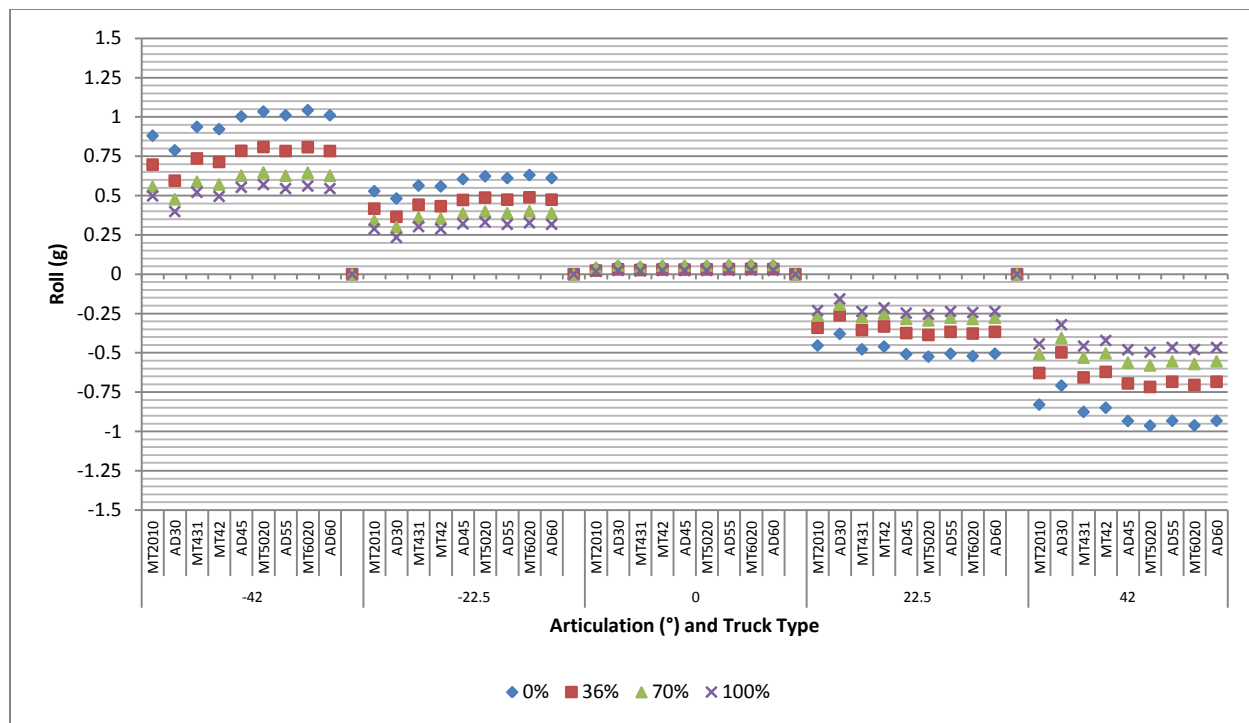


Figure 5.24: Cumulative Roll by Payload

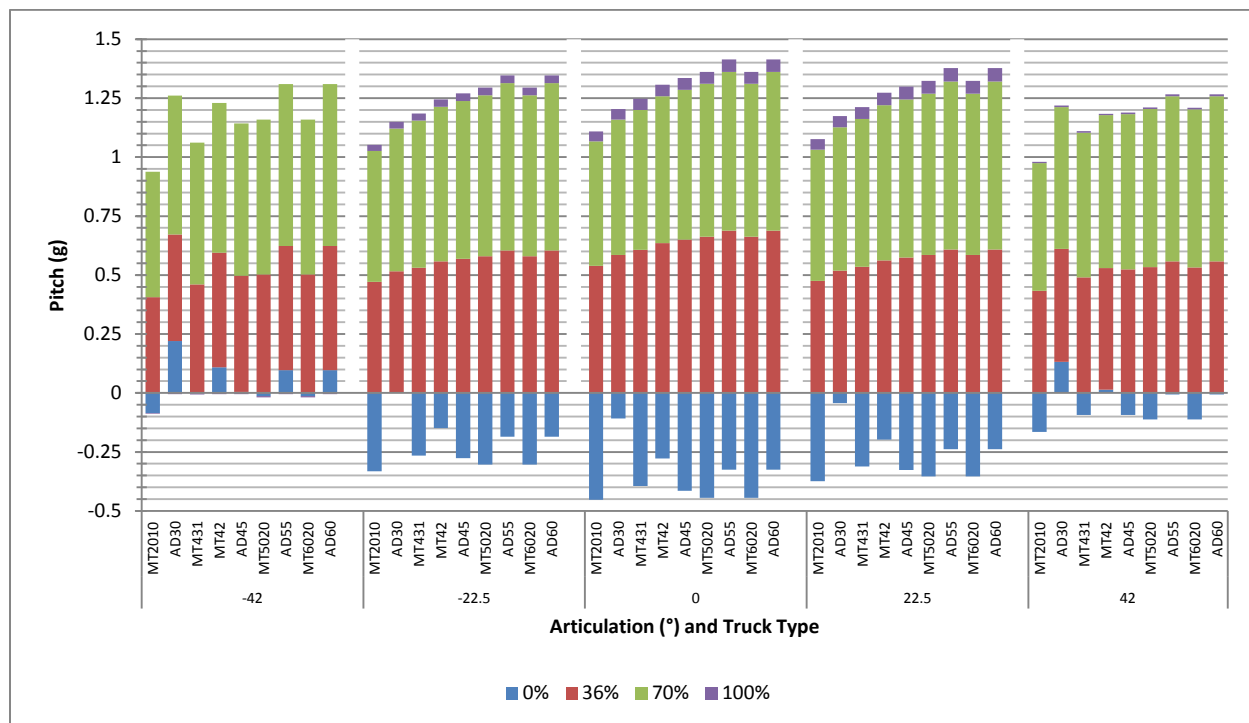


Figure 5.25: Incremental Pitch by Payload



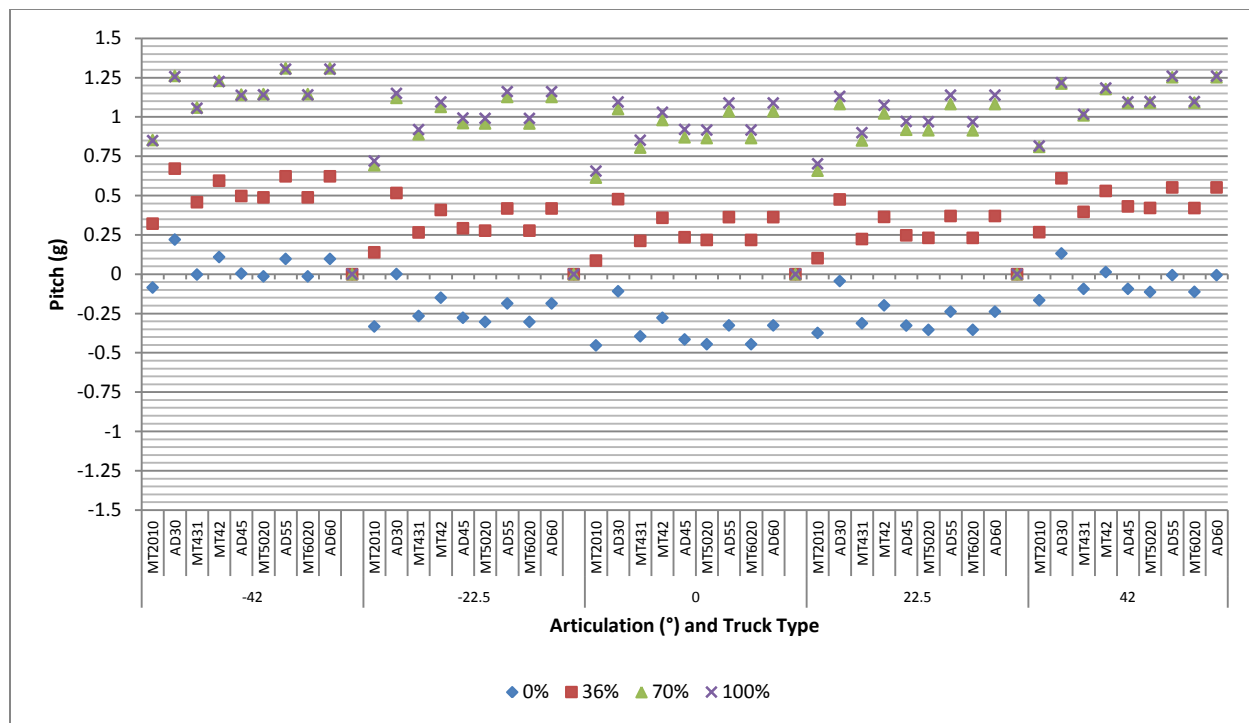


Figure 5.26: Cumulative Pitch by Payload

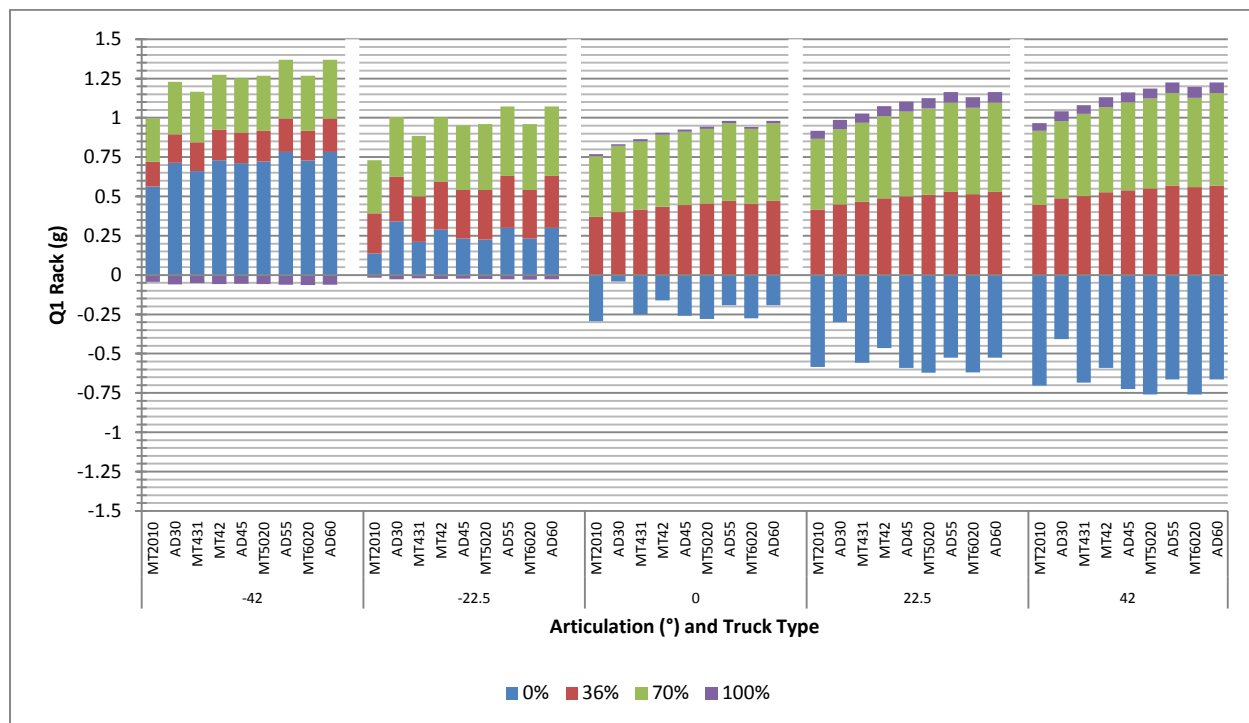


Figure 5.27: Incremental Q1 Rack by Payload

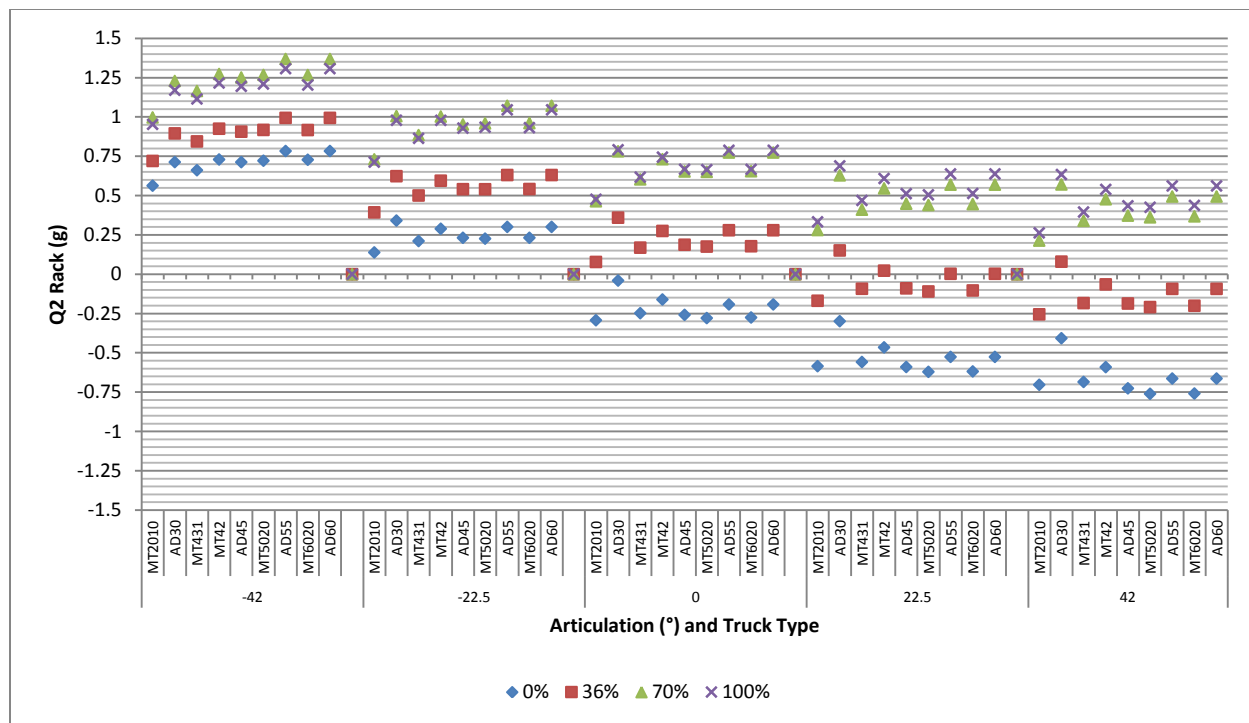


Figure 5.28: Cumulative Q1 Rack by Payload

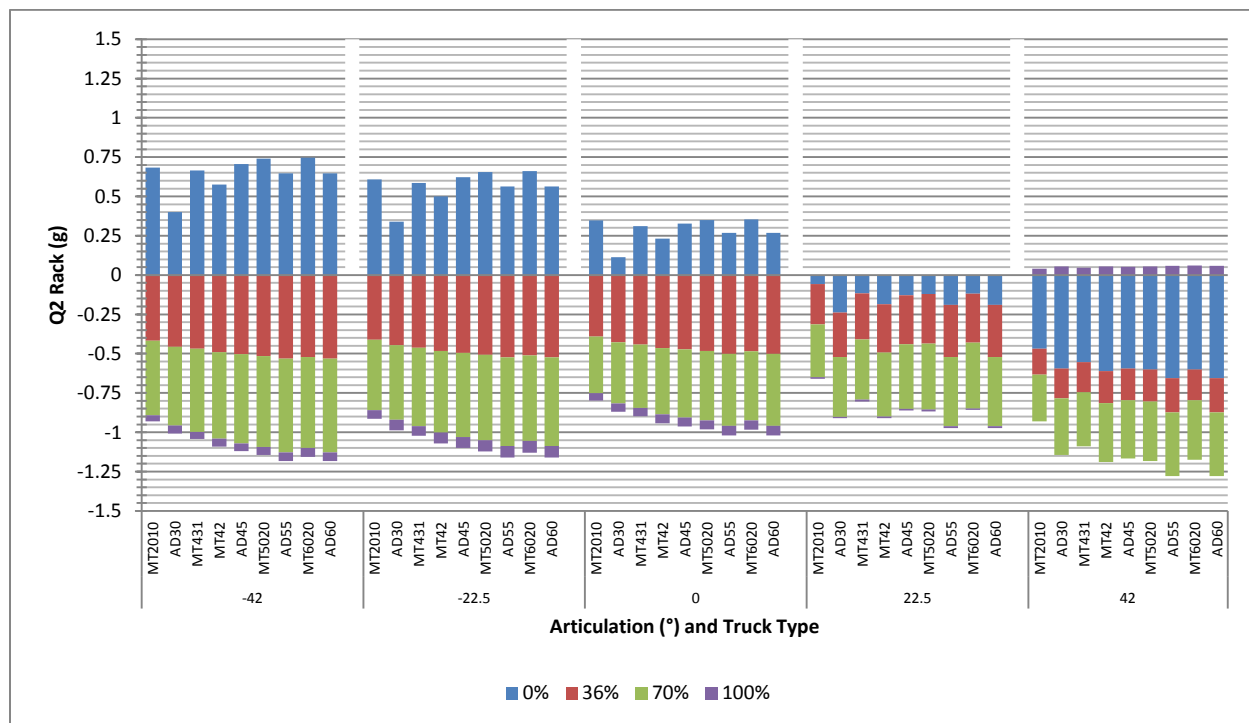


Figure 5.29: Incremental Q2 Rack by Payload

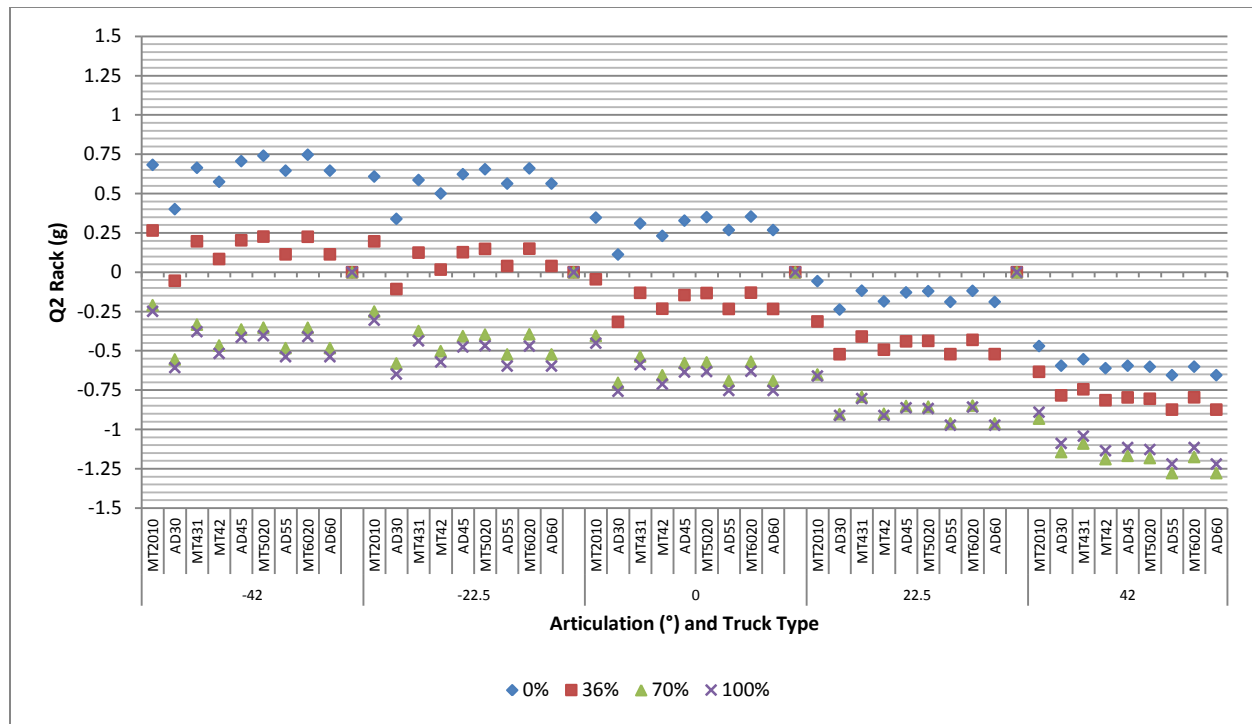


Figure 5.30: Cumulative Q2 Rack by Payload

## 5.2 Full Scale Analysis of Rigid Body Hauler

### 5.2.1 Rigid Body Data

The full scale hauler data used in this study was made available from part of a larger set collected by the University of Alberta in 2004. This data was taken from a Caterpillar 797A operating in a typical Alberta oil sand mining environment on October 21<sup>st</sup>, 2004 between 7:00 and 15:00. All was read at 1hz intervals from Caterpillar's Vital Information Management System (VIMS) and consisted of: time stamp, all four strut pressures, vehicle speed, payload, GPS based latitude and longitude. Table 5.2 below shows a sample of the data collected from the VIMS system.

Date Time	Time	Susp Cyl LTF (kPa)	Susp Cyl LTR (kPa)	Susp Cyl RTF (kPa)	Susp Cyl RTR (kPa)	Ground Speed (km/h)	Payload (tons)	Longitude Deg	Latitude Deg
10/21/2004 12:35:05	12:35:05 PM	8295	11123	4336	9992	23.3	312.9	-111.70827	57.03075
10/21/2004 12:35:07	12:35:07 PM	7352	10746	7352	11312	22.5	312.9	-111.70847	57.03077
10/21/2004 12:35:08	12:35:08 PM	8578	12631	5184	6221	20.9	312.9	-111.70847	57.03077
10/21/2004 12:35:10	12:35:10 PM	8578	12631	5184	6221	20.9	312.9	-111.70866	57.03077
10/21/2004 12:35:11	12:35:11 PM	8578	12631	5184	6221	20.9	312.9	-111.70866	57.03077
10/21/2004 12:35:12	12:35:12 PM	9992	10935	6410	7541	19.3	312.9	-111.70894	57.0308

Table 5.2: Sample Caterpillar 797A Data

Although the available data consisted of fifteen complete load, haul, dump cycles only the peak three cycles in terms of g levels generated are presented in detail. These peak cycles occur between approximately 10:11 and 11:40. For simplicity each reading has been assigned a sample number corresponding to each second after the initial time stamped reading of 07:00 in the original data set. Using this numbered sample system, analysis of the peak three cycles begins at sample number 6500 and ends at 10116.

### 5.2.2 Caterpillar 797 Analysis

The information in Table and figure present the information required for analysis. Note that all required geometry is sourced from the basic 797 equipment data sheets[72].

#### Caterpillar 797

Tare Weight (kg)	146,000	Length AB (m)	5.2
Front Strut Dia. (m)	0.400	Length CD (m)	2.5
Rear Strut Dia (m)	0.381	Length BC (m)	7.2

Table 5.3: Caterpillar 797 Data

#### 5.2.2.1 797 Analysis – About Geometric Center

Section 3.4 contains possible reference points to consider when analyzing rigid bodied haulers. This analysis of the 797 haul truck begins with an analysis about the geometric center of the longitudinal and lateral axes of the vehicle. This reference point is chosen simply because it is a point which is convenient and most simple for cross vehicle comparisons, it also allows for an illustration of the effect reference location has on field data.

The analysis of an UAHT found previously in this research was conducted using scale model laboratory testing which allowed the hub forces to be measured directly at the real world hub locations. When using real world data such as is retrieved from the VIMS system the force data is collected from the struts which are not located directly at the hubs. A further difference is that the 797, like most mining grade haul trucks, utilizes dual rear tires which forces the rear suspension struts to be mounted inside the inner duals resulting in approximately double the distance between the front struts compared to the rears. The overall implication of this is that there is asymmetry of the lateral distances between the front and rear struts. Table 5.4 and Figure 5.31 below illustrates this asymmetry between front and rear strut position vectors on a simple plot.

Geometric Centre Position Vectors (Distance from Reference)	i	j	k
A	2.6	3.6	0
B	-2.6	3.6	0
C	-1.25	-3.6	0
D	1.25	-3.6	0

Table 5.4: Position Vectors - About Geometric Center

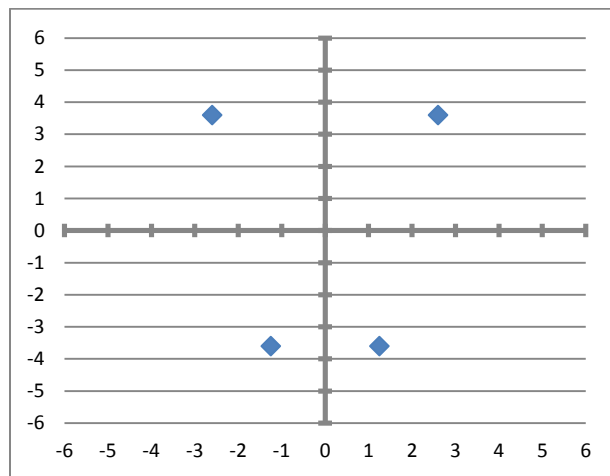


Figure 5.31: Illustrated Position Vectors - Geometric Centre

Analysis of the rigid bodied hauler data was carried out as demonstrated in Sections 3 and 4 with the natural simplifications which follow from the rigid bodied vehicle always having an articulation angle equal to zero which implies that the moment arms of all strut forces are fixed relative to the reference point.

Figure 5.32 to Figure 5.37 below display the 797 hauler results in a similar fashion as the simulated full scale UAHT and Test Unit results expressed in Section 5.1.2. Note that a primary difference is that the effect of the dynamic force due to loading component in the 797 field data yields much more volatility in the results.

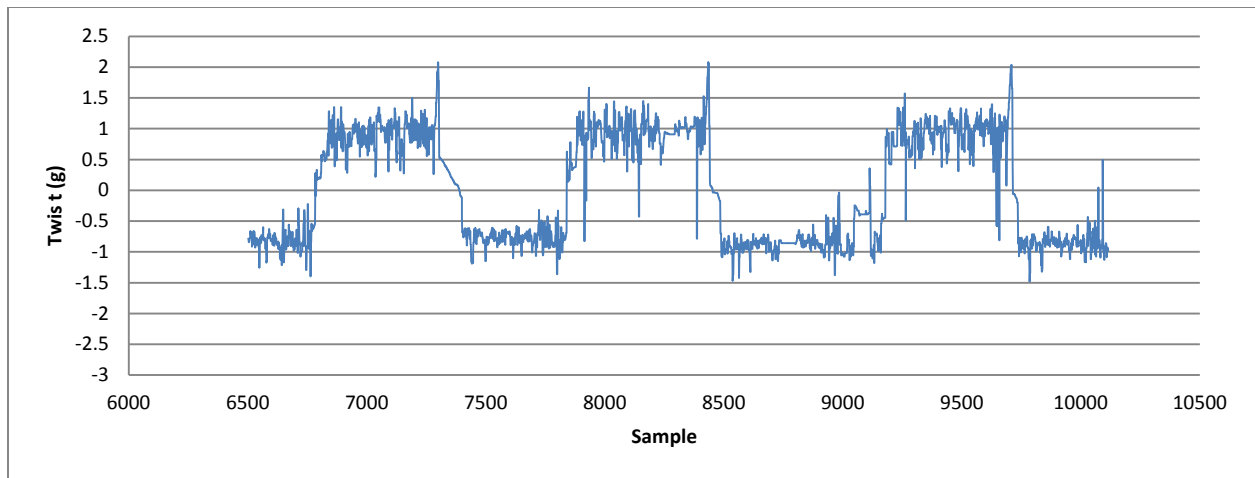


Figure 5.32: 797 g Level Results - Total About Geometric Centre

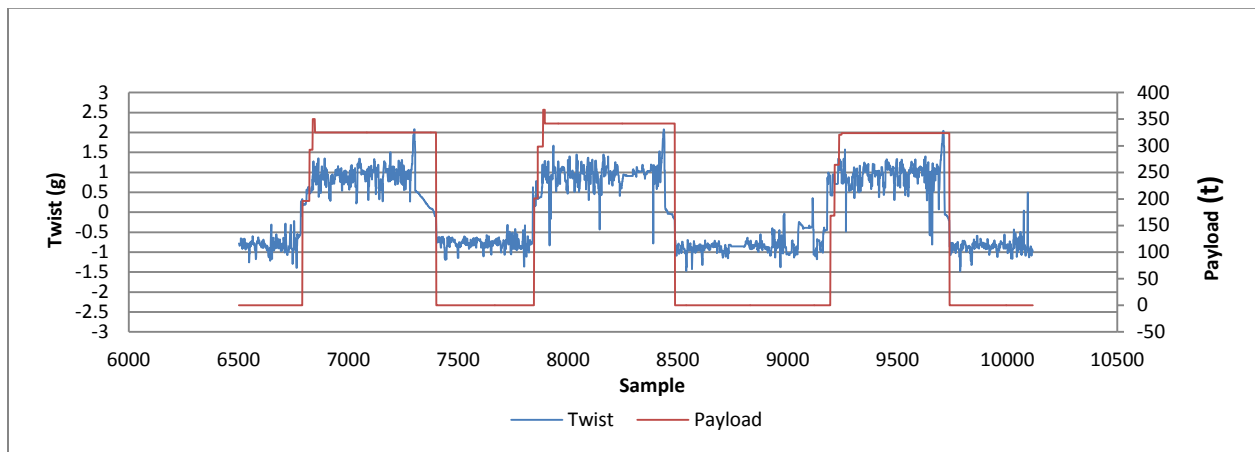


Figure 5.33: 797 g Level Results Total Twist and Payload

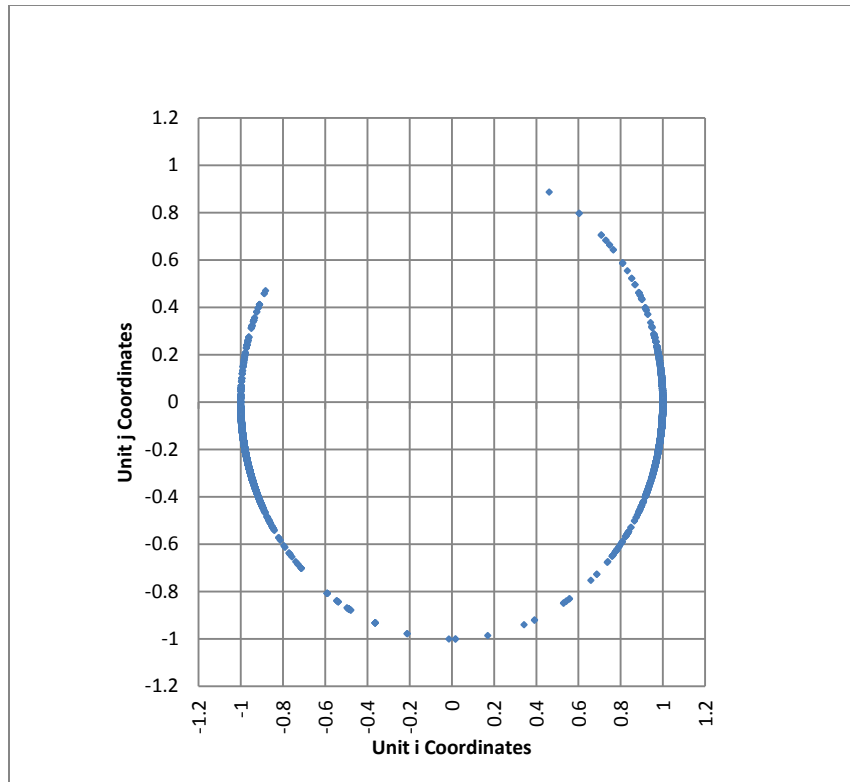


Figure 5.34: 797 Results Direction Plot - About Geometric Centre

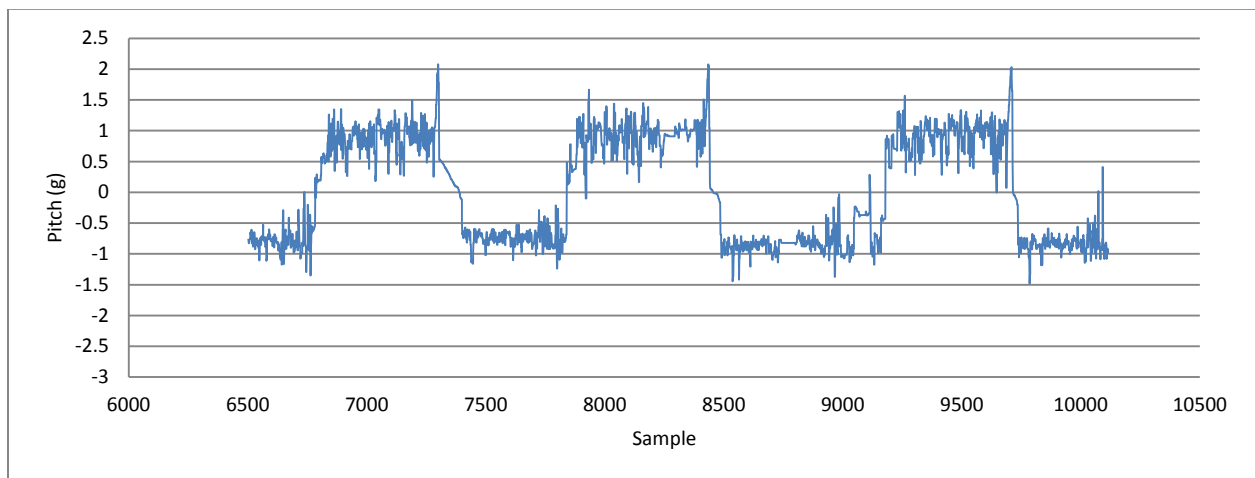


Figure 5.35: 797 Pitch - About Geometric Centre

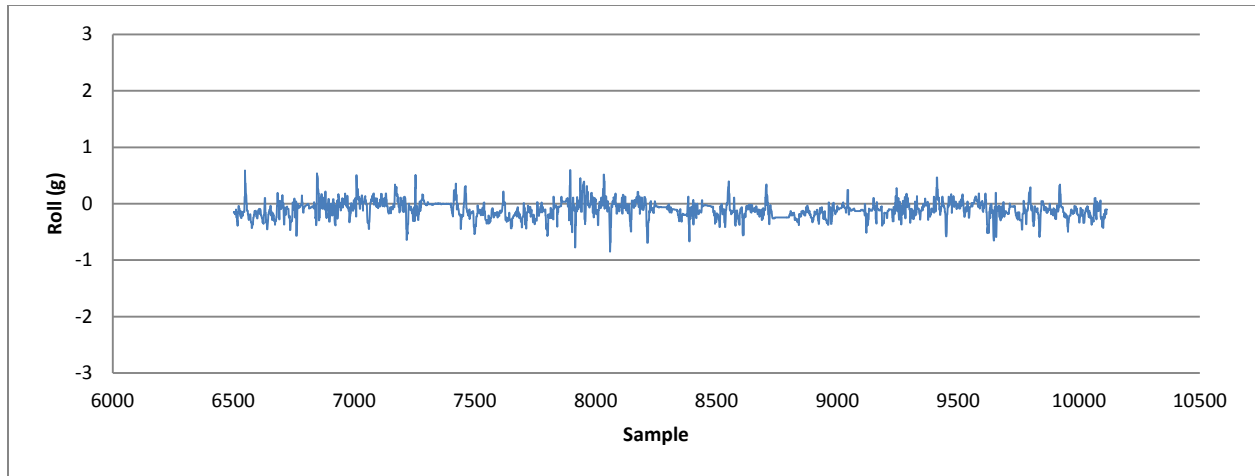


Figure 5.36: 797 Roll - About Geometric Centre

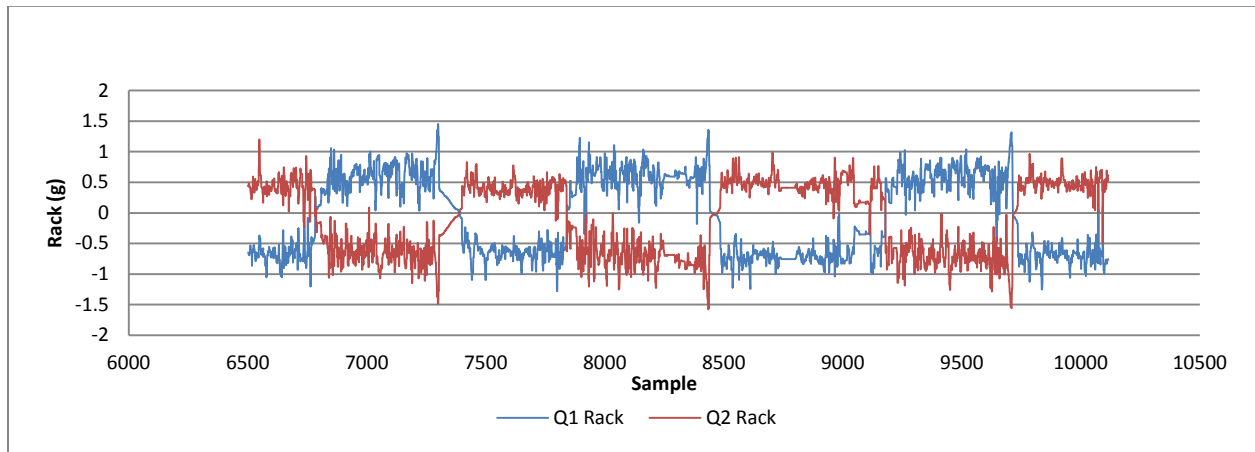


Figure 5.37: 797 Rack - About Geometric Centre

#### 5.2.2.2 797 Analysis - About Theoretical Centre of Gravity

The previous section presented gLA results for the 797 hauler using real world data. The following section provides results calculated from the same 797 data set but about the theoretical centre of gravity of the vehicle under loaded and empty conditions. The calculation of this theoretical COG assumes vehicle symmetry about the longitudinal (Y-Axis). The location of COG along the longitudinal axis is calculated from the manufactures specifications which provide the ideal front to rear weight distribution under loaded and empty conditions. Because the realized COG depends on variable such as load placement, strut condition and the placed location of aftermarket equipment it is important to



note that this analysis is about the theoretical COG. Also note that the distinction between the loaded and empty conditions was nominally chosen to be 180 tonnes as recorded by the VIMS system. Figure 5.40 through Figure 5.45 display the results calculated about the Theoretical COG. Table 5.5 and Table 5.6 along with Figure 5.38 and Figure 5.39 below illustrate the difference between the loaded and empty position vectors of each strut.

Loaded Position Vectors (m)	i	j	k
A	2.6	4.8	0
B	-2.6	4.8	0
C	-1.25	-2.4	0
D	1.25	-2.4	0

Table 5.5:797 Loaded Position Vectors - Ideal COG

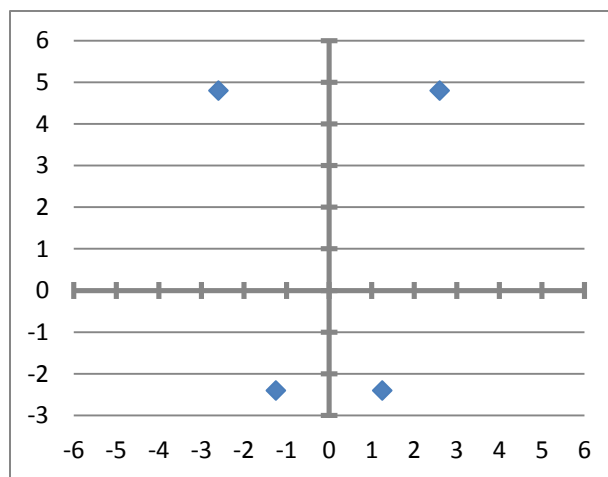


Figure 5.38:797 Illustrated Position Vectors - Loaded COG

Empty Position Vectors (m)	i	j	k
A	2.6	2.88	0
B	-2.6	2.88	0
C	-1.25	-4.32	0
D	1.25	-4.32	0

Table 5.6: 797 Empty Position Vectors - Ideal COG

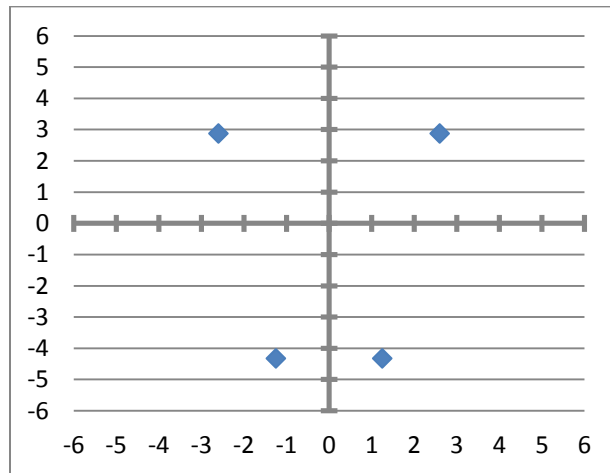


Figure 5.39: 797 Illustrated Position Vectors - Empty COG

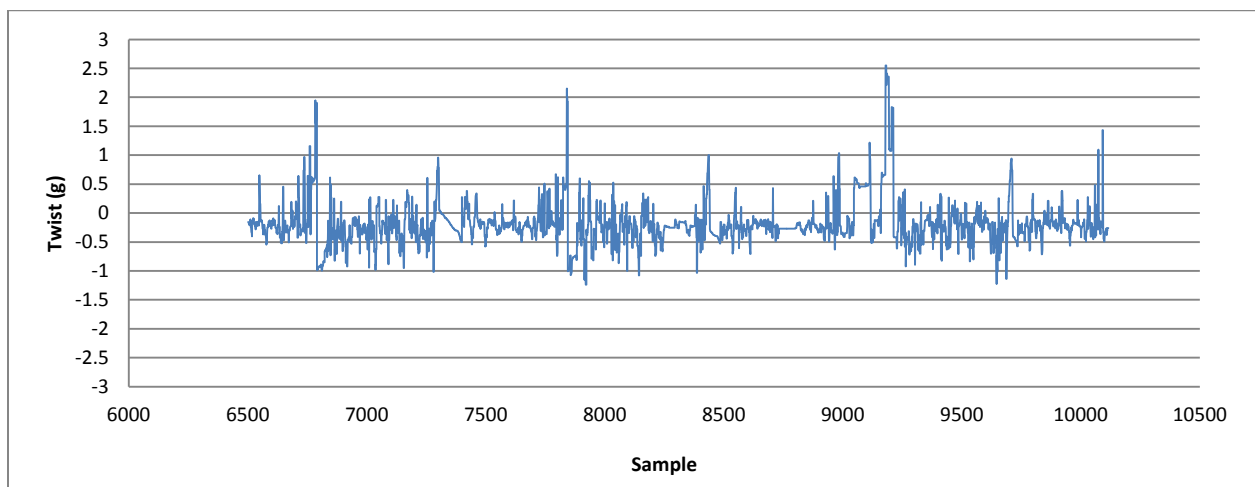


Figure 5.40: 797 Total g Level - About Ideal COG

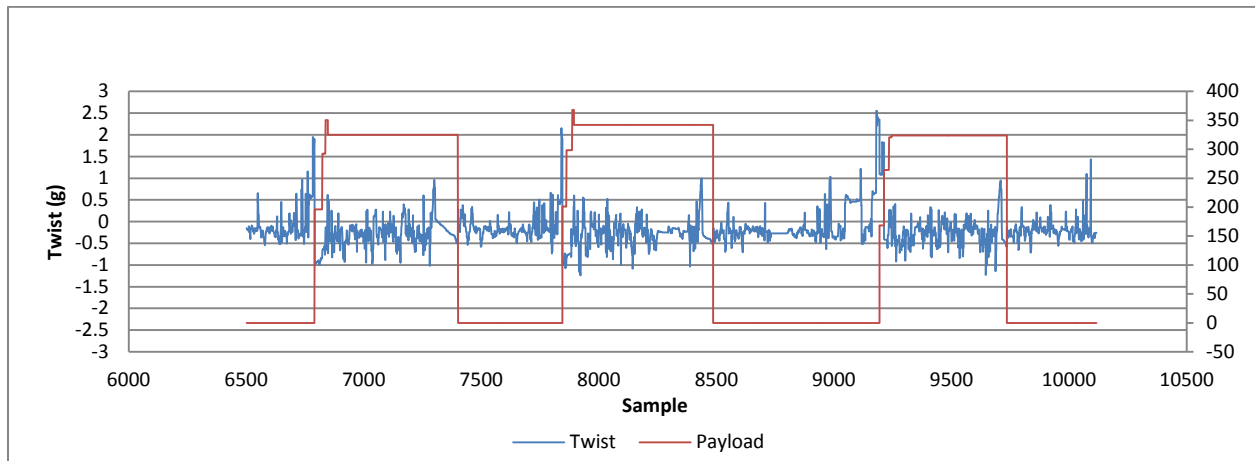


Figure 5.41: 797 Total Twist Results - About Ideal COG

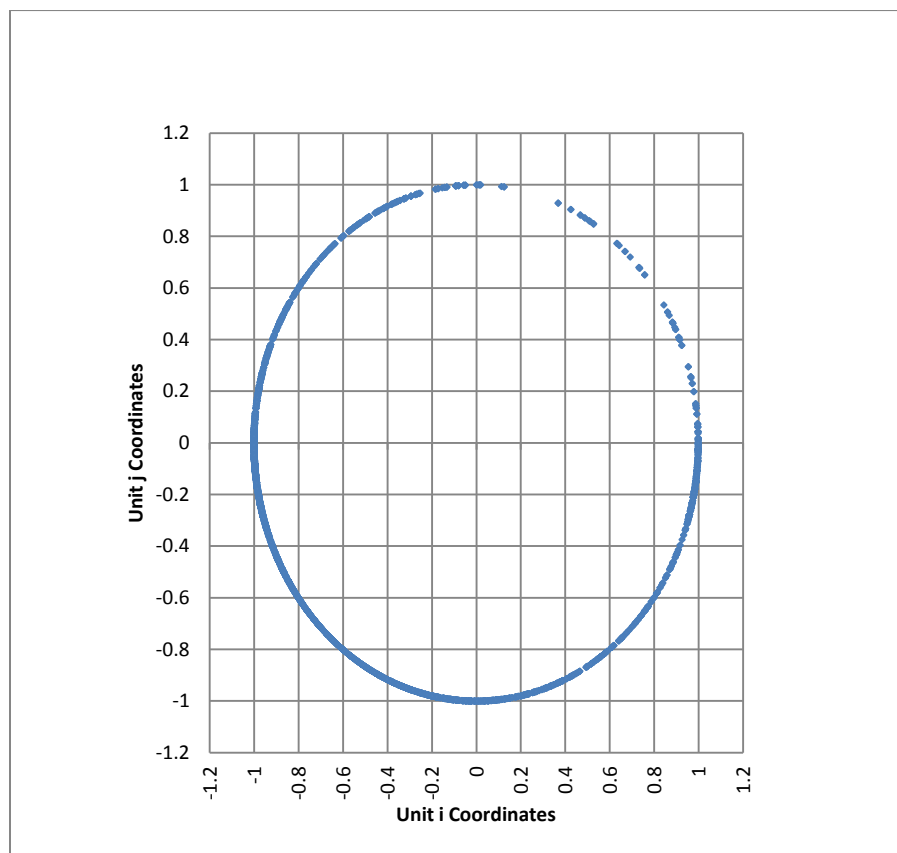


Figure 5.42: 797 Direction Plot - About Ideal COG

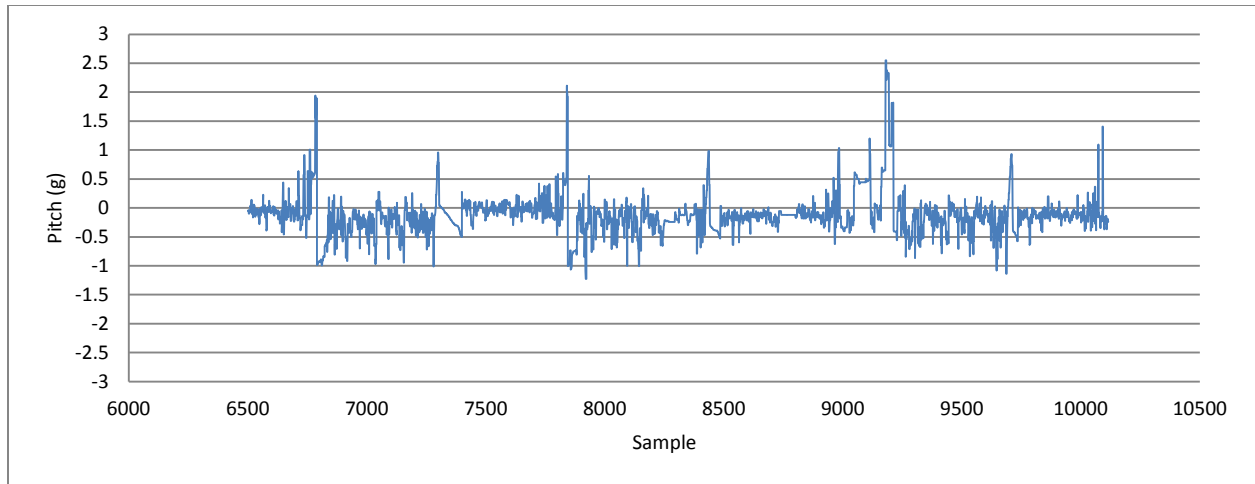


Figure 5.43: 797 Pitch Results - About Ideal COG

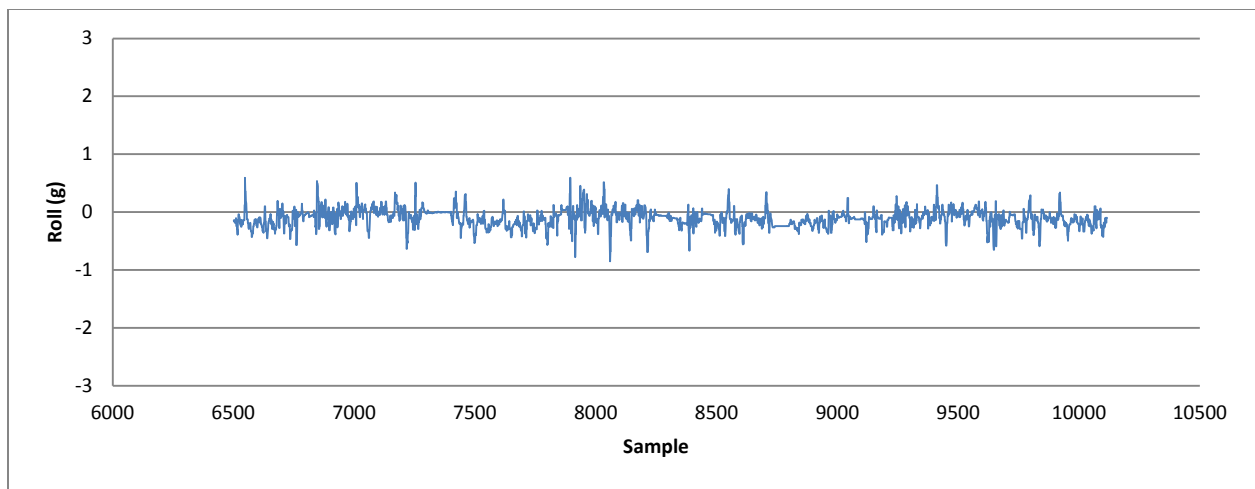


Figure 5.44: 797 Roll Results - About Ideal COG

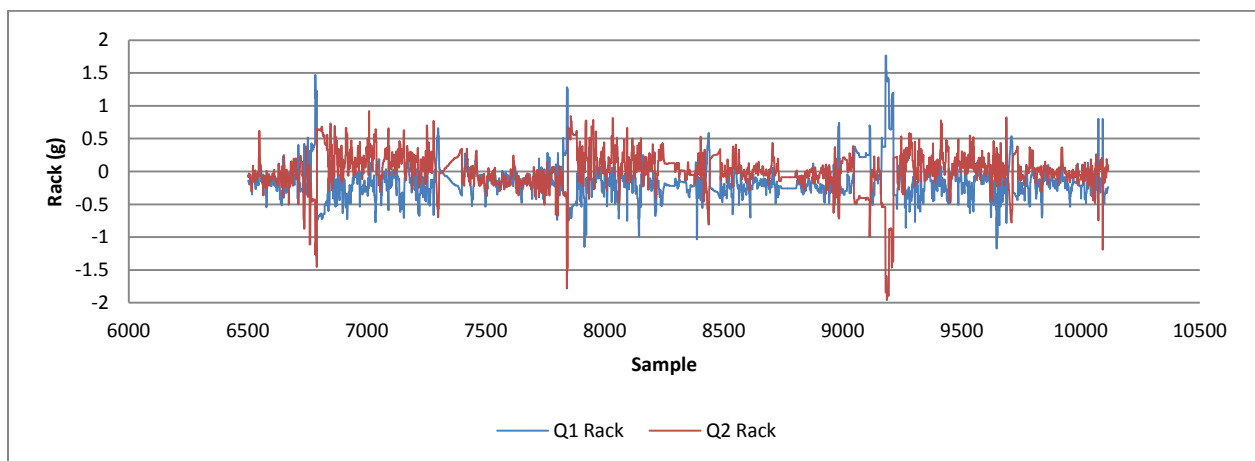


Figure 5.45: 797 Rack Results - About Ideal COG

### 5.2.2.3 Haul Road Analysis

The Literature review included in this study was designed to provide examples of current operational considerations to which the gLA method could be applied. Figure 5.46 below shows the results of a basic application of the gLA method to haul road maintenance. The figure is generated from the same data set used in the previous 797 hauler analysis. See the Discussion section for further comment. Haul road analysis is preformed using the geometric centre as the reference to maintain consistency between loaded and empty hauling. This is considered acceptable because this analysis is concerned with the haulers interaction with the ground rather than the effect on the hauler itself. Figure 5.47 and Figure 5.48 show that in this data set there is no correlation between calculated g level and either vehicle speed or acceleration. From Figure 5.46 the user can easily see which sections of haul road require attention because high g events (red circles) are currently being experienced and which areas require attention (yellow circles) to prevent deterioration to the point that high g levels are induced. For example purposes, sections of Figure 5.46 have been labeled with likely locations of major site components. While these labels may not be completely accurate they serve to demonstrate likely reasons for the path taken by the hauler.

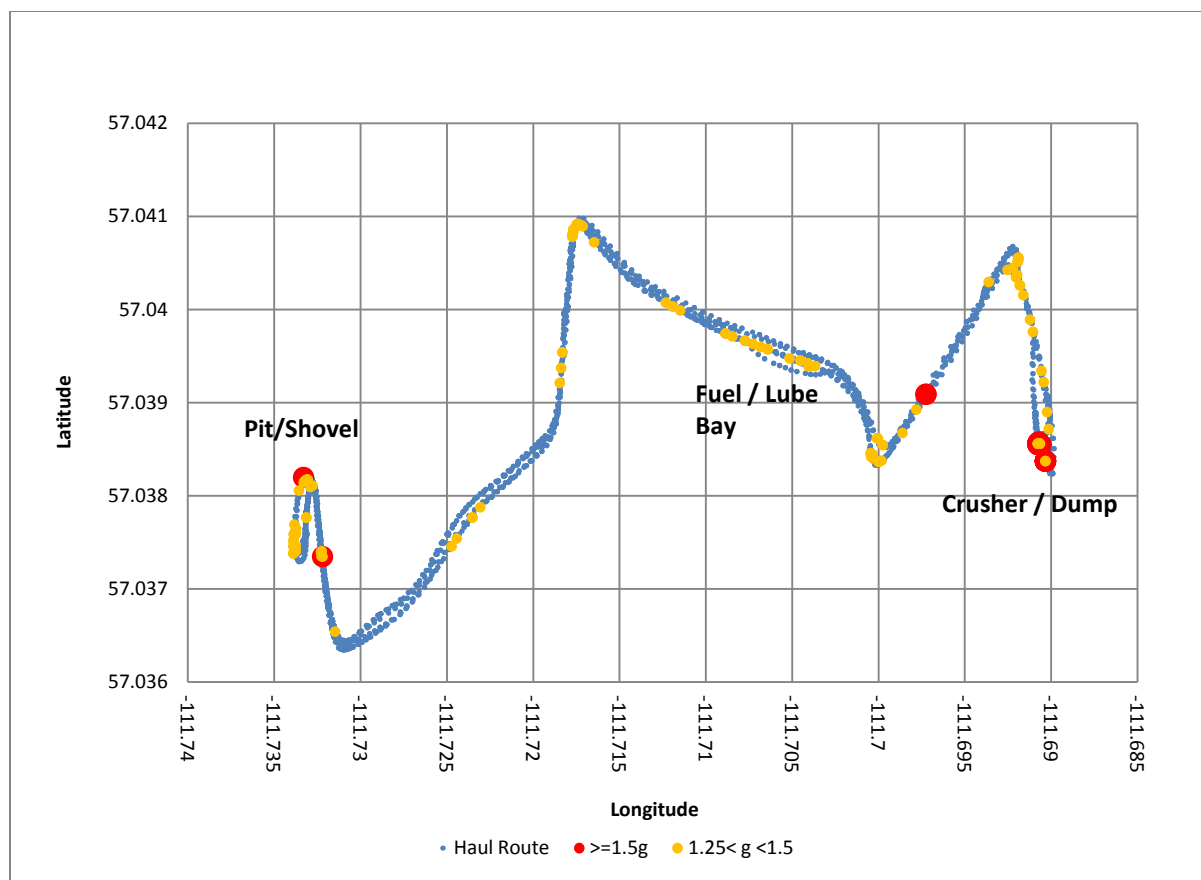


Figure 5.46: 797 Results - Basic Haul Road Analysis

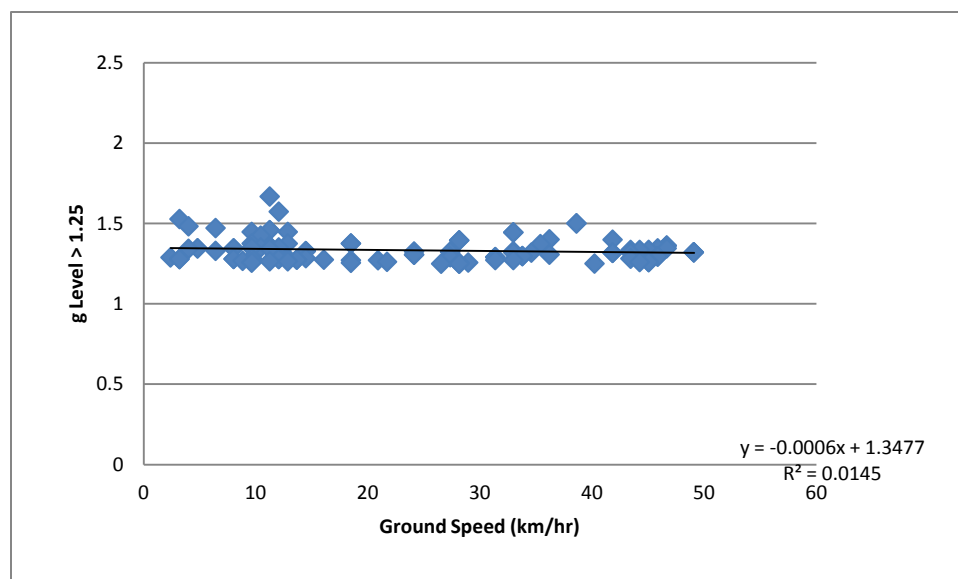


Figure 5.47: 797 Vehicle Ground Speed vs g Level

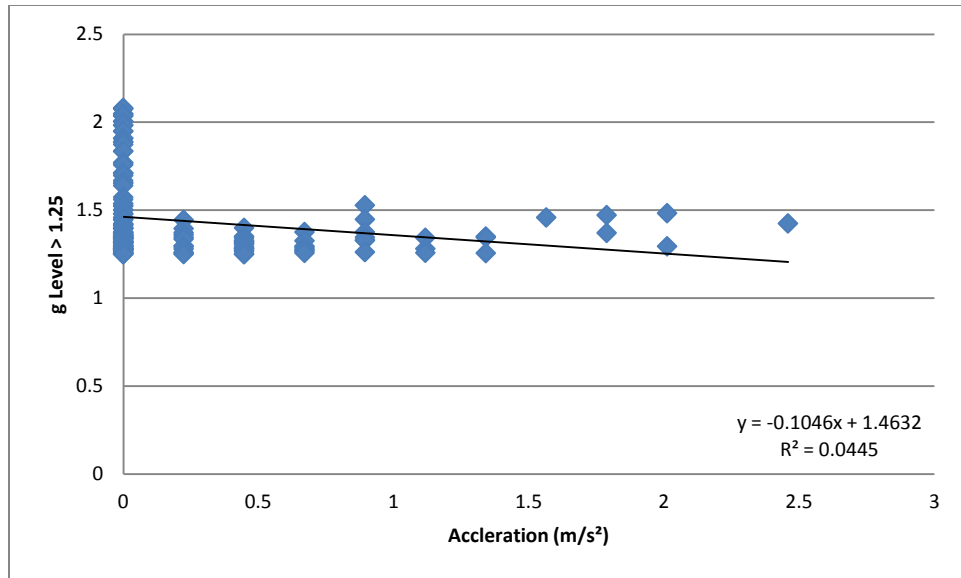


Figure 5.48: 797 Vehicle Acceleration vs g Level

#### 5.2.2.4 Energy Efficiency

The 797 hauler data set used in this section is a discrete data set collected on set time intervals and is representative of what is commonly found with respect to equipment performance data collection. This study initially manipulates this data to calculate a resultant cumulative moment about a chosen reference point. The following section describes a further analysis which allows for an estimate of the amount of energy required to generate this adverse cumulative moments.

The primary task of any hauler is to move material from point A to point B. In carrying out this function useful energy is expended by moving the center of gravity only, all other motion of the hauler can and should be considered waste. Examples of wasted energy are excessive motions or forces as described in this research: Rack, Pitch and Roll. When calculated as a cumulative moment about the appropriate COG, loaded or empty, the degree of rack, pitch and roll represents the degree of efficiency with which the hauler moves the COG. Haul road, truck and operator combinations which create large moments about the COG can be interrupted to be less efficient than those who generate smaller cumulative moments. It is perhaps helpful to note that the term “about the COG” implies motion or forces generating rotational tendency and does not contribute to the movement of the COG directly between two points.

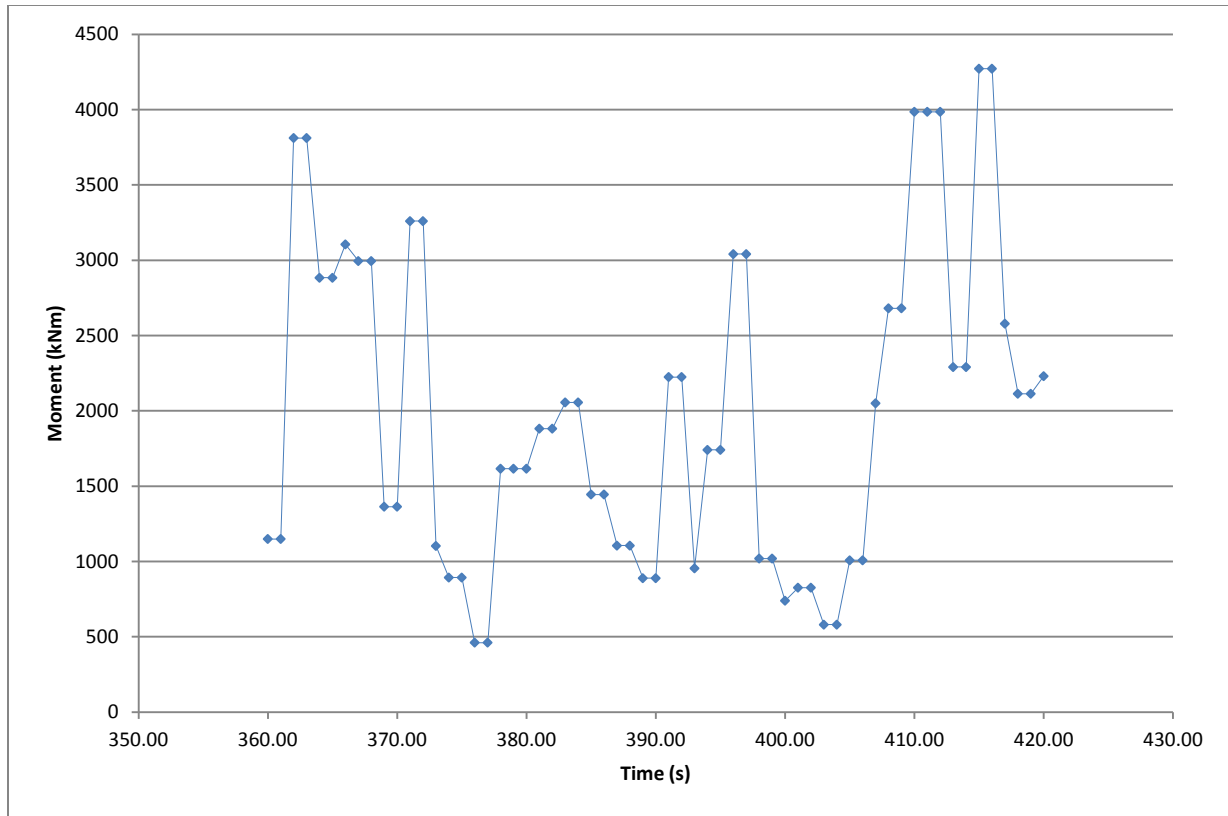


Figure 5.49: 797 Moment About Ideal COG - 60s Sample

Analysis to estimate the amount of moment about the COG in terms of energy is as follows. Using the previously mentioned Cat 797 hauler data Figure 5.49 above shows a 60s sample of the time versus cumulative moment about the haulers COG. The time versus absolute slope between each of the data points from Figure 5.49 is shown in Figure 5.50 and can be observed to have units of Watts. Note that the absolute value of the slopes are used for this analysis as a negative cumulative moment indicates direction and does not imply that useful energy has been created.



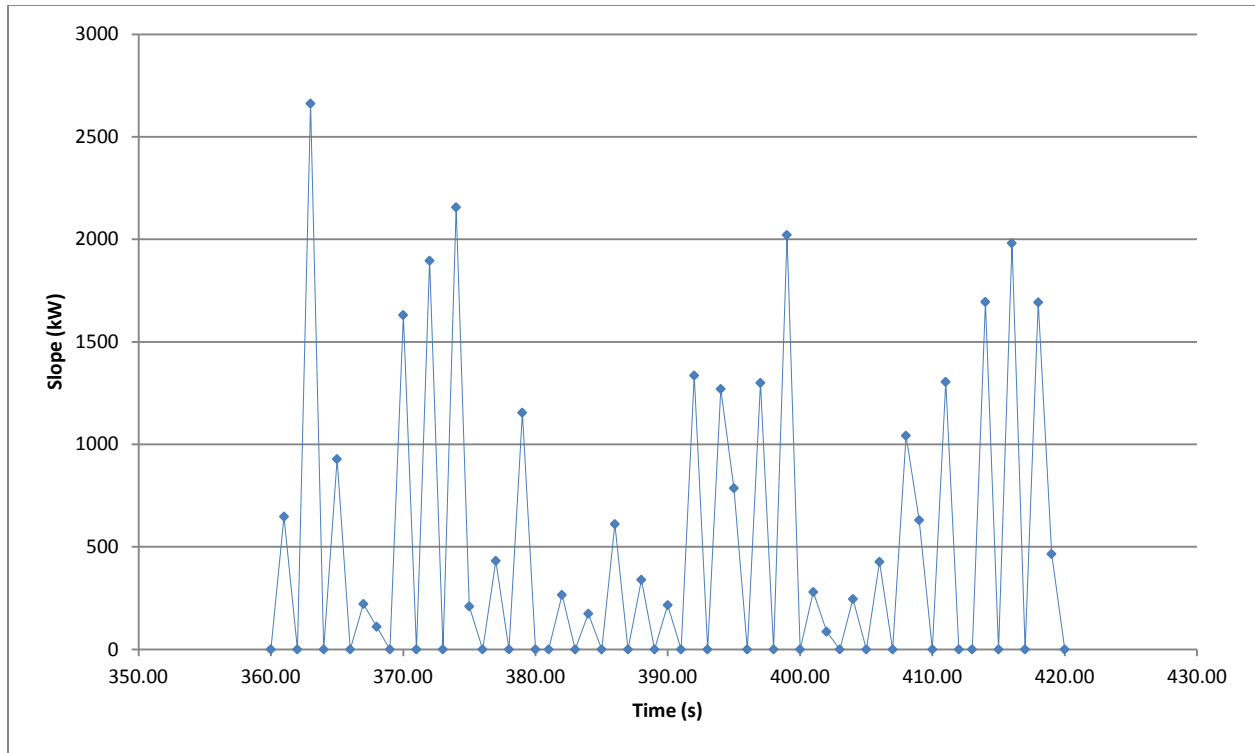


Figure 5.50: Absolute Value Slope of Moment About Ideal COG (60s Sample)

Using the mid-point approximation method to calculate the area under the curve between each of the discrete points in Figure 5.50 which now carries units of Joules, the summation of each of these area approximations provides the estimate of energy wasted in the generation of adverse motions/forces. Table 5.8 below shows these energy results for the 797 hauler data set, Table 5.7 summarizes the general parameters used in this energy analysis.

<b>Sample Time (hr)</b>	1.00
<b>Cumulative Energy About COG (kJ)</b>	645,114
<b>Equivalent Fuel Per Hour (kg)</b>	17.4
<b>Diesel Density (kg/L)</b>	0.88
<b>Energy in Diesel (kJ/kg)</b>	43,400
<b>Mechanical Efficiency</b>	85%
<b>Effective Diesel Energy (kJ/L)</b>	36,890

Table 5.7: Energy Analysis Parameters

	Low	Med	High
<b>797F Fuel Consumption (kg/hr)</b>	130.1	193.6	258.1
<b>% Waste</b>	13%	9%	7%

**Table 5.8: Energy Analysis Results**

Referencing Table 5.8, the results of this study indicate that in extreme cases up to 13% of fuel used could be wasted through unnecessary moments created about the COG of the vehicle. Note that the “Cumulative Energy about the COG” in Table 5.8 is calculated to only include the energy created when the vehicle is in motion. The discussion section further comments on the assumptions and interpretations of the results of these tables.

## 6 Comparison of 2003 Method and gLA

The development and application of the Generalized g Level Analysis method is an extension and improvement of the method presented by Joseph in 2003. It has been shown that the gLA method can be applied to both articulated and rigid frame equipment; this section demonstrates a comparison between Joseph's original 2003 method and gLA method using data from the articulated test unit, Chapter 4, and the ultra class rigid hauler data used in Section 5.2.

### 6.1 Rigid Hauler Comparison

Using each method, g Level calculations were performed on loaded and empty subsets of data from the total data set used in Section 5.2. Specifically the loaded data set consisted of samples 7000 to 7250 while the empty data set consisted of samples 7500 to 7750. Because both loaded and empty conditions were tested the reference point chosen to be used with the gLA was the appropriate loaded or empty ICOG as described in Section 5.2. Calculation of the 2003 method was as described in Joseph, 2003 [3].

Figure 6.1 and Figure 6.2 below, show the roll and pitch results of the two methods for the loaded vehicle. The correlation observed in these plots is verified from the linear regression analysis presented in Figure 6.3 and Figure 6.4. For a rigid framed vehicle this high degree of correlation is expected for the roll and pitch response components. Due to the inherent symmetry of rigid equipment, the 2003 calculation method's treatment of strut forces naturally constructs the vehicle's resultant responses along what is essentially the roll and pitch axes defined by the gLA method.

The results of the two methods do diverge when considering gLA's twist and Q1 or Q2 rack to rack as defined by the 2003 method. It can be seen from Figure 6.5 that there is much less correlation between twist/rack results than was observed between pitch and roll results. This is confirmed by the regression analysis in Figure 6.6 which shows zero correlation. This result is possibly explained by the ability of twist, as defined by gLA, to describe a response in a variable direction while rack, as termed in the 2003 method, is a magnitude in a static direction. Figure 6.7 shows the regression analysis between gLA's Q2 rack and 2003 rack, which shows a low degree of correlation between the two metrics. This is perhaps a more fair comparison as the gLA twist is projected onto a static axis, which is assumed to be the most comparable to the 2003 rack result.

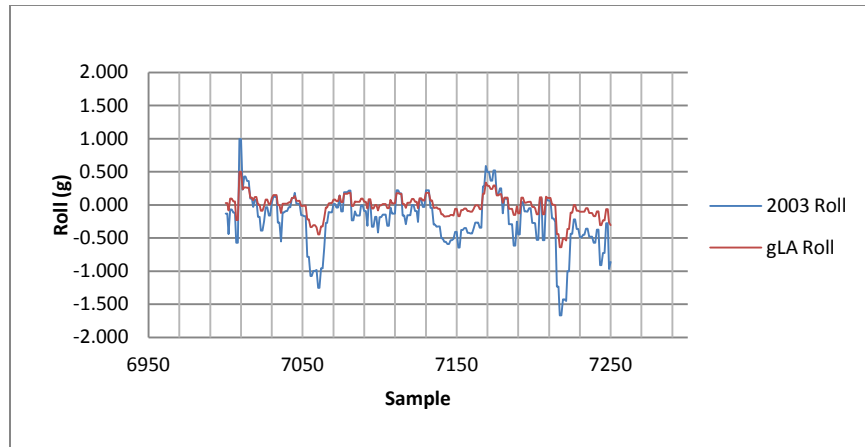


Figure 6.1: Roll Comparison, Loaded Sample

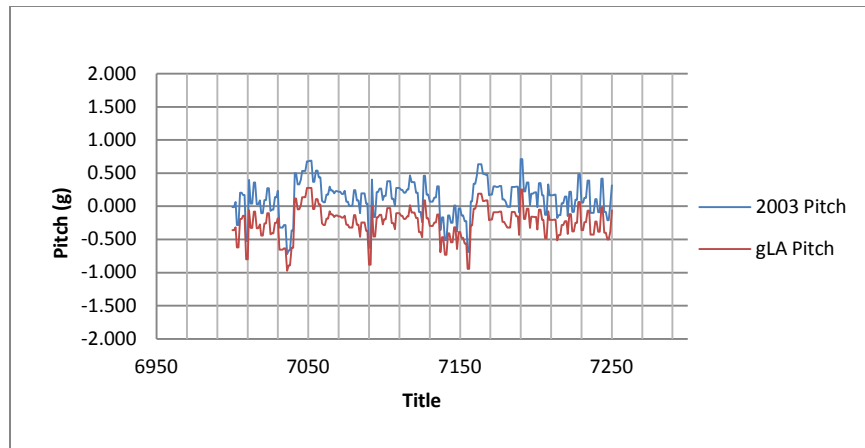


Figure 6.2: Pitch Comparison, Selected Sample

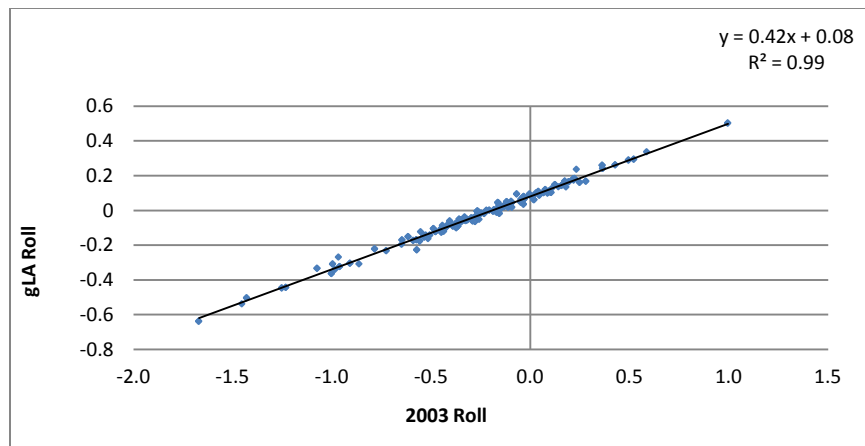


Figure 6.3: Roll Cross Plot

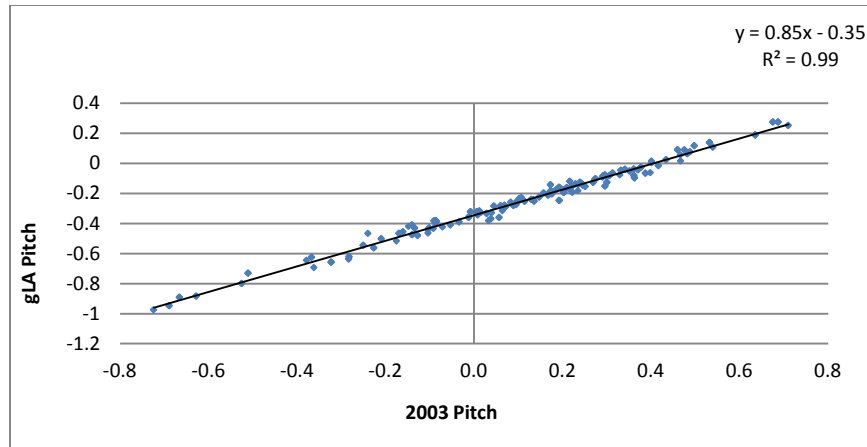


Figure 6.4: Pitch Cross Plot

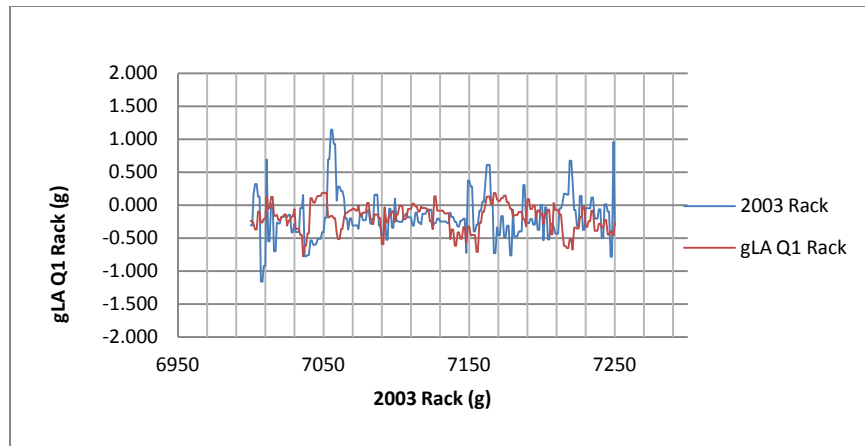


Figure 6.5: Total Twist vs. Rack Comparison, Selected Sample

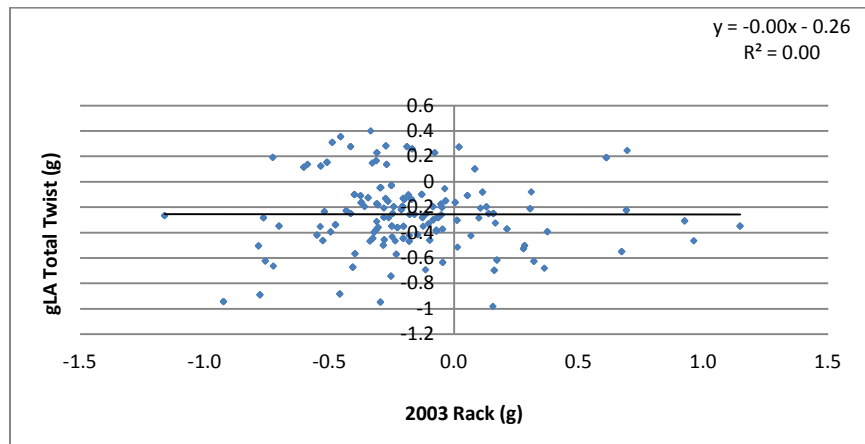


Figure 6.6: Total Twist vs. Rack Cross Plot

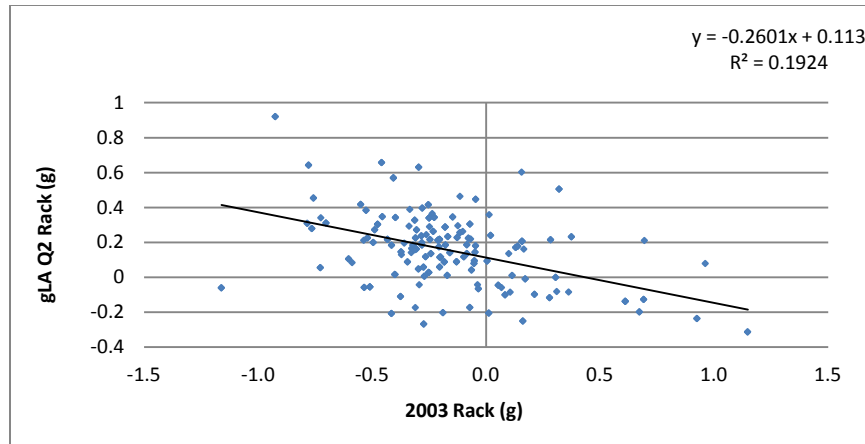


Figure 6.7: Q2 Rack vs. Rack Cross Plot

As a final rigid body hauler comparison between the two methods, the roll and pitch components from the 2003 method results were used to construct a resultant vector response similar to gLA's twist. This construction is illustrated in Figure 6.8. While little correlation was observed from this, a large degree of correlation is found if this constructed response is projected onto either the Q1 or Q2 rack axes as defined by gLA. The Q2 rack result is shown as an example in Figure 6.9. This result is not surprising as it has already been shown that there is correlation between the roll and pitch responses, the construction of a resultant from the 2003 method, and its correlation to gLA rack, shows that the two methods can be correlated if the resultant response direction is considered. This also shows that gLA is a generalized version which can be applied to both rigid and articulated equipment specifically because of its treatment of response direction.

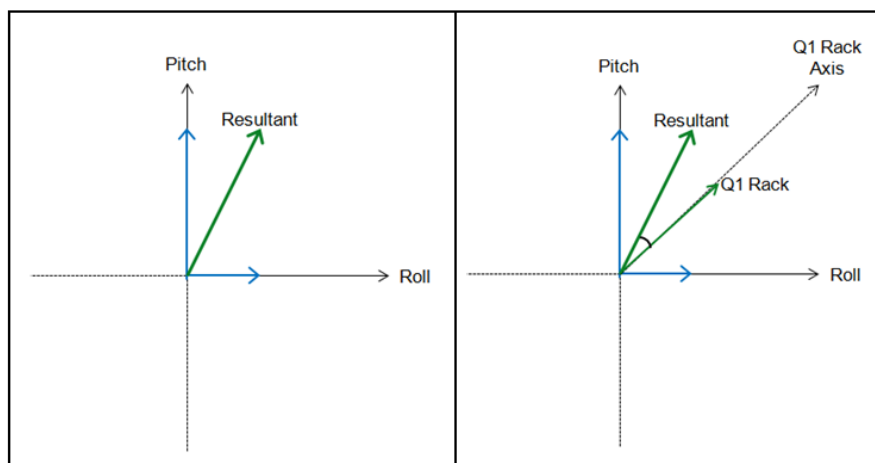


Figure 6.8:(Left) 2003 Resultant Construction, (Right) Q1 Rack Projection

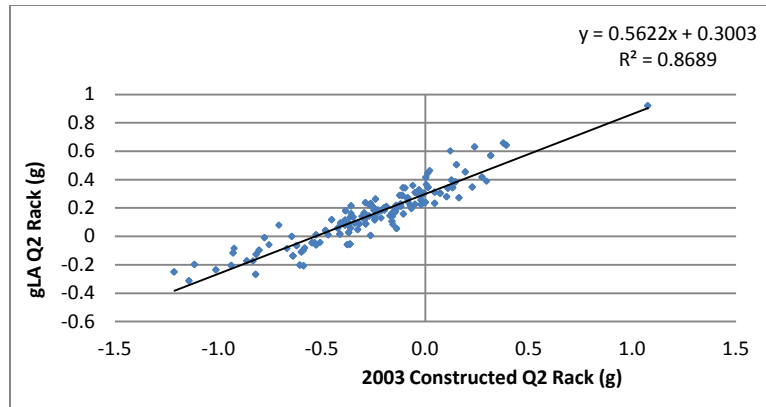


Figure 6.9: gLA Q2 Rack vs. 2003 Constructed Q2 Rack

## 6.2 2003 vs. gLA With Model Data

The previous section has demonstrated that both methods can be applied with a high degree of correlation to rigid body equipment, the intent of this section is to show that gLA is an extension and improvement on the 2003 method in that it can be applied to articulated equipment as well. To compare the 2003 and gLA methods were tested using the scale model data described in Sectionxxx. Results from the 2003 method were calculated exactly as described in Joseph, 2003, with no other data processing or calculations used to accommodate changes in vehicle geometry. The gLA method results used in this section are the same as those presented in Section 4.8.

Figure 6.10 and Figure 6.11 present the results of the 2003 method applied to the articulated scale model data set. These figures present only the magnitude of the response and it can be seen that as the degree of articulation is increased, so too does the magnitude of the response. This variation is explained by the results of Appendix 1 which verified that as the vehicle articulates the weight distribution also varies. Figure 6.12 shows the rack results using the 2003 method. When considering only magnitude, the 2003 method is capable of capturing the overall trends in vehicle response as is the gLA method, this is verified in the provided example regression analysis shown in Figure 6.13 through Figure 6.16. However, the linear nature of the 2003 results for pitch and rack begin to show that while trends in magnitude may be similarly captured, the direction of the overall response may not be.

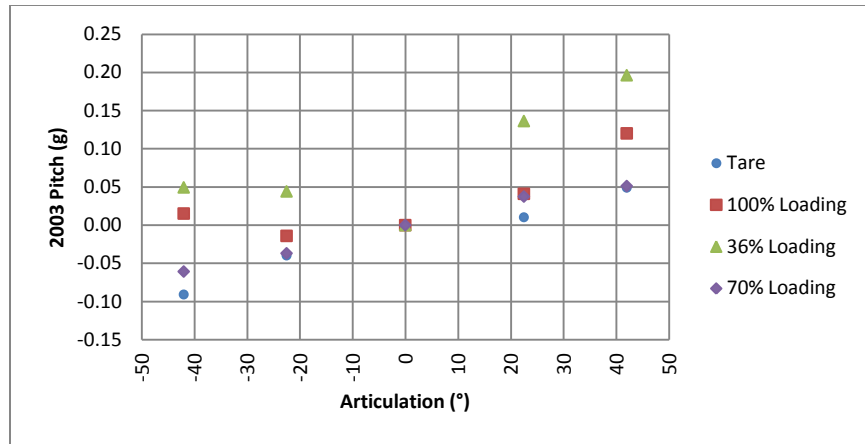


Figure 6.10: 2003 Articulated Pitch

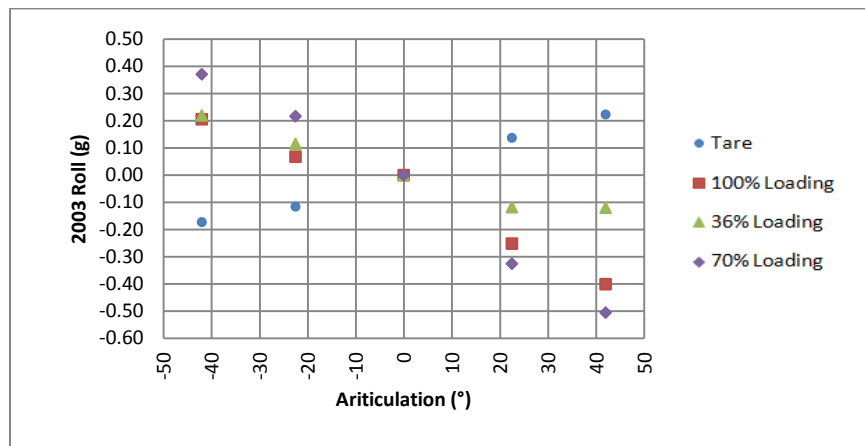


Figure 6.11: 2003 Articulated Roll

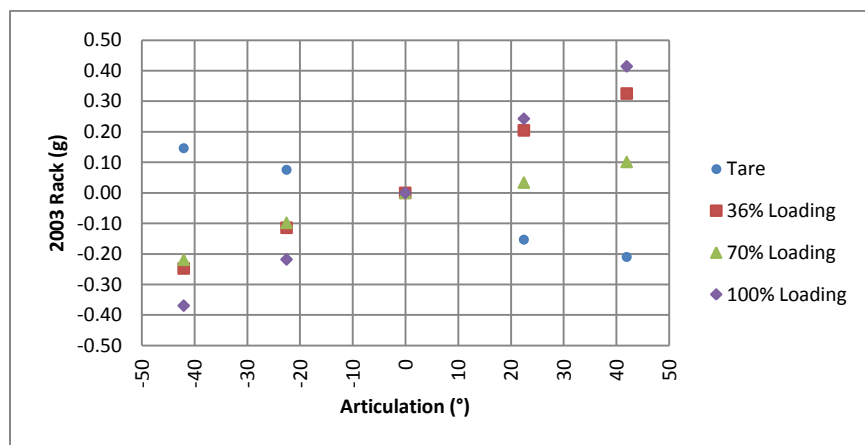


Figure 6.12: 2003 Articulated Rack



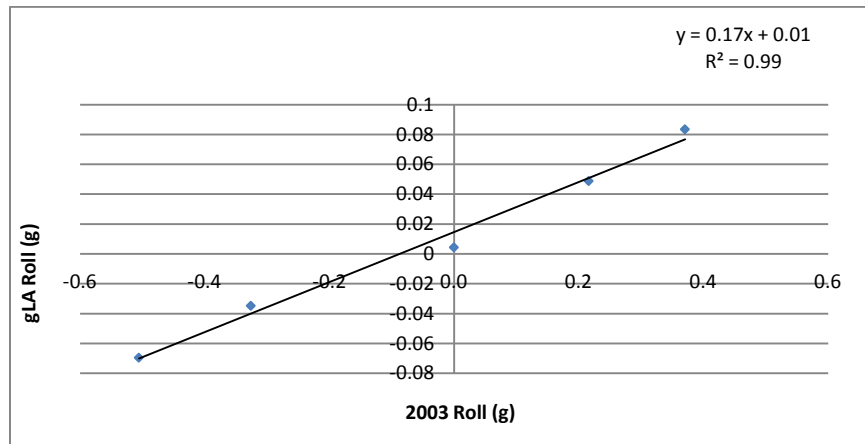


Figure 6.13: Articulated Roll Cross Plot, 100% Loading

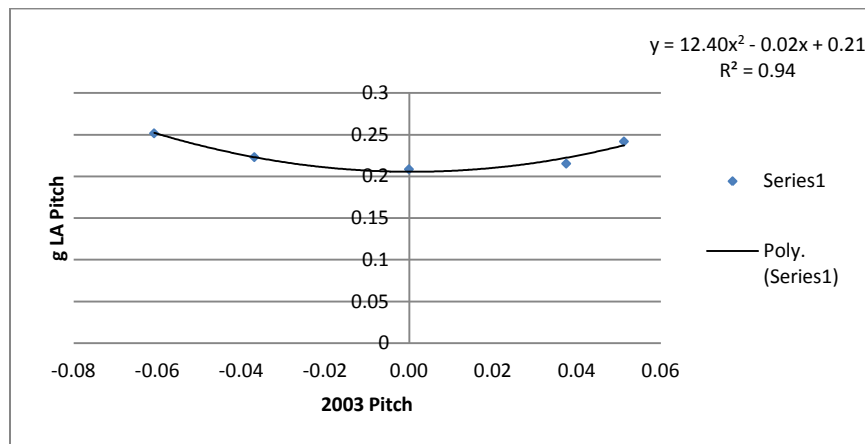


Figure 6.14: Articulated Pitch Cross Plot, 70% Loading Sample

To compare the two methods ability to capture the direction of the overall response, the 2003 roll and pitch results were used, as with the rigid body comparison, to construct a resultant response vector. Figure 6.15 shows this constructed Q1 response, a cross-plot of the Q1 rack results, at the 100% loading condition, is shown in Figure 6.16 from which it can be seen that the magnitude of the responses are highly correlated.

The difference between the two methods becomes apparent when comparing the calculated response direction, Figure 6.17 shows the resultant direction plot for the gLA's twist vector, and the constructed overall response vector from the 2003 pitch and roll calculation. From this figure it is clear that the two methods do not capture the overall response direction in the same manner, which is verified by the regression analysis shown in Figure 6.18 and Figure 6.19. Further, while it may appear that the gLA and

2003 method directions are translated 90° this is shown not to be the case by Figure 6.20 and Figure 6.21.

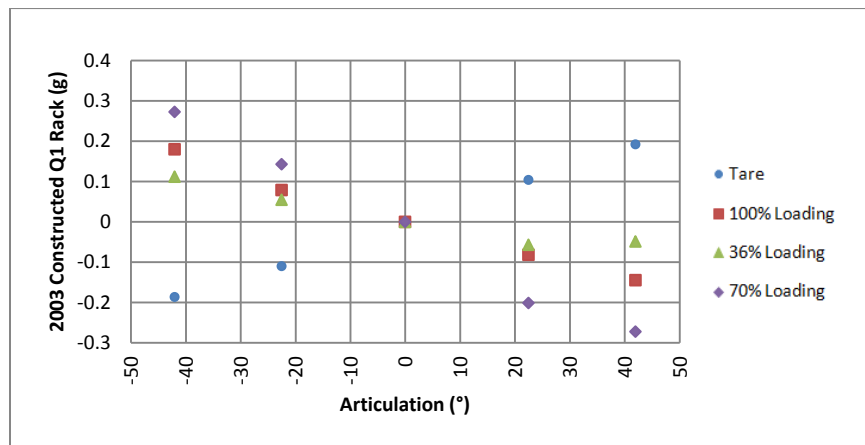


Figure 6.15: 2003 Articulated Constructed Q1 Rack

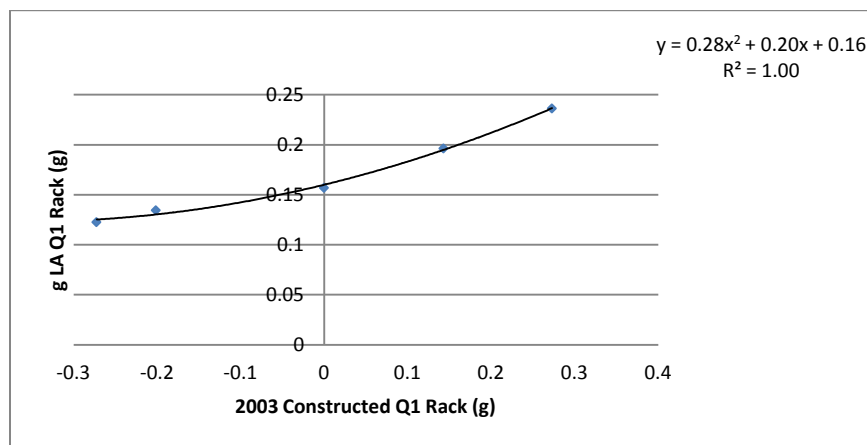


Figure 6.16: Articulated Q1 Rack Cross Plot, 100% Loading

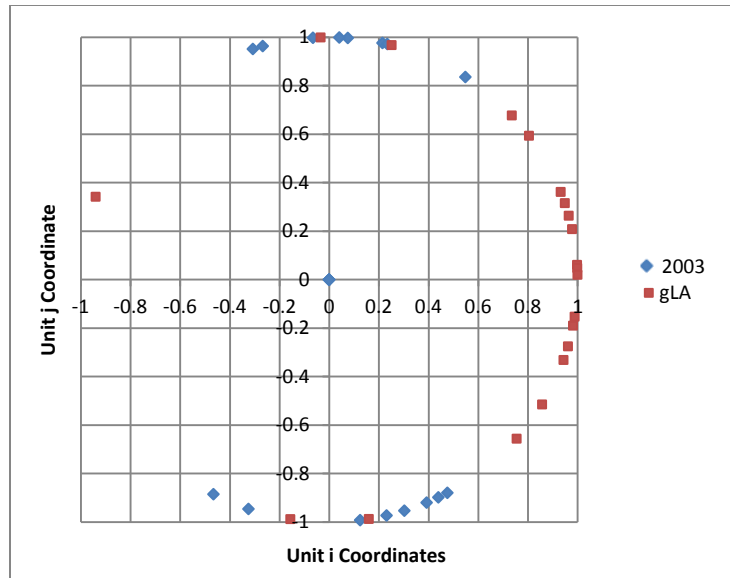


Figure 6.17: Articulated Direction Plot, All Loadings

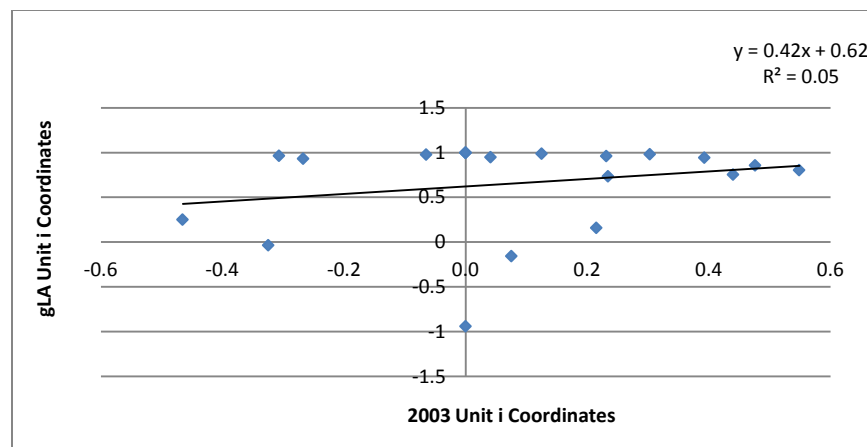


Figure 6.18: Articulated Unit i Cross Plot

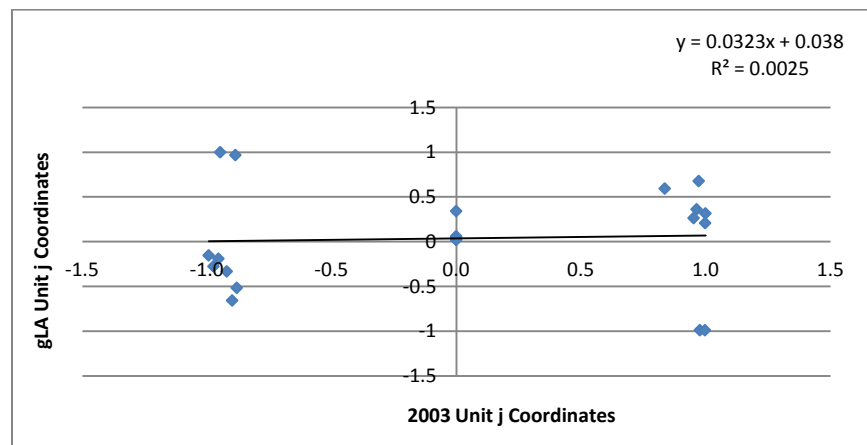


Figure 6.19: Articulated Unit j Cross Plot

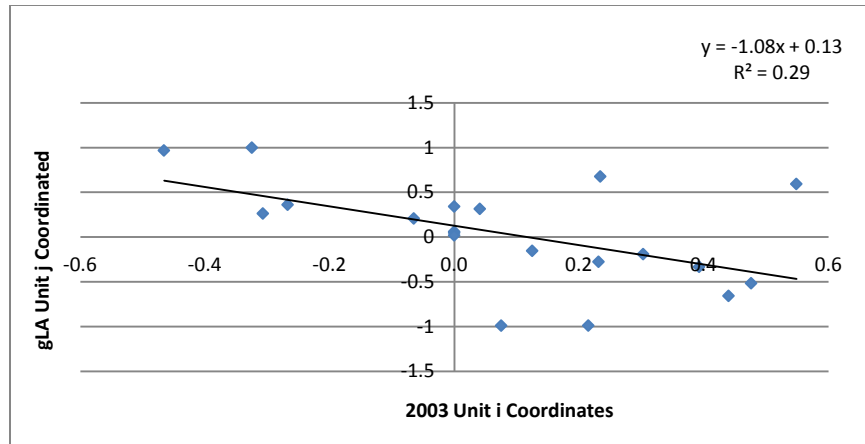


Figure 6.20: Articulated Unit i vs. Unit j Cross Plot

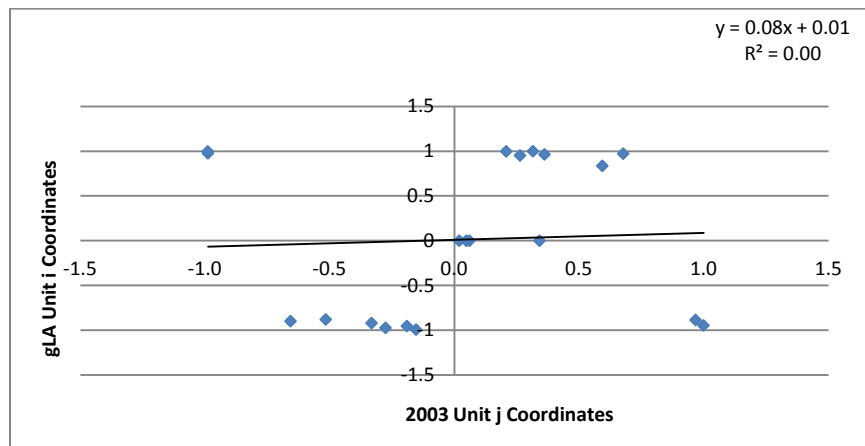


Figure 6.21: Articulated Unit j vs. Unit i Cross Plot

The results of this section have shown that gLA is a complimentary extension to the method presented to Joseph, 2003, through its ability to describe both the magnitude and direction of the vehicle response without excessive effort. It should be noted that the method described in this research is a generalized method and so it is to gLA's advantage that the results of the 2003 method correlate well until the direction of the resultant vector is considered. Alternatively stated, it is intended that both methods can be applied to rigid bodied equipment but it is the position of this author that to accurately consider the g level response of an articulated vehicle both the magnitude and direction must be considered, which can only be accomplished by acknowledging the location of the applied forces, as proposed by the Generalized g Level Analysis method.

## 7 Discussion

Equipment evaluation is complicated by differences in operating surfaces, operator ability, even site specific standards such as speed limits impact results. There are also complications associated with attempting to compare equipment performance between varying size classes of equipment and equipment with extremely different design parameters. It is for these reasons that a generalized method which allows performance comparisons across sites and vehicle ranges is valuable. This investigation has derived such a method which can be applied to any size and type of hauler from ultra class rigid bodied surface equipment to low profile articulating haulers designed for underground environments.

The gLA is derived from the perspective of a mining engineer and provides an acceptable, simple analysis which can be employed at an operations level with data and skills at a mining engineer's disposal. Because gLA is a performance indicator rather than a true dynamic equipment model it is intended to guide decision making. gLA is very much designed in the spirit of doing more with what is available rather than more with exceptional additional effort. The first figure included in this study, Figure 1.1, shows where gLA fits into a model of a simplified scientific method. Its usefulness is rooted in its ability to quickly and easily aid decisions regarding interactions between equipment and its operating environment. The demonstrations provided in this research: energy analysis, haul road performance and general equipment performance are not exhaustive but are rather only examples designed to aid the reader in understanding how gLA may be applied to unique problems.

As stated earlier, gLA is not intended to be, nor can it be, a replacement for dynamic modeling or simulation. Rather, gLA is an alternative, which approximates insight provided by modeling but with some advantages. Chiefly gLA is much simpler than either rigid body or multi body modeling, ideally gLA draws its input forces from the suspension of haul trucks which are not only convenient data collection points but also summarize a large amount of information about a vehicles responses. With the exception of the dampening effect of tires, suspension conveys information on all forces passed from the ground to the load frame and vice-versa. Each suspension strut can be viewed as summarizing the instantaneous distribution across the vehicles load frame of the combined effect of each of the four loading components: Tare, Payload, Articulation (if applicable), and Force Due to Motion. By using this type of force summary from actual field performance detailed dynamic models are not required to provide insight into the type and severity of the interactions the vehicle has with its environment.

The following sections complete the discussion on the study results, significant research contributions and a suggested course for future research which builds from the conclusions of this study.

## 7.1 Significant Research Contributions

The goal of this research was to generate an improved, generalized method of g Level based equipment analysis and to provide examples of how this approach can provide insight into haulage system performance. Below is a list of significant contributions to the existing body of knowledge generated from this study:

- The generation of a generalized g Level based equipment evaluation method and performance indicator which extends previous methodologies by considering the direction and magnitude of the g Level response.
- A baseline study into the adverse moments created by Underground Articulated Haul Trucks.
- A demonstration into how g Level based analysis and its associated metrics can be used to investigate the performance of a surface haulage system including energy based efficiency.

Each of the above results are discussed in greater detail in the remainder of this section.

### 7.1.1 Benefits to Researchers and Industry

Building on the research contributions listed above; g Level analysis will benefit researchers and industry in the following ways:

#### *Researchers*

- gLA functions as a simplified alternative to classical modeling in applications where overall trends are the target result.
- Because of its simplicity gLA can allow researchers in a variety of fields to incorporate vehicle performance into their studies.
- Provides a metric that can be incorporated into computer models and other software which can then be used to help verify model performance with simple field data.

## Industry

- gLA can aid operational decision makers by providing insight into haulage system performance.
- Provide operators with a tool for identifying best practices and areas of improvement.
- Allow for benchmarking comparisons across equipment sizes, types and operating conditions

### 7.1.2 Generation and Demonstration of the Generalized g Level Method

The primary goal of this study was the detailed development of a generalized g level based approach for mobile equipment monitoring. The strength of this tool lies in its ability to provide fleet management with insight into how equipment interacts with both the operator and its environment. The generalized g Level method developed is a continuation of and improvement on the g Level based analysis first proposed by Joseph in 2003. Specifically this is a generalized method can be applied to articulating as well as rigid bodied equipment and is an improvement in that it provides a quantifiable direction to the cumulative instantaneous twist on the vehicle as well as clearly defining how the effect of equipment geometry is accounted for. Another improvement on Joseph, 2003 is that the generalized approach provides both the magnitude and direction of each event where as the previous work only provided definitive directions for pitch and roll motions in addition to magnitude. Another result of this study was to formalize many of the terms and parameters associated with gLA. It is hoped that should this research be continued by others, this basic foundation will prove useful. It is asserted that this investigation is clearly successful in creating the desired equipment analysis approach with not only support for this conclusion generated from the scale model demonstration of the method included in Section 4, but also from the additional results to be discussed.

#### A note on the Interpretation of the g Level

Throughout his work Joseph refers to resultant g Levels as “adverse motions”. While it may be true that high g events are often associated with actual vehicle motions a high g event does not necessitate motion. To illustrate the difference consider a hauler being loaded in a conventional truck and shovel configuration; if the shovel were to load the hauler extremely unevenly the hauler would initially experience true motion when the load is physically placed in the box. This motion will stop once the load settles, however, when this motion ceases there will still be a high g level event as calculated by the methods described in both this work and Joseph, 2003. This high g event is due to the off centered

loading by the shovel and will persist even when all motion of the vehicle has ceased. The foundation of this study is built on the concept of the adverse moment which can be replicated by the equivalent force,  $\vec{F}_{EQ}$ , and so this equivalent force concept can be used to further explain the interpretation of g levels in the current context. The adverse g level as calculated in Equation 3.2 is defined as the cumulative moment about the reference, scaled by the instantaneous mass of the vehicle acting on a moment arm equal to the radius of the unit sphere. Using this definition a hauler experiencing 1g and 2g pure roll events can be interpreted as depicted in Figure 7.1 and Figure 7.2, respectively.

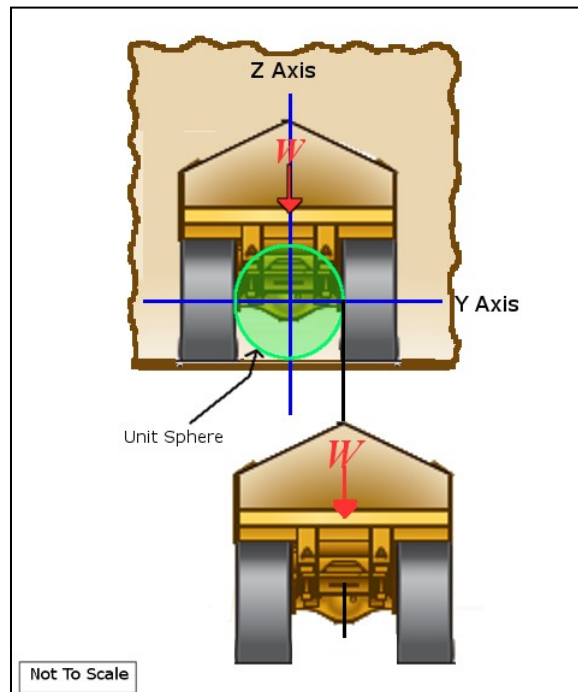


Figure 7.1: 1g Roll Event



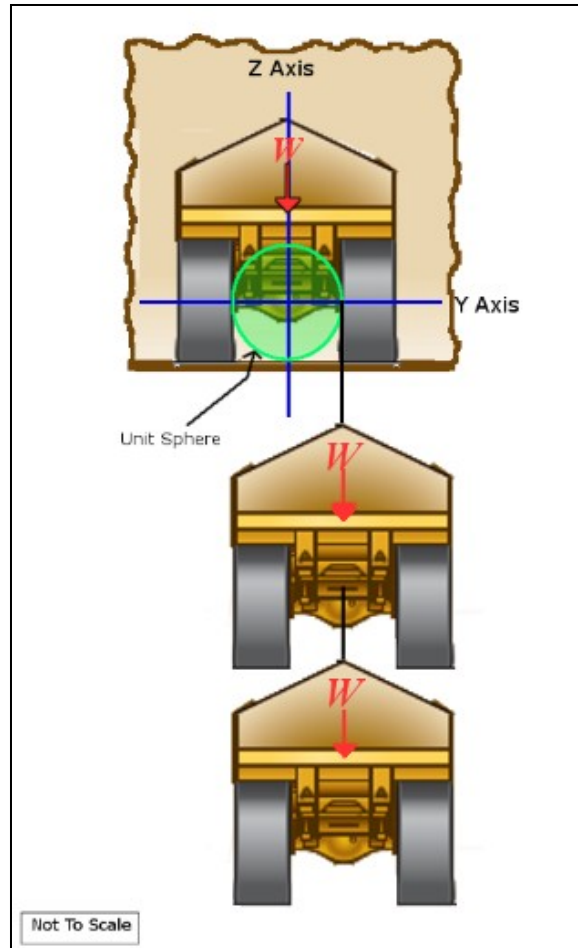


Figure 7.2: 2g Roll Event

The goal of the figures above is to demonstrate that although the g level has units of acceleration it is in reality a description of a force magnitude acting on the vehicle; where a 2g event is equivalent to two times the instantaneous mass of the vehicle applied at the appropriate location on the unit sphere. By fixing the distance from the reference point upon which this force is applied, the g level describes a force action on a moment arm, thus describing the adverse *moment* rather than adverse *motion*. It is felt that one of the important concepts defined during the course of this study has been the concept that an adverse g Level event describes a force moment and does necessarily imply high degrees of actual motion.

### 7.1.3 Baseline Study into Adverse Moments Created by UAHT

The scale model testing included in this study was designed for two purposes. Firstly; the scale model testing provides a controlled and detailed example as to how the mathematics behind the generalized g

level based equipment evaluation methodology can be applied. Secondly, the testing provided insight into the levels of twist that can be expected from today's modern generation of UAHT. Section 5.1.1 Through Section 5.1.5 of this study has shown that under static conditions total g levels induced by articulation and loading in a UAHT can approach the 1.5g level. Although it was shown that deviating the analysis from the COG location affects results this baseline level which approaches 1.5g is considered high as testing did not include the adverse effects of motion. This finding also quantifies the severity of impact and twist which can be generated about the mid-ship components of an UAHT under even ideal conditions. These components could include tires, steering cylinders, mid-ship pins and bushings as well as drive line components. While this study has not included the effects of motion on total induced g level the findings are still important because they help to explain why an UAHT would see events surpassing 1.5g even if operating on near ideal surfaces. The results of Section 5.1.4 can be interpreted as the baseline minimum g levels which should be expected from UAHT. This baseline is representative of near perfectly loaded trucks operating under at constant velocity on a perfectly smooth operating surface. While this is probably not attainable in practice it provides exactly what it is: a baseline against which operations can begin to place themselves against both the ideal and each other.

A further finding from the UAHT simulation was the confirmation of a direct correlation between equipment size, payload and induced g levels as is evident from the figures in the Group Hauler Comparison section 5.1.5. This finding is not surprising, as payload increases, the tare and gross loaded vehicle weight increases which results in larger masses operating on the resultant moment arms. Also induced twist levels also increase with payload class because the box size of the hauler must be increased to accommodate larger payloads inherently increasing the distance from mid-ship to rear axle. Similarly, the distance from the mid-ship to the front axle would also be increased to accommodate a larger engine and its associated components. It would therefore be expected that equipment manufacturers could benefit by incorporating a g Level based analysis as a decision making tool during the equipment design process.

#### **7.1.4 Field Data Analysis of Rigid Framed Hauler**

This study was able to investigate the performance of a modern ultra class hauler using gLA. The data used was taken from a Caterpillar 797 haul truck operating in a typical Alberta Oilsands environment. The opportunity to study a rigid frame hauler is beneficial because it shows potential performance

contrasts from the previously discussed UAHT as well as demonstrating the impact and results of motions on g Level based analysis. Making a direct comparison of the static scale model testing of Section 4 to the field data investigation of section 5.2 is not possible as the scale model testing was conducted under static conditions while the full scale data is primarily when the vehicle is experiencing motion. What can be stated though is that motion not only imparts higher hub forces, over static conditions, but also creates the random appearance of results in figures 5.2.2 when compared to the static results shown in the figures from section 5.1.2. The randomness associated with the real world data should be expected as typical haul road conditions are not perfectly smooth surfaces.

An interesting analysis carried out using the 797 hauler data set was to demonstrate the ability to move the reference point about which the g Levels are calculated. The decision of which reference point to use is one which can be a topic of debate. Section 5.2 of this study used gLA about both the geometric centre of the vehicle and about the ideal centre of gravity (ICOG) of the vehicle where the ICOG is the design COG of the vehicle under either empty or loaded conditions. This is an approximation to the actual COG under empty or loaded conditions as the true COG will depend on the size and placement of each load as well as any auxiliary equipment which is mounted on the vehicle and is not included in the manufactures calculations. The ideal COG location has the benefit of consistency between loads. As with many choices there are benefits and draw backs to the choice of reference point. Benefits of the geometric centre are that it is consistent and unaffected by load placement and weight of the vehicle; is the simplest calculation method as the reference point does not change based on load, and can be considered the most convenient and simple location if comparing g Level performance across payload based vehicle classes. Drawbacks to the geometric centre are that certain types of analysis; such as the energy analysis of section 5.2.2.4 are not possible unless calculated about the COG, or at least the ideal COG. It should be noted that, with regard to articulated equipment, the choice of reference point is complicated further by the articulation variable. It is the opinion of this researcher that the mid-ship is remains the best choice of reference point for articulated equipment for all analysis other than an energy analysis. The reason for this statement is that the mid-ship is a commonly found location across all articulated equipment and that it provides consistency across results by remaining stationary while the vehicle articulates. The mid-ship is also a convenient point to visualize gLA results because all adverse moments or forces will affect the mid-ship as it is literally the pin connection between the front and rear frames of an articulating vehicle.

Referring to Figure 5.37 and Figure 5.45, which show g Level based rack results about the geometric centre and ideal COG respectively; it can be seen that the choice of reference point affects the magnitude of the calculated moment and g Level. Specifically using the ideal COG centers the calculations much more consistently at the zero g level while the geometric centre calculations show symmetry about the zero level but have a much greater range between the loaded and empty conditions. This discrepancy is explained by the fact that when using the ideal COG as the reference the moment arms of each hub force change between the loaded and unloaded conditions keeping the adverse moments much lower. In the geometric centre calculations the reference point remains constant and therefore the hub forces act on consistent, but not necessary balanced, moment arms. As stated earlier it should not be said that the calculations about the geometric centre do not have value, it is just that the results do become more qualitatively valuable because the reference point is more arbitrary.

#### **7.1.4.1 Haul Road Analysis**

An excellent example as to where gLA about the geometric centre has value is in the example haul road analysis of Section 5.2.2.3. This analysis is intended to be a simple extension of gLA and as an example of how changing the variables with which the g Level results are presented can expand the scope of the analysis. Figure 5.46 shows g level results above 1.25g overlaid on the GPS coordinates which were recorded with the original data set. The purpose of this type of figure is to quickly show the user locations on their haul roads which are contributing substantial adverse g level events. While any locations populated with adverse events should be investigated it can be seen that high levels around corners likely contain high levels of roll and may not be considered particularly damaging to the frame, but may be considered damaging to other components such as tires. Although g level values between 1.25g and 1.5g are not as adverse as those above 1.5g it can be seen in Figure 5.46 that a substantial number of events are occurring on the relatively straight sections of haul road. While it is highly likely that these mid level events on straight sections are a result of poor road maintenance, this may only be part of the explanation. Adverse g levels may be in part caused by poor operation of the vehicle either in the form of extreme acceleration or simply travelling too fast for the haul road conditions. Mine operators can begin to isolate the cause of adverse g levels with two additional simple analysis. Figure 5.47 and Figure 5.48 show cross plots of g level vs. vehicle speed and g level vs. vehicle acceleration respectively. As can be seen in these figures there is no correlation between either vehicle speed or

acceleration and degree of g level; this provides support to the theory that the adverse g levels seen in Figure 5.46 are indeed caused by poor road conditions. Knowing this the mine operator can now choose an action to improve haul roads in the areas showing elevated g levels before they exceed the 1.5g level. The value of gLA to haul road monitoring could easily be exploited with automated report generation continuously using data from an entire fleet of vehicles.

#### **7.1.4.2 Energy Analysis**

This study has applied the concept of g Level based monitoring to basic equipment analysis, and shown examples how this process can be used to improve haul road and operator performance. The final application of this method relating to energy efficiency is not only the one which arguably yields the most interesting results but also provides the best conceptualization into what is meant by the term “adverse g Level”.

The results of Section 5.2.2.4, specifically Table 5.8, show that up to 13% of fuel energy could be wasted through the generation of adverse g levels, dependent on overall working conditions. Because the data set used in this investigation did not include a method to determine the exact amount of fuel burned during the time interval in which the data was collected low, medium and high fuel consumption rates from Caterpillar’s performance handbook were used to estimate the efficiency percentage. Because it has been shown in Haul Road Analysis of Section 5.2.2.3 that a substantial number of elevated g level events are likely the result of haul road conditions it is more likely that the hauler is operating in either a medium or high fuel consumption application as described by Caterpillar [73]. Using these estimated fuel consumption rates decreases the estimated energy loss to between 7% and 9% which implies that other factors must be contributing to increased fuel consumption such as higher payload levels or increased climb gradients. Given these results it is apparent that there is an incentive for mine operators to use gLA to benchmark and monitor haulage system efficiency.

Section 7.1.4.2 defined useful energy, in the context of a hauler, as energy which helps move the COG of the hauler between two points. In a mining context this would most often be a loaded COG from the shovel to the crusher or dump and then an empty COG back to the shovel. In contrast the energy used by an adverse moment expressed as an adverse g level is defined as acting about the reference point. The adverse g Level is actually quantifying the energy expended to rotate the vehicle mass around a given reference point, if the reference point used is the instantaneous COG (or at least estimated COG),

the cumulative energy must be considered wasted because it does not contribute to actually moving the vehicle in the intended direction. If it is the case where the vehicle is moving on a negative gradient the wasted energy should be interpreted to include wasted potential energy which, unless the vehicle is under constant braking, could have been used to move the COG in the intended direction.

It stands to reason that better quality roads improve hauler efficiency, hence the common industry expression “Roads make Loads”, but the connection between haul road condition and the wasted energy quantified by gLA is considered to be a very good explanation as to how this relationship may work.

### *Study Limitations*

The largest limitation to the method developed within this study is a lack of understanding in regards to what degree of g level should be considered detrimental to equipment, operator or haul road. It is strongly suspected that this will be dependent on individual components and design. Although this study was not able to address this issue it is considered to be one of the future uses for the gLA method itself and has been included in the recommended future work section.

A second limitation of this study was also one of the primary drivers. As mentioned several times previously, the difficulty in monitoring suspension-less equipment is not conducive to analysis in the same way this study demonstrated using the data recorded by a Caterpillar 797 onboard computer. The corollary to this data acquisition difficulty is that scale model and computer simulation is likely to be as far as gLA can be applied to suspension-less equipment until practical instrumentation solutions can be implemented. Again this is mentioned in the recommendations for future work.

## 8 Conclusions

This primary goal of this study has been to develop a method of equipment analysis which can convey to the user information regarding the equipment's interaction with its operator and its operating environment

This method has been successfully designed to remain useably simple by incorporating data such as strut pressures, vehicle speed, GPS coordinates and basic equipment geometry which owners, operators, and researchers have reasonable access to. This study has also demonstrated that the generalized gLA can be applied to both articulated and rigid body equipment by using a combination of scale model testing and analysis of field collected data.

Although the purpose of this study is to develop an equipment analysis method which meets the criteria above, several significant empirical results have been reached during the course of demonstrating the method. While these results have been expressed in their respective sections and the discussion the following bullets convey these findings as related to the goal of the research:

- A primary driver of this study was to quantify the potential for high g level events in typical underground articulated haul trucks. Sections 4 through 5.1.5 have shown that even under ideal conditions the varying geometry inherent in the articulating design is capable of producing elevated g levels and that there is a direct relationship between payload and the degree of adverse moments generated.
- gLA presented with additional parameters such as time, speed and position can yield insight into haul road performance and efficiency.

The major theoretical contributions of this study are, firstly; the use of g level as a means of conveying the degree of adverse force; or moment when considering said force acting at a distance from an arbitrary reference point. And secondly; that the explanation as to why elevated levels of these forces are considered detrimental to equipment performance is because these forces about the reference point, by definition, do not contribute to the equipments goal of moving its instantaneous COG between points but rather reduce efficiency at the expense of component life.

## 8.1 Future Work

The primary contribution of this work is the generation of a versatile and simple mobile equipment analysis tool. This tool is intended to provide owners and operators of haul trucks with insight into many aspects of their haulage system performance, using data they already have access to. Although the demonstrated uses presented in this study are practical and useful there is still much to be done in the field of g Level based equipment analysis. The following section outlines areas which should be explored by building on the work included in this investigation.

### *Articulated Equipment Simulation and Monitoring*

Given that there are currently no easily feasible hub force monitoring points on typical UAHT's, or generally any other suspension-less equipment, a next logical step in the investigation of such equipment would be to use the algorithms described in this paper to simulate UAHT performance. Part of this investigation would require appropriate modeling of typical underground haulage conditions as well as loading and operational practices. The foremost benefit of a simulated investigation would be to observe the effect of motion as well as to provide an adequate platform for a comparative error analysis between a dynamic articulated vehicle model and the gLA approach.

A second opportunity with certain suspension-less equipment would be to investigate the potential of certain automated guidance systems which use gyroscopes or similar equipment and whether any of these data sources can be incorporated into the g Level based analysis. One of the primary reasons the mid-ship is chosen as the primary reference point on an UAHT is that as the connection between the front and rear frame components all adverse forces must be directed through these pins. Although considered beyond the scope of this investigation, it may be worthwhile investigating the feasibility of instrumenting the mid-ship components in order to record strain readings which would allow for the direct monitoring of the cumulative moment or  $\vec{F}_{EQ}$ .

### *Defining Acceptable g Level Magnitude and Component Monitoring*

The energy analysis section of this study establishes a clear link between g level and energy however what is not clear is what absolute magnitude of g level should be considered detrimental to short, medium and long term component life. It is suspected that different components will have different



tolerances which are dependent on the nature of the high g Level event, their magnitude and orientation. This is considered the most difficult of the recommended future work.

### *Haul Road Perspective*

This investigation was completed from the point of view of the equipment. Even the haul road analysis presents data as the equipment passes across the haulge path. Another perspective could be to look at the cumulative effect from the point of view of the haul road. In this method each arbitrary section of area can be thought of as a single entity which is then exposed repeatedly to potentially destructive force by each tire that travels across it. Using this approach real time condition mapping of a haul road might be established.

### *Training Tools*

Simulation based training is becoming more prevalent. It would be interesting to benchmark and gauge individual operators skill using g level based analysis during training which can then continue to be monitored once the operator is on-board live equipment. This application could also be used to isolate and identify operators who meet production requirements with proportionately lower adverse g levels with the goal of implementing any novel techniques across the fleet.

### *Industry Wide Benchmarking*

One of the initial criteria for the successful generation of a g level based monitoring tool is if it could be applied to industry wide benchmarking. The method developed in the course of this research has the ability to provide industry wide benchmarking, especially in the ultra class hauler range. Now that the method exists, research can begin which will help identify best practices and areas of improvement.

### *Application to WBV and Component Monitoring*

The literature review and motivation sections of this study indicated that a substantial application of g level based analysis would be in the study of WBV and component monitoring. As research progressed it has become apparent that the method derived in this study is not applicable in this form. The reason this method was not used to attempt either WBV analysis or component monitoring is that although the choice of reference point is arbitrary, simply moving the reference point to the location of a component it is thought that a kinematic transform could be used to the operator location could be used to estimate levels of WBV.

With regards to component monitoring, it is likely that gLA can be used in fatigue analysis of components under alternative loading by treating frame and axle components as a simplified beam model. A similar application could be to investigate axial stresses in a quarter car model. It is also believed that gLA can be used as a forensic tool where, for example, a particular component failure is observed in the field and then a correlation is found within the distribution of adverse moments the vehicle had been exposed to leading up to the component failure. If such a statistically significant correlation is found between observed failures and an exposure to adverse moments then corrective actions could then be taken to reduce this exposure, thus reducing the rate of component failure.

### *Final Remarks*

This study has demonstrated the mechanics of g level based analysis and presented examples of its use as well as work required to minimize its limitations. Because it is built on a foundation of simplicity and versatility the potential for gLA to help equipment users, owners and researcher to better understand the interactions between machine, operator and environment is substantial. Most simply gLA is a tool; it is hoped this tool will be employed to enhance the users overall understanding of equipment performance.

## References

- [1] J. J. Berezan. Human vibration monitoring system. *ProQuest Dissertations and Theses* 2006. Available: <http://search.proquest.com/login.ezproxy.library.ualberta.ca/docview/304959726?accountid=14474>.
- [2] O. W. Eshbach, "Moments and couples," in *Eshbach's Handbook of Engineering Fundamentals*, 5th ed., M. Kutz, Ed. Hoboken, New Jersey: John Wiley and Sons, 2009, pp. 311.
- [3] T. G. Joseph. Large mobile mining equipment operating on soft ground. Presented at International Mining Congress and Exhibition. 2003, .
- [4] R. Jazar, *Vehicle Dynamics, Theory and Application*. New York: Springer Science+Business Media, 2014.
- [5] K. Popp and W. Schiehlen, *Ground Vehicle Dynamics*. Berlin: Springer-Verlag, 2010.
- [6] C. Senatore and C. Sandu, "Off-road tire modeling and the multi-pass effect for vehicel dynamics simulation," *Journal of Terramechanics*, pp. 265, 2011.
- [7] S. Taheri, C. Sandu, S. Taheri, E. Pinto and D. Gorsich, "A technical survey on terramechanics models for tire-terrain interaction used in modeling and simulation of wheeled vehicles," *Journal of Terramechanics*, pp. 1, 2015.
- [8] C. Ghike and T. Shim, "14 Degree of Freedom Vehicle Model for Roll Dynamics Study," *SAE Technical Paper Series*, pp. December 10, 2014, 2006.
- [9] R. Brown, M. Mazza, D. Le and M. Murugan, "Comparison of Generalized Predictive Control Algorithms Using a FULL Vehicle Multi-Body Dynamics Model," *SAE International*, 2012.
- [10] N. Laghari. Simulation analysis of the effect of tire and suspension non-linearities on the handling response of rigid and articulated vehicles. *SAE International* 2011. . DOI: 10.4271/2011-01-0962.
- [11] X. Huang, Y. Shen and W. Zhang, "Analysis of Articulated Dump Trucks Vibration and Rear Suspension Stiffness Sensitivity," *SAE International*, 04/12/2010, 2010.
- [12] A. Pazooki, S. Rakheja and D. Cao, "Effect of Terrain Roughness on the Roll and Uaw Directional Stability of an Articulated Freame Steer Vehicle," *SAE International Journal of Commercial Vehicles*, vol. 6, pp. 325, 2013.
- [13] Y. He and M. Islam, "An Automated Design Method for Active Trailer Steering Systems of Articulated Heavy Vehicles," *Journal of Mechanical Design*, vol. 134, 2012.
- [14] M. Islam, X. Ding and H. Yuping, "A closed-loop dynamic simulation-based design method for articulated heavy vehicles with active trailer steering systems," *International Journal of Vehicle Mechanics and Mobility*, vol. 50, pp. 675, 07/10/2011, 2011.

- [15] A. Miede and D. Cebon, "Optimal roll control of an articulated vehicle: theory and model validation," *International Journal of Vehicle Mechanics and Mobility*, vol. 43, pp. 867, 2005.
- [16] B. Chen and H. Peng, "Rollover Warning for Articulated Heavy Vehicles Based on a Time-to-Rollover Metric," *Journal of Dynamic Systems, Measurement and Control*, vol. 127, pp. 406, 2005.
- [17] A. Pazooki, "Ride and Directional Dynamic Analysis of Articulated Frame Steer Vehicles," 2012.
- [18] N. Azas, J. McPhee and A. Khajepour, "Tire forces and moments and on-road lateral stability of articulated steer vehicles," *SAE International Journal of Commercial Vehicles*, 2005.
- [19] X. Li, G. Wang, Z. Yao and J. Qu, "Dynamic Model and Validation of an articulated steering wheel loader on slopes and over obstacles," *International Journal of Vehicle Mechanics and Mobility*, vol. 51, pp. 1305, 2013.
- [20] Y. Yavin, "Modelling the motion of an underground mining vehicle," *Mathematical and Computer Modelling*, vol. 42, pp. 1123, 2005.
- [21] A. Pazooki, D. Cao, S. Rakheja and P. E. Boileau, "Ride dynamic evaluations and design optimisation of a torsio-elastic off-road vehicle suspension," *International Journal of Vehicle Mechanics and Mobility*, vol. 49, pp. 1455, 2011.
- [22] T. Langer, T. Iversen, O. Mouritsen, M. Ebbesen and M. Hansen, "Suspension system performance optimization with discrete design variables," *Structural and Multidisciplinary Optimization*, vol. 47, pp. 621, 2013.
- [23] A. Pakowski and D. Cao, "Effect of soil deformability on off-road vehicle ride dynamics," *SAE International*, 09/24/2013, 2013.
- [24] D. S. Ardeshtir and T. Joseph, "Oil sand deformation under cyclic loading of ultra-class mobile mining equipment," *Journal of Terramechanics*, vol. 47, pp. 75, 2010.
- [25] D. D. Tannant and B. Regensburg, "Guidelines for Mine Haul Road Design," 2001.
- [26] ASTM. Standard test method for CBR (californian bearing ratio) of laboratory-compacted soils. 2007.
- [27] R. J. Thompson, "Building Better Haul Roads," *E&MJ*, pp. 48, 2011.
- [28] R. Thompson. The design and management of surface mine haul roads. 1996.
- [29] R. J. Thompson and A. T. Visser, "Selection and maintenance of mine haul road wearing course materials," *Mining Technology*, vol. 115, pp. 140, 2006.
- [30] R. J. Thompson and A. T. Visser, "Selection, performance and economic evaluation of dust palliatives on surface mine haul roads," *Journal of the Southern African Institute of Mining and Metallurgy*, vol. 107, pp. 435, 2007.

- [31] S. Ambani and L. Li, "Condition-Based Maintenance Decision-Making for Multiple Machine Systems," *Journal of Manufacturing Science and Engineering*, vol. 131, 2009.
- [32] L. Wang, J. Chu and J. Mao, "A condition-based replacement and spare provisioning policy for deteriorating systems with uncertain deterioration to failure," *Journal of Operational Research*, vol. 194, pp. 184, 2009.
- [33] E. Chanda and S. Gardiner, "A comparative study of truck cycle time prediction methods in open pit mining," *Engineering, Construction and Architectural Management*, vol. 17, pp. 446, 2010.
- [34] R. J. Thompson and A. T. Visser, "Mine haul road maintenance management systems," *The Journal of the South African Institute of Mining and Metallurgy*, pp. 306, 2003.
- [35] R. J. Thompson. "Design construction and maintenance of haul roads," in *SME Mining Engineering Handbook* (3rd ed.) Anonymous 2011, .
- [36] C. W. Plackett. A review of force prediction methods for off road wheels. *J. Agric. Engng Res* 31(1), pp. 1. 1985.
- [37] Caterpillar Inc. Haul road design and management. 2006.
- [38] Pea et al, "A Guidline for Maintenance and Service of Unpaved Roads," 2000.
- [39] T. Lee, "Development and Validation of Rolling Resistance-Based Haul Road Management," 2010.
- [40] R. E. Miller, N. T. Lowe and R. Thompson, "A GPS based system for minimizing jolts to heavy equipment operators," *SAE International*, 2004.
- [41] F. Liu, N. Dembski and G. Rizzoni, "An improved design of a behicle based off-road terrain profile measurement system," *SAE International*, 2008.
- [42] H. M. Ngwangwa and P. S. Heyns, "Application of an ANN-based methodology for road surface condition identification on mining vehicles and roads," *Journal of Terramechanics*, vol. 53, pp. 59, 2014.
- [43] T. Heyns, J. P. de Villiers and P. S. Heyns, "Consistent haul road condition monitoring by mean of vehicle response normalisation with Gaussian processes," *Engineering Applications of Artificial Intelligence*, vol. 25, pp. 1752, 2012.
- [44] R. J. Thompson, A. T. Visser, P. S. Heyns and D. Hugo, "Mine Road Maintenance Management Using Haul Truck Response Measurements," *Mining Technology*, vol. 115, pp. 123, 2006.
- [45] S. Park, A. A. Popov and D. J. Cole, "Influence of soild deformation on off-road heavy vehicle suspension vibration," *Journal of Terramechanics*, vol. 41, pp. 41, 2004.
- [46] D. Hugo, P. S. Heyns, R. J. Thompson and A. T. Visser, "Haul road defect identification using measured truck response," *Journal of Terramechanics*, vol. 45, pp. 79, 2008.

- [47] T. Eger, "WBV: Investigation of Health Risks Associated with Vibration Exposure, Transmissibility and Posture During Operation of Mining Vehicles," 2007.
- [48] M. Smets, "The Effecto of WBV Exposure as Experienced During the Operation of Surface Haulage Trucks on Proprioception in the Lumar Spine," 2006.
- [49] S. A. Aye and P. S. Heyns, "The evaluation of whole body-vibration in a South African opencast mine," *Journal of the Southren African Institute of Mining and Metallurgy*, vol. 111, pp. 751, 2011.
- [50] K. N. Kittusamy and B. Bucholz, "Whole-body vibration and postural stress among operators of construction equipment: A literature review," *Journal of Safety Research*, vol. 35, pp. 255, 2004.
- [51] A. P. Vanerkar, N. P. Kulkarni, P. D. Zade and A. S. Kamavisdar, "Whole body vibration exposure in heavy earth moving machinery operators of metalliferous mines," *Environmental Monitoring and Assessment*, vol. 143, pp. 239, 2008.
- [52] R. P. Blood, J. D. Ploger and P. W. Johnson, "Whole body vibration exposures in forklift operators: comparison of a mechanical and air suspension seat," *Ergonomics*, vol. 53, pp. 1385, 2010.
- [53] S. G. Grenier, T. R. Eger and J. P. Dickey, "Predicting Discomfort Scores Reported by LHD Operators Using WBV Exposure Values and Musculoskeletal Pain Scores," *Work*, vol. 35, pp. 49, 2010.
- [54] ISO, "ISO 2631-1 Mechanical Vibration and Shock - Evaluation of Human Exposure to WBV, Part 1 General Requirements," 1997.
- [55] J. DeShaw, "Effect of Head-Neck Postur on Human Discomfort During WBV," 2010.
- [56] K. Routsalainen, T. Rantaharju, A. Partanen and P. Romppainen, "Wireless system for the continuous observation of whole-body vibration in heavy machinery," *IEEE Instrumentation and Measurement Magazine*, pp. 26, 2013.
- [57] W. Wolfgang, L. Di Corleto and R. Burgess-Limerick, "Can an iPod touch be used to assess whole-body vibration associated with mining equipment," *Annals of Occupational Hygiene*, vol. 58, pp. 1200, 2014.
- [58] US Army, "Engineering design handbook, automotive series-automotive suspensions," in Anonymous US Army Material Command, 1967, pp. 1-20.
- [59] R. E. Miller. Methods to assess jolting and jarring events: A surface mining case study. *SAE International* 1(2830), 2009.
- [60] A. Schaum, A. Nieto, S. Scharfrik and M. Karmis, "Haul truck safety and virtual environments training," *Mining Engineering*, vol. 60, pp. 56, 2008.
- [61] R. A. Diaz Borquez, "Haul truck operator training at the Esperanza mine project," *Engineering and Mining Journal*, pp. 48, 2010.

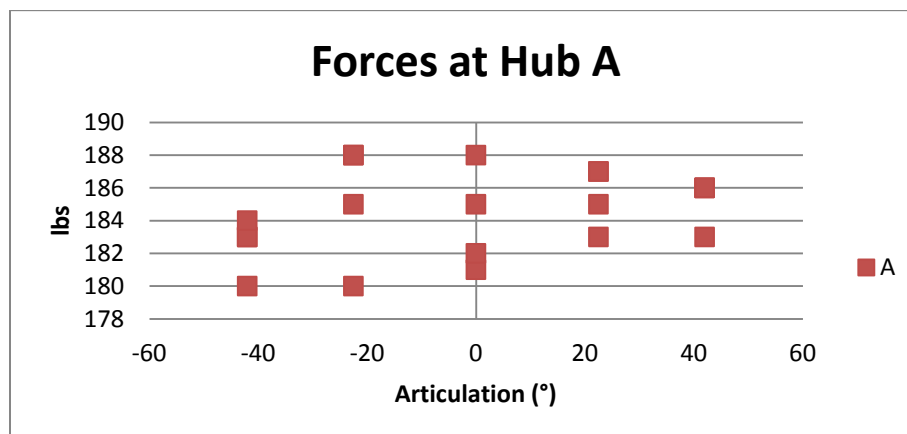
- [62] J. Tichon and P. Diver, "Interactive simulator training in civil construction: Evaluation form the trainer's perspective," *Journal of Interactive Learning Research*, vol. 23, pp. 143, 2012.
- [63] M. A. Oskouei and K. Awuah-Offei, "Statistical methods for evaluating the effect of operators on energy efficiency of mining machines," *Mining Technology*, vol. 123, pp. 175, 2014.
- [64] T. H. Langer, T. K. Iversen, N. K. Andersen, O. Mouritsen and R. Hansen, "Reducing whole-body vibration exposure in backhoe loaders by education of operators," *International Journal of Industrial Ergonomics*, vol. 42, pp. 304, 2012.
- [65] S. T. McClain, R. A. Harris and W. R. Peters, "A Fuel Consumption Simulator for Teaching Efficient Driving Practices," *SAE International*, 2008.
- [66] SAE, "Surface vehicle recommended practice," Society of Automotive Engineers, Tech. Rep. J1100, 2009.
- [67] R. C. Hibbeler, "Moment of a force," in *Engineering Mechanics Static and Dynamics*, 10th ed. Anonymous Upper Saddle River New Jersey: Pearson Prentice Hall, 2004, pp. 113.
- [68] K. W. Nicholson, "The dot product and projections," in *Linear Algebra with Applications*, 4th ed. Anonymous McGraw-Hill Ryerson Limited, 2003, pp. 156-159.
- [69] Aviation Publishers Ltd., "Aircraft operations," in *From the Ground Up*, 26th ed. Anonymous Aviation Publishers Co., 1991, pp. 11.
- [70] Tesis DYNAware GnbH, "veDYNA 3.10.6-Entry Edition," 2014.
- [71] Detroit Diesel Corporation. Series 60 engine. 2005.
- [72] Caterpillar Inc. Large specalog for 797F mining truck. 2012.
- [73] Caterpillar Inc. "Caterpillar performance handbook," in (44th ed.) Anonymous 2013, .

## Appendix

### 1. Statistical Evaluation of Weight Distribution vs Articulation

The following section contains statistical analysis regarding the effect of articulation on weight distribution between the four hubs of the Test Unit. Note that three of the evaluations are considered statistically insignificant. Specifically the tare weight Forces at A, 36% loading Forces at B, 70% loading Forces at B and the 100% Loading Forces at B are statistically insignificant. It is suspected that slight issues with torsional stress on the load cell are the cause of slight reading error which caused non parabolic readings in the previously mentioned conditions. There is also a possible outlier effect in the 100% Loading Forces at B which severely affect the statistical analysis. Even with the previously mentioned statistical issues this paper considers the effect of articulation on weight distribution to be relevant. As all readings contained in this section were used in the total analysis of this paper all readings were deemed legitimate for statistical evaluation.

#### Tare Weight

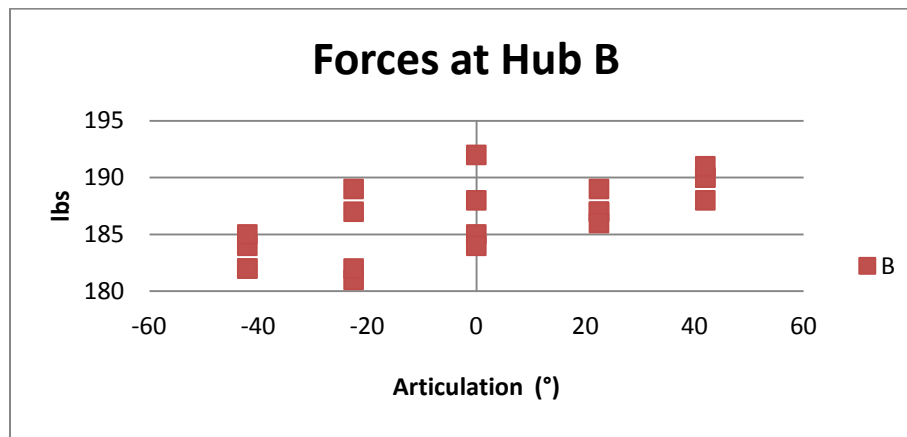


Forces at A Polynomial Regression	
Regression Statistics	
R	0.35
R Square	0.12
Adjusted R Square	0.02
Standard Error	2.54
Total number of observations	20
a = + 184.9585 + 0.0267 * phi - 0.0005 * phi**2	



## ANOVA

	<i>d.f.</i>	<i>SS</i>	<i>MS</i>	<i>F</i>	<i>p-level</i>
<i>Regression</i>	2	15.59	7.79	1.21	0.32
<i>Residual</i>	17	109.41	6.44		
<i>Total</i>	19	125.			



## Forces at B Polynomial Regression

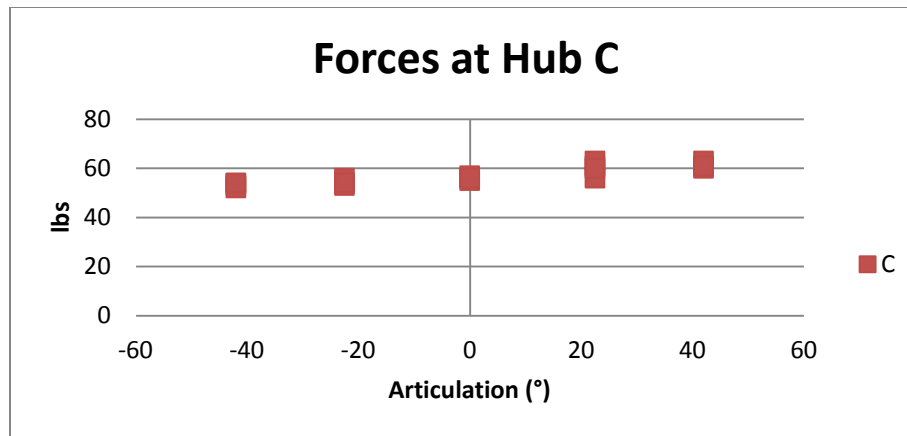
## Regression Statistics

<i>R</i>	0.69
<i>R Square</i>	0.48
<i>Adjusted R Square</i>	0.41
<i>Standard Error</i>	2.49
<i>Total number of observations</i>	20

$$b = +186.5470 + 0.0725 * \text{phi} - 0.0001 * \text{phi}^2$$

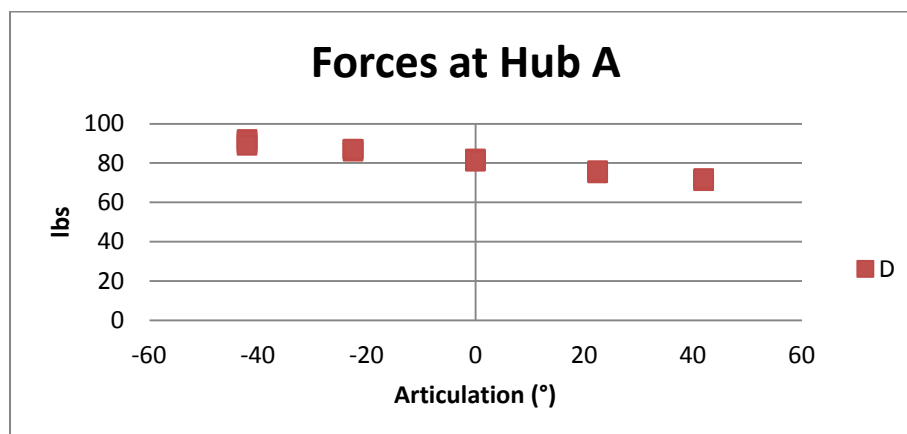
## ANOVA

	<i>d.f.</i>	<i>SS</i>	<i>MS</i>	<i>F</i>	<i>p-level</i>
<i>Regression</i>	2	95.62	47.81	7.72	0.0041
<i>Residual</i>	17	105.33	6.2		
<i>Total</i>	19	200.95			



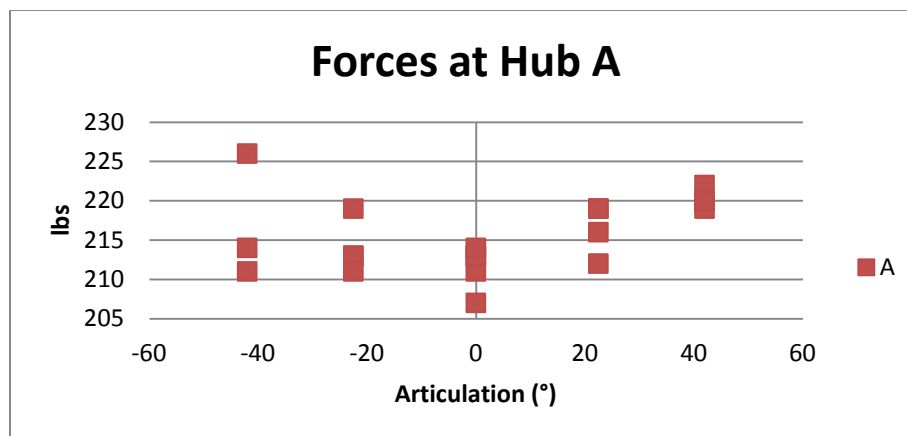
Forces At C Polynomial Regression	
<i>Regression Statistics</i>	
<i>R</i>	0.9
<i>R Square</i>	0.81
<i>Adjusted R Square</i>	0.79
<i>Standard Error</i>	1.64
<i>Total number of observations</i>	20
<b><math>c = + 56.5206 + 0.1025 * \text{phi} + 0.0005 * \text{phi}^2</math></b>	

<i>ANOVA</i>					
	<i>d.f.</i>	<i>SS</i>	<i>MS</i>	<i>F</i>	<i>p-level</i>
<i>Regression</i>	2	193.13	96.57	35.83	0.
<i>Residual</i>	17	45.82	2.7		
<i>Total</i>	19	238.95			

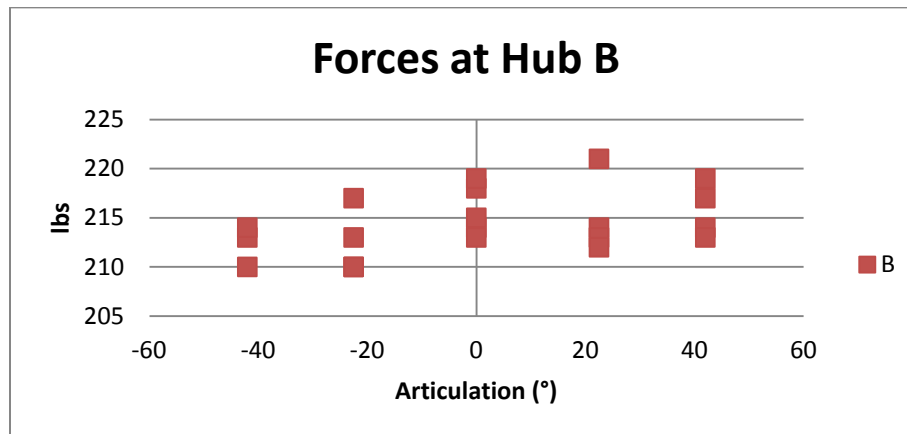


Forces at D Polynomial Regression					
<i>Regression Statistics</i>					
<i>R</i>	0.99				
<i>R Square</i>	0.99				
<i>Adjusted R Square</i>	0.99				
<i>Standard Error</i>	0.79				
<i>Total number of observations</i>	20				
<b><math>d = + 81.3427 - 0.2315 * \phi - 0.0002 * \phi^{**2}</math></b>					
<i>ANOVA</i>					
	<i>d.f.</i>	<i>SS</i>	<i>MS</i>	<i>F</i>	<i>p-level</i>
<i>Regression</i>	2	973.81	486.91	770.84	0.E+0
<i>Residual</i>	17	10.74	0.63		
<i>Total</i>	19	984.55			

### 36% Loading

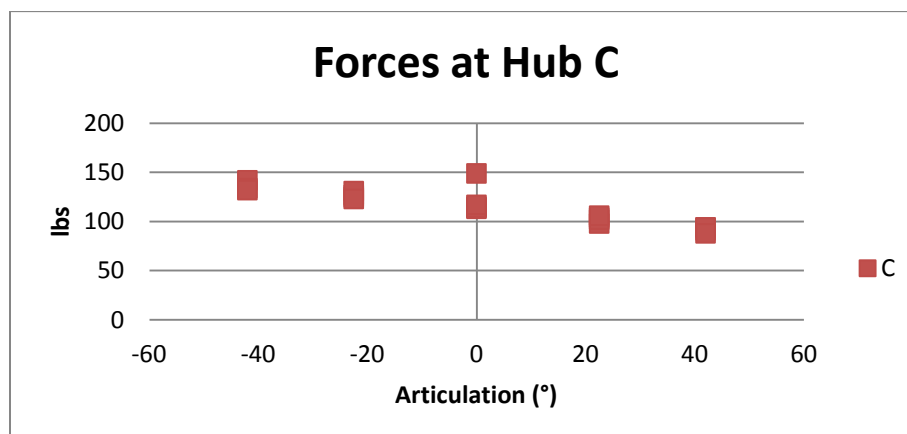


Forces at A Polynomial Regression					
<i>Regression Statistics</i>					
<i>R</i>	0.65				
<i>R Square</i>	0.42				
<i>Adjusted R Square</i>	0.35				
<i>Standard Error</i>	3.78				
<i>Total number of observations</i>	20				
<b><math>a = + 212.5808 + 0.0422 * \phi + 0.0036 * \phi^{**2}</math></b>					
<i>ANOVA</i>					
	<i>d.f.</i>	<i>SS</i>	<i>MS</i>	<i>F</i>	<i>p-level</i>
<i>Regression</i>	2	173.7	86.85	6.07	0.0102
<i>Residual</i>	17	243.1	14.3		
<i>Total</i>	19	416.8			



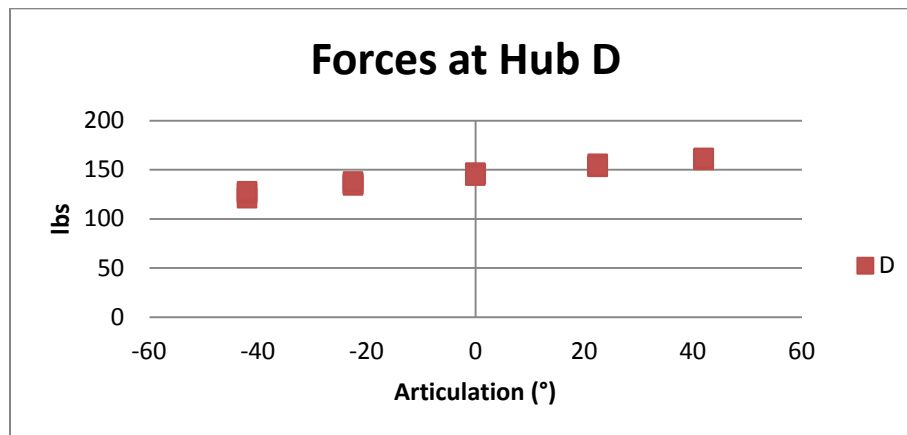
Forces at B Polynomial Regression	
<i>Regression Statistics</i>	
<i>R</i>	0.43
<i>R Square</i>	0.19
<i>Adjusted R Square</i>	0.09
<i>Standard Error</i>	2.99
<i>Total number of observations</i>	20
<b><math>b = + 214.8803 + 0.0451 * PHI - 0.0006 * PHI**2</math></b>	

ANOVA					
	<i>d.f.</i>	<i>SS</i>	<i>MS</i>	<i>F</i>	<i>p-level</i>
<i>Regression</i>	2	35.14	17.57	1.97	0.17
<i>Residual</i>	17	151.81	8.93		
<i>Total</i>	19	186.95			



Forces at C Polynomial Regression	
<i>Regression Statistics</i>	
<i>R</i>	0.89
<i>R Square</i>	0.8
<i>Adjusted R Square</i>	0.78
<i>Standard Error</i>	8.4
<i>Total number of observations</i>	20
<b><math>C = + 118.6803 - 0.5262 * PHI - 0.0032 * PHI^{**2}</math></b>	

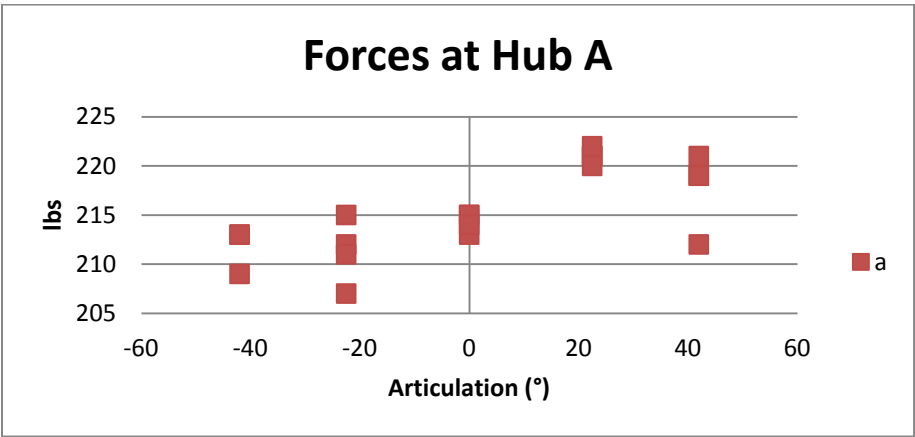
ANOVA					
	<i>d.f.</i>	<i>SS</i>	<i>MS</i>	<i>F</i>	<i>p-level</i>
<i>Regression</i>	2	4,756.83	2,378.42	33.75	0.00
<i>Residual</i>	17	1,198.12	70.48		
<i>Total</i>	19	5,954.95			



Forces at D Polynomial Regression	
<i>Regression Statistics</i>	
<i>R</i>	0.99
<i>R Square</i>	0.98
<i>Adjusted R Square</i>	0.98
<i>Standard Error</i>	1.7
<i>Total number of observations</i>	20
<b><math>d = + 145.7215 + 0.4229 * PHI - 0.0015 * PHI^{**2}</math></b>	

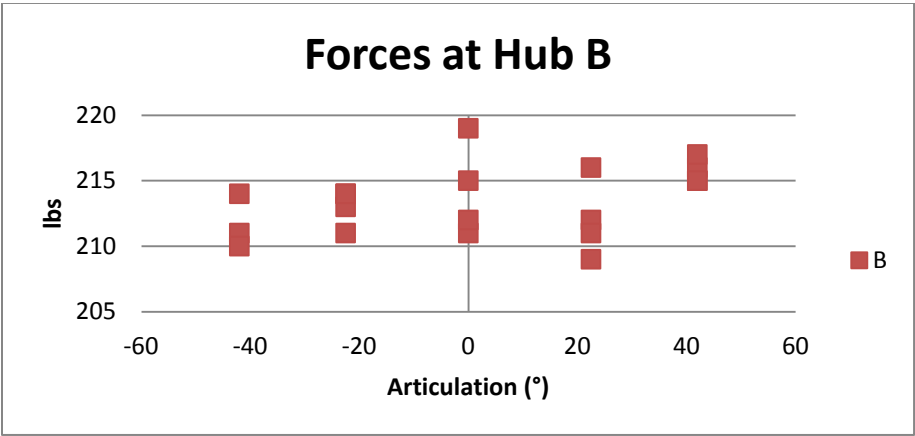
ANOVA					
	<i>d.f.</i>	<i>SS</i>	<i>MS</i>	<i>F</i>	<i>p-level</i>
<i>Regression</i>	2	2,889.32	1,444.66	498.87	7.77E-16
<i>Residual</i>	17	49.23	2.9		
<i>Total</i>	19	2,938.55			

70% Loading



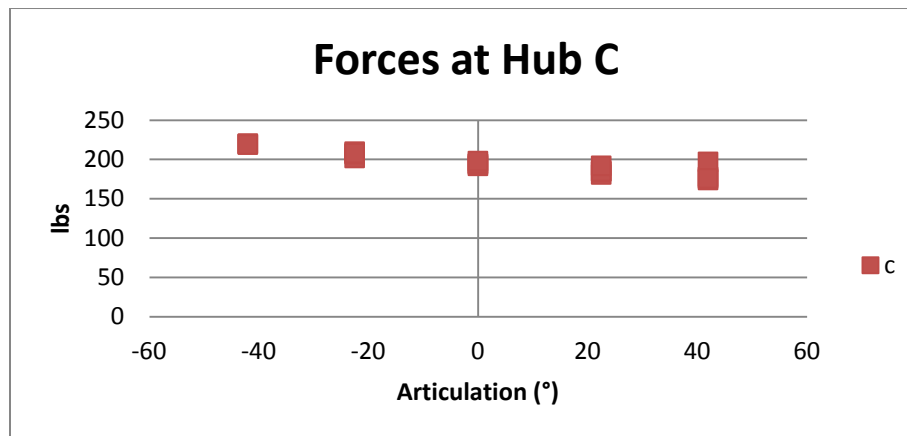
Forces at A Polynomial Regression	
Regression Statistics	
R	0.72
R Square	0.52
Adjusted R Square	0.47
Standard Error	3.26
Total number of observations	19
a = + 215.4690 + 0.1079 * Phi - 0.0004 * Phi**2	

ANOVA					
	d.f.	SS	MS	F	p-level
Regression	2	188.02	94.01	8.83	0.
Residual	16	170.4	10.65		
Total	18	358.42			



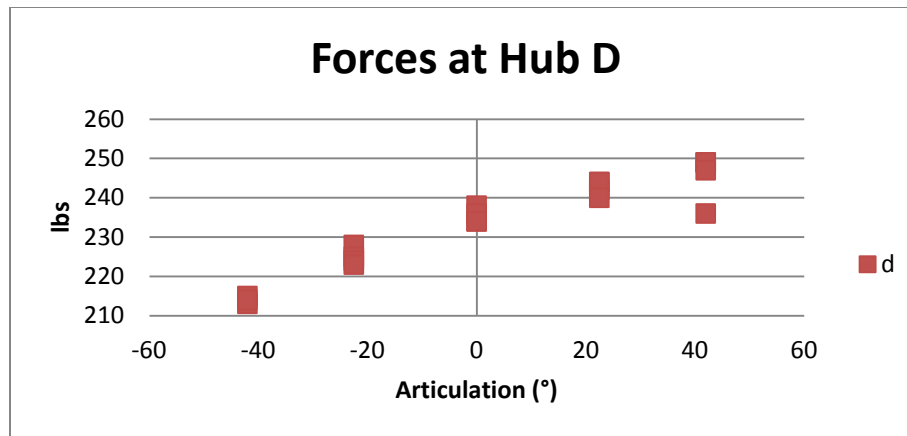
Forces at B Polynomial Regression	
<i>Regression Statistics</i>	
<i>R</i>	0.37
<i>R Square</i>	0.14
<i>Adjusted R Square</i>	0.03
<i>Standard Error</i>	2.59
<i>Total number of observations</i>	19
<b><math>b = + 213.1529 + 0.0315 * \text{Phi} + 0.0002 * \text{Phi}^{**2}</math></b>	

ANOVA					
	<i>d.f.</i>	<i>SS</i>	<i>MS</i>	<i>F</i>	<i>p-level</i>
<i>Regression</i>	2	17.24	8.62	1.28	0.3
<i>Residual</i>	16	107.39	6.71		
<i>Total</i>	18	124.63			



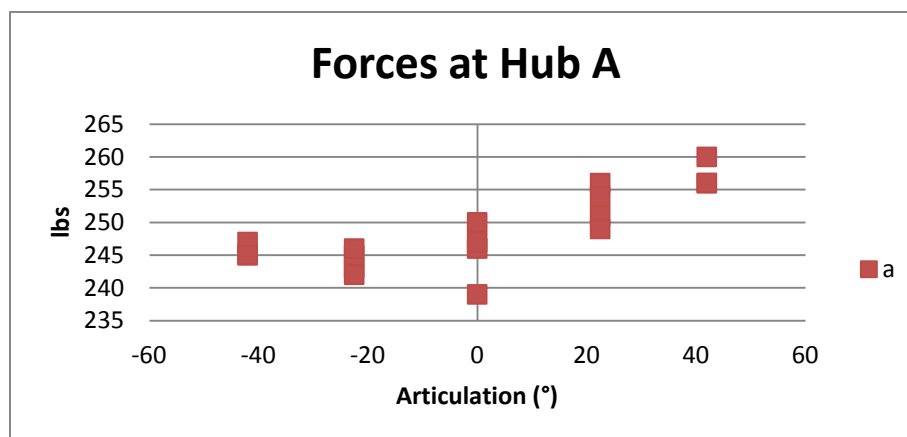
Forces at C Polynomial Regression	
<i>Regression Statistics</i>	
<i>R</i>	0.94
<i>R Square</i>	0.88
<i>Adjusted R Square</i>	0.87
<i>Standard Error</i>	5.34
<i>Total number of observations</i>	19
<b><math>c = + 194.6540 - 0.4596 * \text{Phi} + 0.0033 * \text{Phi}^{**2}</math></b>	

ANOVA					
	<i>d.f.</i>	<i>SS</i>	<i>MS</i>	<i>F</i>	<i>p-level</i>
<i>Regression</i>	2	3,434.73	1,717.36	60.26	0.
<i>Residual</i>	16	456.01	28.5		
<i>Total</i>	18	3,890.74			



Forces at D Polynomial Regression					
Regression Statistics					
R	0.97				
R Square	0.94				
Adjusted R Square	0.93				
Standard Error	3.12				
Total number of observations	19				
d = + 235.4618 + 0.3763 * Phi - 0.0033 * Phi**2					
ANOVA					
	d.f.	SS	MS	F	p-level
Regression	2	2,321.01	1,160.5	119.31	0.
Residual	16	155.63	9.73		
Total	18	2,476.63			

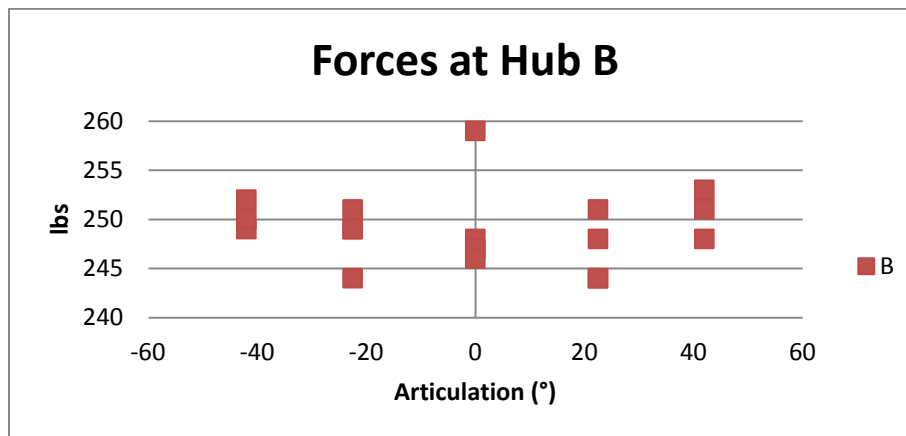
## 100% Loading





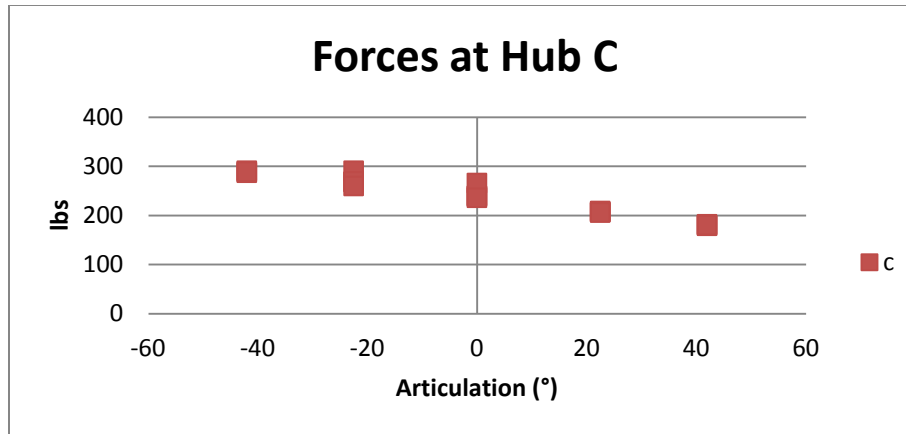
Forces at A Polynomial Regression	
<i>Regression Statistics</i>	
<i>R</i>	0.88
<i>R Square</i>	0.77
<i>Adjusted R Square</i>	0.74
<i>Standard Error</i>	2.93
<i>Total number of observations</i>	18
<b><math>a = + 246.1894 + 0.1527 * \text{Phi} + 0.0031 * \text{Phi}^{**2}</math></b>	

ANOVA					
	<i>d.f.</i>	<i>SS</i>	<i>MS</i>	<i>F</i>	<i>p-level</i>
<i>Regression</i>	2	426.98	213.49	24.9	0.
<i>Residual</i>	15	128.63	8.58		
<i>Total</i>	17	555.61			



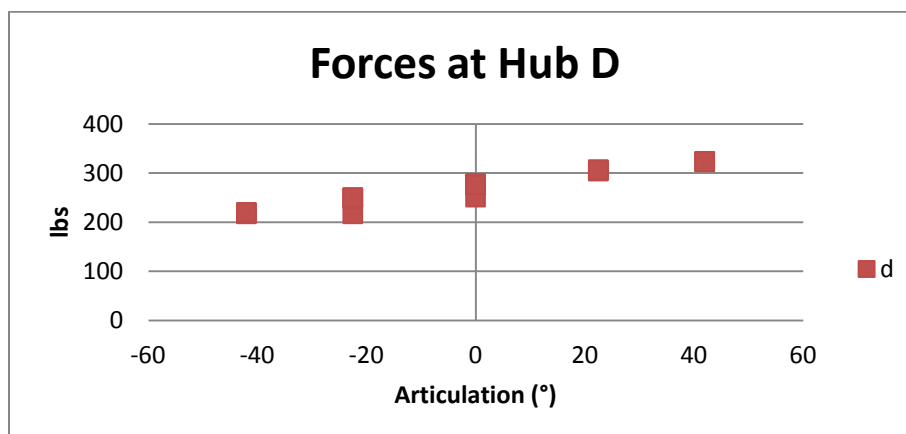
Forces at B Polynomial Regression	
<i>Regression Statistics</i>	
<i>R</i>	0.21
<i>R Square</i>	0.04
	-
<i>Adjusted R Square</i>	0.09
<i>Standard Error</i>	3.82
<i>Total number of observations</i>	18
<b><math>b = + 248.2274 - 0.0064 * \text{Phi} + 0.0010 * \text{Phi}^{**2}</math></b>	

ANOVA					
	<i>d.f.</i>	<i>SS</i>	<i>MS</i>	<i>F</i>	<i>p-level</i>
<i>Regression</i>	2	9.75	4.87	0.33	0.72
<i>Residual</i>	15	219.2	14.61		
<i>Total</i>	17	228.94			



Forces at C Polynomial Regression	
<i>Regression Statistics</i>	
<i>R</i>	0.98
<i>R Square</i>	0.96
<i>Adjusted R Square</i>	0.95
<i>Standard Error</i>	9.01
<i>Total number of observations</i>	18
<b><math>c = + 243.5148 - 1.3338 * \text{Phi} - 0.0053 * \text{Phi}^{**2}</math></b>	

ANOVA					
	<i>d.f.</i>	<i>SS</i>	<i>MS</i>	<i>F</i>	<i>p-level</i>
<i>Regression</i>	2	26,281.97	13,140.98	161.95	7.E-11
<i>Residual</i>	15	1,217.14	81.14		
<i>Total</i>	17	27,499.11			



Forces at D Polynomial Regression
-----------------------------------

<i>Regression Statistics</i>					
<i>R</i>			0.97		
<i>R Square</i>			0.94		
<i>Adjusted R Square</i>			0.94		
<i>Standard Error</i>			9.78		
<i>Total number of observations</i>			18		
<b>d = + 272.3317 + 1.2963 * Phi - 0.0005 * Phi**2</b>					
<i>ANOVA</i>					
	<i>d.f.</i>	<i>SS</i>	<i>MS</i>	<i>F</i>	<i>p-level</i>
<i>Regression</i>	2	24,594.04	12,297.02	128.55	0.
<i>Residual</i>	15	1,434.91	95.66		
<i>Total</i>	17	26,028.94			

## 2. Detailed derivation of the direction of $\vec{F}_{Eq}$

From Figure 2.8 we can determine the slope of line  $\ell$  from the derivative of the equation of the relevant unit circle at point  $(P_y, P_z)$ . Specifically this derivation is as follows:

$$\text{Equation of Unit Circle} = x^2 + z^2 = 1$$

Whose derivative, using implicit differentiation is equal to:

$$2x + 2z \frac{dz}{dx} = 0$$

Which yields;

$$\frac{dz}{dx} = \frac{-x}{z} = m_T$$

Where  $\frac{-x}{z}$  is the slope, denoted by  $m_T$ , of  $\ell$  when evaluated using  $(P_y, P_z)$ . . By default the direction of  $\vec{F}_{Eq}$  is calculated using Tip-Tail with point  $\ell_z$  as the tip and point P as the tail, however; to establish agreement between the sense of  $\vec{M}_{oT}$  and the moment created by  $\vec{F}_{Eq}$  the following manipulations must be made based on which quadrant P falls in and if the  $\vec{M}_{oT}$  is either positive or negative by right hand rule.

### 3. Load Cell Calibration Certificates

OMEGADYNE INC.

A

#### LOAD CELL FINAL CALIBRATION

0.00 - 1000.00 LBS  
Excitation 10.000 Vdc

Job: RMLS11837                      Serial: 304793  
Model: LC101-1K                      Tested By: CAG  
Date: 6/6/2012                      Temperature Range: 60 to 160 F  
Calibrated: 0.00 - 1000.00 LBS                      Specfile: LC101 750-30K

Force LBS	Unit Data mVdc	Normalized Data
0.00	0.164	0.000
500.00	15.177	15.013
1000.00	30.198	30.034
500.00	15.173	15.009
0.00	0.168	0.004

Balance	0.164	mVdc
Sensitivity	30.034	mVdc
In Resist	349.60	Ohms
Out Resist	351.40	Ohms
59K Shunt	14.855	mVdc

Calibration Factors:  
Sensitivity = 3.003 mV/V      59K Shunt = 1.486 mV/V

ELECTRICAL LEAKAGE: PASS  
ELECTRICAL WIRING/CONNECTOR: RED = +INPUT (EXC)  
BLACK = -INPUT (EXC)  
GREEN = +OUTPUT  
WHITE = -OUTPUT

This Calibration was performed using Instruments and Standards that are traceable to the United States National Institute of Standards Technology.

S/N	Description	Range	Reference	Cal Cert
SN15	1000lb Dead-Weights	0 - 1000 LBS	C-2690	
US36037936	HP34401A DMM	UUT Unit Under Test	C-2448	C-2448

Q.A. Representative : *Carol Griffin*                      Date: 6/6/2012

This transducer is tested to & meets published specifications. After final calibration our products are stored in a controlled stock room & considered in bonded storage. Depending on environment & severity of use factory calibration is recommended every one to three years after initial service installation date.  
COMMENTS: FINAL TEST IN TENSION.

Omegadyne, Inc., 149 Stelzer Court, Sunbury, OH 43074      (740) 965-9340  
http://www.omegadyne.com      email: info@omegadyne.com      (800) USA-DYNE

OMEGADYNE INC.

B

LOAD CELL  
FINAL CALIBRATION

0.00 - 1000.00 LBS  
Excitation 10.000 Vdc

Job: RMLS11837 Serial: 304863  
Model: LC101-1K Tested By: WF  
Date: 6/5/2012 Temperature Range: 60 to 160 F  
Calibrated: 0.00 - 1000.00 LBS Specfile: LC101 750-30K

Force LBS	Unit Data mVdc	Normalized Data
0.00	0.022	0.000
500.00	15.027	15.005
1000.00	30.037	30.015
500.00	15.031	15.009
0.00	0.023	0.001

Balance 0.022 mVdc  
Sensitivity 30.015 mVdc  
In Resist 349.90 Ohms  
Out Resist 351.90 Ohms  
59K Shunt 14.786 mVdc

Calibration Factors:  
Sensitivity = 3.002 mV/V 59K Shunt = 1.479 mV/V

ELECTRICAL LEAKAGE: PASS  
ELECTRICAL WIRING/CONNECTOR: RED = +INPUT (EXC)  
BLACK = -INPUT (EXC)  
GREEN = +OUTPUT  
WHITE = -OUTPUT

This Calibration was performed using Instruments and Standards that are traceable to the United States National Institute of Standards Technology.

S/N	Description	Range	Reference	Cal Cert
US36037936	1000lb Reference STD	0 - 1000 LBS	C-2692	C-2692
	HP34401A DMM	UUT Unit Under Test	C-2448	C-2448

Q.A. Representative : *William Fleeter*

Date: 6/5/2012

This transducer is tested to & meets published specifications. After final calibration our products are stored in a controlled stock room & considered in bonded storage. Depending on environment & severity of use factory calibration is recommended every one to three years after initial service installation date.  
COMMENTS: FINAL TEST.

Omegadyne, Inc., 149 Stelzer Court, Sunbury, OH 43074 (740) 965-9340  
<http://www.omegadyne.com> email: [info@omegadyne.com](mailto:info@omegadyne.com) (800) USA-DYNE



Δ

Job: RMLS12385                      Serial: 297815  
Model: LC101-1K                    Tested By: WF  
Date: 8/28/2012                  Temperature Range: 60 to 160 F  
Calibrated: 0.00 - 1000.00 LBS      Specfile: LC101 750-30K

Force LBS	Unit Data mVdc	Normalized Data
0.00	- 0.072	0.000
500.00	14.934	15.006
1000.00	29.949	30.021
500.00	14.940	15.012
0.00	- 0.071	0.001
Balance	- 0.072	mVdc
Sensitivity	30.021	mVdc
In Resist	349.90	Ohms
Out Resist	351.40	Ohms
59K Shunt	14.907	mVdc

Calibration Factors:  
Sensitivity = 3.002 mV/V      59K Shunt = 1.491 mV/V

ELECTRICAL LEAKAGE: PASS

ELECTRICAL WIRING/CONNECTOR:

RED	= +INPUT (EXC)
BLACK	= -INPUT (EXC)
GREEN	= +OUTPUT
WHITE	= -OUTPUT

This Calibration was performed using Instruments and Standards that are traceable to the United States National Institute of Standards Technology.

S/N	Description	Range	Reference	Cal Cert
SN15	1000lb Dead-Weights	0 - 1000 LBS	C-2690	
US36037936	HP34401A DMM UUT	Unit Under Test	C-2448	C-2448

Q.A. Representative : *William Fleeter*

Date: 8/28/2012

This transducer is tested to & meets published specifications. After final calibration our products are stored in a controlled stock room & considered in bonded storage. Depending on environment & severity of use factory calibration is recommended every one to three years after initial service installation date.

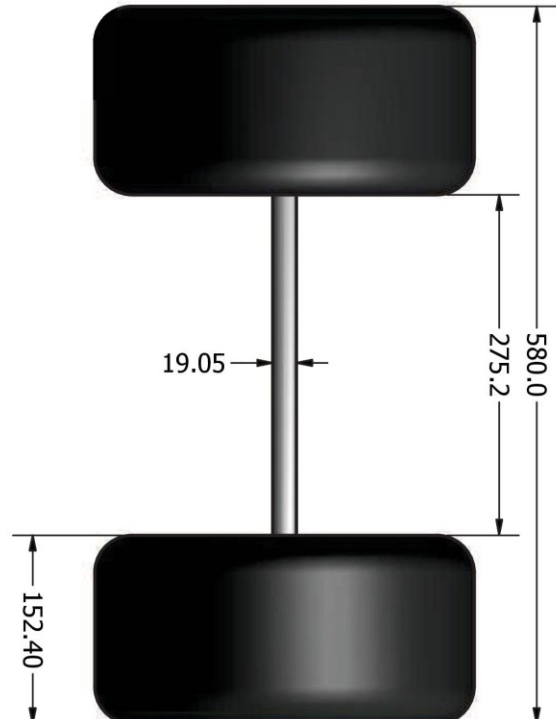
COMMENTS: FINAL TEST.


Omegadyne, Inc., 149 Stelzer Court, Sunbury, OH 43074 (740) 965-9340  
<http://www.omegadyne.com> email: [info@omegadyne.com](mailto:info@omegadyne.com) (800) USA-DYNE

REV	DATE	DESCRIPTION
0	6/14/2012	No Revisions



Ø304.8



	
University of Alberta Chemical & Materials Engineering Machine Shop	
PART NAME (Part #)  Axle & Wheel Assy	
PART CREATION DATE 5/17/2012	
SHEET SIZE W.O.# (Title) A W.O.#1256	
REV # 0	
Designed By DAVE PARLIN	SHEET 1 OF 1

2 Complete Axle & Wheel Assemblies Required

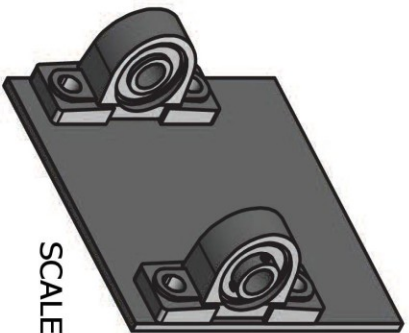
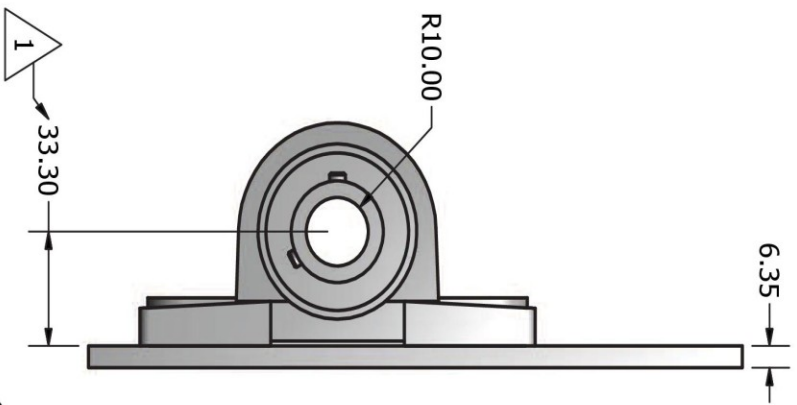
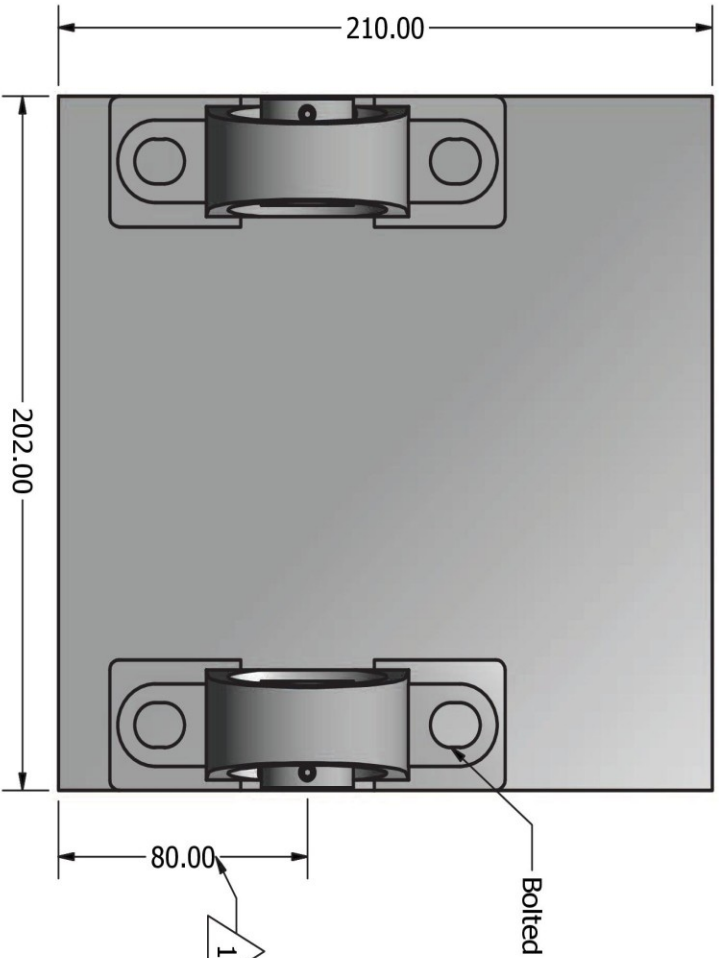
SCALE 1 / 5

#### 4. Detailed Design Drawings of Test Unit





REV	DATE	DESCRIPTION
0	6/14/2012	No Revisions
1	6/14/2012	Minor dimension changes



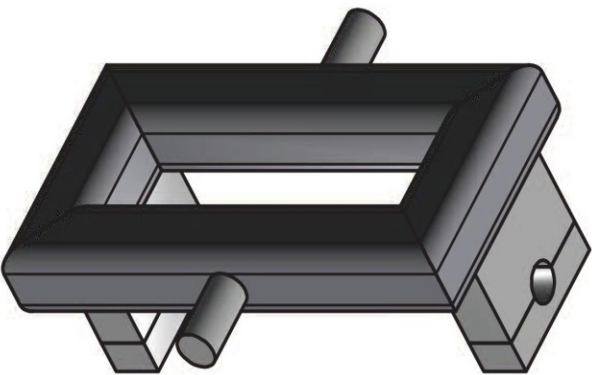
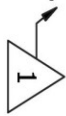
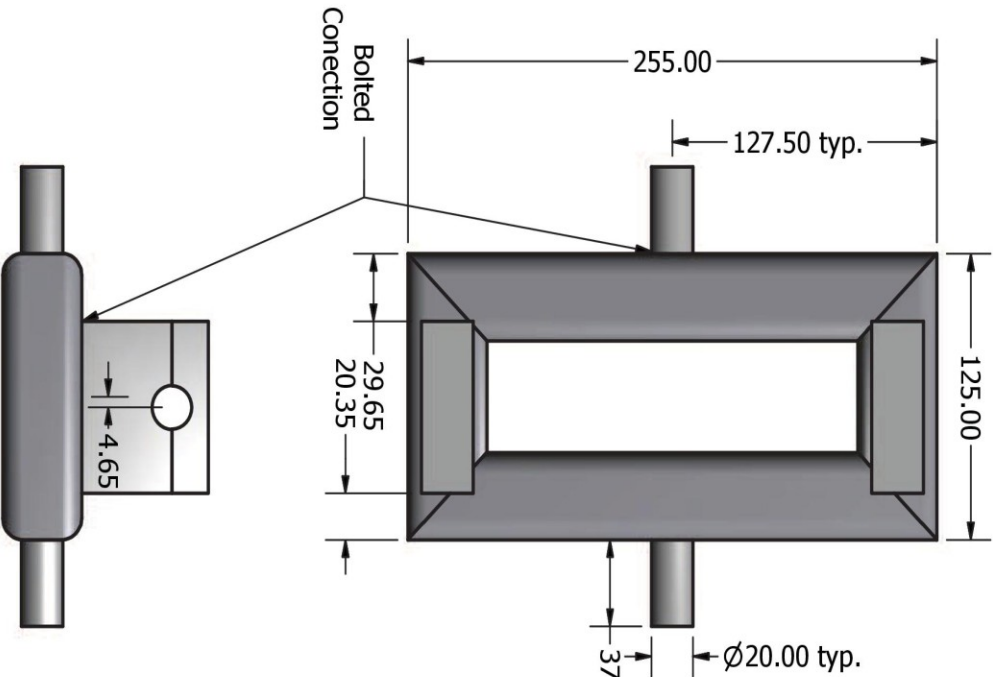
SCALE 1 / 4



PART NAME (Part #)			
University of Alberta Chemical & Materials Engineering Machine Shop			
Front_Axle Plate			
PART CREATION DATE	SHEET SIZE W.O.# (Title)	REV #	
5/17/2012	A W.O.# 1256	1	
Designed By		SHEET 1 OF 1	
DAVE PARLIN			

SCALE 1 / 2  
 $\frac{1}{2}$ " Mild Steel Plate  
 Bearing =

REV	DATE	DESCRIPTION
0	6/14/2012	No Revisions
1	6/14/2012	Tube Size Changed to 1 $\frac{1}{2}$ " + Minor Dimension Changes



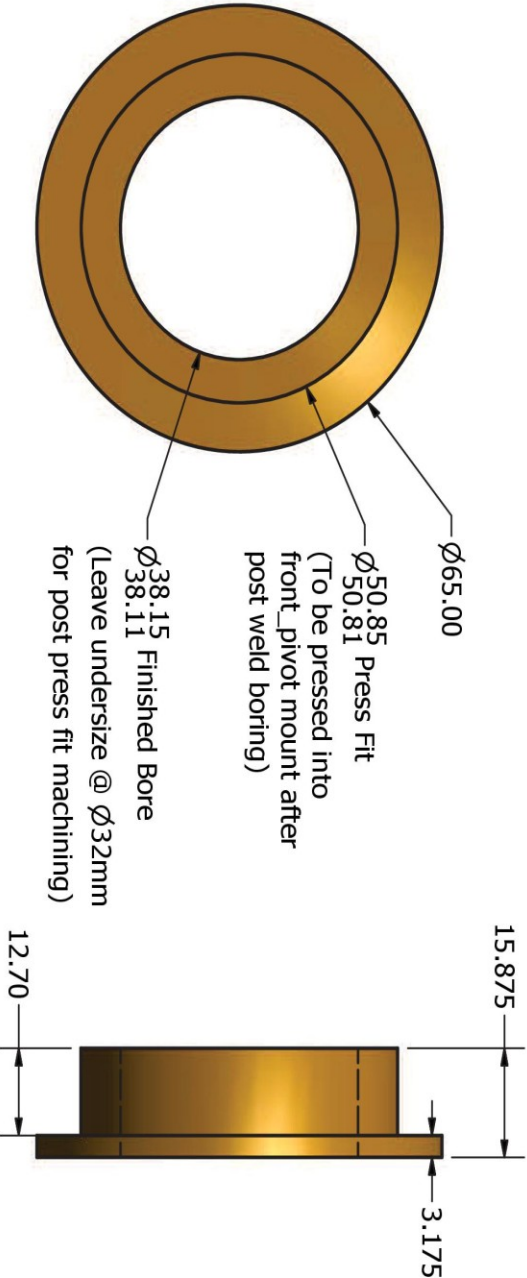
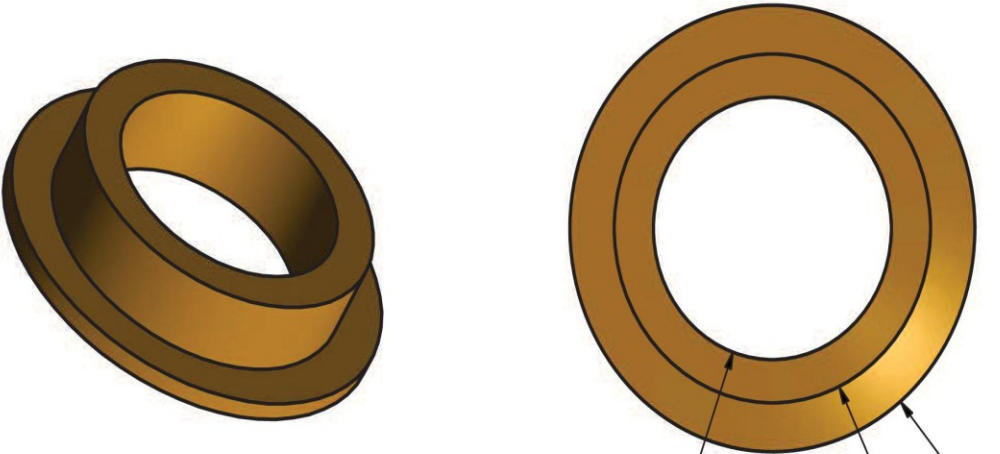
SCALE 1 / 3

1  $\frac{1}{2}$ " Square Tube  $\frac{3}{16}$ " Wall  
All other parts = Mild Steel



PART NAME (Part #) <b>Front_Axle Trunion</b>			
University of Alberta Chemical & Materials Engineering Machine Shop			
PART CREATION DATE 5/17/2012	SHEET SIZE W.O.# (Title) A W.O.#1256	REV # 1	Designed By DAVE PARLIN
SHEET 1 OF 1			

REV	DATE	DESCRIPTION
0	6/14/2012	No Revisions



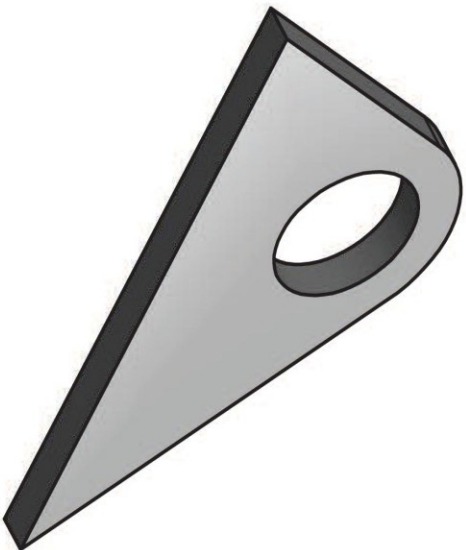
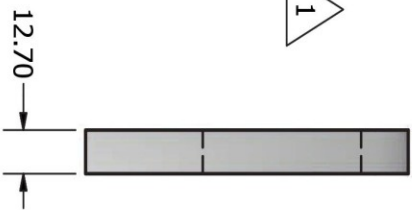
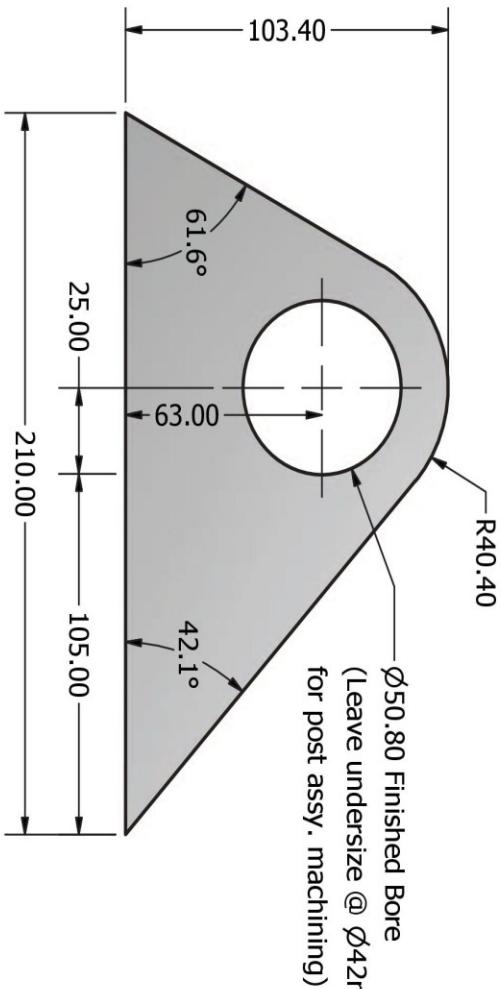
PART NAME (Part #)		University of Alberta Chemical & Materials Engineering Machine Shop	
SHEET SIZE W.O.# (Title)		Front_Brass Bushing	
PART CREATION DATE	4/27/2012	W.O.# 1256	REV # 0
Designed By	DAVE PARLIN	SHEET 1 OF 1	


SCALE 1 : 1  
4 Pieces Required  
Matl. = Brass





REV	DATE	DESCRIPTION
0	6/14/2012	No Revisions
1	6/14/2012	Minor Dimension Changes



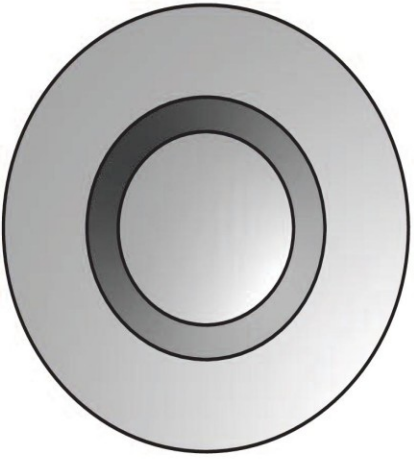
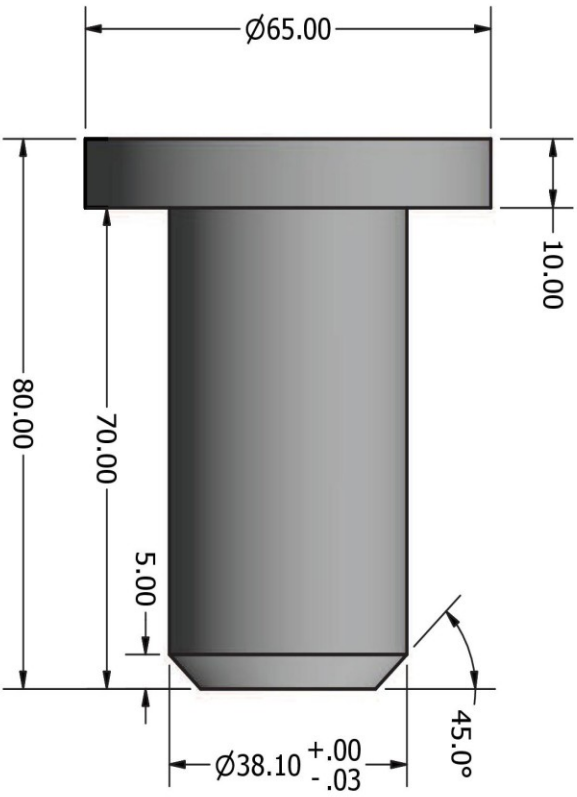
		University of Alberta Chemical & Materials Engineering Machine Shop	
PART CREATION DATE 4/26/2012		PART NAME (Part #)  Front_Pivot Mount	
SHEET SIZE W.O.# (Title) A W.O.#1256		REV # 1	
Designed By DAVE PARLIN		SHEET 1 OF 1	

SCALE 1 / 2  
4 Pieces Required  
Matl. = Mild Steel

University of Alberta  
Chemical & Materials Engineering  
Machine Shop



REV	DATE	DESCRIPTION
0	6/14/2012	No Revisions




A

B

A

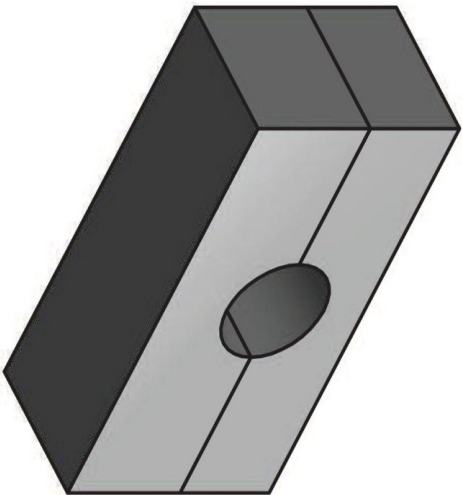
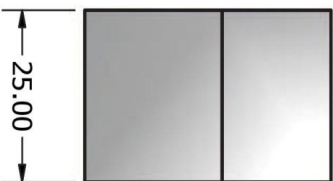
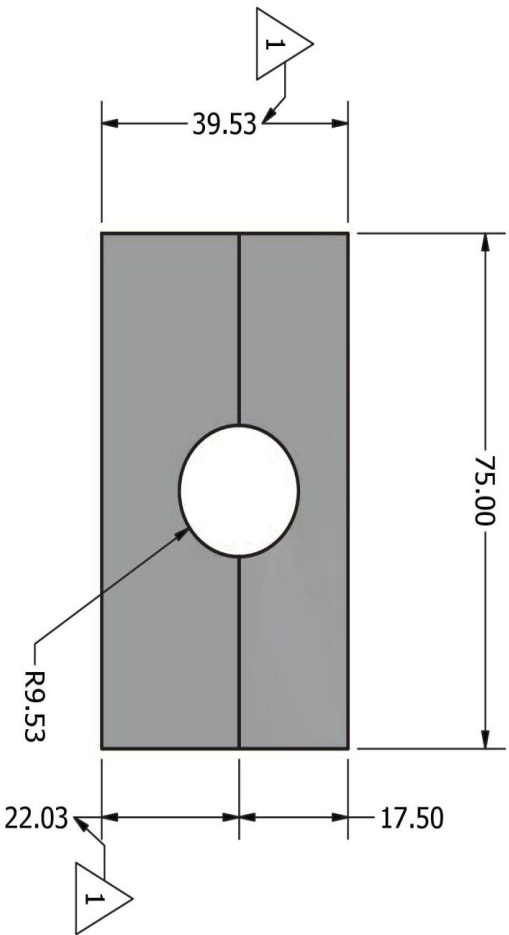
B

		<b>University of Alberta</b> Chemical & Materials Engineering Machine Shop	
PART NAME (part #) <b>Pin</b>		SHEET SIZE W.O.# (Title) <b>W.O.# 1256</b>	
PART CREATION DATE <b>4/27/2012</b>		REV # <b>0</b>	
Designed By <b>DAVE PARLIN</b>		SHEET 1 OF 1	

**SCALE 1 : 1**  
 2 Pieces Required  
 Matl. = Mild Steel



REV	DATE	DESCRIPTION
0	6/14/2012	No Revisions
1	6/14/2012	Minor Dimension Changes

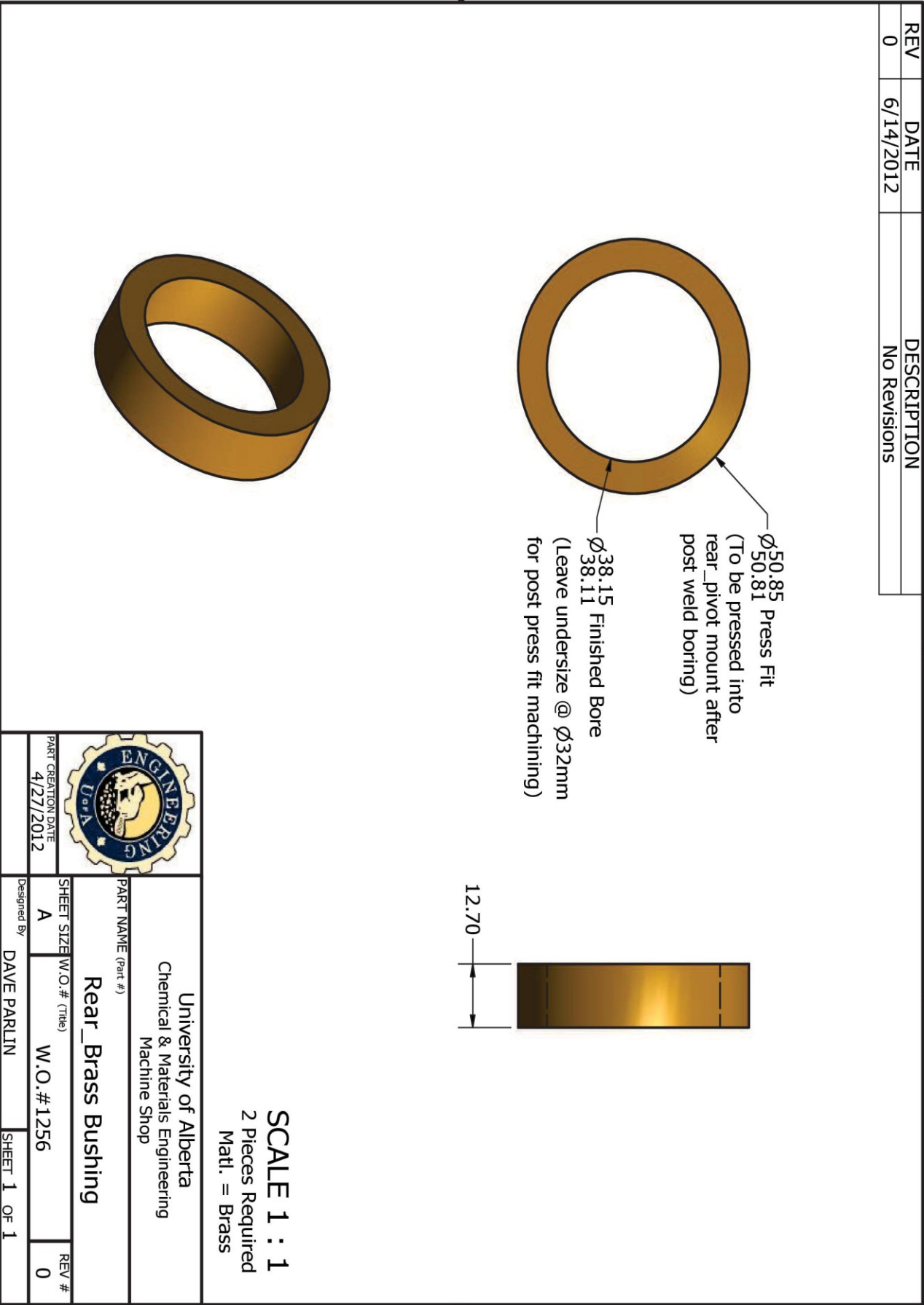


**SCALE 1 : 1**  
2 Pieces Required  
Matl. = Mild Steel



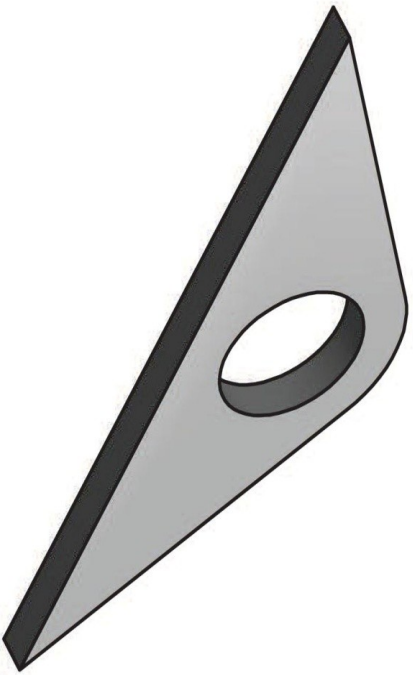
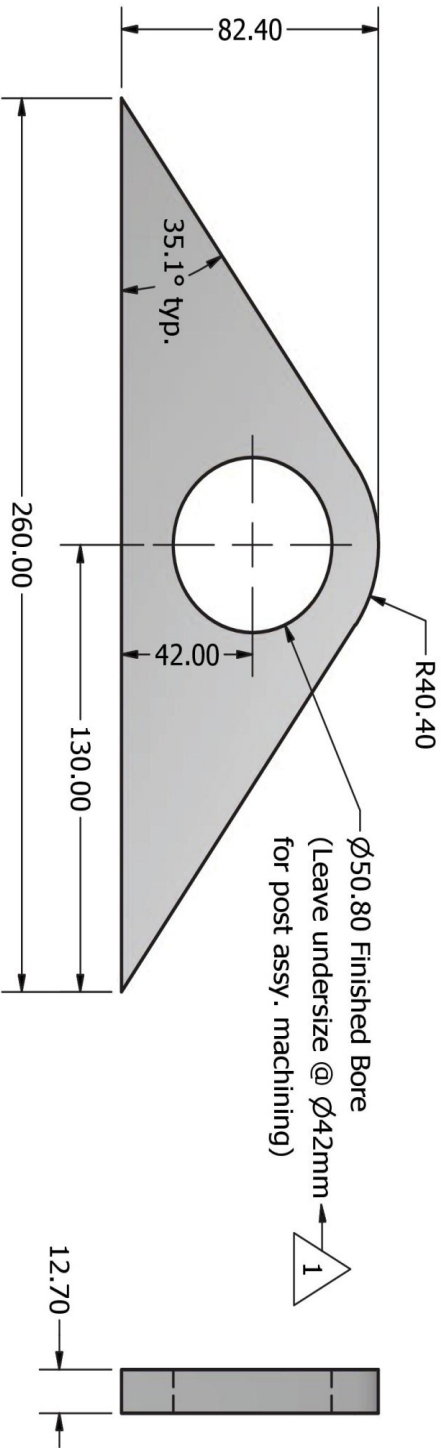
<b>University of Alberta</b> Chemical & Materials Engineering Machine Shop			
PART NAME (part #) <b>Rear_Axle Clamp</b>			
SHEET SIZE W.O.# (Title) <b>A</b>		REV # <b>1</b>	
PART CREATION DATE 5/18/2012		Designed By <b>DAVE PARLIN</b>	
		SHEET 1 OF 1	

REV	DATE	DESCRIPTION
0	6/14/2012	No Revisions






REV	DATE	DESCRIPTION
0	6/14/2012	No Revisions
1	6/14/2012	Minor Dimension Changes



**SCALE 1 / 2**  
 2 Pieces Required  
 Matl. = Mild Steel

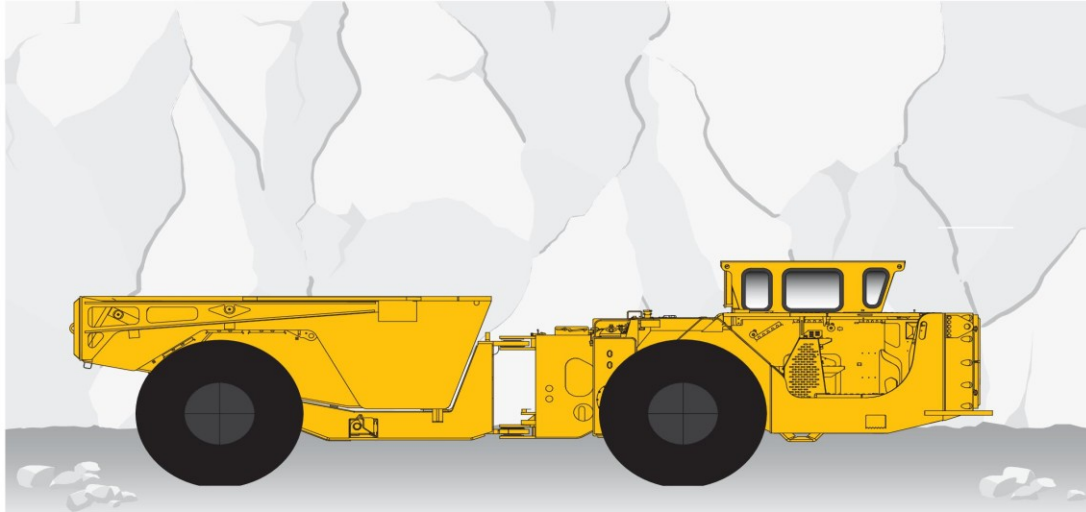
		<b>University of Alberta</b> Chemical & Materials Engineering Machine Shop	
PART NAME (Part #) <b>Rear_Pivot Bracket</b>		REV # <b>1</b>	
SHEET SIZE W.O.# (Title) <b>A</b>		W.O.# 1256	
PART CREATION DATE 4/26/2012		Designed By <b>DAVE PARLIN</b>	
		SHEET 1 OF 1	

## 5. Example Equipment Specification Sheets

**Atlas Copco** Underground trucks

# Minetruck MT2010

## Technical specification



The Minetruck MT2010 is a 20 metric tonne underground truck, designed for small to medium-scale underground operations and high speed development.

### Features

#### Dump box

- Optimum box profile for clean and fast dumping
- Box support for safe work under box

#### Operator's compartment

- FOPS/ROPS approved canopy with back protection
- 3 point mounting access for entry and exit from operator's compartment
- Optional back up camera and monitor for maximum safety and operator assistance
- Optional spacious and ergonomically designed compartment for maximum safety and minimal operator fatigue with:
  - Forward seated enclosed cabin
  - ISO ROPS/FOPS certified for maximum safety
  - Air conditioning for convenient working conditions

#### Power frame

- A high power-to-weight ratio for high ramp haulage performance
- Oversized power train components for long life and low costs

#### General

- Great serviceability with centralized service points
- Long-life roller bearing centre hinge
- Anti skid material at service access points
- Central manual lubrication
- Hydraulic hoses, electric cables and hot surfaces are well routed and protected
- SAHR brake system
- CE certified

**Atlas Copco**



# Specifications

## CAPACITIES

kg	Tramming capacity	20 000
m³	Standard box volume (SAE heaped)	9.0

## MOTION TIMES

sec	Dumping	15
-----	---------	----

## WEIGHTS

Standard equipped vehicle (empty weight)		
kg	Approximate weight	20 500
	Front axle load	13 800
	Rear axle load	6 700

## Engine

- Cummins..... QSL9C300, Tier/Stage 3
- Power rating at 2 100 rpm ..... 224 kW/300 hp
- Maximum torque at 1 350 rpm ..... 1 369 Nm
- MSHA Part 7 ventilation rate ..... 368 m³/min
- MSHA Part 7 particulate index ..... 396 m³/min
- Rock Tough purifier and silencer
- Dry type air cleaner
- Exhaust heat protection
- Cooling package with tube type radiator

## Transmission and converter

- Converter, single stage with automatic lock-up
- Dana..... 5000 Series

## Axles

- Spiral bevel differential, full floating, planetary wheel end drive Rock Tough ..... Model 457
- Conventional front and rear differential
- Degree of oscillation ..... 20° (10° on each side)

## Brakes

- Fully enclosed, force cooled, multiple wet discs at each wheel end
- Service/parking/emergency ..... SAHR

## Tyres

- Tubeless, steel radial, lug tread design for underground mine service
- Dimension ..... 18.00R25

*\* As applications and conditions vary, Atlas Copco recommends that the user consults with tyre suppliers to obtain the optimum tyre selection*

## Operator's compartment

- Side seated operator for bi-directional operation
- Canopy FOPS/ROPS approved
- Grammer seat with retractable seat belt
- Two pilot operated levers for steering and gear shifting
- External sound level according to ISO 6393 LwA 122 dB(A)
- Sound level in canopy according to ISO 6394 LpA 108 dB(A)
- Sound level in cabin according to ISO 6394 LpA 85 dB(A)
- Whole body vibration value A(8)w in range of 0.5 to 2m/s² (typical value for similar machines).

## Hydraulic system

- Filtration type ..... suction
- Heavy duty gear type pumps
- Hydraulic tank capacity ..... 223 litres
- Cylinders, double acting, chrome plated stems, diameter:
  - Steer cylinders (2) ..... 115 mm
  - Dump cylinders (2) ..... 140 mm
- System pressure ..... 15.5 MPa

## Electrical system

- Voltage, system start & accessories ..... 24 V
- Alternator, high output ..... 140 A
- Hydraulic warning system; temperature, level
- LED lights 8 x 40W
- Isolation switch lockout

## Fuel

- Fuel tank capacity ..... 379 litres

## Other

- Central manual lubrication
- Fire extinguisher ..... 2x6 kg
- Fuel gauge in panel

# Optional equipment

## Main frame

- Optional box sizes
- Shipping covers
- Wheel chocks
- Tele dump CE certification

## Ergonomics

- Forward facing enclosed cab with wheel control steering
- Low built canopy
- Heater (not for low built)
- Air conditioner, cabin

## System

- Ansul Checkfire, autofire suppression
- Ansul single bottle fire suppression with engine shutdown
- Lincoln auto lube with timer
- Wiggins fast fuel fill
- Back up camera and monitor
- Manual hydraulic tank fill pump

## Drive train

- Neutral break apply

## Electrical system

- Tail and brake lights
- Block heater (120V or 240V)

## Controls and instruments

- Blockout 3<sup>rd</sup> and/or 4<sup>th</sup> gears
- Speedometer

## Power unit

- Corrosion resistant radiator

## Documentation

- LinkOne parts book, CD
- Operator's and maintenance manual - plasticized

## Parts kit

- 1 000 hour consumables

## Other

- Tool box

# Grade performance

STANDARD CONFIGURATION, BOX EMPTY												
%	Grade	0.0	2.0	4.0	6.0	8.3	10.0	12.5	14.3	16.0	18.0	20.0
Ratio	Grade	—	—	—	—	1:12	1:10	1:8	1:7	—	—	1:5
km/h	1st gear	4.5	4.5	4.5	4.5	4.5	4.4	4.4	4.4	4.4	4.4	4.4
	2nd gear	8.0	8.0	8.0	8.0	8.0	7.9	7.9	7.9	7.9	7.8	7.8
	3rd gear	14.1	14.1	14.0	13.9	13.8	13.8	13.7	13.6	13.5	13.5	13.1
	4th gear	25.1	24.9	24.7	24.4	24.2	23.4	21.9	19.6			

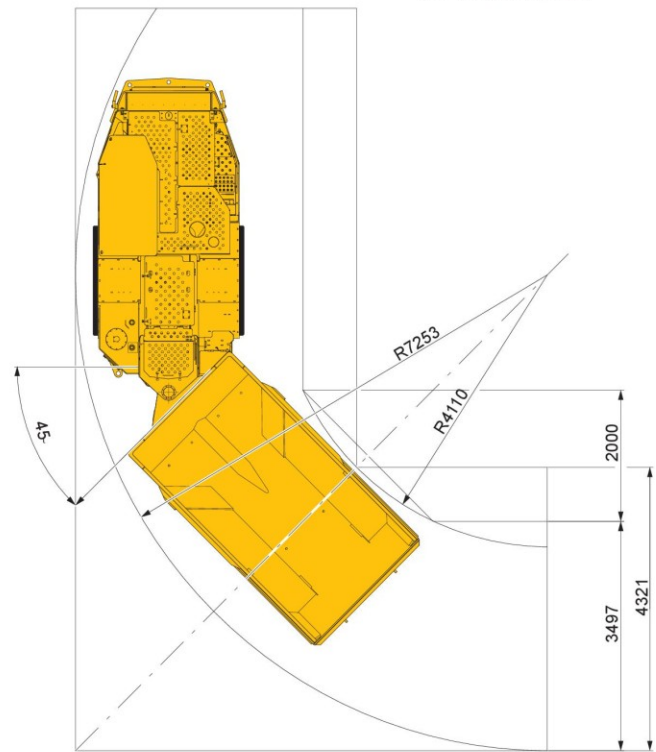
3% rolling resistance assumed. Actual performance may vary depending on the application.

STANDARD CONFIGURATION, BOX LOADED												
%	Grade	0.0	2.0	4.0	6.0	8.3	10.0	12.5	14.3	16.0	18.0	20.0
Ratio	Grade	—	—	—	—	1:12	1:10	1:8	1:7	—	—	1:5
km/h	1st gear	4.5	4.5	4.4	4.4	4.4	4.4	4.4	4.4	4.3	4.3	4.3
	2nd gear	8.0	7.9	7.9	7.8	7.8	7.8	7.7	7.7	7.6	7.3	7.0
	3rd gear	14.0	13.8	13.7	13.5	13.2	12.3	10.9				
	4th gear	24.7	24.2	22.4	17.6							

3% rolling resistance assumed. Actual performance may vary depending on the application.

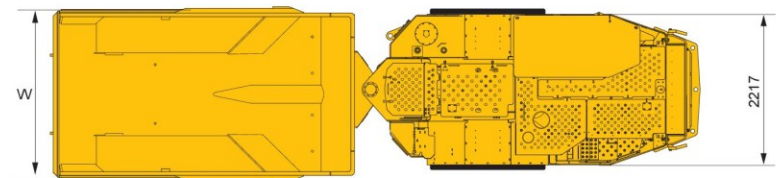
## Measurements

### TURNING RADIUS



### » Dimensions

- All dimensions are shown in millimetres
- All dimensions shown are based on standard vehicle configuration with 27 mm tyre deflection, unloaded



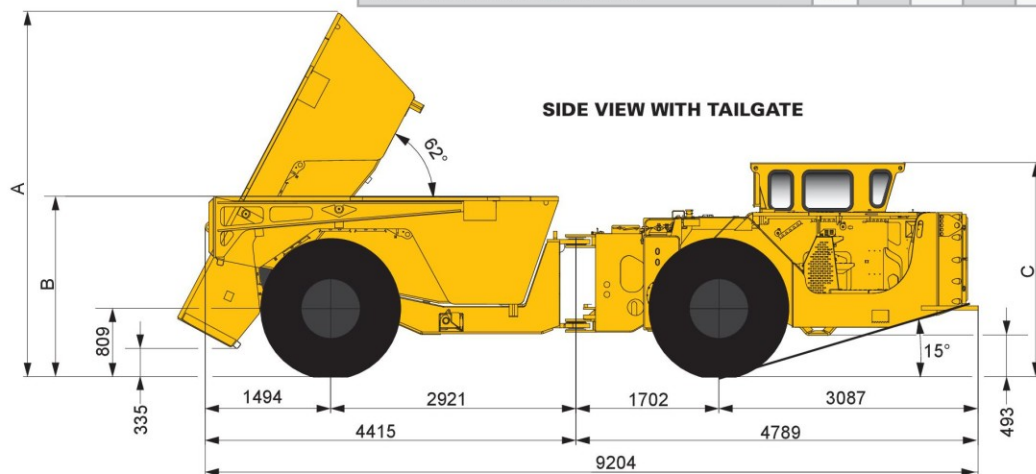
### TOP VIEW BOX WITH TAILGATE

## Measurements and weights

### DUMP BOXES WITH TAILGATE

### STD

Volume, SAE heaped (m <sup>3</sup> )		11.0	10.0	9.1	8.4
Volume, SAE struck (m <sup>3</sup> )		9.2	8.0	7.1	6.5
Maximum material density (t/m <sup>3</sup> )		1.8	2.0	2.2	2.4
Width, dump box (mm)	(W)	2 400	2 400	2 400	2 400
Dump position: box height, max (mm)	(A)	4 445	4 341	4 301	4 199
Tramming position: dump box height (mm)	(B)	2 358	2 230	2 131	2 059



SIDE VIEW WITH TAILGATE

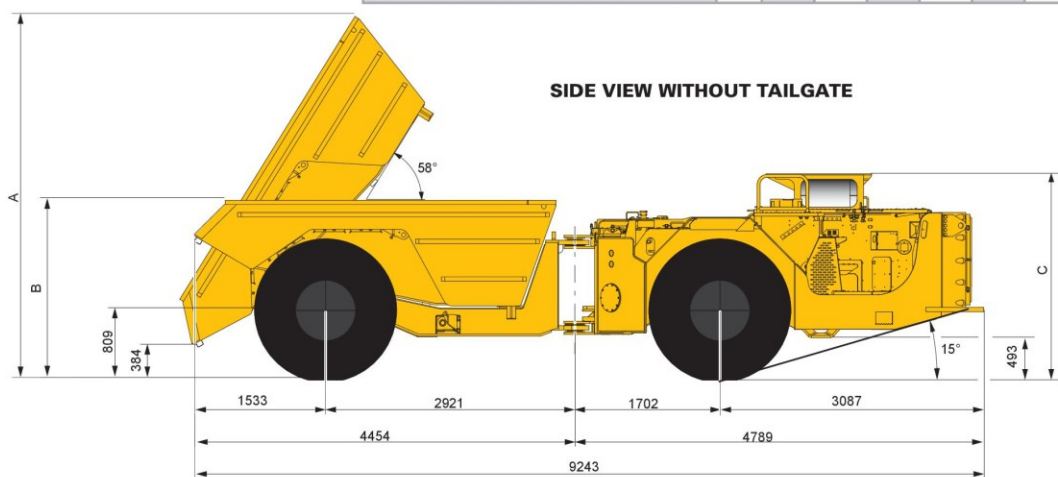
### OPERATORS COMPARTMENT

Height (mm)	C
Cabin	2 530
Canopy standard	2 510
Canopy low profile	2 400

### DUMP BOXES WITHOUT TAILGATE

### STD

Volume, SAE heaped (m <sup>3</sup> )		11.0	10.0	9.0	8.4	7.7	6.7
Volume, SAE struck (m <sup>3</sup> )		9.2	8.0	7.0	6.3	5.6	4.6
Maximum material density (t/m <sup>3</sup> )		1.8	2.0	2.2	2.4	2.6	3.0
Width, dump box (mm)	(W)	2 435	2 435	2 435	2 435	2 435	2 435
Dump position: box height, max (mm)	(A)	4 444	4 330	4 226	4 197	4 097	4 097
Tramming position: dump box height (mm)	(B)	2 351	2 214	2 089	2 054	1 934	1 934



SIDE VIEW WITHOUT TAILGATE

**Atlas Copco**

© Copyright 2011, Atlas Copco Rock Drills AB, Örebro, Sweden. All product names in this publication are trademarks of Atlas Copco. Any unauthorized use or copying of the contents or any part thereof is prohibited. Illustrations and photos may show equipment with optional extras. No warranty is made regarding specifications or otherwise. Specifications and equipment are subject to change without notice. Consult your Atlas Copco Customer Center for specific information.

9851 2464 01 k  
02/2011



# **Minetruck 431B**

## **Technical specification**



The Minetruck MT431B is a 28.1 metric ton capacity underground truck, for large operations, in mining and construction.

### **Features**

- ROPS/FOPS canopy with back protection
- Jacobs engine brake increase brake life, automatic engine overspeed protection, and reduced heat from breaking
- Electric transmission shift control for convenient shifting
- Converter lockup offers better power transfer, less heat and longer component life
- Centralized lubrication simplifies maintenance
- SAHR brake system offers long component life and very reliable breaking

# Specifications

Capacity	
Tramming	28 125 kg

Motion times	
Dump box	
Dumping	14 seconds

## Engine

- Detroit Diesel engine ..... Series 60, EPA Tier 2/EU Stage II
- Power rating at 2 100 rpm ..... 298 kW/400 hp
- Maximum torque at 1 350 rpm ..... 1 898 Nm
- MSHA Part 7 ventilation rate ..... 793 m<sup>3</sup>/min
- MSHA Part 7 particulate index ..... 241 m<sup>3</sup>/min
- Dry type air cleaner
- Exhaust heat protection
- Remote engine oil drain
- Cooling package with V-core radiator

## Transmission

- Full power shift, 4 speed forward/reverse
- Dana ..... 6000 Series

## Converter

- Single stage with Lock Up
- Dana ..... CL-8000 Series

## Axles

- Spiral bevel differential, full floating, planetary wheel end drive
- Rock Tough ..... 508
- Conventional front differential
- Rear axle, trunnion mounted, self-lubricating bushings
- Degree of oscillation ..... 18° (9° each side)

## Brakes

- Fully enclosed, force cooled, multiple wet discs at each wheel end
- Service/parking/emergency ..... SAHR

## Tyres

- Tubeless, nylon, smooth tread design for underground mine service, on demountable rims
- Dimension ..... 18.00R33
- Ply rating ..... MS

*\* As applications and conditions vary, Atlas Copco recommends that the user consults with tyre suppliers to obtain the optimum tyre selection*

## Operator's compartment

- Canopy; MSHA-ISO ROPS/FOPS approved
- Side seated operator for bi-directional operation
- Grammer seat with retractable seat belts
- Two pilot operated joysticks for steering and dump control

## Hydraulic system

- System pressure ..... 15.8 MPa
- Hydraulic tank capacity ..... 238 litres
- Filtration, return line ..... 4.0 µm
- Heavy duty gear type pumps
- Cylinders, double acting, chrome plated stems, diameter:
  - Steer cylinders (2) ..... 152 mm
  - Dump cylinder ..... 228 mm

## Electrical system

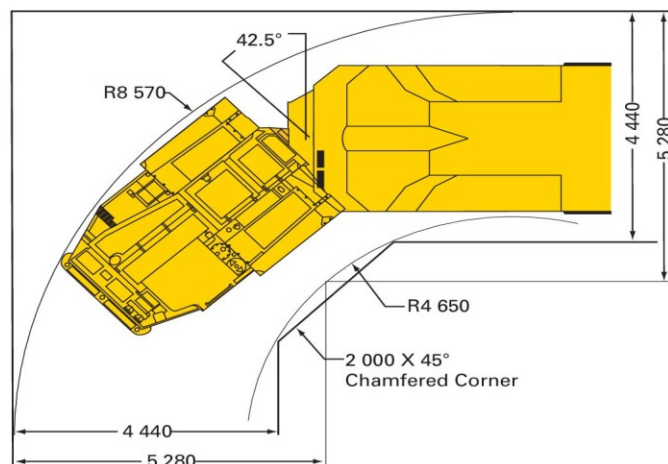
- Voltage, system start & accessories ..... 24 V
- Alternator, high output ..... 140 A
- Hydraulic warning system ..... level, hyd. temp.
- Hella protection lights
- Isolation switch lockout

## Fuel

- Fuel tank capacity ..... 439 litres
- Fuel consumption, full load ..... 35.5 litres/hour
- Fuel filtration ..... 8.0 µm
- Anti-siphon fuel supply



## Turning radius



- Turning angle +/- 42.5°
- Turning radius left and right are symmetrical
- Dimensions shown are based on standard vehicle configuration with 25 mm tyre deflection
- All dimensions are shown in millimetres

## Grade performance

NB. 3% rolling resistance assumed. Actual performance may vary depending on the application

### Standard configuration, box empty

Percent grade	0.0	2.0	4.0	6.0	8.0	10.0	12.0	14.0	16.0	18.0	20.0
Ratio					1:12	1:10	1:8	1:7			1:5
1st gear (km/h)	5.72	5.70	5.69	5.68	5.66	5.65	5.63	5.62	5.61	5.59	5.58
2nd gear (km/h)	10.22	10.17	10.13	10.08	10.03	9.99	9.94	9.90	9.85	9.80	9.76
3rd gear (km/h)	18.05	17.90	17.76	17.61	17.47	17.32	16.65	15.27	13.56	11.54	
4th gear (km/h)	32.0	31.5	31.0	28.4	23.0						

### Standard configuration, box loaded

Percent grade	0.0	2.0	4.0	6.0	8.0	10.0	12.0	14.0	16.0	18.0	20.0
Ratio					1:12	1:10	1:8	1:7			1:5
1st gear (km/h)	5.70	5.67	5.64	5.61	5.59	5.56	5.53	5.50	5.47	5.45	5.42
2nd gear (km/h)	10.15	10.06	9.97	9.88	9.79	9.65	8.77	7.77	6.51		
3rd gear (km/h)	17.84	17.55	17.27	14.85	10.95						
4th gear (km/h)	31.36	26.70									

## Optional equipment

### Main frame

- Shipping covers, cabin
- Wheel chocks
- Tele dump

### Ergonomic

- Forward facing cab
- KAB 555 seat with retractable seatbelts cabin
- Heater
- Air condition, cabin
- Side seated with steering wheel, canopy

### System

- Ansul dual bottle fire suppression with engine shutdown
- Electric hydraulic tank fill pump
- Lincoln auto lube with timer
- Wiggins fast fuel fill

### Electrical system

- Amber strobe light - power on
- 24/12 V power converter, cabin
- Load lights

- Side light opposite operator, cabin
- Tail and brake lights
- Front and rear red lights 2 each

### Controls and instruments

- Blockout 3rd and/or 4th gears
- Load man, cabin
- Speedometer
- Automatic transmission control
- Back up camera and monitor

### Power unit

- Epoxy coated radiator

### Documentation

- LinkOne parts catalogue, CD
- Parts and service manual - plasticized
- Extra DDEC manual kit

### Parts kit

- 1 000 hour consumables
- Articulation repair kit
- Maintenance kit

### Other

- Tool box, cabin

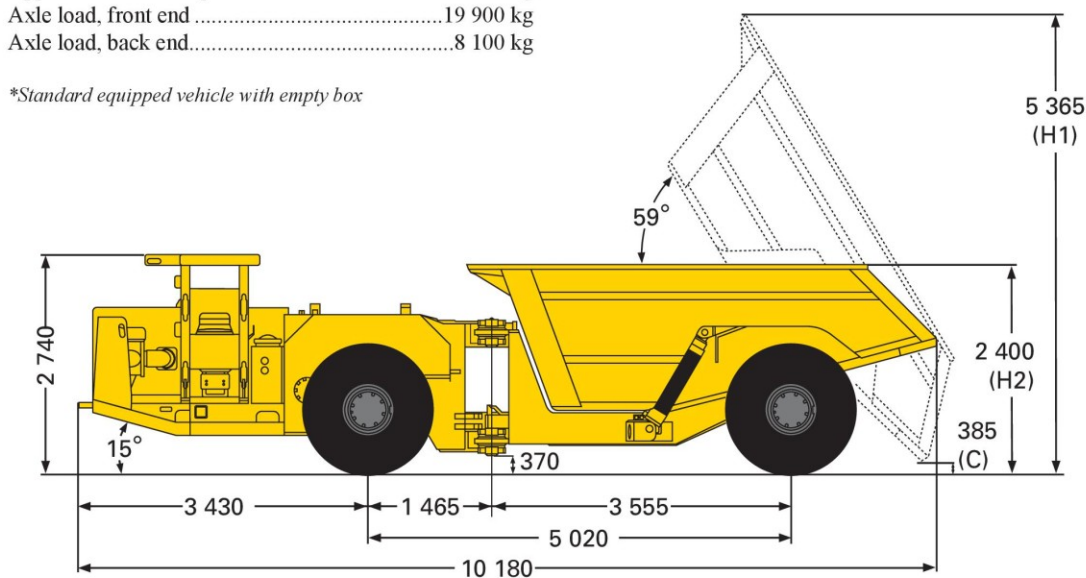
## Dump boxes

Dump box data		STD			
Material density (t/m <sup>3</sup> )		1.6	1.8	2.0	2.4
Volume, SEA struck (m <sup>3</sup> )		16.2	13.7	12.3	9.8
Volume, Semi-heaped (m <sup>3</sup> )		17.3	15.2	13.9	11.5
Volume, SAE heaped (m <sup>3</sup> )		18.5	16.7	15.5	13.2
Width, dump box (mm)	W	3 050	2 795	2 795	2 795
Dump position: Box height, max (mm)	H1	4 650	5 420	5 365	5 200
Tramming position: Dump box height (mm)	H2	2 600	2 445	2 400	2 175
Dump position: Clearance (mm)	C	350	300	385	-

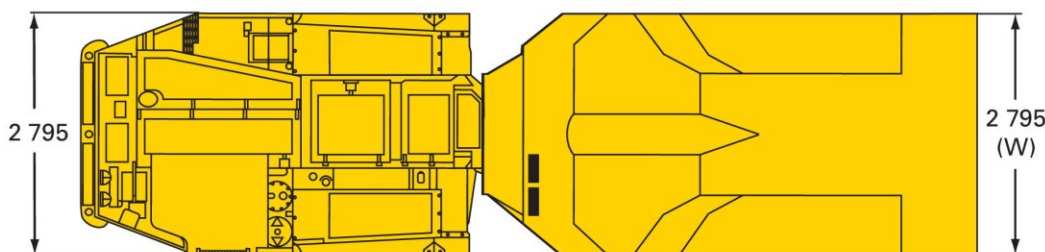
## Dimensions and weights\*

Approximate net weight.....28 000 kg  
 Axle load, front end .....19 900 kg  
 Axle load, back end.....8 100 kg

\*Standard equipped vehicle with empty box



Side view



Top view

- Dimensions shown are based on standard vehicle configuration with 25 mm tyre deflection
- All dimensions are shown in millimetres

**Atlas Copco**

© Copyright 2010, Atlas Copco Rock Drills AB, Örebro, Sweden. All product names in this publication are trademarks of Atlas Copco. Any unauthorized use or copying of the contents or any part thereof is prohibited. Illustrations and photos may show equipment with optional extras. No warranty is made regarding specifications or otherwise. Specifications and equipment are subject to change without notice. Consult your Atlas Copco Customer Center for specific information.

9851 2356 01 k  
10/2010



## 6. Payload Sieve Analysis

### Sample 1

CSA A23.2-2A

Sieve Analysis for Coarse Aggregates

Project:

Sample Material:

1

Test by:

r. mariano

Test on:

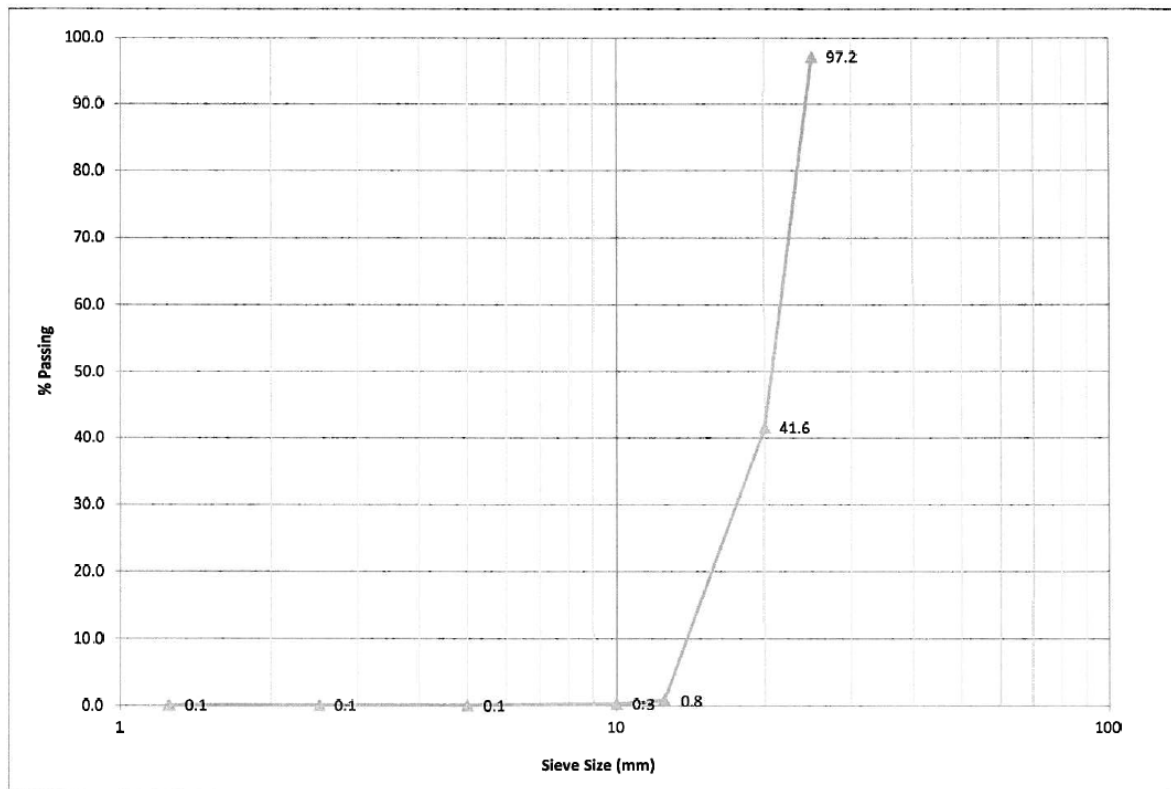
Dec. 19, 2012

Weight original dry sample

4710.5 g

Sieve	Sieve + Material	Retained	% Retained	Cumulative % Retained	Cumulative Passing
Size mm	Weight g	Weight g	%	%	%
25	490.1	622.9	132.8	3	97
20	1564.8	4184.8	2620.0	56	42
12.5	1589.1	3509.6	1920.5	41	1
10	1575.8	1598.6	22.8	0	0
5	1535.5	1545.9	10.4	0	0
2.5	1445.9	1446.1	0.2	0	0
1.25	0.0	0.0	0.0	0	0
Pan	893.1	896.6	3.5	0	0
		Sum	4710.2	399	

Fineness Modulus: 3.99



## Sample 2

CSA A23.2-2A

Sieve Analysis for Coarse Aggregates

Project:

Sample Material:

2

Test by:

r. mariano

Test on:

Dec. 19, 2012

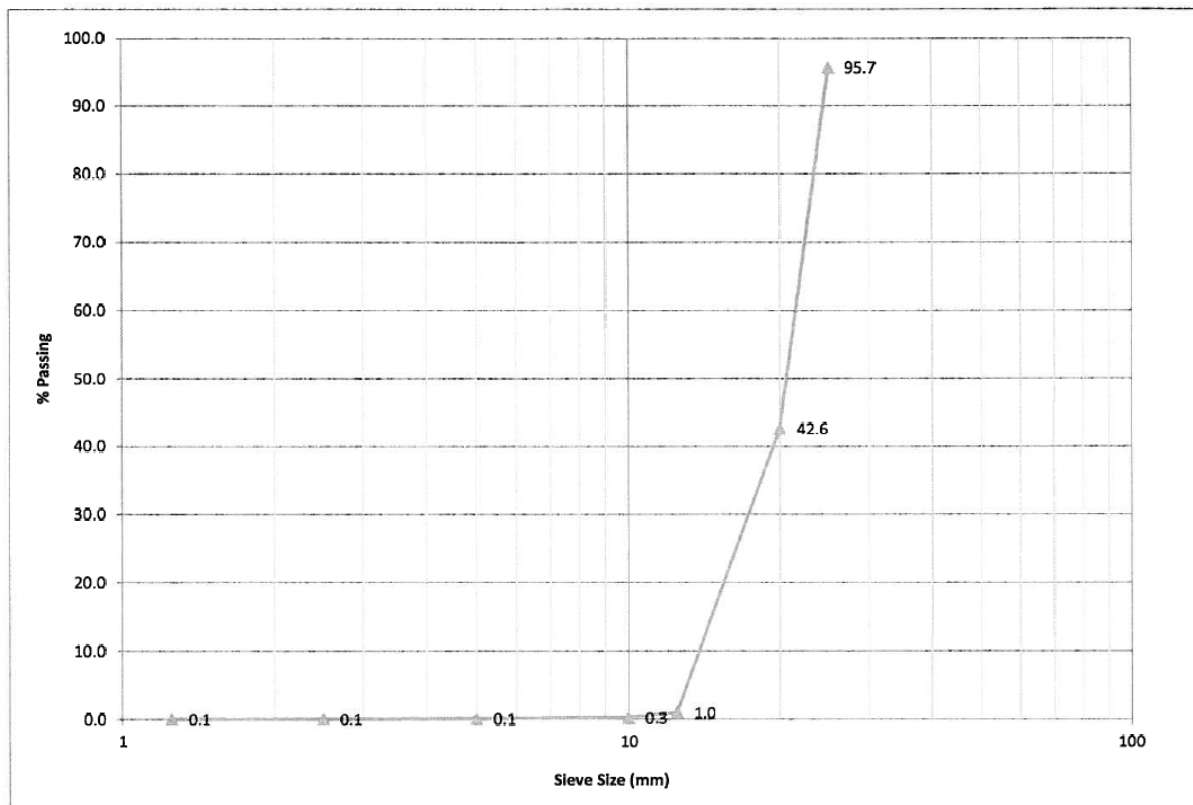
Weight original dry sample

4698.5

g

Sieve	Sieve + Material	Retained	% Retained	Cumulative % Retained	Cumulative Passing
Size mm	Weight g	Weight g	%	%	%
25	490.1	692.6	202.5	4	96
20	1564.8	4056.6	2491.8	53	43
12.5	1589.1	3544.1	1955.0	42	1
10	1575.8	1611.1	35.3	1	0
5	1535.5	1544.5	9.0	0	0
2.5	1445.9	1446.7	0.8	0	0
1.25	0.0	0.0	0.0	0	0
Pan	893.1	896.6	3.5	0	0
		Sum	4697.9	399	

Fineness Modulus: 3.99



## 7. Determination of Scaling Factor

Determination of the appropriate scaling factor was achieved via the Buckingham Pi Theorem using units of force, length and time as reference units. The goal of this dimensional analysis is to determine a scale relationship between the payload of the vehicle and the hub force generated. From the Buckingham Pi Method it was determined that hub force was could be functionally described as follows:

$$F_H \doteq f(W, \phi, P)$$

Equation 0.1

Where:

$$F_H = A \text{ generic hub force}$$

$$W = \text{The tare weight of the vehicle}$$

$$\phi = \text{Articulation angle of the vehicle}$$

$$P = \text{Payload of the vehicle}$$

Given the above parameters it can be seen that there is only one reference dimension, F, as phi is already dimensionless. Form inspection the following three Pi groups can be determined using payload as the repeating variable:

$$\pi_1 = \phi$$

$$\pi_2 = F_H/P$$

$$\pi_3 = W/P$$

Using **Error! Reference source not found.** above we can observe that:

$$F_H/P = f(\phi, W/P)$$

The functional equality above can be applied to solve for the appropriate scaling factor using:

$$\left(F_H/P\right)_{Model} = \left(F_H/P\right)_{Prototype}$$

Which yields:

$$F_{H_{Prototype}} = F_{H_{Model}} \left( P_{Prototype} / P_{Model} \right)$$

0.2

Because the ratio of the payload of the prototype to payload of the scale model is equal to the scaling factor cubed **Error! Reference source not found.** can be simplified to:

$$F_{H_{Prototype}} = F_{H_{Model}}(PSF^3)$$



## 8. Scale Model Testing Raw Data

Test #	Phi (°)		FA Jack 1	FB Jack 2	FC Jack 3	FD Jack 4
	Degrees	Degrees	lbs	lbs	lbs	lbs
1	0	0	181	188	56	82
2	22.5	0	183	187	56	76
3	42	0	183	190	60	72
4	22.5	0	185	189	61	75
5	0	0	182	192	55	81
6	-22.5	0	180	189	54	87
7	-42	0	183	184	53	90
8	-22.5	0	185	187	53	87
9	0	0	185	185	57	82
10	22.5	0	187	187	63	75
11	42	0	186	188	61	71
12	22.5	0	187	186	60	76
13	42	0	186	190	63	71
14	0	0	188	184	56	81
15	-22.5	0	188	181	56	86
16	-42	0	180	185	52	92
17	-22.5	0	188	182	54	87
18	-42	0	183	182	54	91
19	42	0	186	191	61	72
20	-42	0	184	182	54	89
21	0	0	211	218	113	146
22	0	0	207	214	149	146
23	22.5	0	216	214	104	153
24	42	0	219	217	91	160
25	22.5	0	212	221	98	156
26	0	0	213	213	115	146
27	-22.5	0	213	217	127	135
28	-42	0	226	210	142	121
29	-22.5	0	213	210	125	136
30	0	0	213	215	114	147
31	22.5	0	219	213	102	153
32	42	0	220	214	94	161
33	22.5	0	219	212	106	154
34	42	0	222	213	94	161
35	0	0	214	219	117	144
36	-22.5	0	219	210	131	134

37	-42	0	214	213	134	126
38	-22.5	0	211	213	123	138
39	-42	0	211	214	132	128
40	42	0	220	219	88	162
41	-42	0	207	217	132	129
42	0	0	213	219	192	234
43	22.5	0	221	216	181	242
44	42	0	221	215	174	249
45	22.5	0	221	212	185	244
46	0	0	215	211	194	238
47	-22.5	0	207	214	202	228
48	-42	0	209	214	220	213
49	-22.5	0	212	213	207	225
50	0	0	215	212	195	236
51	22.5	0	220	211	185	244
52	42	0	219	216	178	249
53	22.5	0	222	209	192	240
54	42	0	212	215	197	236
55	-22.5	0	215	211	210	224
56	-42	0	213	211	220	215
57	-22.5	0	211	214	208	223
58	42	0	219	217	176	247
59	-42	0	213	210	219	214
60	0	0	214	215	198	234
61	0	0	246	248	240	276
62	22.5	0	251	251	207	304
63	42	0	256	253	182	323
64	22.5	0	249	248	207	307
65	0	0	247	247	239	279
66	-22.5	0	243	249	268	250
67	-42	0	245	249	291	217
68	-22.5	0	245	249	291	217
69	0	0	239	259	266	251
70	22.5	0	256	244	209	305
71	42	0	256	251	179	324
72	22.5	0	254	244	206	306
73	0	0	250	246	236	276
74	-22.5	0	246	244	269	248
75	-42	0	247	252	287	219
76	-22.5	0	242	251	260	250
77	-42	0	245	250	289	220

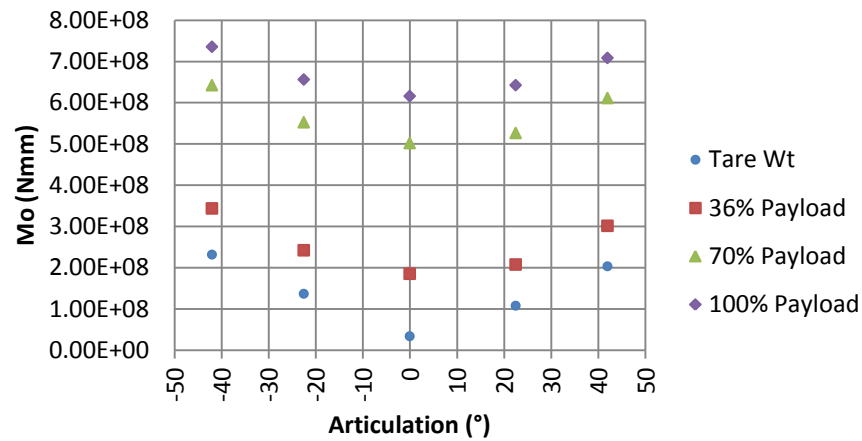
78	42	0	260	248	180	323
79	0	3.15	242	247	234	280
80	-22.5	3.15	241	245	267	255
81	-42	3.15	241	249	291	226
82	-22.5	3.15	241	242	273	249
83	0	3.15	252	236	244	279
84	22.5	3.15	252	239	216	303
85	42	3.15	247	261	142	357
86	22.5	3.15	257	244	175	336
87	0	3.15	233	262	201	315
88	-22.5	3.15	237	257	241	283
89	-42	3.15	248	251	262	254
90	-22.5	3.15	243	250	234	283
91	-42	3.15	249	244	260	255
92	22.5	3.15	243	254	178	336
93	42	3.15	247	258	146	354
94	22.5	3.15	248	246	186	333
95	42	3.15	252	252	147	355
96	0	4.5	251	244	208	311
97	-22.5	4.5	248	244	236	281
98	-42	4.5	246	250	262	253
99	-22.5	4.5	246	245	236	283
100	0	4.5	245	244	206	313
101	22.5	4.5	239	259	171	340
102	42	4.5	255	246	160	349
103	22.5	4.5	246	247	181	337
104	0	4.5	244	245	210	313
105	-22.5	4.5	240	247	239	286
106	-42	4.5	248	247	270	246
107	22.5	4.5	251	241	182	336
108	42	4.5	247	247	158	351
109	-42	4.5	257	237	266	247
110	0	7.7	239	241	224	304
111	-22.5	7.7	238	238	262	274
112	-42	7.7	240	241	274	252
113	-22.5	7.7	236	241	255	275
114	0	7.7	236	238	222	305
115	22.5	7.7	243	239	198	326
116	42	7.7	249	241	169	347
117	22.5	7.7	251	231	205	324
118	0	7.7	253.4	230	224	302

119	-22.5	7.7	244	236	255	277
120	-42	7.7	237	243	276	256
121	-22.5	7.7	234	242	257	279
122	0	7.7	232	248	279	248
123	22.5	7.7	243	241	205	324
124	42	7.7	245	243	173	344
125	22.5	7.7	246	239	205	324
126	-42	7.7	239	241	283	249
127	42	7.7	244	243	184	337
128	0	3.2	244	241	235	293

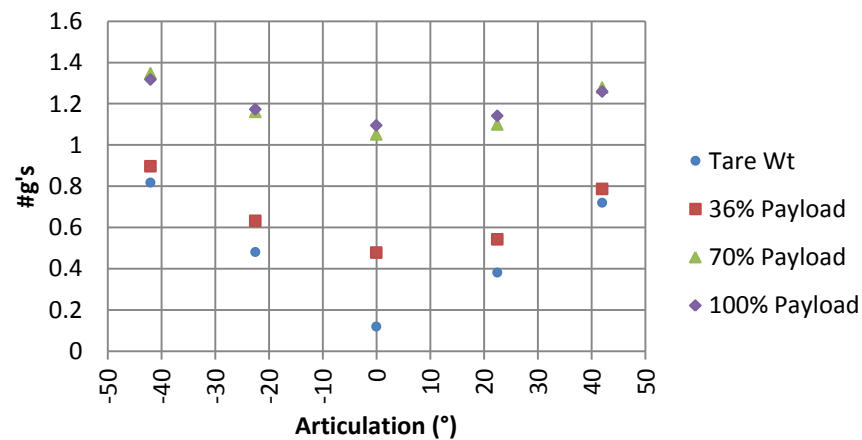
## 9. Complete Full Scale Simulation Results

### MT431B

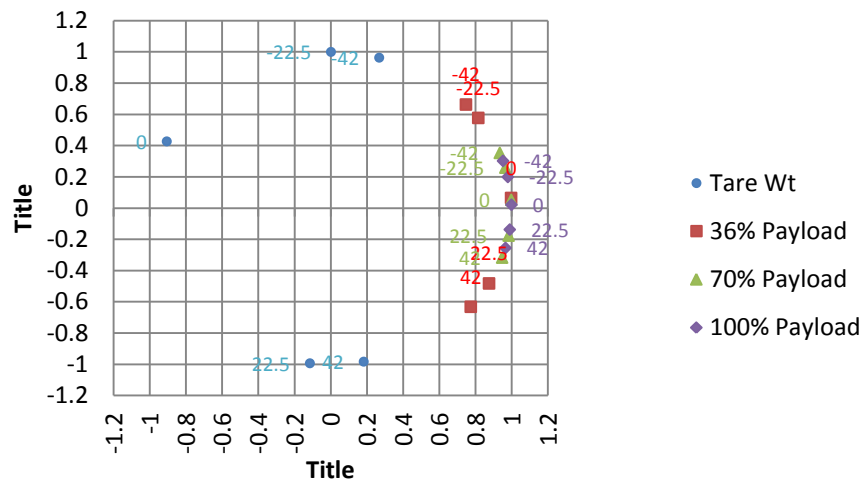
**MT431B Total Moment About Reference Point By Payload**



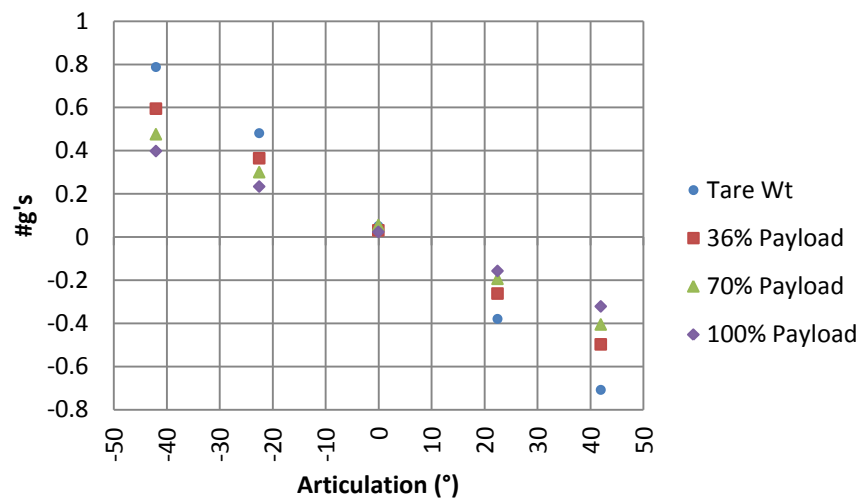
**MT431B Total g Level About Reference Point By Payload**



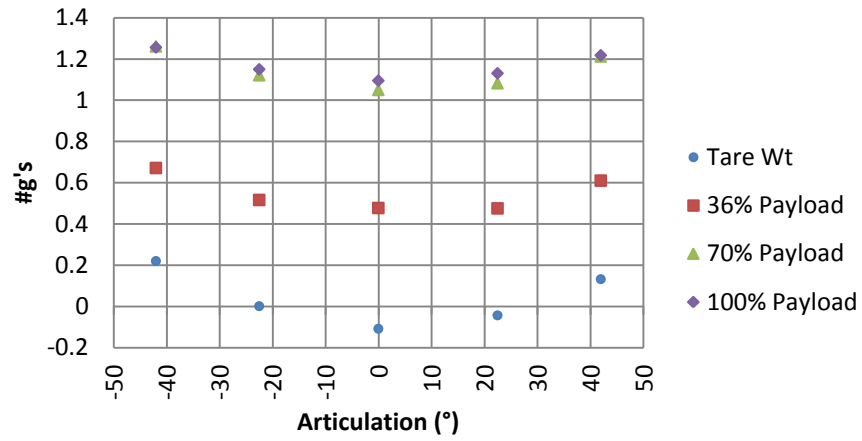
## MT431B Mo Unit i, j Coordinates



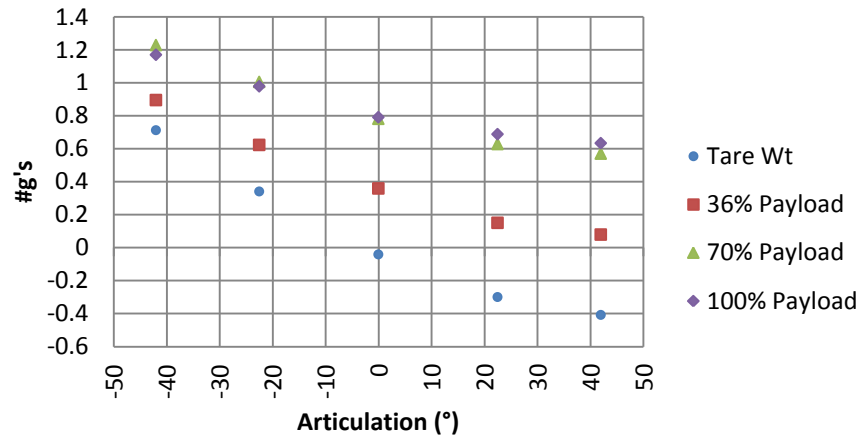
## MT431B Total Vehicle Roll In g Level



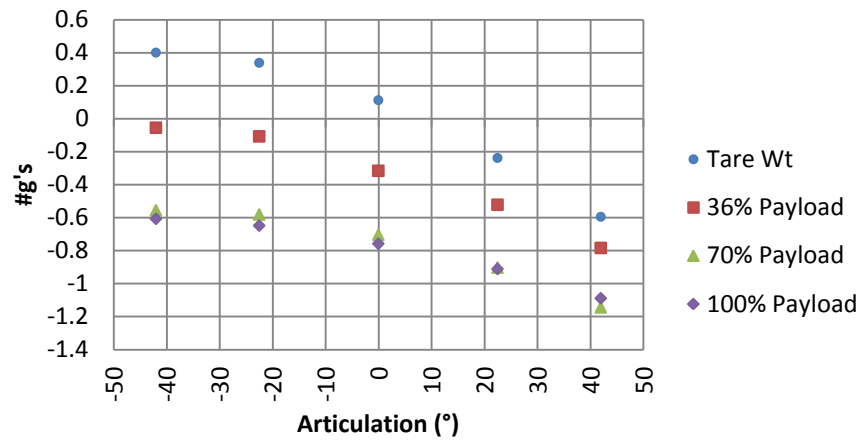
### MT431B Total Vehicle Pitch In g Level



### MT431B Total Rack Level About Q1 45° Axis

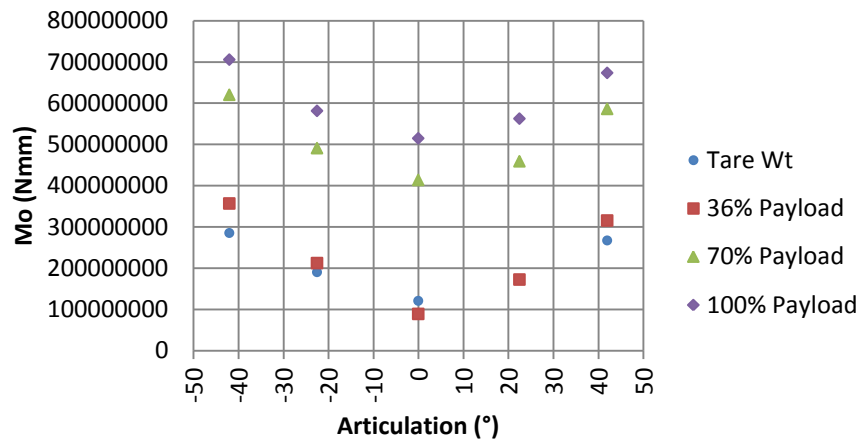


## MT431B Total Rack Level About Q2 45° Axis



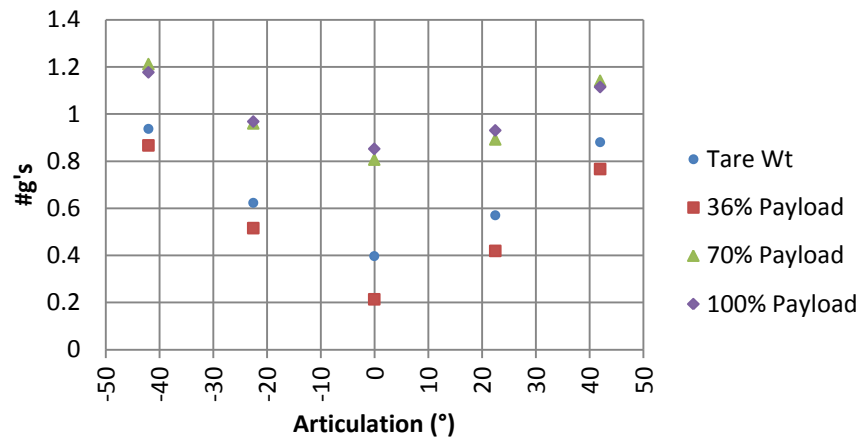
AD30

## AD30 Total Moment About Reference Point By Payload

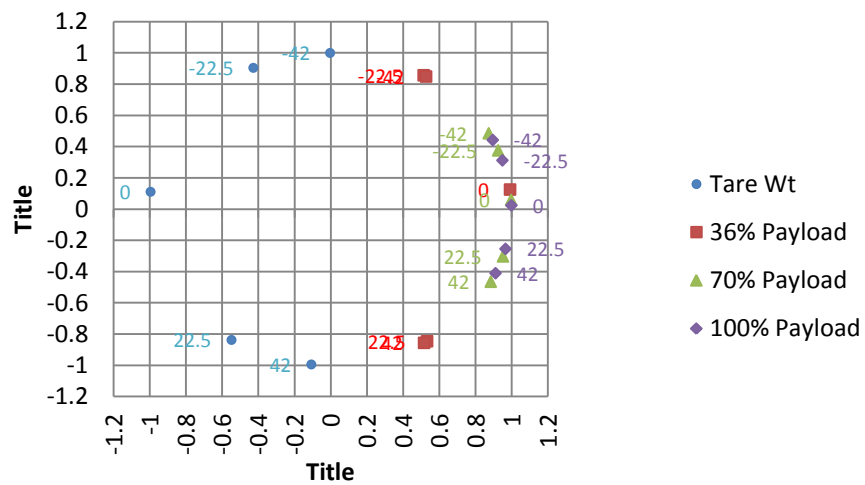




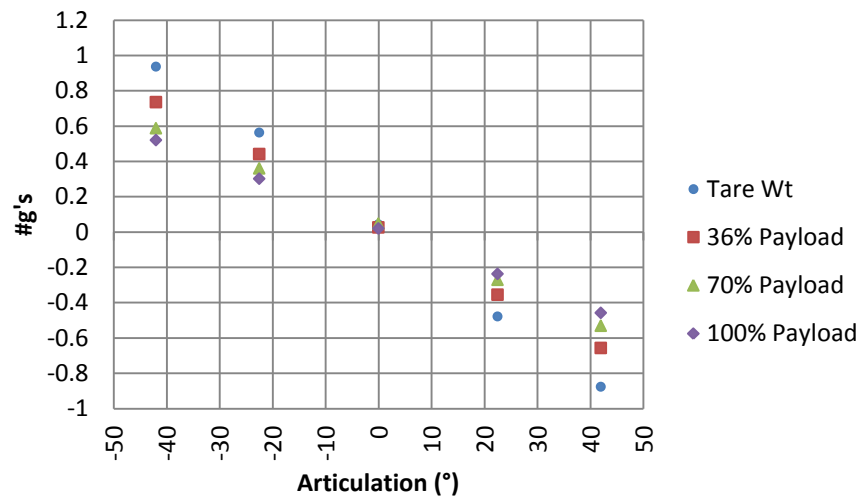
## AD30 Total g Level About Reference Point By Payload



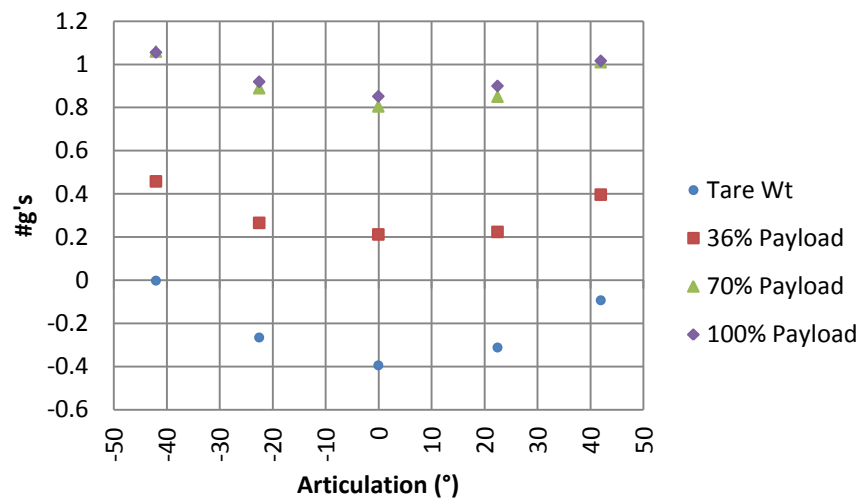
## AD30 Mo Unit i, j Coordinates



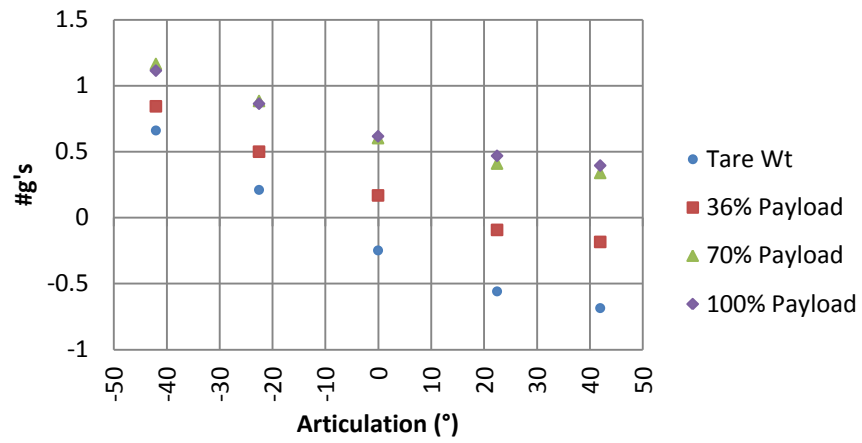
### AD30 Total Vehicle Roll In g Level



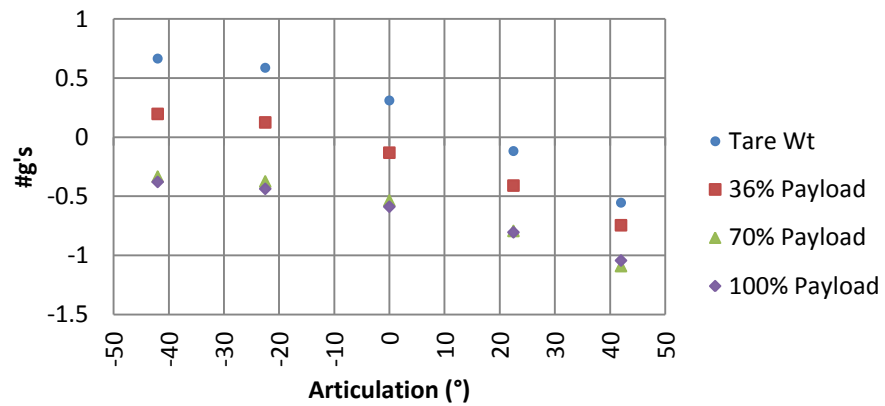
### AD30 Total Vehicle Pitch In g Level



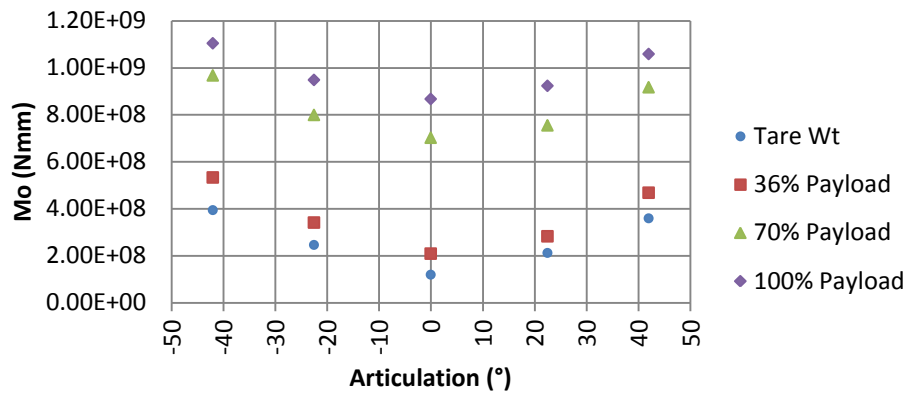
### AD30 Total Rack Level About Q1 45° Axis



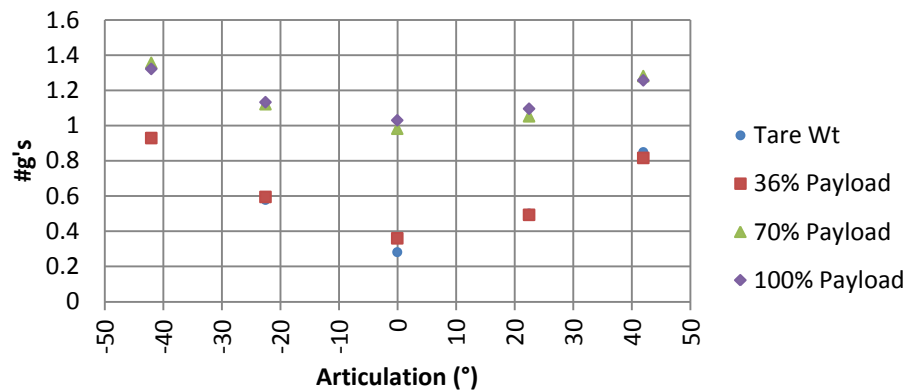
### AD30 Total Rack Level About Q2 45° Axis



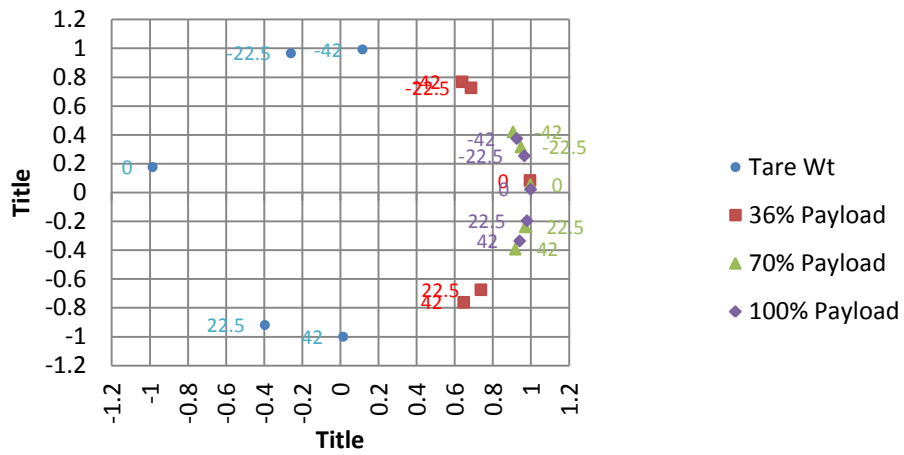
### MT42 Total Moment About Reference Point By Payload



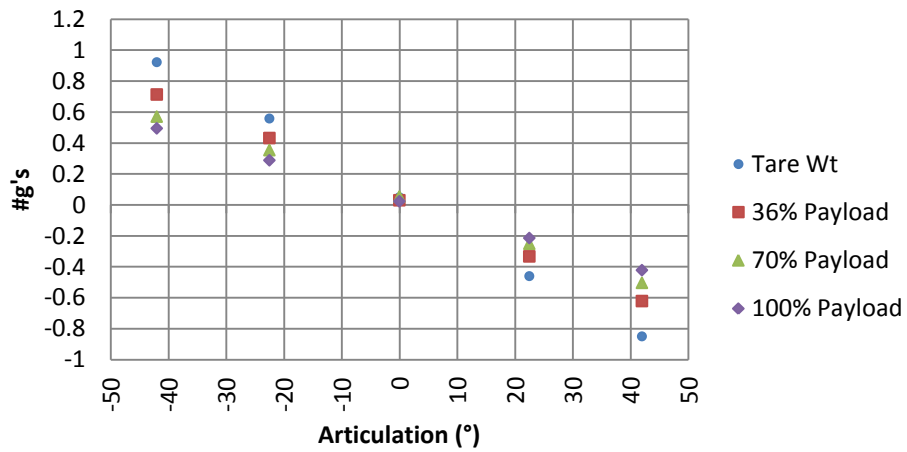
### MT42 Total g Level About Reference Point By Payload



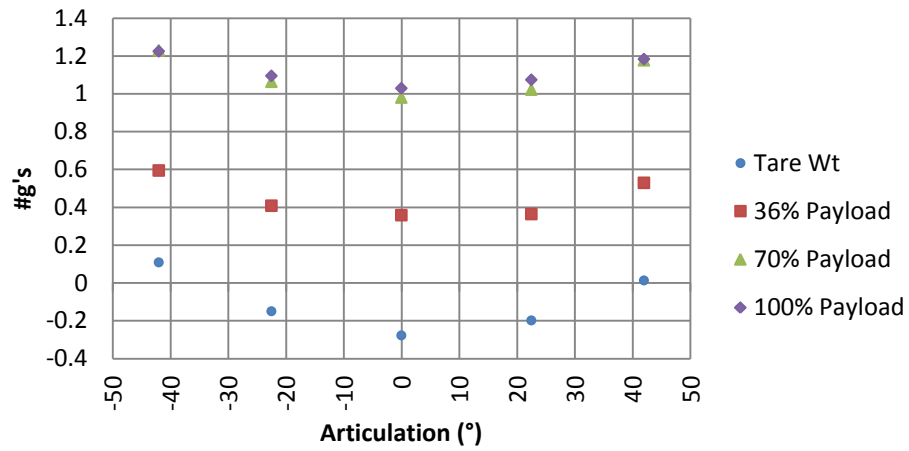
## MT42 Mo Unit i, j Coordinates



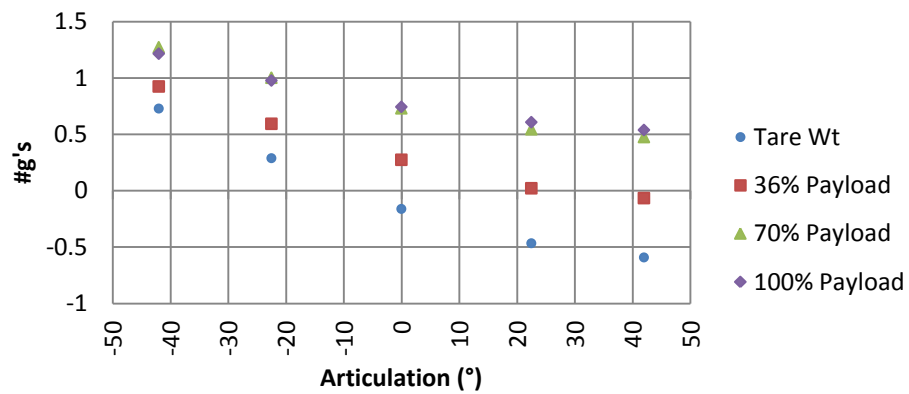
## MT42 Total Vehicle Roll In g Level



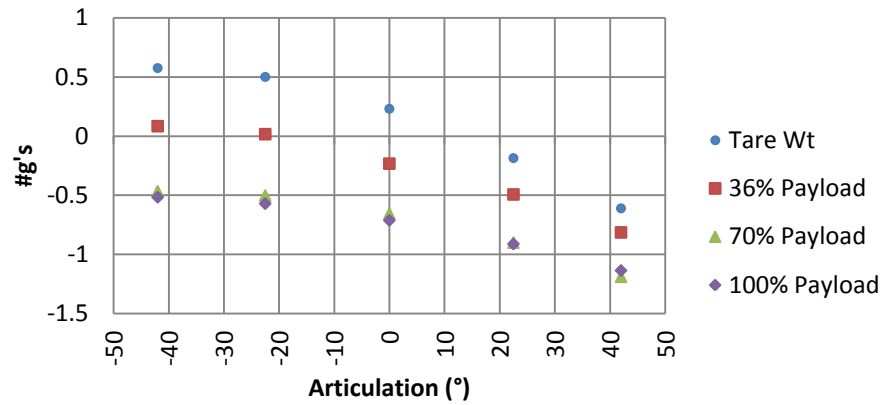
### MT42 Total Vehicle Pitch In g Level



### MT42 Total Rack Level About Q1 45° Axis

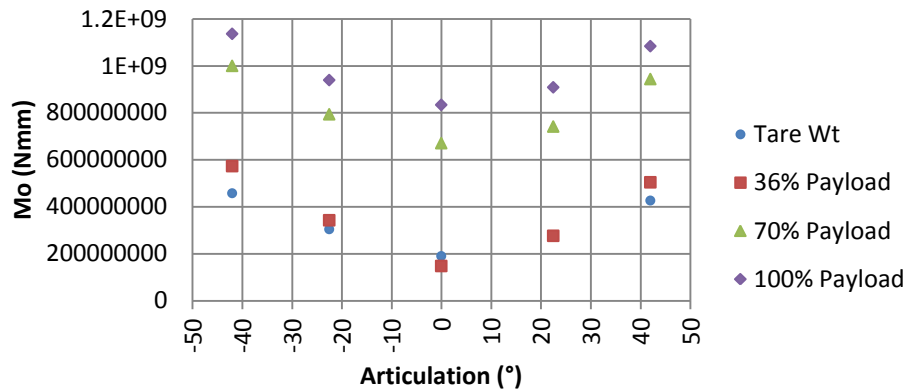


### MT42 Total Rack Level About Q2 45° Axis

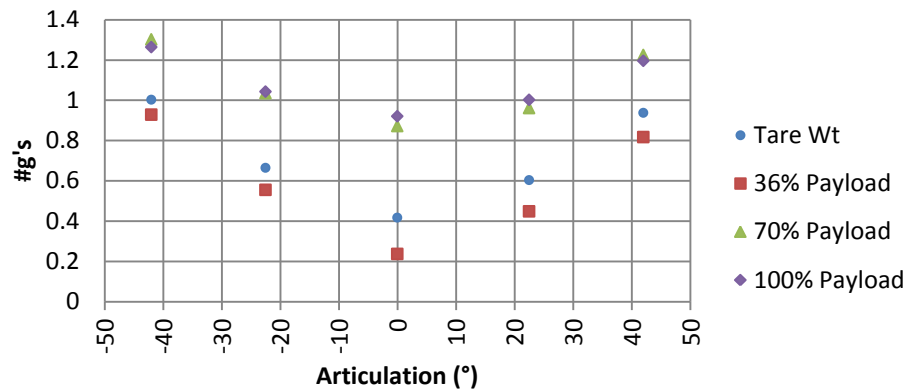


AD45B

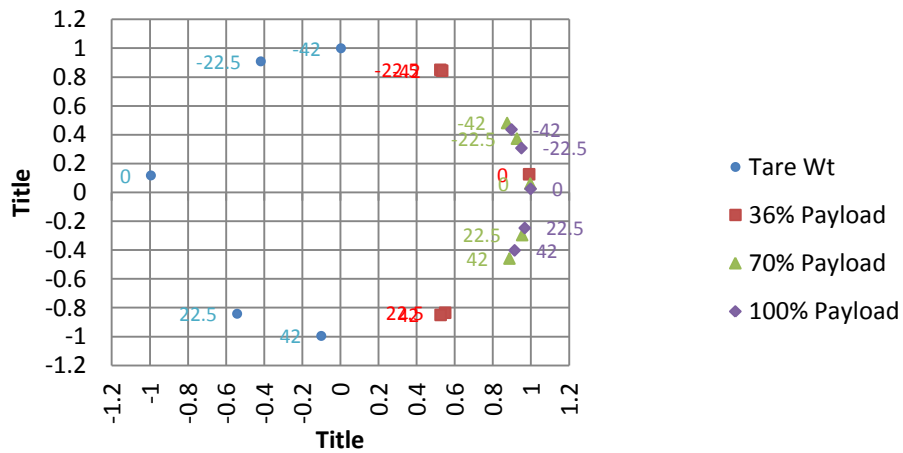
### AD45B Total Moment About Reference Point By Payload



## AD45B Total g Level About Reference Point By Payload

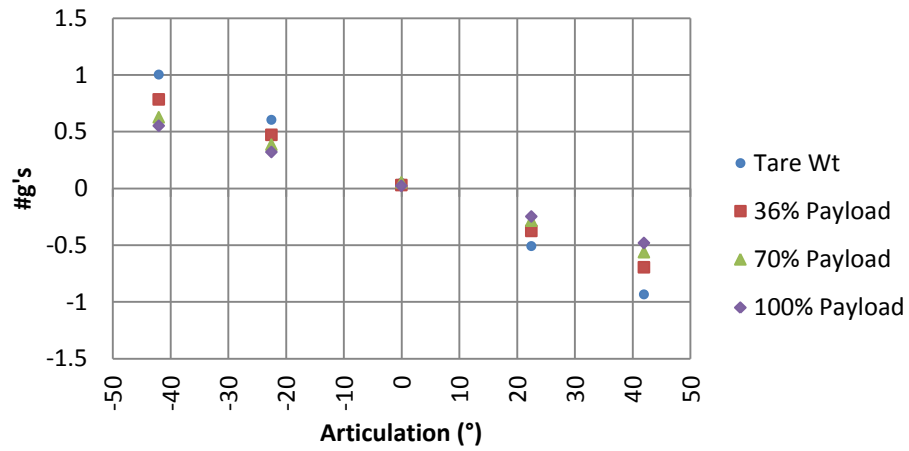


## AD45B Mo Unit i, j Coordinates

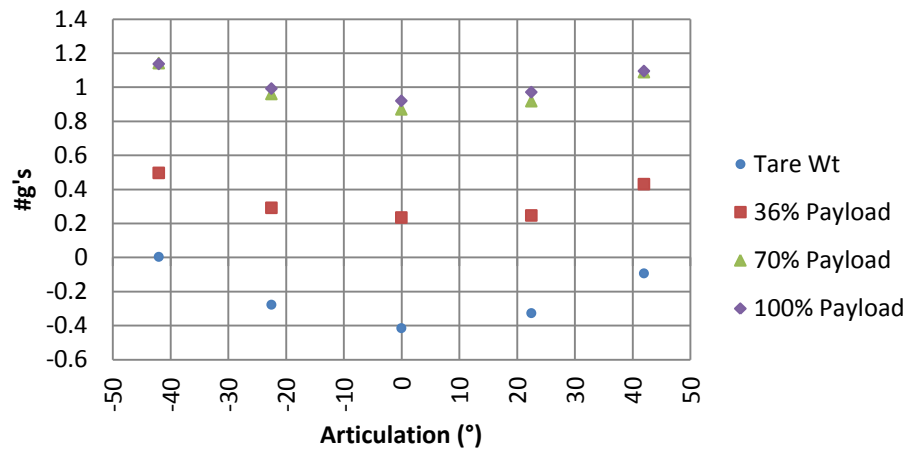




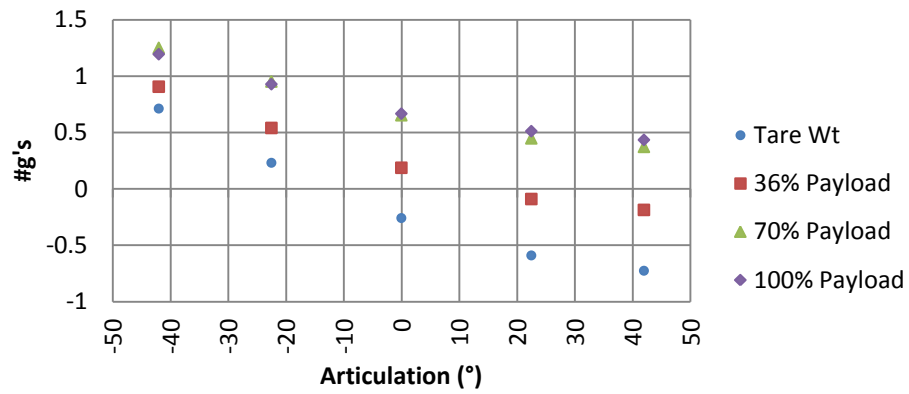
### AD45B Total Vehicle Roll In g Level



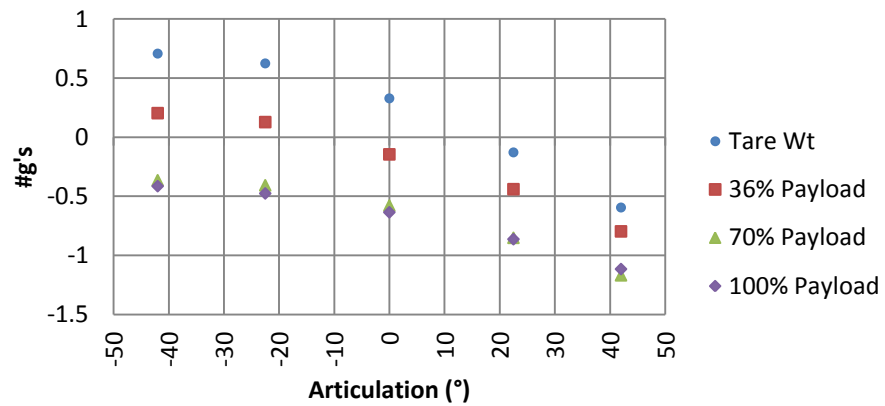
### AD45B Total Vehicle Pitch In g Level



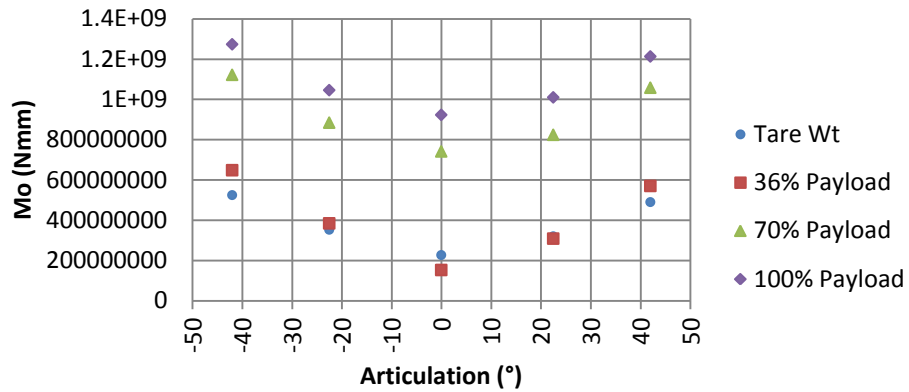
### AD45B Total Rack Level About Q1 45° Axis



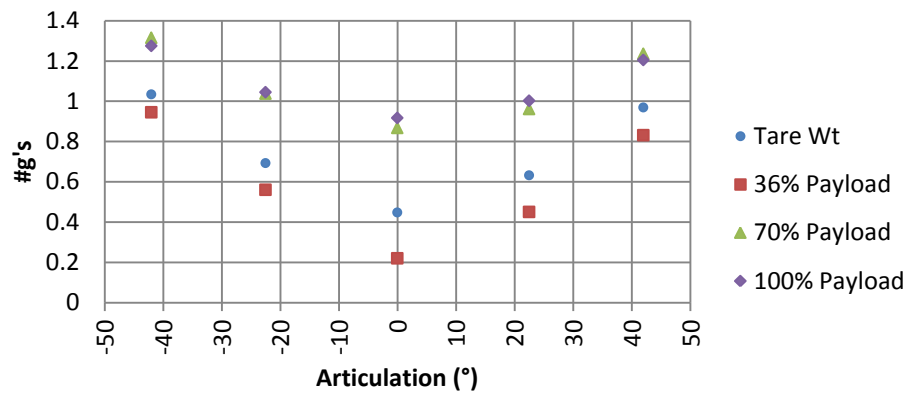
### AD45B Total Rack Level About Q2 45° Axis



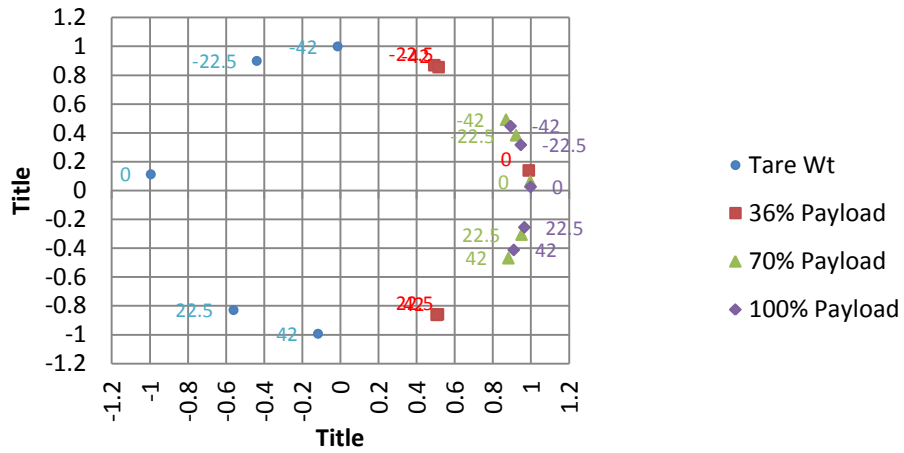
### MT 5020 Total Moment About Reference Point By Payload



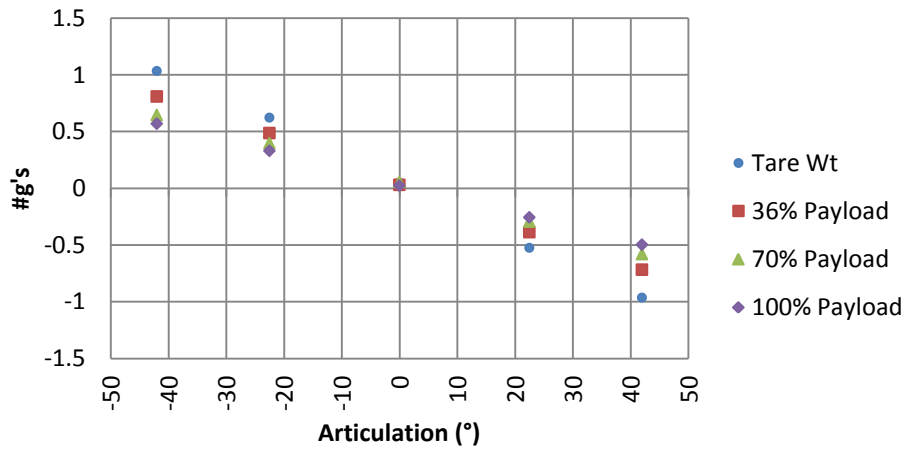
### MT 5020 Total g Level About Reference Point By Payload



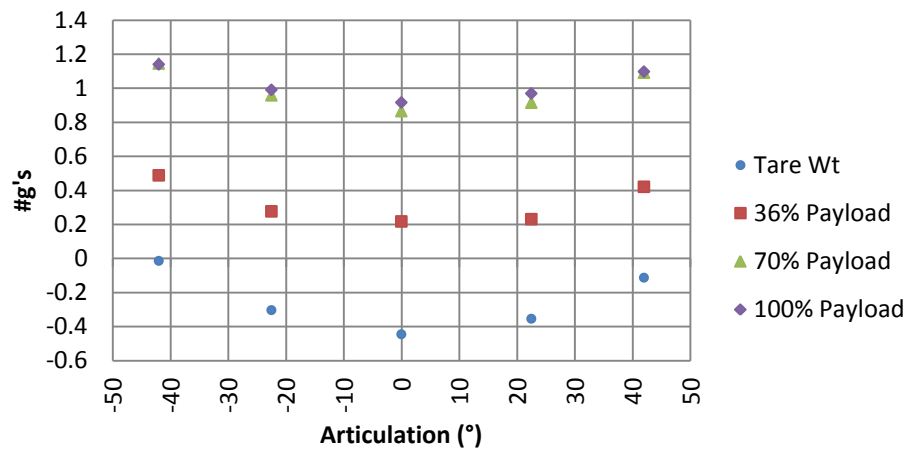
### MT 5020 Mo Unit i, j Coordinates



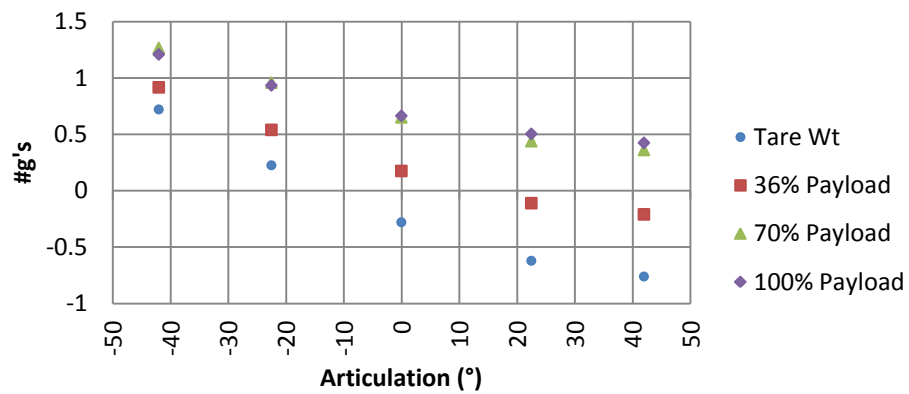
### MT 5020 Total Vehicle Roll In g Level



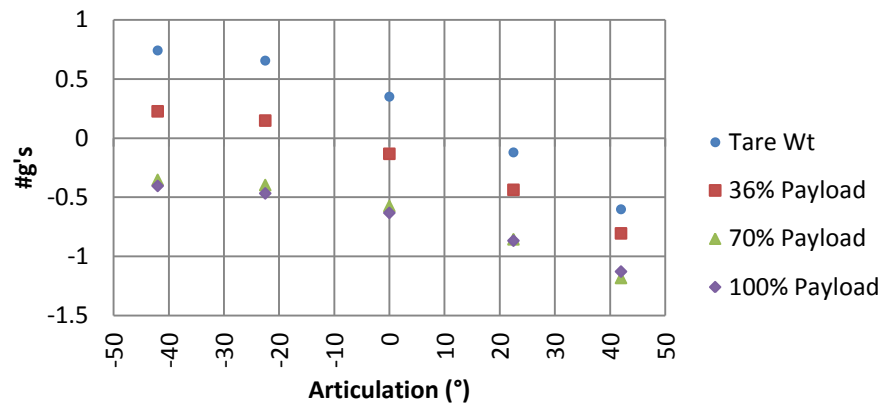
## MT 5020 Total Vehicle Pitch In g Level



## MT 5020 Total Rack Level About Q1 45° Axis

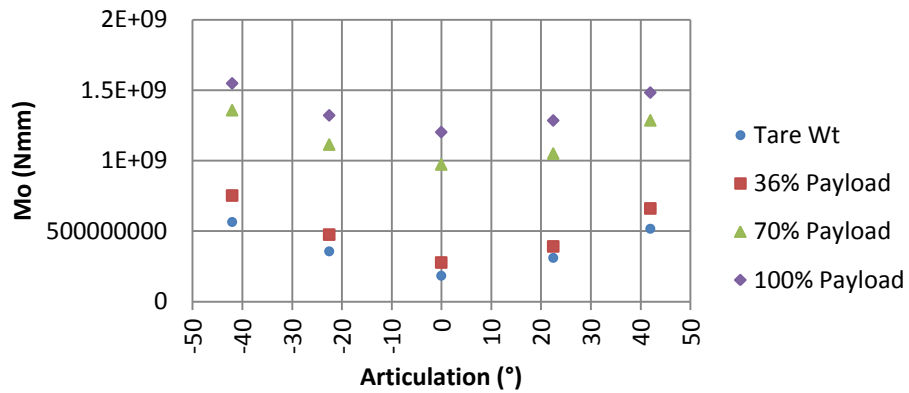


## MT 5020 Total Rack Level About Q2 45° Axis

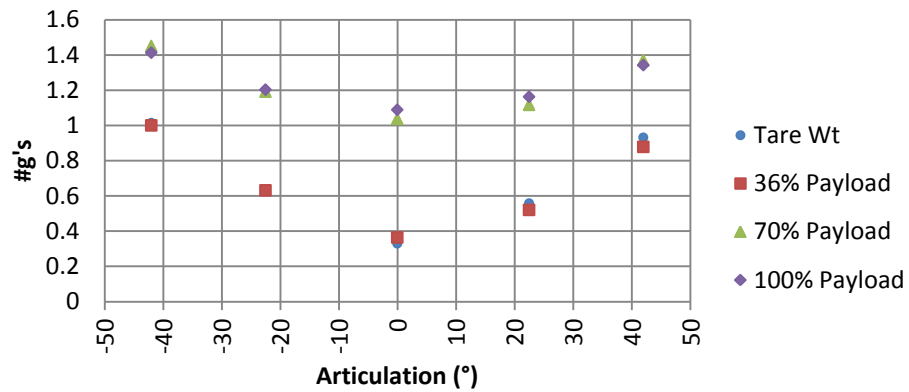


AD55

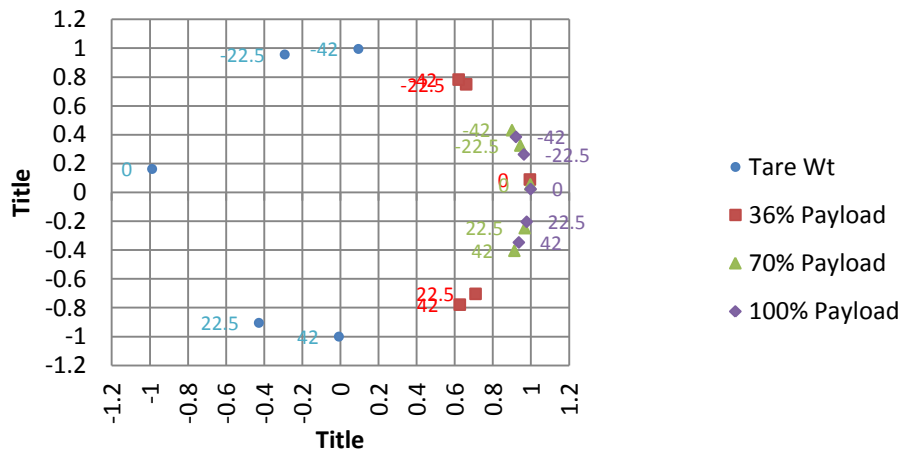
## AD55 Total Moment About Reference Point By Payload



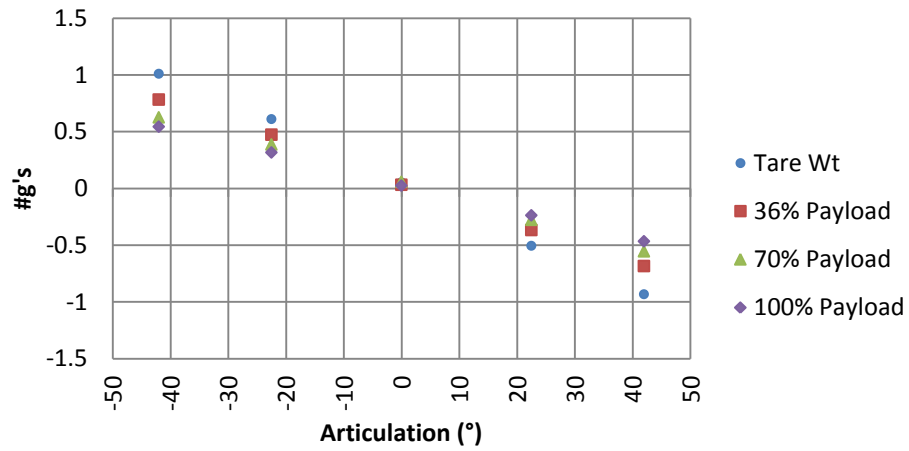
## AD55 Total g Level About Reference Point By Payload



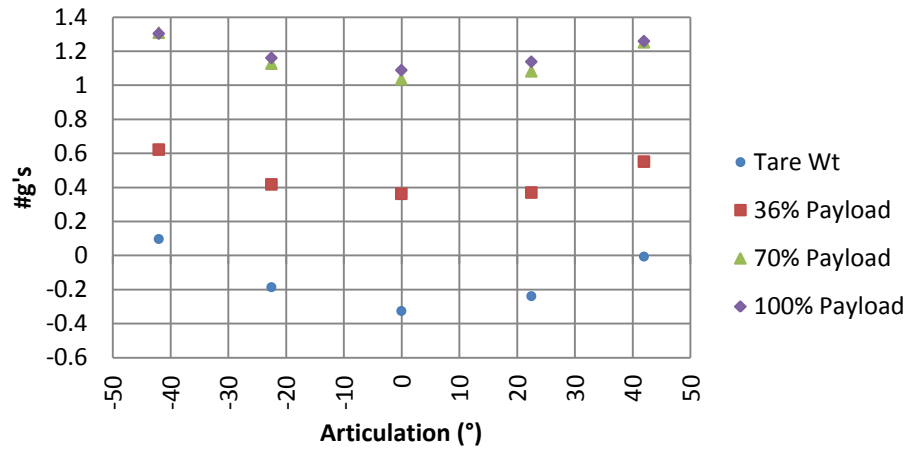
## AD55 Mo Unit i, j Coordinates



### AD55 Total Vehicle Roll In g Level

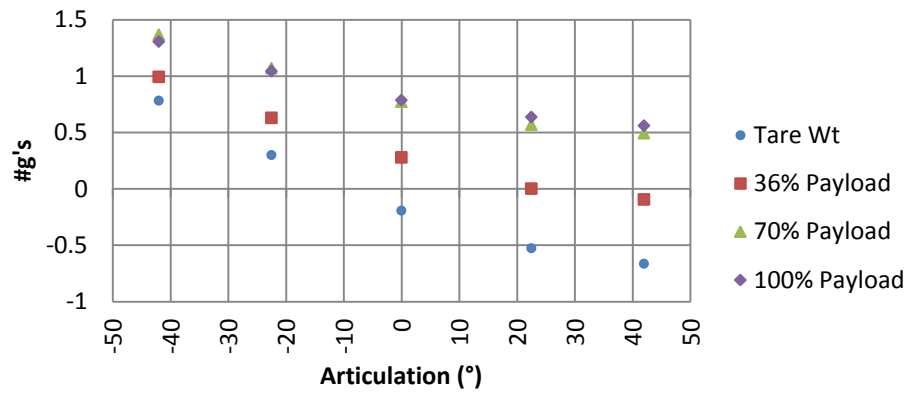


### AD55 Total Vehicle Pitch In g Level

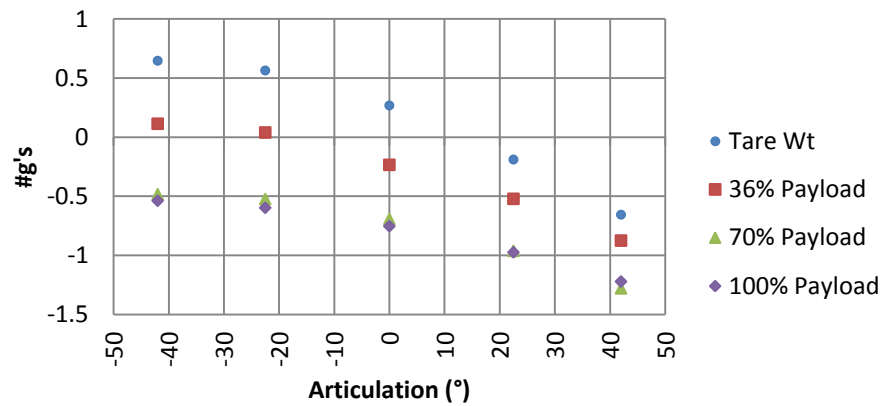




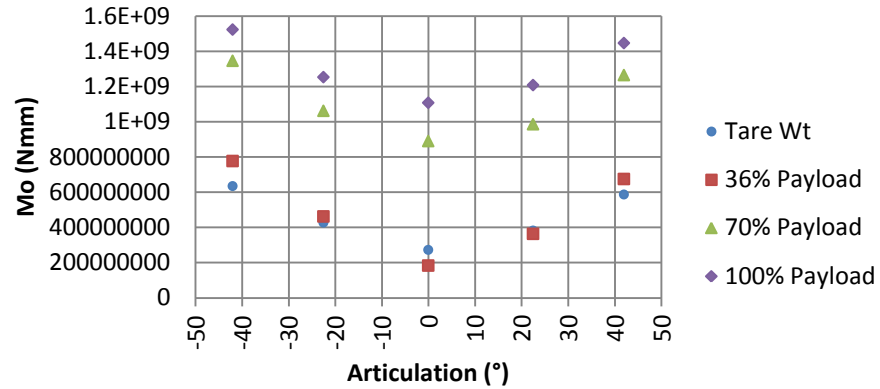
### AD55 Total Rack Level About Q1 45° Axis



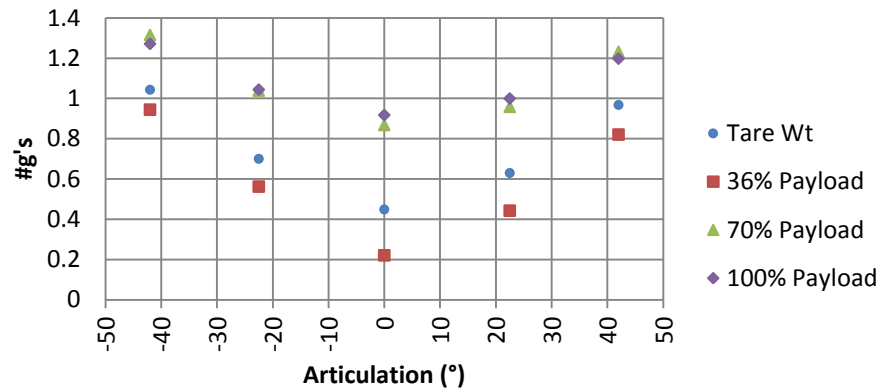
### AD55 Total Rack Level About Q2 45° Axis



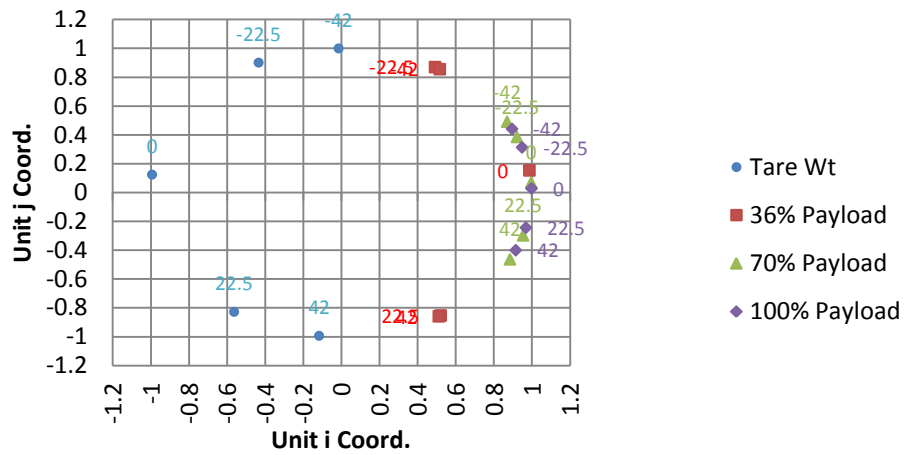
### MT6020 Total Moment About Reference Point By Payload



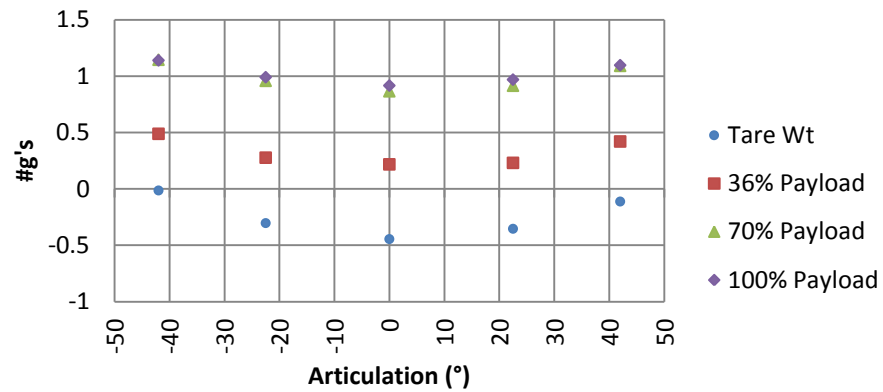
### MT6020 Total g Level About Reference Point By Payload



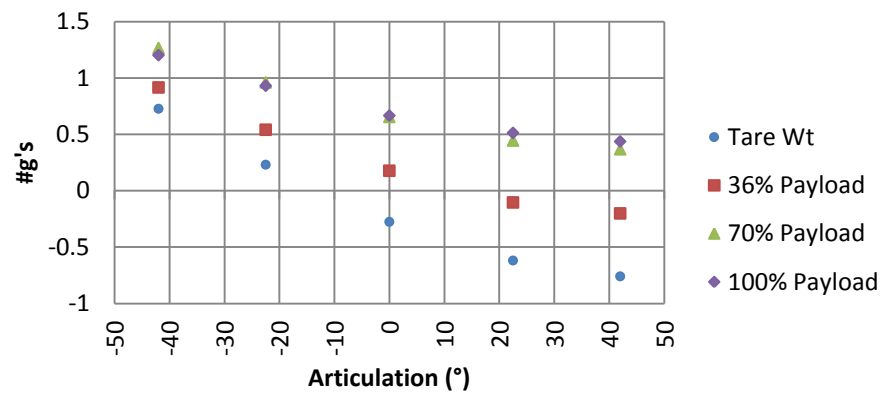
## MT6020 Mo Unit i, j Coordinates



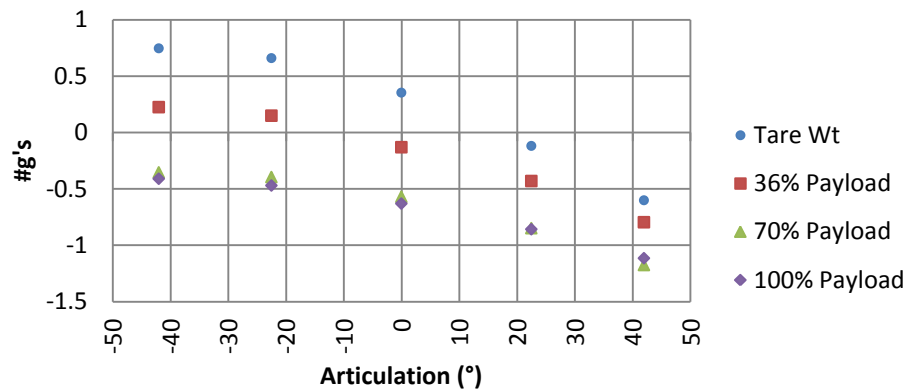
## MT6020 Total Vehicle Pitch In g Level



## MT6020 Total Rack Level About Q1 45° Axis

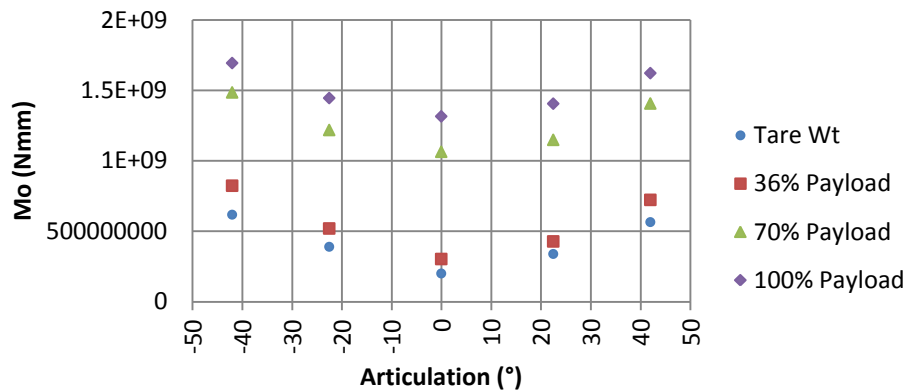


## MT6020 Total Rack Level About Q2 45° Axis

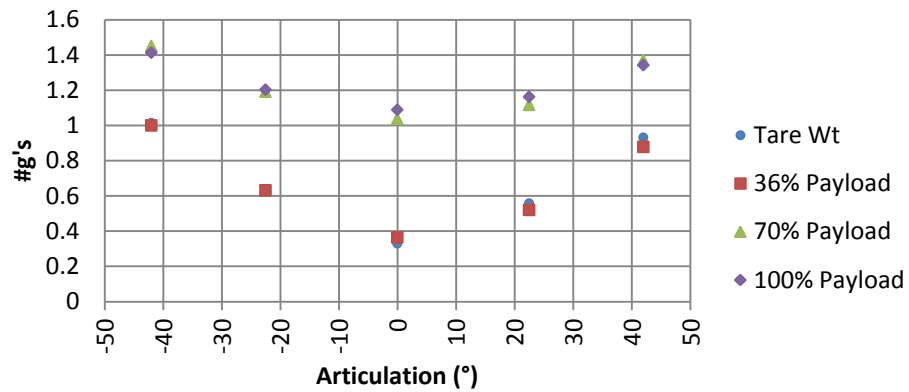


AD60

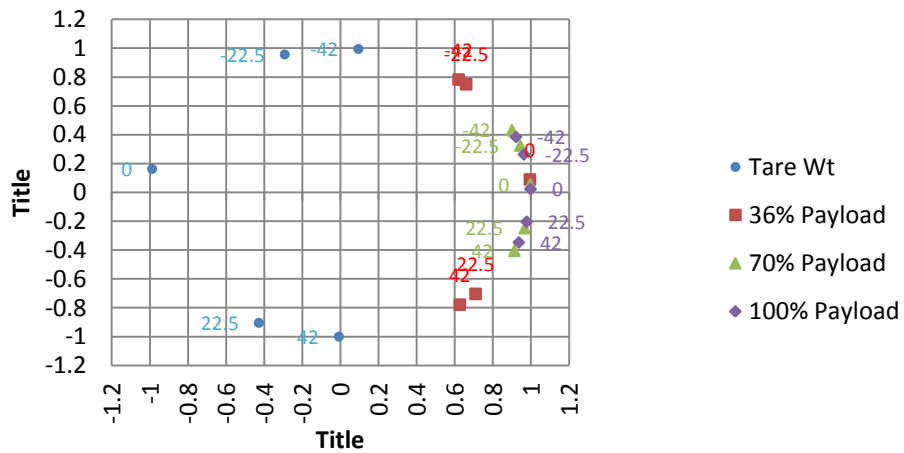
## AD60 Total Moment About Reference Point By Payload



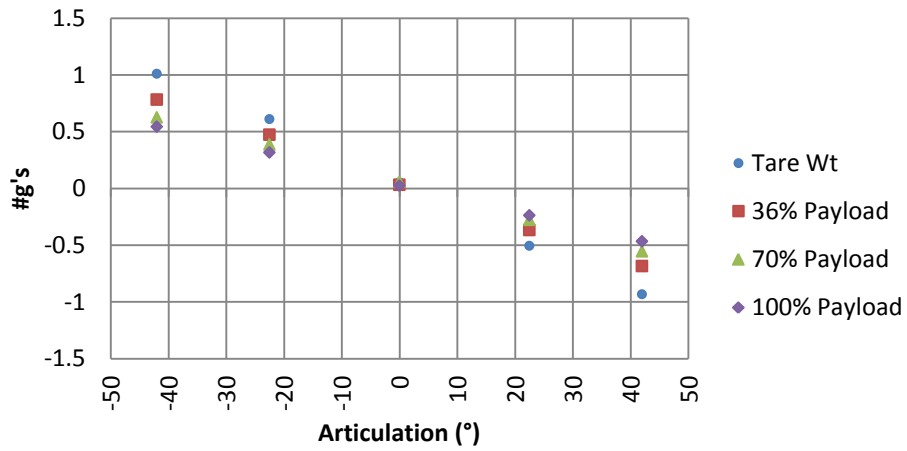
## AD60 Total g Level About Reference Point By Payload



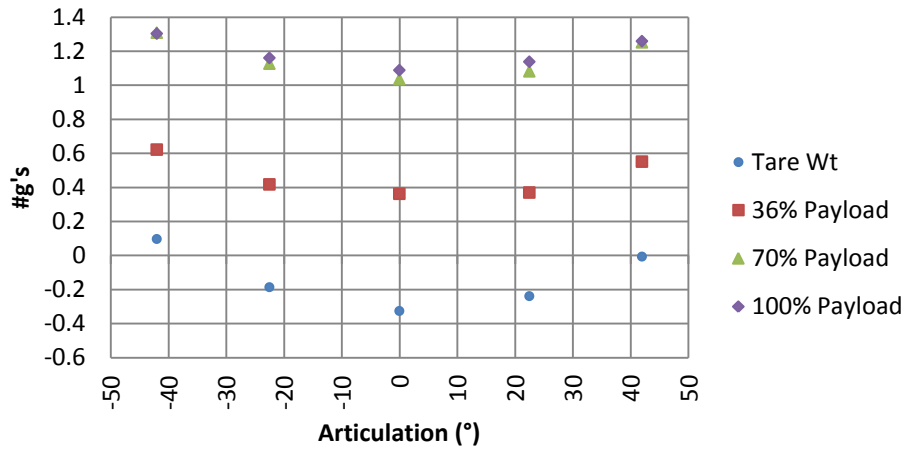
## AD60 Mo Unit i, j Coordinates



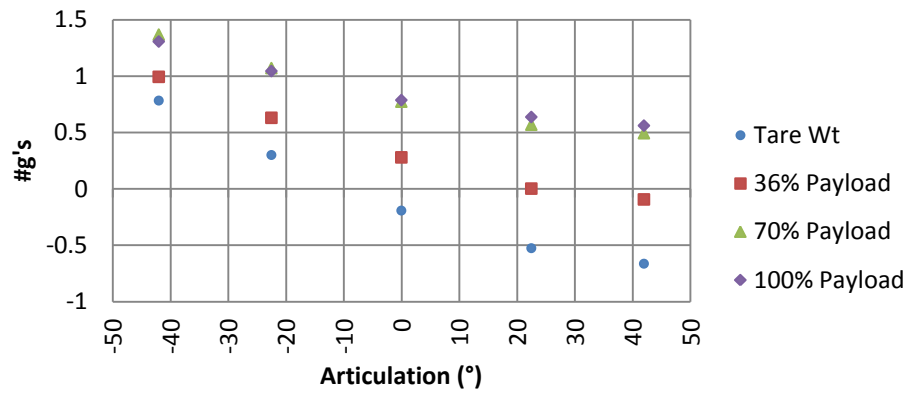
### AD60 Total Vehicle Roll In g Level



### AD60 Total Vehicle Pitch In g Level



## AD60 Total Rack Level About Q1 45° Axis





## 10. veDYNA Entry Vehicle Parameters

veDYNA Entry Vehicle Data: truck



February 1, 2015

# Contents

<b>1</b>	<b>General Vehicle Data</b>	<b>3</b>
1.1	Vehicle Dimensions . . . . .	3
1.2	Mass & Load . . . . .	3
1.3	Aerodynamics . . . . .	4
1.4	Brake System . . . . .	4
<b>2</b>	<b>Front Axle</b>	<b>5</b>
2.1	Tyre . . . . .	5
2.2	Brake . . . . .	5
2.3	Steering . . . . .	5
2.4	Axle Mass & Inertia . . . . .	5
2.5	Initial Wheel Orientation . . . . .	6
2.6	Axle Kinematics . . . . .	6
2.7	Axle Compliance . . . . .	6
2.8	Spring . . . . .	6
2.9	Damper . . . . .	7
2.10	Stabi . . . . .	7
<b>3</b>	<b>Rear Axle</b>	<b>8</b>
3.1	Tyre . . . . .	8
3.2	Brake . . . . .	8
3.3	Axle Mass & Inertia . . . . .	8
3.4	Initial Wheel Orientation . . . . .	8
3.5	Axle Kinematics . . . . .	9
3.6	Axle Compliance . . . . .	9
3.7	Spring . . . . .	9
3.8	Damper . . . . .	9
3.9	Stabi . . . . .	10
<b>4</b>	<b>Drive Train</b>	<b>11</b>
4.1	Engine . . . . .	11
4.2	Driveline . . . . .	11
4.2.1	Rear Differential . . . . .	11
4.3	Manual Transmission . . . . .	12
4.3.1	Gear Data . . . . .	12
4.3.2	Shift Control . . . . .	12

---

# 1 General Vehicle Data

Vehicle Type: Truck

## 1.1 Vehicle Dimensions

Vehicle Length [ m ]:	7.5		
Vehicle Width [ m ]:	2.55		
Vehicle Height [ m ]:	3.1		
Wheel Base [ m ]:	3.88		
Wheel Track front [ m ]:	2.2		
Wheel Track rear [ m ]:	2.2		
Vehicle Geometry:	vehicle_body_truck.wrl		
Scaling for Vehicle Geometry:	1	1	1
Tyre Geometry:	tire_truck.wrl		
Scaling for Tyre Geometry:	1	1	1
Steering Wheel Geometry:	steeringwheel_truck.wrl		
Steering Wheel Position:	0.9	0.69	1.3

## 1.2 Mass & Load

Vehicle Mass [ kg ]:	8830		
Vehicle Centre of Gravity x [ m ]:	-1.542		
Vehicle Centre of Gravity y [ m ]:	0		
Vehicle Centre of Gravity z [ m ]:	0.915		
Inertia Matrix at CoG [ kgm <sup>2</sup> ]:	301413	0	0
	0	107000	0
	0	0	107000
Load Mass [ kg ]:	0		
Load Centre of Gravity x [ m ]:	0		
Load Centre of Gravity y [ m ]:	0		
Load Centre of Gravity z [ m ]:	0		
Load Inertia Matrix [ kgm <sup>2</sup> ]:	0	0	0
	0	0	0
	0	0	0

### 1.3 Aerodynamics

CW Coefficient in x-direction:	0.8		
CW Coefficient in y-direction:	0.9		
CW Coefficient in z-direction:	0		
Shadow area in x-direction [ m <sup>2</sup> ]:	8.9		
Shadow area in y-direction [ m <sup>2</sup> ]:	38.9		
Shadow area in z-direction [ m <sup>2</sup> ]:	30		
Centre of Forces [ m ]:	-3.8	0	1.4
Wind Speed [ m/s ]:	0	0	0

### 1.4 Brake System

Maximum Brake Pressure [ bar ]:	20		
Brake Pressure Distribution:	overall [ % ]:		rear [ % ]:
	0		0
	50		50
	100		100
Time Constant for Pressure Build-up [ s ]:	0		

---

## 2 Front Axle

### 2.1 Tyre

Tyre Width [ mm ]:	290
Ratio of Tyre Height to Tyre Width [ x100 ]:	80
Tyre Rim Diameter [ inch ]:	22.5
Load Index [ - ], Range: 50...209:	156
Tyre Speed Symbol:	L = 120 km/h
Reference Load [ N ]:	16000
Longitudinal Slip Gradient [ N/- ]:	150000
$F_{x,max}$ [ N ]:	12800
Lateral Slip Gradient [ N/- ]:	104200
$F_{y,max}$ [ N ]:	10000
Sliding Friction Ratio:	0.95
Vertical Stiffness [ N/m ]:	1090000
Load Degression for Lateral Force:	1.8

### 2.2 Brake

Friction Coefficient:	0.35
Effective Brake Disc Radius [ m ]:	0.155
Effective Brake Cylinder Area [ m <sup>2</sup> ]:	0.081

### 2.3 Steering

Steering Type:	Parallel Steering
Steering Column Stiffness [ Nm/deg ]:	52.36
Steering Column Damping [ Nms/deg ]:	0.8727
Maximum Steering Wheel Angle (one direction) [ deg ]:	864
Steering Ratio (Steering Wheel Angle / Steering Angle):	24.4

### 2.4 Axle Mass & Inertia

Unsprung Mass located in WC [ kg ]:	190		
Inertia of Rotating Parts about Wheel Spin Axis (1/2 Drive Shaft, Brake Disk, Wheel) [ kgm <sup>2</sup> ]:	4.1		
Inertia Matrix of Non-Rotating Parts about Wheel Centre (Wheel Body, Wheel Carrier) [ kgm <sup>2</sup> ]:	30	0	0
	0	15	0
	0	0	32

## 2.5 Initial Wheel Orientation

Toe-In Angle [ deg ]:	0.1098
Camber Angle [ deg ]:	0.5

## 2.6 Axle Kinematics

Wheel Position at Wheel Lift [ m ]:	-0.0670079	0	0.0608345
x [ m ]:	0.0179379	0	-0.010001
y [ m ]:	-4.15e-05	0	-6.1e-06
Camber [ deg ]:	-0.04282	0	0.0280692
Caster [ deg ]:	0.14725015	0	-0.08981686
Toe-In [ deg ]:	1.1172677	0	-0.68181977
x [ m ]:	0.0570211	0	-0.0593618
y [ m ]:	-0.0099124	0	-0.0107162
Camber [ deg ]:	-0.35139501	0	1.398017
Caster [ deg ]:	2.5897692	0	-2.7788453

## 2.7 Axle Compliance

x Displacement / Fx [ m/N ]:	0
Bounce Force [ N ]:	0
Bounce x Displacement [ m ]:	0
Toe-In / Fx [ deg/N ]:	0
Bounce Force [ N ]:	0
Bounce Toe-In Angle [ deg ]:	0
Toe-In / Fy [ deg/N ]:	0
Bounce Force [ N ]:	0
Bounce Toe-In Angle [ deg ]:	0
Toe-In / Mz [ deg/Nm ]:	0

## 2.8 Spring

Pre-Load [ N ]:	18557
Spring Stiffness [ N/m ]:	300000
Jounce Stop [ m ]:	0.186
Jounce Stiffness [ N/m ]:	100000000
Rebound Stop [ m ]:	-0.179
Rebound Stiffness [ N/m ]:	100000000

## 2.9 Damper

Table of vertical force at wheel center due to damper, dependent on wheel lift velocity.:	Wheel Center Velocity [ m/s ]:	Force at Wheel Center [ N ]:
	-0.6	-3373
	-0.3	-2178
	-0.1	-775
	-0.05	-451
	0	0
	0.05	941
	0.1	2099
	0.3	5580
	0.6	8257

## 2.10 Stabi

Stabi Roll Stiffness front [ Nm/deg ]:	33113.78
--	----------

---

## 3 Rear Axle

### 3.1 Tyre

Tyre Width [ mm ]:	265
Ratio of Tyre Height to Tyre Width [ x100 ]:	90
Tyre Rim Diameter [ inch ]:	22.5
Load Index [ - ], Range: 50...209:	156
Tyre Speed Symbol:	L = 120 km/h
Reference Load [ N ]:	12260
Longitudinal Slip Gradient [ N/- ]:	150000
$F_{x,max}$ [ N ]:	9800
Lateral Slip Gradient [ N/- ]:	86000
$F_{y,max}$ [ N ]:	7700
Sliding Friction Ratio:	0.95
Vertical Stiffness [ N/m ]:	824000
Load Degression for Lateral Force:	1.8

### 3.2 Brake

Friction Coefficient:	0.35
Effective Brake Disc Radius [ m ]:	0.155
Effective Brake Cylinder Area [ m <sup>2</sup> ]:	0.081

### 3.3 Axle Mass & Inertia

Unsprung Mass located in WC [ kg ]:	190		
Inertia of Rotating Parts about Wheel Spin Axis (1/2 Drive Shaft, Brake Disk, Wheel) [ kgm <sup>2</sup> ]:	4.1		
Inertia Matrix of Non-Rotating Parts about Wheel Centre (Wheel Body, Wheel Carrier) [ kgm <sup>2</sup> ]:	30	0	0
	0	15	0
	0	0	32

### 3.4 Initial Wheel Orientation

Toe-In Angle [ deg ]:	0.1098
Camber Angle [ deg ]:	0.5



### 3.5 Axle Kinematics

Wheel Position at Wheel Lift [ m ]:	-0.0434496	0	0.0597272
x [ m ]:	0.0086685	0	-0.0079549
y [ m ]:	-0.1027	-0.1	-0.097
Camber [ deg ]:	1.2433184	0	-1.7131438
Caster [ deg ]:	-0.13765311	0	-0.24608537
Toe-In [ deg ]:	0.2482053	0	-0.22700587
Axle Type:	Rigid Axle		

### 3.6 Axle Compliance

x Displacement / Fx [ m/N ]:	0
Bounce Force [ N ]:	0
Bounce x Displacement [ m ]:	0
Toe-In / Fx [ deg/N ]:	0
Bounce Force [ N ]:	0
Bounce Toe-In Angle [ deg ]:	0
Toe-In / Fy [ deg/N ]:	0
Bounce Force [ N ]:	0
Bounce Toe-In Angle [ deg ]:	0
Toe-In / Mz [ deg/Nm ]:	0

### 3.7 Spring

Pre-Load [ N ]:	18857
Spring Stiffness [ N/m ]:	300000
Jounce Stop [ m ]:	0.1
Jounce Stiffness [ N/m ]:	614715
Rebound Stop [ m ]:	-0.191
Rebound Stiffness [ N/m ]:	1000000

### 3.8 Damper

Table of vertical force at wheel center due to damper, dependent on wheel lift velocity.:	Wheel Center Velocity [ m/s ]:	Force at Wheel Center [ N ]:
	-0.6	-2648.7
	-0.3	-1962
	-0.1	-1471.5
	-0.05	-735.8
	0	0
	0.05	1814.9
	0.1	3629.7
	0.3	6376.5
	0.6	7848

### 3.9 Stabi

Stabi Roll Stiffness rear [ Nm/deg ]: 0

---

## 4 Drive Train

Transmission Type: Manual

### 4.1 Engine

Inertia of Flywheel [ kgm <sup>2</sup> ]:	1.211
Torque Delay [ s ]:	0.1
Scaling Factor:	1
Idle Speed [ rpm ]:	800
Torque at 1.2 * Idle Speed [ Nm ]:	1510
Friction Torque at 1.2 * Idle Speed [ Nm ]:	-134
Engine Speed at Maximum Engine Torque [ rpm ]:	1600
Maximum Torque [ Nm ]:	1520
Engine Speed at Maximum Engine Power [ rpm ]:	2100
Torque at Maximum Power [ Nm ]:	1180
Friction Torque at Maximum Engine Speed [ Nm ]:	-260
Maximum Engine Speed [ rpm ]:	2400

### 4.2 Driveline

Driveline Type: Rear Drive

#### 4.2.1 Rear Differential

Input Shaft (rear) Stiffness [ Nm/deg ]:	5240
Input Shaft (rear) Damping [ Nms/rad ]:	0.02
Wheel Shaft (left) Stiffness [ Nm/deg ]:	10110
Wheel Shaft (left) Damping [ Nms/rad ]:	0.2
Inertia of Output to Left [ kgm <sup>2</sup> ]:	0.0468
Wheel Shaft (right) Stiffness [ Nm/deg ]:	10110
Wheel Shaft (right) Damping [ Nms/rad ]:	0.2
Inertia of Output to Right [ kgm <sup>2</sup> ]:	0.0468
Inertia Housing & Bevel Wheel [ kgm <sup>2</sup> ]:	0.0959
Inertia Rear Differential Input [ kgm <sup>2</sup> ]:	0.1057
Inertia Planetary Gear Set [ kgm <sup>2</sup> ]:	0.0096
Maximum Dry Friction Locking Torque [ Nm ]:	0
Transmission Ratio:	5.285

## 4.3 Manual Transmission

### 4.3.1 Gear Data

Number of Forward Driving Gears:	7
Reverse Gear [ - ]:	-6.552
1st Gear [ - ]:	6.59
2nd Gear [ - ]:	3.4
3rd Gear [ - ]:	2.04
4th Gear [ - ]:	1.407
5th Gear [ - ]:	1
6th Gear [ - ]:	0.743
7th Gear [ - ]:	0.61
Maximum Clutch Torque [ Nm ]:	2882.4
Moments of Inertia:	
Transmission Input [ kgm <sup>2</sup> ]:	0.0062
Transmission Output [ kgm <sup>2</sup> ]:	0.0268
Clutch Wheel [ kgm <sup>2</sup> ]:	0.0243
Between Clutch Driven Plate and Layshaft:	
Stiffness [ Nm/deg ]:	200
Maximum Torsion Angle [ deg ]:	8
Damping Coefficient [ Nms/rad ]:	0.05

### 4.3.2 Shift Control

Engine Speed to Shift Up [ rpm ]:	2000
Engine Speed to Shift Down [ rpm ]:	1000
Engine Speed to Disengage Clutch [ rpm ]:	400
Engine Speed to Engage Clutch [ rpm ]:	1000
Gear Ratio Synchronisation Time Constant [ s ]:	0.2
Clutch Time Constant [ s ]:	1